

**Development of novel CO<sub>2</sub>-stable oxygen  
permeable dual phase membranes for CO<sub>2</sub>  
capture in an oxy-fuel process**

Von der Naturwissenschaftlichen Fakultät  
der Gottfried Wilhelm Leibniz Universität Hannover  
zur Erlangung des Grades

**Doktorin der Naturwissenschaften**

**Dr. rer. nat.**

genehmigte Dissertation

von

**Huixia Luo**

(Master of Engineering)

geboren am 29.07.1984 in Guangdong, China

**2012**

**Referent:** Uni.-Prof. Juergen Caro

**Korreferent:** Univ.-Prof. Haihui Wang

**Tag der Promotion:** 19<sup>th</sup> July, 2012

## Preface

The presented results of this thesis were obtained since August 24, 2009 during my Ph. D. study at the Institute of Physical Chemistry and Electrochemistry at the Gottfried Wilhelm Leibniz Universität Hannover under the supervision of Prof. Dr. Jürgen Caro. In this period, I was a Fellow of the Chinese government (stipendium) and was also a member of scientific research staff and worked for the European project NASA-OTM.

Six research articles in which I have been the first author or the co-author are presented within this thesis. The following statement will point out my contribution to the articles collected in this thesis. For all these articles, I would like to acknowledge the fruitful discussions and valuable comments from the co-authors and referees, particularly from Prof. Dr. J. Caro, Prof. Dr. H. Wang, Dr. H. Jiang and Priv.-Doz. Dr. A. Feldhoff.

The first article, *Phase stability and permeation behavior of a dead-end  $Ba_{0.5}Sr_{0.5}Co_{0.8}Fe_{0.2}O_{3-\delta}$  tube membrane in high-purity oxygen production*, was written by Priv.-Doz. Dr. A. Feldhoff and my colleague Fangyi Liang. My contribution was to assist in performing long-term oxygen permeation measurements and to share experimental knowledge.

The four articles in Chapter 3, are on studying the preparation and testing of novel  $CO_2$ -stable dual phase membranes for oxygen separation. The first article,  *$CO_2$ -stable and cobalt-free dual phase membrane for oxygen separation*, was written by me. I got support on the manuscript preparation from all the co-authors, especially from Prof. Dr. J. Caro, Prof. Dr. H. Wang and Priv.-Doz. Dr. A. Feldhoff. The development and preparation of novel dual phase membranes and all the measurements of oxygen permeation were mainly completed by myself. (HR)TEM, HAAD, EELS and SEAD characterizations and data interpretation were done by Priv.-Doz. Dr. A. Feldhoff. Frank Steinbach conducted me to carry out the EDXS and SEM characterizations. And BSEM characterizations were done by Frank Steinbach and me together. Dr. Konstantin Efimov conducted me to carry out the XRD measurements and did the *in-situ* XRD measurements in different atmosphere. The second article, *Influence of the preparation methods on the microstructure and oxygen permeability of a  $CO_2$ -stable dual phase membrane*, was written by me. The experimental data and calculations were performed by myself. Dr. Konstantin Efimov carried out the *in-situ* XRD measurements in different gaseous atmospheres. And the *in-situ* data calculation and interpretation were done by myself. Frank Steinbach and I did the BSEM

characterizations together. Prof. Dr. J. Caro, Prof. Dr. H. Wang and Dr. H. Jiang provided strong support on the manuscript preparation. The third article, *CO<sub>2</sub>-tolerant oxygen-permeable Fe<sub>2</sub>O<sub>3</sub>-Ce<sub>0.9</sub>Gd<sub>0.1</sub>O<sub>2-δ</sub> dual phase membranes*, was also written by me, and Prof. Dr. J. Caro improved it. And Prof. Dr. H. Wang offered strong support on the manuscript preparation. Dr. H. Jiang and Dr. A. Huang also gave many valuable suggestions to improve it. The oxygen permeation measurements and SEM, EDXS characterizations were conducted by myself. *In-situ* XRD measurement was done by Dr. Konstantin Efimov. And the *in-situ* data calculation and interpretation were done by myself. The fourth article, *Rapid glycine-nitrate combustion synthesis of CO<sub>2</sub>-stable dual phase membrane 40Mn<sub>1.5</sub>Co<sub>1.5</sub>O<sub>4-δ</sub>-60Ce<sub>0.9</sub>Pr<sub>0.1</sub>O<sub>2-δ</sub> for CO<sub>2</sub> capture via an oxyfuel process*, was written by me with the help of Prof. Dr. J. Caro. EDXS, SEM and BSEM characterizations were done by Frank Steinbach and me together. Tobias Klande helped me to analysis the XRD. The oxygen permeation measurements and the interpretation were carried out by myself.

Another article focusing on dual phase membrane for partial oxidative methane conversion was collected in Chapter 4. I wrote the first draft: *A novel cobalt-free noble metal-free oxygen-permeable 40Pr<sub>0.6</sub>Sr<sub>0.4</sub>FeO<sub>3-δ</sub>-60Ce<sub>0.9</sub>Pr<sub>0.1</sub>O<sub>2-δ</sub> composite membrane*, Prof. Dr. J. Caro and Prof. H. Wang spent much time on correcting and improving it. EDXS, SEM and BSESEM characterizations were done by Frank Steinbach and me together. *In-situ* XRD measurements in different gaseous atmospheres were carried out by my colleague, Tobias Klande. Additionally, I obtained support on the manuscript preparation from all co-authors.

All together, I have developed four novel dual phase membranes with oxygen transport: (1) NiFe<sub>2</sub>O<sub>4-δ</sub>-Ce<sub>0.9</sub>Gd<sub>0.1</sub>O<sub>2-δ</sub> (2) Fe<sub>2</sub>O<sub>3-δ</sub>-Ce<sub>0.9</sub>Gd<sub>0.1</sub>O<sub>2-δ</sub> (3) Mn<sub>1.5</sub>Co<sub>1.5</sub>O<sub>4-δ</sub>-Ce<sub>0.9</sub>Pr<sub>0.1</sub>O<sub>2-δ</sub> (4) Pr<sub>0.6</sub>Sr<sub>0.4</sub>FeO<sub>3-δ</sub>-Ce<sub>0.9</sub>Pr<sub>0.1</sub>O<sub>2-δ</sub>. The chemical composition of these four CO<sub>2</sub>-stable oxygen-transporting dual phase membranes was proposed by me. It was also my idea to adopt novel preparation concepts like one-pot single-step EDTA citric acid method and one-pot single-step glycine-nitrate combustion process for the first time to the development of these dual phase membranes.

# Acknowledgement

I would like to express my grateful appreciation to all the persons who have helped and encouraged me during my Ph.D. thesis research at the Institute of Physical Chemistry and Electrochemistry at the Gottfried Wilhelm Leibniz Universität Hannover.

First of all, I would like to give my appreciation to my supervisors, Prof. Dr. Caro for giving me this opportunity to study and carry out this interesting scientific work in his group. During the past three years, I am deeply grateful for his fruitful support and patient guidance throughout my entire Ph.D. thesis. Without him, this dissertation would not have been finished. In addition, I deeply appreciate to his kind suggestions to improve my languages not only in writing but also in speaking. Especially, I am profoundly impressed by his kindness, his passion and his hard-working attitude. I have been fortunate to benefit from his many years of experience in research and his research insight.

Furthermore, I am grateful to Prof. Wang from South China University of Technology for his kindness allowing me to obtain the master degree one-year in advance and encouraging and helping me to apply for the stipend organized by the China Scholarship Council. I am deeply indebted to him for his so valuable suggestions and help during my Ph.D. Meanwhile, I acknowledge his promotion and understanding during my work.

I would also like to thank Dr. Heqing Jiang, Priv.-Doz. Dr. Armin Feldhoff and Dr. Aisheng Huang for their valuable discussions and comments throughout my work. Special thanks goes to Dr. Heqing Jiang for his help in the beginning of my Ph.D. study and life in Germany. Exceptional thanks go to Priv.-Doz. Dr. Armin Feldhoff for his valuable cooperation on TEM measurements.

I am very grateful to Fangyi Liang, Dr. Konstantin Efimov, Tobias Klande, Zhengwen Cao, Dr. Oliver Czuprat, and Dr. Helge Bux for their assistance and helpful cooperation in the past three years. Special gratitude goes to Fangyi Liang and Zhengwen Cao. I am very pleased to

share the office with them. Meanwhile, I am also glad to work with Fangyi with the same GC. Furthermore, I thank Dr. Konstantin Efimov and Tobias Klande for their so kind help for *in-situ* XRD measurements.

I would like to give many thanks to Yvonne Gabbey-Uebe, Kerstin Janze, and Frank Steinbach for their kind supports in the technical or the administrative aspects in the past three years. Exceptional thanks go to Frank Steinbach for his valuable cooperation on BSEM and EDXS measurements. He initially taught me how to operate the SEM and EDXS instruments. I am very happy with the nice atmosphere in Prof. Caro's group. I want to express my gratitude to all the former and current members of our group for their kindness, help and friendship, especially Prof. Dr. Michael Wark, Dr. Yanshuo Li, Dr. Dirk Dorfs, Dr. Juan Du, Dr. Oliver Merka, Dr. Monir Sharifi, Dr. Christian Dunkel, Dr. Olga Wittich, Dr. Jana Panke, Dr. Amira Ahmed, Dr. Florian Bittner, Nanyi Wang, Kaveh Partovi, Lisa Diestel, Alexander Mundstock and Olga Wittich. I appreciate the great job done by the mechanical and electrical workshop, my special thanks to Mr. Bieder, Mr. Egly, Mr. Becker, Mr. Rogge, and Mr. Ribbe.

I kindly acknowledge the financial support of the China Scholarship Council (CSC) and the European project NASA-OTM.

Finally, but not the least, I would like to express my deepest thanks and regards to my great parents, brother, sisters, my boyfriend and friends, for their understandings, unlimited support, unconditional love, sacrifice and encouragement.

## Abstract

The combustion of fossil fuels in power stations with pure oxygen following the oxy-fuel process allows the sequestration of CO<sub>2</sub>. The pure oxygen needed can be separated from air by oxygen transporting ceramics like single phase perovskites. However, most of the so far developed single phase perovskites have stability problems in a CO<sub>2</sub> containing atmosphere. Dual phase membranes are micro-scale mixtures of an electron conducting phase and an oxygen ion conducting phase and their compositions can be tailored according to practical requirements, which are considered to be promising substitutes for the single phase perovskite materials. In my thesis the issues of phase stability for perovskite-type material with the common composition Ba<sub>0.5</sub>Sr<sub>0.5</sub>Co<sub>0.8</sub>Fe<sub>0.2</sub>O<sub>3-δ</sub> (BSCF) as well as the development of a series of novel CO<sub>2</sub>-stable dual phase membranes were studied.

In Chapter 2, the phase stability and permeation behavior of a dead-end BSCF tube membrane in high-purity oxygen at temperatures below 750 °C, were elucidated using powder X-ray diffraction (XRD), energy dispersive X-ray spectroscopy (EDXS), high-angle annular dark-field (HAADF) and scanning transmission electron microscopy (STEM). It was found that parts of the cubic perovskite BSCF transformed into a hexagonal perovskite Ba<sub>0.5±x</sub>Sr<sub>0.5±x</sub>CoO<sub>3-δ</sub> (x ≈ 0.1) and a trigonal mixed oxide Ba<sub>1-x</sub>Sr<sub>x</sub>Co<sub>2-y</sub>Fe<sub>y</sub>O<sub>5±δ</sub> (x ≈ 0.15, y ≈ 0.25) in high-purity oxygen at 750 °C. On the other hand, it was found that the partial degradation of cubic BSCF perovskite at 750 °C was more pronounced under the strongly oxidizing conditions on the oxygen supply (feed) side than on the oxygen release (permeate) side of the membrane. The structural instability of BSCF is attributed to an oxidation of cobalt from Co<sup>2+</sup> to Co<sup>3+</sup> and Co<sup>4+</sup>, which exhibits an ionic radius that is too small to be tolerated by the cubic perovskite structure, which then becomes unstable.

Chapter 3 demonstrated the development of the CO<sub>2</sub>-stable alkaline-earth metals-free dual phase membranes. There novel dual phase membranes of the compositions: 40 wt.% NiFe<sub>2</sub>O<sub>4-δ</sub> - 60 wt.% Ce<sub>0.9</sub>Gd<sub>0.1</sub>O<sub>2-δ</sub> (40NFO-60CGO), 40 wt.% Fe<sub>2</sub>O<sub>3-δ</sub> - 60 wt.% Ce<sub>0.9</sub>Gd<sub>0.1</sub>O<sub>2-δ</sub> (40FO-60CGO), 40 wt.% Mn<sub>1.5</sub>Co<sub>1.5</sub>O<sub>4-δ</sub> - 60 wt.% Ce<sub>0.9</sub>Pr<sub>0.1</sub>O<sub>2-δ</sub> (40MCO-60CPO) were developed using different methods, including mixing powder by hand, mixing powder by

ball-milling, one-pot single-step sol-gel method. The structures of the dual phase membranes were studied in detail by various analytical techniques such as *in-situ* XRD, SEM, back-scattered SEM (BSEM), EDXS, STEM and selected-area electron diffraction (SAED). It was found that all these dual phase membranes show two well separated phases. Moreover, the *in-situ* one-pot single-step sol-gel method was found to be the best way to prepare well-distribution dual phase membranes. On the other hand, since our dual phase membranes do not contain alkaline-earth metals, it can be expected that they are CO<sub>2</sub>-stable. The oxygen permeation flux measurements were performed for a few days and no decrease of the oxygen permeation flux was observed, which confirms that these dual phase membranes are CO<sub>2</sub>-stable. However, it is shown that all these materials are not stable in reducing atmosphere, since they contain easily reducible metals oxides of Co, Ni in their compositions.

Chapter 4 demonstrated the development of a novel cobalt-free noble metal-free oxygen-permeable 40 wt.% Pr<sub>0.6</sub>Sr<sub>0.4</sub>FeO<sub>3-δ</sub> - 60 wt.% Ce<sub>0.9</sub>Pr<sub>0.1</sub>O<sub>2-δ</sub> (40PSFO-60CPO) dual phase membrane. The structures of the dual phase membranes were investigated in detail by various analytical techniques such as *in-situ* XRD, SEM, BSEM and EDXS. *In-situ* XRD measurements in 50 vol.% N<sub>2</sub>/50vol.% CO<sub>2</sub> atmosphere confirmed that the dual phase 40PSFO-60CPO membrane showed good CO<sub>2</sub> stability since no change of the reflections and no carbonate formation was observed. The partial oxidation of methane (POM) to synthesis gas reaction was successfully performed with a 40PSFO-60CPO membrane reactor, indicating its high stability in reducing atmosphere.

**Keywords:** Dual phase membrane, CO<sub>2</sub>-stable membrane, Oxygen permeation, *In-situ* one-pot single-step sol-gel method.



# Zusammenfassung

Die Verbrennung von fossilen Rohstoffen in Kraftwerken nach dem Oxy-Fuel-Verfahren erlaubt die Abtrennung des klimaschädlichen CO<sub>2</sub>. Hierbei kann der benötigte reine Sauerstoff durch keramische Perowskitmembranen aus der Luft abgetrennt werden. Allerdings weisen die bisher entwickelten Perowskitmaterialien ein großes Stabilitätsdefizit bei extrem kleinen Sauerstoffpartialdrücken auf. In der praktischen Anwendung ist die eine Seite der Membran einer oxidierenden Atmosphäre (z.B. Luft) und die andere Seite der Membran reduzierenden oder CO<sub>2</sub>-haltigen Atmosphären ausgesetzt. Die hier vorgestellten Zweiphasen-Membranen bestehen aus einer Mischung aus einem Elektronen- und einem Sauerstoffionenleiter, die im Mikrometermaßstab streng getrennt als zwei Phasen vorliegen. Die Eigenschaften können durch Variation der chemischen Zusammensetzung und des Mischverhältnisses auf den jeweiligen Einsatzzweck maßgeschneidert werden. Das macht Zweiphasen-Membranen zu einer Alternative zu den bekannten einphasigen Perowskitmaterialien. In der vorliegenden Doktorarbeit wird die Phasenstabilität des bekannten Perowskitmaterials Ba<sub>0.5</sub>Sr<sub>0.5</sub>Co<sub>0.8</sub>Fe<sub>0.2</sub>O<sub>3-δ</sub> (BSCF) untersucht und die Entwicklung neuartiger CO<sub>2</sub>-stabiler Zweiphasenmembranen berichtet.

In Kapitel 2 wird die Phasenstabilität und das Sauerstofftransportverhalten einer einseitig verschlossenen BSCF-Rohrmembran in hochreinem Sauerstoff bei Temperaturen über und unter 750 °C mittels Röntgendiffraktometrie (XRD), Energie dispersive Röntgenspektroskopie (EDXS) und Transmissionselektronenmikroskopie (TEM) untersucht. Es wird gezeigt, dass sich die kubische BSCF Struktur in reinem Sauerstoff im intermediären Temperaturbereich (750 °C) teilweise in einen hexagonalen Pervoskiten Ba<sub>0.5±x</sub>Sr<sub>0.5±x</sub>CoO<sub>3-δ</sub> und in ein trigonales Mischoxid Ba<sub>1-x</sub>Sr<sub>x</sub>Co<sub>2-y</sub>Fe<sub>y</sub>O<sub>5±δ</sub> zersetzt.

In Kapitel 3 wird die Entwicklung von CO<sub>2</sub>-stabilen Erdalkaliemetall-freien Zweiphasen-Membranen beschrieben. Drei neuartige Membranen folgender Zusammensetzung wurden entwickelt: 40 wt.% NiFe<sub>2</sub>O<sub>4-δ</sub> - 60 wt.% Ce<sub>0.9</sub>Gd<sub>0.1</sub>O<sub>2-δ</sub> (40NFO-60CGO), 40 wt.% Fe<sub>2</sub>O<sub>3-δ</sub> - 60 wt.% Ce<sub>0.9</sub>Gd<sub>0.1</sub>O<sub>2-δ</sub> (40FO-60CGO), 40 wt.% Mn<sub>1.5</sub>Co<sub>1.5</sub>O<sub>4-δ</sub> - 60 wt.% Ce<sub>0.9</sub>Pr<sub>0.1</sub>O<sub>2-δ</sub> (40MCO-60CPO). Dabei wurde der Einfluss verschiedener Herstellungsprozesse auf die

Membraneigenschaften untersucht: Pulvermischen in einem Mörser, Mischen mittels Kugelmühle und Eintopf-Sol-Gel-Synthese. Die Struktur der Membranen wurde mittels einer Vielzahl analytischer Methoden untersucht, wie zum Beispiel *in-situ* Röntgendiffraktometrie (XRD), Rasterelektronenmikroskopie (REM), Rückstreuetelektronen-Rasterelektronenmikroskopie (BREM), Energie-dispersive Röntgenspektroskopie (EDXS), Transmissionselektronenmikroskopie (TEM) und Feinbereichselektronenbeugung (SAED) untersucht. Alle Membranen zeigen eine eindeutige Phasentrennung, das heißt, die beiden Phasen liegen getrennt vor, es bilden sich keine Mischphasen. Die Herstellungsweise mittels *in-situ* Eintopf-Sol-Gel-Synthese zeigt die besten Ergebnisse in Bezug auf eine feine Homogenisierung (kleine Körner mit enger Korngrößenverteilung) der Phasen und den Sauerstofffluss. Durch die Abwesenheit von Erdalkalimetallen kann auf eine gute CO<sub>2</sub>-Verträglichkeit geschlossen werden. In der Tat zeigen Langzeitsauerstoffpermeationsmessungen, die über mehrere Tage in CO<sub>2</sub>-haltigen Atmosphären ausgeführt wurden, keine Verringerung des Sauerstoffflusses. Nichtsdestotrotz wurde eine schlechte Stabilität in reduzierenden Atmosphären, bedingt durch die leicht reduzierbaren Cobalt- und Nickelionen in den Membranen, gefunden.

In Kapitel 4 wird die Entwicklung einer neuartigen Cobalt- und Edelmetall-freien sauerstoffleitenden 40 wt.% Pr<sub>0.6</sub>Sr<sub>0.4</sub>FeO<sub>3-δ</sub> - 60 wt.% Ce<sub>0.9</sub>Pr<sub>0.1</sub>O<sub>2-δ</sub> (40PSFO-60CPO) Zweiphasen-Membran beschrieben. Die Struktur der Membranen wurde mittels einer Vielzahl analytischer Methoden untersucht, wie zum Beispiel *in-situ* XRD, REM, BREM und EDXS. *In-situ* XRD-Messungen in 50 vol.% N<sub>2</sub> und 50 vol.% CO<sub>2</sub> bestätigen die gute CO<sub>2</sub>-Toleranz des Materials, da keine Änderungen der Reflexe oder eine Carbonatbildung beobachtet wurde. Die partielle Oxidation von Methan (POM) zu Synthesegas wurde erfolgreich in einem Membranreaktor durchgeführt. Dies zeigt die hohe Stabilität dieser Zweiphasenmembran in reduzierenden Atmosphären.

**Schlagwörter:** Zweiphasen-Membran, CO<sub>2</sub>-stabile Membran, Sauerstoffpermeation, *In-situ* Eintopf-Sol-Gel-Synthese

# Content

<b>Preface.....</b>	<b>I</b>
<b>Acknowledgement .....</b>	<b>III</b>
<b>Abstract.....</b>	<b>V</b>
<b>Zusammenfassung.....</b>	<b>VII</b>
<b>Content.....</b>	<b>1</b>
<b>1. Introduction.....</b>	<b>3</b>
1.1 Motivation .....	3
1.2 Basic aspects of dense oxygen permeable membranes .....	6
1.2.1 Concepts of dense ceramic oxygen permeable membranes .....	6
1.2.2 Structures of dense ceramic oxygen permeable materials.....	9
1.3 Perovskite-type oxygen permeable membranes .....	11
1.3.1 Preparation of perovskite-type oxygen permeable oxides.....	11
1.3.2 Issues of perovskite-type oxygen permeable membranes .....	14
1.4 Dual phase oxygen permeable membranes .....	15
1.4.1 Preparation of dual phase oxygen permeable membranes.....	15
1.4.2 Oxygen transport through dual phase oxygen permeable membranes.....	21
1.4.3 Applications of dual phase oxygen permeable membranes.....	28
1.5 Bibliography .....	33
<b>2. Phase stability and permeation behavior of BSCF perovskite membrane.....</b>	<b>43</b>
2.1 Summary .....	43
2.2 Phase stability and permeation behavior of a dead-end $\text{Ba}_{0.5}\text{Sr}_{0.5}\text{Co}_{0.8}\text{Fe}_{0.2}\text{O}_{3-\delta}$ tube	

membrane in high-purity oxygen production .....	44
<b>3. Preparation and characterization of alkaline-earth metals-free CO<sub>2</sub>-stable dual phase membranes.....</b>	<b>54</b>
3.1 Summary .....	54
3.2 CO <sub>2</sub> -stable and cobalt-free dual phase membrane for oxygen separation .....	56
3.3 Influence of the preparation methods on the microstructure and oxygen permeability of a CO <sub>2</sub> -stable dual phase membrane .....	69
3.4 CO <sub>2</sub> -tolerant oxygen-permeable Fe <sub>2</sub> O <sub>3</sub> - Ce <sub>0.9</sub> Gd <sub>0.1</sub> O <sub>2-δ</sub> dual phase membranes.....	78
3.5 Rapid glycine-nitrate combustion synthesis of the CO <sub>2</sub> -stable dual phase membrane 40Mn <sub>1.5</sub> Co <sub>1.5</sub> O <sub>4-δ</sub> - 60Ce <sub>0.9</sub> Pr <sub>0.1</sub> O <sub>2-δ</sub> for CO <sub>2</sub> capture via an oxy-fuel process.....	89
<b>4. Dual phase membrane as reactor for partial oxidation of methane .....</b>	<b>99</b>
4.1 Summary .....	99
4.2 A novel cobalt-free noble-free oxygen-permeable 40Pr <sub>0.6</sub> Sr <sub>0.4</sub> FeO <sub>3-δ</sub> - 60Ce <sub>0.9</sub> Pr <sub>0.1</sub> O <sub>2-δ</sub> dual phase membrane .....	100
<b>5. Conclusions.....</b>	<b>110</b>
<b>Publications and conferences.....</b>	<b>112</b>
<b>Curriculum Vitae .....</b>	<b>115</b>
<b>Erklärung zur Dissertation.....</b>	<b>117</b>

# Chapter 1

## 1. Introduction

### 1.1 Motivation

It is now widely accepted that CO<sub>2</sub> emission is the main contribution to the global warming via the greenhouse effect. Especially the CO<sub>2</sub> emitted from the power plants accounts for more than 40 % of the global anthropogenic CO<sub>2</sub> emissions.<sup>[1]</sup> Therefore, there is an urgent need to develop efficient and cost-effective methods for reducing the emissions of CO<sub>2</sub> from the power plants into the atmosphere. Recently, CO<sub>2</sub> capture and storage technologies to reduce the CO<sub>2</sub> emissions from coal-fired power plants have gained great attentions of decision makers in governments, industry and academia. There are three major concepts for CO<sub>2</sub> sequestration: post-combustion capture, pre-combustion separation and oxy-fuel techniques.<sup>[2]</sup> Among these promising strategies to integrate the existing coal-fired power plants with CO<sub>2</sub> capture to produce low emission electricity, oxy-fuel combustion is considered to be more economically feasible than other strategies. So far, several big projects have been initiated such as CS Callide (Australia), Vattenfal (Germany), Inabensa (Spain), OXY-CFB-300 (Spain), TotalLacq (France) and FutureGen2 (USA) program with billion dollar investments for each of these projects.<sup>[3]</sup>

In oxy-fuel combustion, the combustion process is accomplished with pure O<sub>2</sub> or an O<sub>2</sub>/CO<sub>2</sub> mixture in steady of air, thus major waste gas produced is CO<sub>2</sub>, enabling the CO<sub>2</sub> capture more energy-efficient.<sup>[4]</sup> Mixed ion electron conducting (MIEC) ceramic membranes have gained increasing attention due to their potential applications in oxygen supply to power stations for CO<sub>2</sub> capture according to the oxy-fuel concept by using flue gas as sweep gas, which reduce O<sub>2</sub> production cost by 35 % or more comparing the conditional oxygen separation methods (e.g. cryogenic distillation and pressure swing adsorption). Two different methods of membrane integration (three-end operation and four-end operation)<sup>[5]</sup> have been presented in the membrane-based oxy-fuel power plant. In the other hand, MIEC ceramic membranes could be promising applications are high-temperature catalytic membrane reactors for hydrocarbon conversion

into syngas and added-value products and the thermal decomposition of carbon dioxide in combination with the partial oxidation of methane to syngas. In these applications, MIECMs enable thermal integration and energy saving and allow process intensification and thus realizing the process with highest efficiency.<sup>[6]</sup> However, in the real process conditions which include the presence of highly concentrated CO<sub>2</sub>, it is considered that a dense oxygen separation membrane should possess the following properties: (i) high oxygen permeation flux, i.e. having both high oxygen ion and electron conductivities; (ii) good structural stability within appropriate ranges of temperature and oxygen partial pressure; (iii) sufficient chemical compatibility and mechanical strength.<sup>[7]</sup> Figure 1.1 shows the most important issues for the application of MIEC ceramic membranes in the membrane-based oxy-fuel power plant.

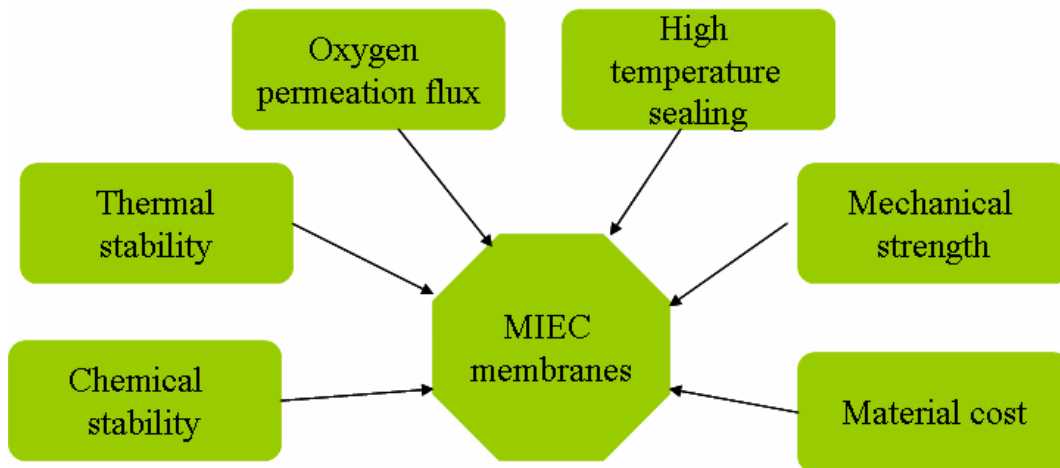


**Figure 1.1** Critical issues of mixed ion electron conducting ceramic membranes.<sup>[7]</sup>

Over the last two decades, large efforts have been made to develop perovskite-type oxides with the general formula of ABO<sub>3</sub> (A = alkaline-earth metals or lanthanide elements; B = transition metals) membrane since a high oxygen permeation flux could be obtained. The highest oxygen permeation is observed for alkaline-earth cobaltites such as Ba<sub>1-x</sub>Sr<sub>x</sub>Co<sub>1-y</sub>Fe<sub>y</sub>O<sub>3-δ</sub>,<sup>[8,9]</sup> BaCo<sub>1-y</sub>Fe<sub>y</sub>O<sub>3-δ</sub>,<sup>[10]</sup> and SrCo<sub>1-y</sub>Fe<sub>y</sub>O<sub>3-δ</sub>.<sup>[11,12]</sup> Even though a high oxygen permeation flux of these materials could be obtained, their widespread adoption are hampered owing to phase instability of cobalt-based perovskite at intermediate temperatures<sup>[13,14]</sup> and the poor chemical stability under a large oxygen concentration gradient.<sup>[15,16]</sup> The phase and chemical stability of single phase perovskite MIEC membrane

materials can be enhanced by removal cobalt elements. Many cobalt-free materials (e.g  $\text{BaCe}_{0.15}\text{Fe}_{0.85}\text{O}_{3-\delta}$ ,<sup>[17]</sup>  $\text{Ba}_{0.95}\text{La}_{0.05}\text{Fe}_0\text{O}_{3-\delta}$ ,<sup>[18]</sup>  $\text{Ba}_{0.5}\text{Sr}_{0.5}\text{Fe}_{0.8}\text{Zn}_{0.2}\text{O}_{3-\delta}$ ,<sup>[19]</sup>  $\text{Ba}_{0.5}\text{Sr}_{0.5}\text{Fe}_{0.8}\text{Cu}_{0.2}\text{O}_{3-\delta}$ <sup>[20]</sup> and  $\text{Ba}_{0.5}\text{Sr}_{0.5}\text{Fe}_{0.9}\text{Al}_{0.1}\text{O}_{3-\delta}$ ,<sup>[21]</sup>) have been developed and offered much higher stability comparing with the cobalt-based perovskites. However, for numerous applications like for the oxy-fuel process or hydrocarbon partial oxidations, where some  $\text{CO}_2$  is formed as by-product of an undesired deeper oxidation, the oxygen transporting membranes must sustain their phase stability and oxygen transport property.<sup>[22,23]</sup> Generally speaking, it is difficult to meet all above-mentioned requirements in a single phase perovskite MIEC membrane because of its improvement in one aspect but often accompanying by the deterioration in others. Therefore, the dual phase oxygen permeable membranes have been proposed to avoid this dilemma since their compositions can be tailoring in the practical applications, in which oxygen ions are transported through the oxygen ion conducting phase (OIC-phase), while electrons are carried by the electron conducting phase (EC-phase). The oxygen permeation properties of dual phase membrane are dependent on their electronic and ionic conductivity, chemical stability, phase stability, as well as thermal expansion compatibility between the two OIC and EC phases.<sup>[24]</sup>

Until now, numerous dual phase materials have been developed which can be divided into two major groups: (i) The first generation of dual phase membranes consist of noble metal (such as Ag, Pd) powders as electronic and a ceramic particles as ionic conductors.<sup>[25-28]</sup> However, these dual phase membranes are expensive, a mismatch of the thermal expansion coefficients (TEC) of the metallic and the ceramic phase exists, and the oxygen permeabilities were found to be low. (ii) The second generation of dual phase membranes compose of two oxides, where one of the oxides acts as electron conductor instead of the noble metal.<sup>[29-32]</sup> These dual phase membranes of the second generation show higher oxygen permeabilities, but they usually contain a perovskite phase ( $\text{ABO}_3$ , A= alkaline-earth metals or lanthanide element; B = transition metal). The alkaline-earth metals on the A site easily form carbonates if  $\text{CO}_2$  is present. This carbonate formation is found to be reversible but it immediately stops the oxygen flux.<sup>[33,34]</sup> These dual phase membranes also suffer from a mechanical stress and can mechanically decompose due to swelling by carbonate formation. On the other hand, reactions between OIC and EC phases in the second generation of dual phase membranes at high operation temperature limited their wide application.

The main aims of this thesis are to elucidate the issues of single phase perovskite-type oxygen permeable membrane and develop novel CO<sub>2</sub>-stable dual phase membranes targeted in CO<sub>2</sub> capture in an oxy-fuel process or thermal decomposition of carbon dioxide in combination with the partial oxidation of methane to syngas. The issue of phase stability of perovskite-type Ba<sub>0.5</sub>Sr<sub>0.5</sub>Co<sub>0.8</sub>Fe<sub>0.2</sub>O<sub>3-δ</sub> (BSCF) was discussed first in Chapter 2. With taking advantages of the flexibility of dual phase materials, a series of novel CO<sub>2</sub>-stable dual phase membrane were designed and investigated. Since these new dual phase membranes do not contain alkaline-earth metals, it can be expected that they are CO<sub>2</sub>-stable. The effects of preparation methods and composition ratios on the oxygen permeabilities through these dual phase membranes were investigated in detail. The phase and CO<sub>2</sub> stability was studied in detail in Chapter 3. In Chapter 4, partial oxidation of methane (POM) to synthesis gas with a novel CO<sub>2</sub>-stable dual phase membrane was investigated in the dual phase membrane reactor.

## 1.2 Basic aspects of dense oxygen permeable membranes

### 1.2.1 Concepts of dense ceramic oxygen permeable membranes

Up to now, several dense oxygen permeable membrane concepts have been proposed, all of them incorporating a dense ceramic oxygen ion conducting materials. Figure 1.2 shows four membrane concepts employing a dense oxygen ion conducting materials. In concept (a),<sup>[35]</sup> solid state cell also called oxygen pump, is based on a solid oxide electrolyte, which is only for oxygen ions transportation. Electrodes and wiring are required for the external transport of electrons (see Figure 1.2a). The driving force for overall oxygen transport is applied as a potential difference between the electrodes. In concept (b) shown in Figure 1.2b, mixed ion and electron conducting (MIEC) oxides materials were used.<sup>[36]</sup> These MIEC membranes can operate without external electrodes and circuits since they can transport oxygen ions as well as electrons. The driving force for overall oxygen transport is the differential oxygen partial pressure applied across the membrane. The selectivity can be reached 100 % in theory since the MIEC membranes are dense and tight and the oxygen transport is in ionic form. Since Teraoka et al.<sup>[37]</sup> first reported a MIEC



perovskite-type membrane,  $\text{La}_x\text{Sr}_{1-x}\text{Fe}_y\text{Co}_{1-y}\text{O}_{3-\delta}$ , with high oxygen permeability, extensive efforts have been made to study such MIEC perovskite-type membranes. However, as mentioned in section 1.1, it is difficult to meet all requirements in a single phase membrane because of its improvement in one aspect but often accompanying by the deterioration in others. Therefore, the dual phase membranes have been proposed to avoid this dilemma since their compositions can be tailoring in the practical applications.

Figure 1.2c presents a schematic of dual phase membrane, which consists of two phases. [24] Therefore, a dual phase membrane also can be considered as a dispersion of one phase into the other phase. Usually, in such a dual phase membrane, oxygen ions transport through the oxygen ion conducting phase (OIC-phase), while electrons are carried by the electron conducting phase (EC-phase). OIC-phases were usually made from solid oxide electrolytes (fast oxygen ionic conductor, e.g.  $\text{Y}_{0.15}\text{Zr}_{0.85}\text{O}_{2-\delta}$ ,  $\text{Ce}_{0.8}\text{Gd}_{0.2}\text{O}_{2-\delta}$ ) and EC-phases can be made from pure electron conductors (e.g. Pd, Ag, Pt, Au) or MIEC conductors. The dual phase membrane is first proposed by Mazanec et al. [24], which offers an alternative use of oxide electrolytes in the field of dense oxygen permeable membranes. After that, several research groups [26, 28, 38-42] have reported the improved oxygen permeation flux with different sets of dual phase membranes by mixing of ceramic materials (e.g stabilized zirconia or bismuth oxides) and noble metal powders. For example, Chen et al. [28] has reported the 60 vol.% yttria-stabilized zirconia (YSZ) - 40 vol.% palladium (Pd) with 2.0 mm thickness at 1100 °C, which shows a oxygen permeation flux of  $4.3 \times 10^{-8}$  mol/cm<sup>2</sup>·s. Jinsoo Kim et al. [42] developed the 60 vol.%  $\text{Bi}_{1.5}\text{Y}_{0.3}\text{Sm}_{0.2}\text{O}_3$  (BYS) - 40 vol.% Ag with 1.3 mm thickness, which show  $5.8 \times 10^{-7}$  mol/cm<sup>2</sup>·s at 850 °C. However, many problems were found in these dual phase membranes with noble metals as electronic conductors. The major problems are as follows: (i) The cost is too expensive. (ii) A mismatch of the thermal expansion coefficients (TEC) between the metallic and the ceramic phase exists. (iii) The oxygen permeabilities were found to be low. To solve these problems, perovskite oxides are suggested to replace noble metals for electron transport considering their high electronic conductivity and low cost. Many publications have reported these kinds of dual phase membranes. However, these dual phase membranes still have some disadvantages, such as poor chemical compatibility and thermal mismatch between two phases leading to low oxygen permeability. Kharton et al. [43] reported that the dual phase membrane with the compositions of  $\text{Ce}_{0.8}\text{Gd}_{0.2}\text{O}_{1.9}$  -  $\text{La}_{0.7}\text{Sr}_{0.3}\text{MnO}_{3-\delta}$ , whose

oxygen permeation flux decreased with operating time due to the formation of other layers with low ionic conductivity at the phase boundaries. U. Igge et al. [30] described  $\text{Ce}_{0.8}\text{Gd}_{0.2}\text{O}_{1.9} - \text{Gd}_{0.7}\text{Ca}_{0.3}\text{CoO}_{3-\delta}$  oxygen permeable membranes for  $\text{NO}_x$  detection in exhaust gases. However, the decomposition of the perovskite phase and interdiffusion of metal ions resulted in a relatively poor oxygen permeability of this dual phase membrane. Recently, Zhu et al. [33,44] proposed a ceria based oxygen permeable membrane of  $\text{Ce}_{0.8}\text{Gd}_{0.2}\text{O}_{1.92} - \text{Gd}_{0.2}\text{Sr}_{0.8}\text{FeO}_{3-\delta}$  (abbreviated as CGO-GSFO), which showed a good oxygen permeation stability (stable for more than 1100 h operation) and a high oxygen permeation flux of  $0.80 \text{ ml}/\text{min}\cdot\text{cm}^2$  at  $950 \text{ }^\circ\text{C}$  under an oxygen partial pressure gradient of  $21 \text{ kPa}/0.5 \text{ kPa}$ . However,  $\text{SrCO}_3$  phase was also detected in the spent membrane, indicating a decomposition of the perovskite phase to some extent. Therefore, the development of new dual phase membranes with high phase and chemical stability is still highly in demand in practical conditions, especially in  $\text{CO}_2$  and reducing atmospheres. In the Chapter 3 in this thesis, the development of novel  $\text{CO}_2$ -stable dual phase membrane will be addressed in detail.

It is well-known that the oxygen permeability is related to many factors such as the microstructures, temperatures, oxygen partial pressures and thicknesses etc. It is accepted that the decrease of membrane thickness can enhance the oxygen permeation flux though a membrane when the oxygen permeation is limited by bulk diffusion. However, the mechanical strength of a thin membrane also will be decrease when the thickness was decreased. In order to obtain the oxygen permeable membrane with high oxygen permeation flux and sufficient mechanical strength, asymmetric membrane was proposed. Figure 1.2d presents a schematic of an asymmetric membrane, which consist of thin dense layer and porous support. In this structure, the support and the thin layer should have good chemical compatibility and similar expansion coefficients. Teraoka et al. first reported an asymmetric membrane, whose support and thin layer were both fabricated with  $\text{La}_{0.6}\text{Sr}_{0.4}\text{CoO}_{3-\delta}$  perovskite oxides by means of sputtering and spray deposition techniques, [45]

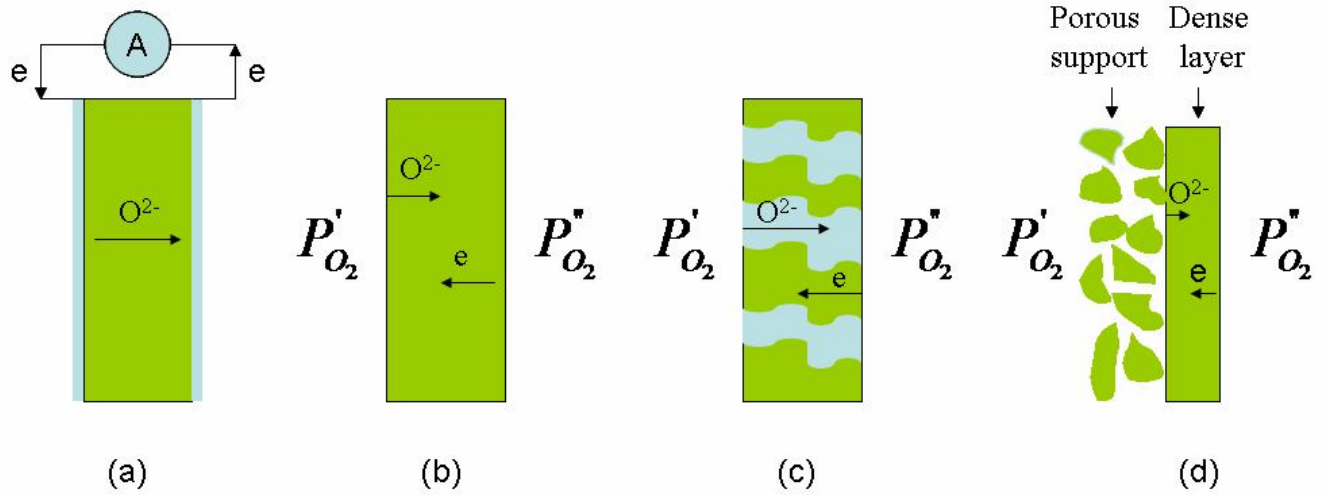


**Figure 1.2** Four membrane concepts employing a dense oxygen ion conducting materials: (a) solid state cell (oxygen pump), (b) MIEC membrane, (c) dual phase membrane and (d) asymmetric membrane.  $P_{O_2}'$  and  $P_{O_2}''$  denote the high oxygen partial pressure on the feed side and low oxygen partial pressure on the permeated side. <sup>[46]</sup>

### 1.2.2 Structures of dense ceramic oxygen permeable materials

It is well-known that the oxygen permeability of any ceramic dense oxygen permeable membrane is related to the materials properties of the membrane. Successively, the properties of the materials highly depend on not only the chemical composition but also the materials structure. There are many structures were found until now. The major structures can be classified into (i) fluorite-type (general formula  $AO_2$ , e.g.  $CeO_2$ ,  $ZrO_2$ ), <sup>[47]</sup> (ii)  $K_2NiF_4$ -type (general formula  $K_2NiF_4$ , e.g.  $La_2NiO_4$ ), <sup>[48]</sup> (iii) brownmillerite-type (general formula  $A_2B_2O_5$ , e.g.  $Ca_2AlFeO_5$ ), <sup>[49]</sup> (iv) pyrochlore-type (general formula  $A_2B_2O_7$ , e.g.  $Ca_2Re_2O_7$ ), <sup>[50]</sup> (v) double perovskite-type (general formula  $A_2B_2O_6$ , e.g.  $Sr_2FeMoO_6$ ), <sup>[51]</sup> (vi) Ruddlesden-Popper series (general formula  $A_{n+1}B_nO_{3n+1}$ , e.g.  $K_2La_2Ti_3O_{10}$ ), <sup>[52]</sup> (vii) single cubic perovskite-type structure. <sup>[53]</sup> Among these MIEC oxygen permeable membrane materials, cubic perovskite-type membranes are studied extensively, since this kind of mixed-conducting dense membranes that show high oxygen permeation rates at high temperatures. The general formula of ideal perovskite oxide is  $ABO_3$ , where A is occupied the large cation (mostly alkaline, alkaline-earth or rare-earth cation) and B is

smaller cation (mostly transition metals).<sup>[54]</sup> In the typical ideal cubic perovskite structure as shown in Figure 1.3, it is clearly to visualize the structure is in terms of the BO<sub>6</sub> octahedra, which share corners infinitely in all 3 dimensions. The ideal cubic perovskite structure has the A cation in 12-fold oxygen coordination and the B-cation in 6-fold oxygen coordination, since the A cations occupy every hole which is created by 8 BO<sub>6</sub> octahedra. In the example shown in Figure 1.3, the Sr atoms are located at the 12 coordinate A site and the Ti atoms occupy the 6 coordinate B site. The B-O distance is equal to  $a/2$  ( $a$  denotes the cubic unit cell parameter) while the A-O distance is  $a/\sqrt{2}$ . The perovskite structure has various representatives compositional combinations such as A<sup>1+</sup>B<sup>5+</sup>O<sub>3</sub>, A<sup>2+</sup>B<sup>4+</sup>O<sub>3</sub>, or A<sup>3+</sup>B<sup>3+</sup>O<sub>3</sub>. Therefore, many cations and their respective atomic radii can be incorporated into the perovskite structure. However, with the wide range of cation combinations available for the perovskite structure, the actual unit cells are orthorhombic instead of cubic. The symmetry of the structures can be described by the tolerance factor ( $t$ ),<sup>[55]</sup> which quantifies the extent to which the perovskite structure varies from the ideal cubic structure by the following equation:

$$t = \frac{r_A + r_O}{\sqrt{2}(r_B + r_O)} \dots\dots\dots (1)$$

where,  $r_A$ ,  $r_B$  and  $r_O$  denoting the radii of the A-site and B-site cations and the oxygen ion. For an ideal cubic structure,  $t$  should equal one. But the perovskite structure is stable if the tolerance factor is in the range of 0.75 - 1.0.<sup>[56]</sup>

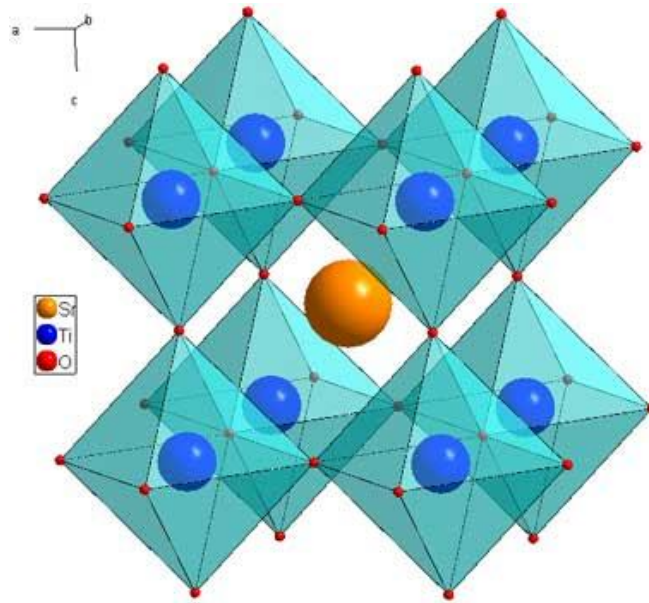


**Figure 1.3** Ideal perovskite structure exhibited by  $\text{SrTiO}_3$ .<sup>[57]</sup>

## 1.3 Perovskite-type oxygen permeable membranes

### 1.3.1 Preparation of perovskite-type oxygen permeable oxides

Numerous methods can be used to prepare perovskite-type oxide powders, such as solid state reaction, chemical vapor deposition, coprecipitation, spray pyrolysis, hydrothermal synthesis, combustion synthesis and EDTA-citric acid sol-gel methods. It is believed that the perovskite-type powders prepared with different methods can result in significantly microstructures, thereby affecting the properties of a performance perovskite-type oxygen permeable membrane. Many researchers have reported the effects of prepared methods on the properties of perovskite-type membrane. For example, Zhu et al.<sup>[58]</sup> found that the  $\text{BaCe}_{0.15}\text{Fe}_{0.85}\text{O}_{3-\delta}$  membrane derived from the EDTA-citric acid sol-gel method showed higher density and pure phase structure but lower oxygen permeability than that derived from the solid state reaction method. Tan et al.<sup>[59]</sup> reported that the oxygen permeation flux through  $\text{Ba}_{0.5}\text{Sr}_{0.5}\text{Ce}_{0.15}\text{Fe}_{0.85}\text{O}_{3-\delta}$  prepared by solid state reaction method was higher than that of prepared

by the EDTA-citric acid sol-gel method.

**Conventional solid state reaction method** Among the aforementioned methods, the conventional solid state reaction method is the most commonly used for preparing the perovskite-type oxide powders. The solid state reaction method generally involves mechanically mixing and grinding the metal precursors. The suitable precursors include, but are not limited to, oxides, hydroxides, acetates, carbonates, chlorides, or nitrates of the desired metal ions. The precursors are usually mixed in appropriate stoichiometric quantities during the grinding process. After grinding, the mixture will be fired at high temperatures which always are higher than two thirds of the melting points for a long time ( $\geq 10$  h), in order to thermally decompose the precursors and form the final desired phase pure perovskite.<sup>[60]</sup> Many perovskite oxide powders have been successfully prepared by the solid state reaction method.<sup>[61-63]</sup> For example, Zhao et al,<sup>[62]</sup> reported that  $\text{BaCo}_{0.7}\text{Fe}_{0.3-x}\text{YO}_{3-\delta}$  (BCFY,  $x = 0.08 - 0.2$ ) was successfully prepared by the conventional solid state reaction process, with  $\text{BaCO}_3$ ,  $\text{Fe}_2\text{O}_3$ ,  $\text{Y}_2\text{O}_3$ , and  $\text{Co}(\text{CH}_3\text{COO})_2 \cdot 4\text{H}_2\text{O}$  as the raw materials. After accurately being weighted, the raw materials were mixed by ball milling for 6 h with ethyl alcohol as the milling medium. The slurries were dried, and the obtained powders were sieved (140 mesh), followed by heating at 1000 °C for 10 h in air. The calcined powders were finely ground to break the soft agglomerations and then ball milled again for 6 h. Dong et al.<sup>[63]</sup> reported that the perovskite-type  $\text{La}_{0.85}\text{Ce}_{0.1}\text{Ga}_{0.3}\text{Fe}_{0.65}\text{Al}_{0.05}\text{O}_{3-\delta}$  (LCGFA) powders were synthesized by the conventional solid state reaction method. The stoichiometric amounts of analytical grade  $\text{La}_2\text{O}_3$ ,  $\text{CeO}_2$ ,  $\text{Ga}_2\text{O}_3$ ,  $\text{Fe}_2\text{O}_3$  and  $\text{Al}_2\text{O}_3$  raw materials were mixed and ball-milled in ethanol for 24 h. These examples demonstrated that the solid state reaction method can be used to synthesize even highly complex composition powders. However, generally speaking, the homogeneity and purity of perovskite powders prepared by the solid state reaction method are poor and show a broad particle size distribution. In addition, in order to get accepted purity, the repeated grinding, calcinations and a long ball-milling period generally would be required, which could be considered energy intensive.

**EDTA-citric acid sol-gel method** The EDTA-citric acid sol-gel method which offers control over both the composition at molecular level and the structure has been used widely. Typically, a metal alkoxide,  $\text{M}(\text{OR})_x$ , undergoes replacement of the OR group by OH via controlled hydrolysis. This results in the formation of very small colloidal particles (the sol), which then

form a gel via condensation reaction. [64] The gel is then dried to produce an oxide. Finally, calcinations at high temperatures are required to produce the oxide. Figure 1.4 shows a flow chart of preparation of common perovskite  $\text{Ba}_{0.5}\text{Sr}_{0.5}\text{Fe}_{0.8}\text{Fe}_{0.2}\text{O}_{3-\delta}$  (BSCF) powder with the EDTA-citric acid sol-gel method. As shown in Figure 1.4, the stoichiometric amounts of  $\text{Ba}(\text{NO}_3)_2$ ,  $\text{Sr}(\text{NO}_3)_2$ ,  $\text{Fe}(\text{NO}_3)_3$ ,  $\text{Co}(\text{NO}_3)_2$  were mixed in a beaker. After stirring the metal nitrate solutions for 20 min, calculated amounts of citric acid and EDTA were added and the pH value was adjusted to around 9 by ammonia. The molar ratio of EDTA : citric acid : total metal ions was 1 : 1.5 : 1. Then, the solutions were stirred when heated to 150 °C, until the water was evaporated and a gel was formed. The gels were heated treatment in air at 600 °C in a furnace to remove the organic compounds by combustion, and the primary powders were obtained. These powders were calcined at 950 °C for 10 h in air.

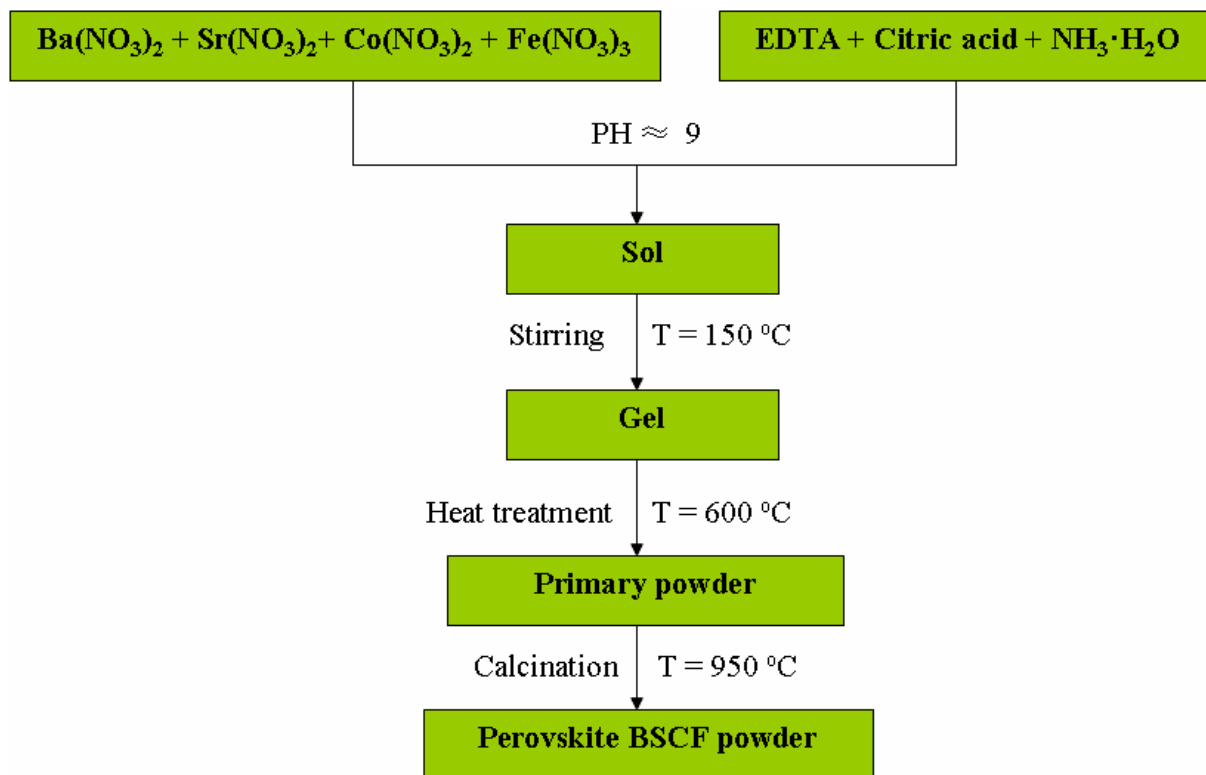


**Figure 1.4** Flow chart of preparation of BSCF powder with the EDTA-citric acid sol-gel method. [65]

### 1.3.2 Issues of perovskite-type oxygen permeable membranes

Over the last decades, the perovskite-type materials have received a lot of attention both in industrial and academia due to their multiple functionality and wide range of applications, including catalysis, superconductors, gas sensors, and as cathodes in solid oxide fuel cells (SOFCs), among others. In addition to the above applications, single phase perovskite-type oxygen permeable membranes with mixed electron-oxide ion conductivity can be separate oxygen from air with infinite permeation selectivity. In the 1980s, Teraoka et al. [66] developed the earliest version of a mixed conducting oxygen-permeable membrane  $\text{SrCo}_{1-x}\text{Fe}_x\text{O}_{3-\delta}$  (SCF), which showed very high oxygen permeation flux ( $3.1 \text{ ml/min}\cdot\text{cm}^2$  with 1 mm thickness at  $850 \text{ }^\circ\text{C}$ ). Unfortunately, it was found that, this material has very limited chemical and structural stability in reduced environments. [67] It was believed that the phase/chemical stability and oxygen permeability can be improved by proper substitution of metals in SCF. Therefore, following Teraoka et al.' pioneering work, a class of Co-based perovskite-type oxides with partial substitution of A or B sites have been intensive researched and developed. [68-70] For example, Shao et al. [65] developed a composition  $\text{Ba}_{0.5}\text{Sr}_{0.5}\text{Co}_{0.8}\text{Fe}_{0.2}\text{O}_{3-\delta}$  (BSCF) perovskite-type material, which showed high oxygen permeation flux over a wide temperatures and improved stability comparing with SCF. After that, BSCF have been widely studied as cathodes in solid state fuel cells, as oxygen permeation membrane and membrane reactor. However, the wide applications of BSCF were still hampered by the following reasons: (i) BSCF material was not stable at temperatures below  $750 \text{ }^\circ\text{C}$ . [71-73] (ii) In the presence of  $\text{CO}_2$ , the oxygen permeation flux through BSCF membrane reduced sharp, even the structure was destroyed since the formation of carbonates. [74,75] The phase stability and permeation behaviour of a dead-end  $\text{Ba}_{0.5}\text{Co}_{0.5}\text{Fe}_{0.2}\text{Co}_{0.8}\text{O}_{3-\delta}$  tube membrane in high purity oxygen production will be discussed in detailed in chapter 2. Generally speaking, the single-phase mixed conducting materials are difficult to meet all the requirements (such as high permeability, stability, mechanical strength, etc.) for application as oxygen separation membranes. Therefore, the dual-phase membrane materials were suggested as the candidates due to their composition can be tailoring in practical conditions. The developments and properties of new  $\text{CO}_2$ -stable dual phase membranes will be described in detail in Chapter 3.



## 1.4 Dual phase oxygen permeable membranes

### 1.4.1 Preparation of dual phase oxygen permeable membranes

**Preparation methods for oxides and membranes** To achieve the target properties of the dual phase powders, the flowing properties of the dual phase powders should be considered: particle size, particle distribution, particle morphology, degree of agglomeration, phase purity and chemical purity. It is important to select a powder with high reactivity for fabrication of dense oxygen permeable membrane materials. Therefore, it is considered that the powder should have a small particle size and a low degree of agglomeration.<sup>[76]</sup> The aforementioned properties of the dual phase powders are directly related to the synthesis methods. Dual phase oxygen permeable powders can be prepared by huge amount of methods, such as in a simple mixing of the two oxide powders, packing method, loading method, one-pot EDTA-citric acid process and the one-pot single-step glycine-nitrate combustion process (GNP).

The dual phase powders are traditionally prepared by the simple mixing of the two oxide powders method. This method generally involves mixing the oxygen ion conducting phase (OIC-phase) powder and the electron conducting phase (EC-phase) powder. In this method, OIC-phase and EC-phase oxides consisting of the dual phase are prepared separately in the first step. The aforementioned methods in section 1.3.1 generally can be used to prepare the OIC-phase and EC-phase oxides. In the next step, the as-obtained OIC-phase and EC-phase powders are mixed in the calculated weight or volume ratios though grinding in a mortar by hand or by mechanical mixing. This traditional synthesized method often not only requires several steps to get a uniform mixture but also gives coarse agglomerated powders with low sintering reactivity.<sup>[60]</sup> To replace this conventional preparation, one-pot single-step methods have been developed such as the one-pot single-step EDTA-citric acid process<sup>[33]</sup> and the one-pot single-step glycine-nitrate combustion process (GNP).<sup>[77]</sup> For the one-pot single-step method, all the required metallic ions solutions are mixed in one beaker, so that every element has the same chemical potential in each phase after synthesis. Therefore, diffusion of metallic elements between the two phases can be avoided during permeation operations. Especially, the GNP is reported to rapidly produce complex oxide ceramic powders of uniform composition on an

atomic scale and fine enough to for sinter to a high density. In this thesis, four types dual phase powders with the following compositions: 40 wt.%  $\text{NiFe}_2\text{O}_{4-\delta}$  - 60 wt.%  $\text{Ce}_{0.9}\text{Gd}_{0.1}\text{O}_{2-\delta}$  (40NFO-60CGO), 40 wt.%  $\text{Fe}_2\text{O}_3$  - 60 wt.%  $\text{Ce}_{0.9}\text{Gd}_{0.1}\text{O}_{2-\delta}$  (40FO-60CGO), 40 wt.%  $\text{Mn}_{1.5}\text{Co}_{1.5}\text{O}_{4-\delta}$  - 60 wt.%  $\text{Ce}_{0.9}\text{Pr}_{0.1}\text{O}_{2-\delta}$  (40MCO-60CPO) and 40 wt.%  $\text{Pr}_{0.6}\text{Sr}_{0.4}\text{FeO}_{3-\delta}$  - 60 wt.%  $\text{Ce}_{0.9}\text{Pr}_{0.1}\text{O}_{2-\delta}$  (40PSFO-60CPO), were involved.

The first 40NFO-60CGO composition is preparing in three methods (see Figure 1.3): (i) Powder mixing in a mortar by hand (40NFO-60CGO 01 powder): The powders of  $\text{Ce}_{0.9}\text{Gd}_{0.1}\text{O}_{2-\delta}$  (CGO),  $\text{NiFe}_2\text{O}_{4-\delta}$  (NFO) and 40 wt. %  $\text{NiFe}_2\text{O}_{4-\delta}$  - 60 wt. %  $\text{Ce}_{0.9}\text{Gd}_{0.1}\text{O}_{2-\delta}$  were synthesized by a combined citric acid and EDTA method. After stirring the metal nitrate solutions for 20 min, equal molar amounts of citrate and EDTA were added and the pH value was adjusted to  $\sim 9$  by ammonia. The molar ratio of EDTA : citric acid : total metal ions was 1 : 1.5 : 1. Then the solutions were stirred while heated to  $150\text{ }^\circ\text{C}$ , until the water was evaporated and a gel was formed. The gels were calcined in air at  $600\text{ }^\circ\text{C}$  in a furnace to remove the organic compounds by combustion, and the primary powders were obtained. The as-obtained CGO and NFO powders were mixed with a weight ratio of 60 : 40. Then the mixed powders were grind in an agate mortar for 1.5 h. (ii) Powder mixing by ball-milling (40NFO-60CGO 02 powder): The powders of CGO, NFO and 40NFO-60CGO were also synthesized by a combined citric acid and EDTA method. But the as-prepared CGO and NFO powders were mixed in a weight ratio 60 : 40 by ball-milling for 4 h. (iii) Direct one-pot single-step EDTA-citric acid synthesis (40NFO-60CGO 03 powder): The powder mixture was obtained by *in-situ* one-pot single-step EDTA-citric acid process. The powders of all three techniques were pressed to disk membranes under a pressure of  $\sim 10\text{ MPa}$  in a stainless steel module with a diameter of 18 mm. Then they were sintered at  $1350\text{ }^\circ\text{C}$  in air for 10 h with heating and cooling rates of  $2\text{ }^\circ\text{C}/\text{min}$ . X-ray diffraction (XRD), scanning electron microscopy (SEM), Backscattered scanning electron microscopy (BSEM), Scanning transmission electron microscopy (STEM) in high-angle annular dark-field (HAADF) mode, electron energy-loss spectroscopy (EELS), selected area electron diffraction (SAED), high-resolution TEM (HRTEM), and energy-dispersive X-ray spectroscopy (EDXS) were used to characterize the samples. The phase stabilities and oxygen behaviors of 40NFO-60CGO membranes obtained in three ways were investigated (chapter 3.2 and 3.3). It was found that the direct one-pot single-step EDTA-citric acid synthesis of 40NFO-60CGO showed the smallest grains in a

homogeneous distribution and the highest oxygen permeability, compared with powder homogenization in the mortar or the ball-milling, the direct one-pot single-step EDTA-citric acid synthesis. Therefore, the direct one-pot single-step EDTA-citric acid synthesis was used to fabricate the second composition of 40FO-60CGO mixture powder. The as-prepared powders were pressed to disk membranes under a pressure of  $\sim 10$  MPa in a stainless steel module with a diameter of 18 mm. Then they were sintered at  $1300$  °C in air for 5 h with heating and cooling rates of  $2$  °C/min.

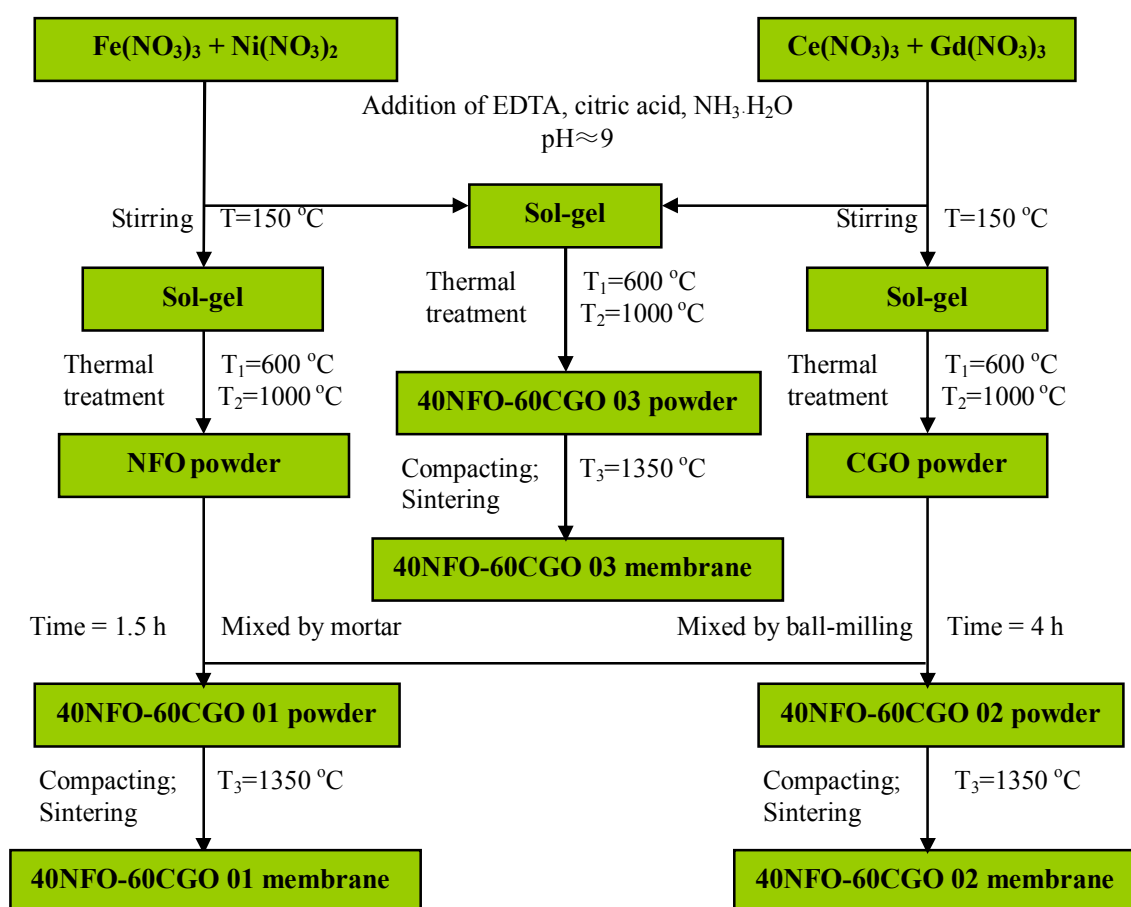


**Figure 1.5** Flow chart for the preparation of 40NFO-60CGO dual oxides in three ways: (i) mixing of two oxides by hand, 40NFO-60CGO 01 powder (ii) mixing of two oxides by ball-milling, 40NFO-60CGO 02 powder (iii) one-pot single-step EDTA-citric acid process, 40NFO-60CGO 03 powder. [78,79]

The 40MCO-60CPO and 40PSFO-60CPO dual phase membrane materials were prepared via the one-pot single-step glycine-nitrate combustion process (GNP). Figure 1.6 shows the flow chart for the preparation of 40PSFO-60CPO dual phase membranes via the one-pot single-step GNP method. As shown in Figure 1.6, a precursor was prepared by combining glycine and metal nitrates  $\text{Sr}(\text{NO}_3)_2$ ,  $\text{Fe}(\text{NO}_3)_3$ ,  $\text{Ce}(\text{NO}_3)_3$  and  $\text{Pr}(\text{NO}_3)_3$  in their appropriate stoichiometric ratios in an aqueous solution. The molar ratio of glycine: total metal ions was 2 : 1. The precursor was stirred and heated at 150 °C in air to evaporate excess water until a viscous liquid was yielded. Further, heating the viscous liquid to 300 °C caused the precursor liquid to auto-ignite. Combustion was rapid and self-sustaining, and a precursor ash was obtained. This precursor ash was calcined at 950 °C for 10 h in air to obtain the powder. The as-prepared powders were pressed to disk membranes under a pressure of 5 MPa in a stainless steel module with a diameter of 18 mm to get the green membranes. These green disks were pressure-less sintered at 1350 °C for 5 h in air.

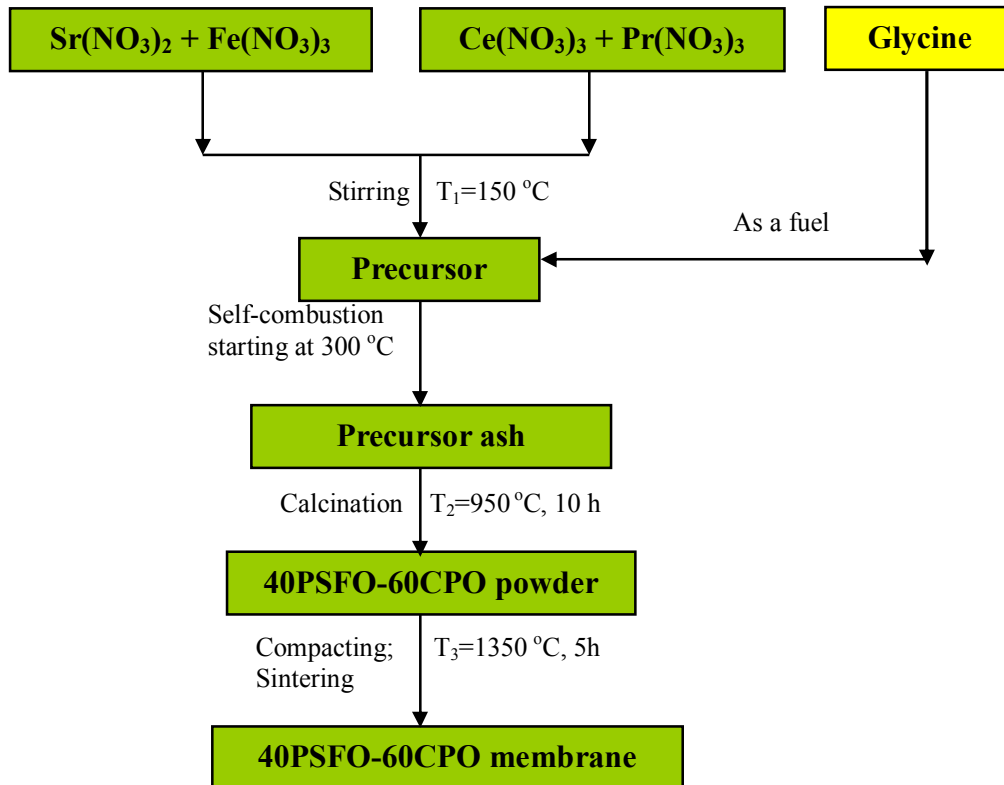


**Figure 1.6** Flow chart for the preparation of 40PSFO-60CPO dual phase membranes. <sup>[80]</sup>

**Sintering temperatures for dual phase oxygen permeable membranes** To obtain a dense and gas tight dual phase membrane, the as-prepared powder will be compacted and shaped by pressing in a rigid die or flexible mold in the desired shape (e.g. disk or tube) and following by sintering into the dense membrane. Sintering refers to this phenomenon: when a compacted powder is heated at an elevated temperature which is below its melting point, powder particles fuse together, voids between the particles reduce, and finally a dense solid body is obtained. [81] In this thesis, the as-prepared dual phase powders were pressed to green disk membranes under a pressure of 5 ~ 10 MPa in a stainless steel module with a diameter of 18 mm, following by sintering at high temperatures (in the range of 1300 - 1450 °C). The sintering temperature affects the microstructure and texture of dual phase membranes thereby influences the oxygen permeability through the dual phase membranes. It has been reported that the grain growth with increasing sintering temperatures will decrease the electrical conductivity and oxygen permeability for the single phase perovskite oxygen permeable membranes, such as  $\text{Ba}_{0.5}\text{Sr}_{0.5}\text{Co}_{0.8}\text{Fe}_{0.2}\text{O}_{3-\delta}$  and  $\text{La}_{0.6}\text{Sr}_{0.4}\text{Co}_{0.2}\text{Fe}_{0.8}\text{O}_{3-\delta}$ . [82,83] They demonstrated that in the case of single-phase membranes the grain growth has a positive effect on the oxygen permeability, since the grain boundaries in single-phase perovskite membranes act as barriers for the oxygen transport. However, the influence of sintering temperature on the microstructure and oxygen permeability of dual phase membrane was more complex because of the components of dual phase membranes are more complex than those of the single phase perovskite membranes. Zhu et al. [84] have investigated the effects of sintering temperature in the range of 1400 - 1525 °C on the 75 wt.%  $\text{Ce}_{0.85}\text{Sm}_{0.15}\text{O}_{2-\delta}$  - 25 wt.%  $\text{Sm}_{0.6}\text{Sr}_{0.4}\text{FeO}_{3-\delta}$  (75CSO-25SSFO) dual phase membranes. They found that when the sintered temperature was below 1425 °C, the oxygen permeation flux through 75CSO-25SSFO dual phase membrane increased with the increasing temperature. However, if the temperature was  $\geq 1425$  °C, the oxygen permeation flux through 75CSO-25SSFO dual phase membrane decreased with the increasing temperature. In this thesis (section 3.4 in chapter 3), it was also found that the grain growth with increasing temperatures from 1300 to 1350 °C has a negative effect on the oxygen permeability in the case of dual phase membranes of 40FO-60CGO dual phase. With increasing sintering temperatures of dual phase membranes, the grain growth can interrupt the continuity of the FO percolation network, which will block the electronic transport through the dual phase 40FO-60CGO membrane. It can be concluded that a

high sintering temperature has a negative influence on the oxygen permeation flux for our dual phase membranes. Therefore, chose of a suitable sintering temperature is very important to get a dual phase membrane with good oxygen permeability.

**Ratio between the two phases in a dual phase oxygen permeable membrane** For the membrane applications, a desired dual phase materials should consist of two continuously distributed phases: one being a good oxygen ionic conducting phase and the other being an electronic conducting phase. In other words, the precondition for the dual phase membrane is that both constituent phases in the composite membranes should form a continuous path for both ionic and electronic conduction, having their concentrations above the critical volume fraction (percolation threshold). This critical volume fraction determines the minimum volume fraction in which conduction is possible and its function of relative dimensions and shape of the particles of both continuous phases. Usually, 30 vol.% of the electronic conducting phase is required to exceed the percolation threshold for a dual phase system where the grain sizes are comparable.<sup>[85]</sup> In this thesis, the influence of the FO : CGO ratio on oxygen permeability of FO-CGO dual phase membranes was investigated. The  $\chi$  wt. % FO - (100 -  $\chi$  wt. %) CGO ( $\chi = 25, 40$  and  $50$ , and denoted 25FO-75CGO, 40FO-60CGO, and 50FO-50CGO, respectively) dual phase powders were synthesized via a one-pot single-step EDTA-citric acid method. It was found that the optimum oxygen permeation flux was the composition 40FO-60CGO dual phase membrane since the electronic conductivity of 40FO ( $0.159 \text{ S}\cdot\text{cm}^{-1}$ ) was equal to the oxygen ionic conductivity of 60CGO ( $0.155 \text{ S}\cdot\text{cm}^{-1}$ ). And in the thesis, in order to obtain a dual phase membrane with a continuous path for both ionic and electronic conduction, 40 wt.% electronic conducting phases were chosen to prepare the 40NFO-60CGO, 40MCO-60CPO and 40PSFO-60CPO dual phase membranes.

**Deposition of porous layer LSC onto dual phase membrane** In order to improve the oxygen surface exchange rate, the perovskite-type  $\text{La}_{0.6}\text{Sr}_{0.4}\text{CoO}_{3-\delta}$  (LSC) oxide, which shows a good oxygen reducing activity when it acts as cathode materials for SOFC, was used to coat the air sides of 40NFO-60CGO and 40FO-60CGO dual phase membranes. First, the membranes were polished to 0.5 mm thickness by using 1200 grit-sand paper (average particle diameter  $15.3 \mu\text{m}$ )

and then the membranes were washed with ethanol. Second, a LSC porous layer was deposited onto the air side the membrane with a paste made of 40 wt.% LSC powder and 60 wt.% terpineol. Third, the membrane with LSC coating was calcined at 950 °C for 2 h in air with a heating and cooling rate of 2 °C/min.

### 1.4.2 Oxygen transport through dual phase oxygen permeable membranes

**Transport mechanisms** Dual phase oxygen permeable membranes can separate oxygen from air at elevated temperature with infinite permeation selectivity. If there is a oxygen chemical potential gradient ( $\nabla \mu_{O_2}$ ) cross the dense dual phase oxygen permeable membrane, the oxygen ions directly can transport from the high oxygen partial pressure ( $p_{O_2}'$ ) side to the low oxygen partial pressure ( $p_{O_2}''$ ) side accompanied by the counter transfer of the electrons. It is generally accepted that the oxygen permeation through the dense dual phase membrane, as shown in Figure 1.7a, mainly involves three steps as follows: (1) oxygen insertion on the air side, (2) the simultaneous bulk diffusion of oxygen ion and electron through membrane bulk phase, and (3) oxygen release on the permeate side. The first and third steps are usually called surface exchange limitation steps and the second step is called bulk diffusion limitation step. The slowest step is considered to control the overall rate of oxygen permeation. [86]

The bulk diffusion is governed by oxygen ionic or electronic conduction (or both). For the dual phase membrane, the oxygen ion and electron transport usually take place separately. The oxygen ionic conduction in a dual phase membrane mainly depends on ion conductor such as Y or Sc-stabilized zirconia or cerium-based electrolytes, which is very stable under reaction environments and lower thermal expansion rates. The electronic conducting oxides in dual phase membranes come from first noble metals to pure ceramic electronic conducting oxides and recently to perovskite MIEC materials. Figure 1.7b shows the schematic illustration of oxygen transport in ionic/pure electronic conductor dual phase membrane oxygen and oxygen ionic/mixed conductor dual phase membrane. As shown in Figure 1.7b, if a dual phase membrane consist of a pure oxygen ion conducting phase and a pure electron conducting phase or ceramic oxides with poor ionic conductivity (such as noble metals: Ag, Pd, Au, spinel-type oxides:

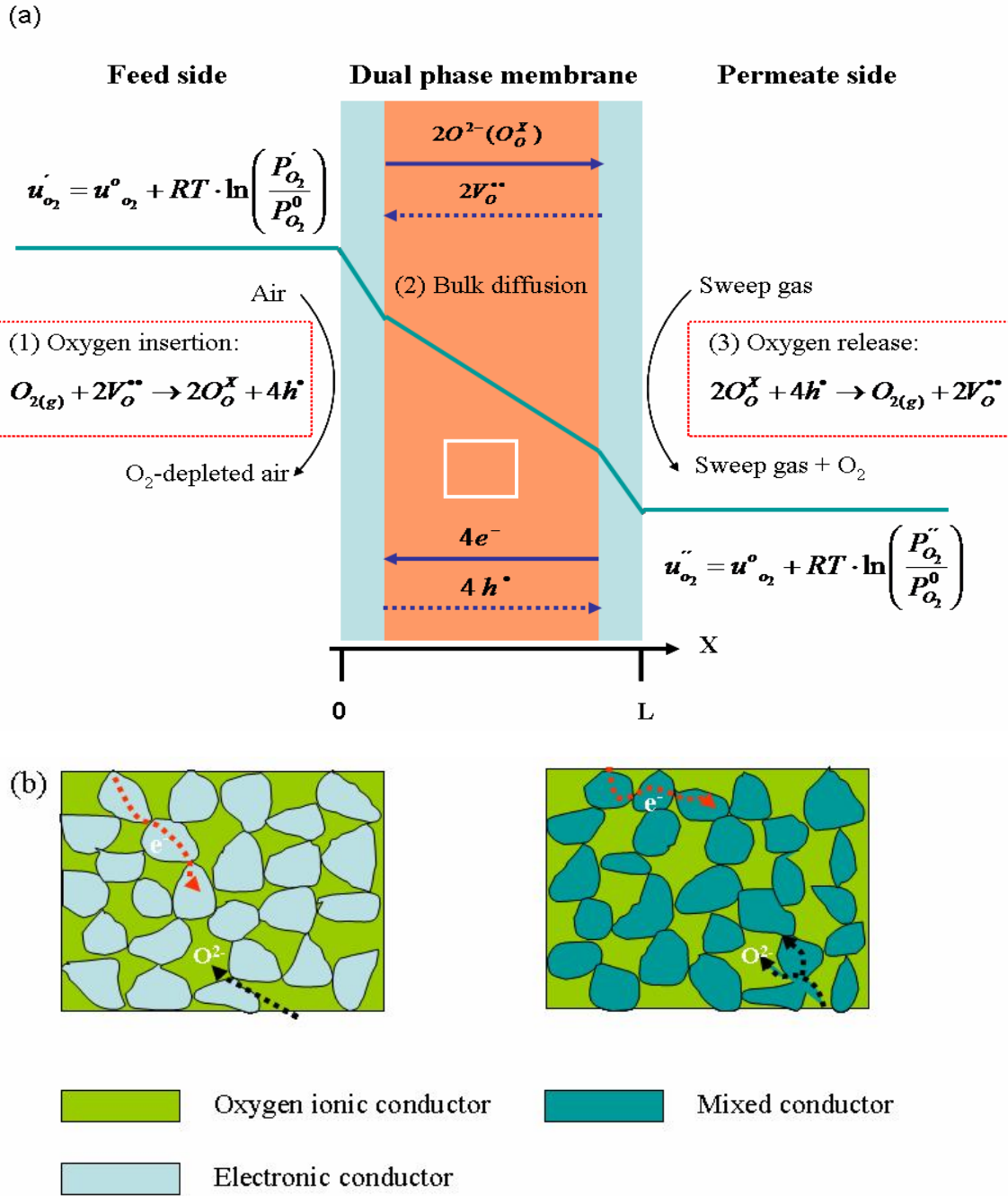


**Figure 1.7** (a) Schematic diagram of oxygen transport through a dual phase membrane. (b) close-up of marked area in (a) denotes oxygen transport in an ionic/pure electronic conductor dual phase membrane (left) and oxygen transport in oxygen ionic/mixed conductor dual phase membrane (right). <sup>[87]</sup>



NiFe<sub>2</sub>O<sub>4-δ</sub>, CoFe<sub>2</sub>O<sub>4-δ</sub>, MnFe<sub>2</sub>O<sub>4-δ</sub>, and perovskite-type oxides: La<sub>x</sub>Sr<sub>1-x</sub>Mn(Cr)O<sub>3-δ</sub>, oxygen ions transport through the oxygen ion conducting phase (OIC-phase), while electrons are carried by the electron conducting phase (EC-phase). In other words, in such a dual phase membrane, the oxygen ions transport will be blocked in the bulk of membrane between ionic conductor grains. If a dual phase membrane consist of a pure oxygen ion conducting phase and a mixed ion-electron conducting phase (such as perovskite-type oxides: Gd<sub>0.2</sub>Sr<sub>0.8</sub>FeO<sub>3-δ</sub>, SmMn<sub>0.5</sub>Co<sub>0.5</sub>O<sub>3-δ</sub>) through the oxygen ion conducting phase transport the oxygen ions while the electron conducting phase (EC-phase) transport the electrons meanwhile assist the transport of the oxygen ions.

It is accepted the different dual phase membranes by varying thickness tend to have different determining steps. [88] The mainly determining steps include bulk diffusion limited step and surface exchange limited step.

**Bulk diffusion limitation** For a relatively thick membrane, the bulk diffusion process is commonly the determining step. In this case, the Wagner’s theory can be used to describe the oxygen permeation flux through the membrane, [89,90] which is restricted to the simultaneous transport of oxygen ions and electrons that are ideally diluted and do not interact. The oxygen permeation flux  $J_{O_2}$  can be described by Wagner’s equation as follows:

$$J_{O_2} = \frac{RT}{(4F)^2 L} \int_{\ln P_2}^{\ln P_1} \frac{\sigma_i \cdot \sigma_e}{\sigma_i + \sigma_e} d \ln P_{O_2} \dots\dots\dots (2)$$

where  $\sigma_e$  and  $\sigma_i$  are the electronic and ionic conductivities, respectively,  $R$ ,  $F$ ,  $T$  and  $L$  denote the gas constant, Faraday constant, temperature and thickness of the membrane, respectively.  $P_1$  and  $P_2$  are the oxygen partial pressure on the permeate side and feed side, respectively. In the case of mixed conductor where electronic conductivity dominates, that is  $\sigma_e \gg \sigma_i$ , the integration of Eq.(2) involves only  $\sigma_i$  as a function of the oxygen partial pressure and gives the following Wagner’s equation

$$J_{O_2} = \frac{RT\sigma_i}{(4F)^2 L} \ln \frac{P_1}{P_2} \dots\dots\dots (3)$$

According to the above equation, the oxygen permeation rate can be increased by increasing the operating temperature, the pressure gradient across the membrane, or by decreasing the thickness of the membrane.

**Surface exchange limitation** If the oxygen transport resistance in the bulk phase becomes very small due to an increase in the ionic or electronic conductivity or the thickness of membranes is below a characteristic thickness ( $L_c$ ), the surface exchange reactions on both sides would become the limiting steps in the oxygen permeation. The surface exchange reaction is a complex process, which consists of the adsorption, dissociation, charge transfer, surface diffusion and oxygen ions incorporation into the lattice on the interface zone of both sides. [28]

In this case, the Wagner equation is not applicable to describe the overall permeation process through the membranes. Other mechanisms and relations have been proposed to explain the oxygen permeation flux within this regime. It has been reported by Kim et al. [91] if the oxygen permeation process is limited by the surface exchange reaction.  $J_{O_2}$  shows a linear relationship with  $(P_2 - P_o)^{0.5} - (P_1 - P_o)^{0.5}$  according to the following equation:

$$J_{O_2} = \frac{1}{2} \frac{C_{i1}C_{i2}}{C_{i1} + C_{i2}} k_{io} [(P_2 / P_o)^n - (P_1 / P_o)^n] \dots\dots\dots (4)$$

where  $J_{O_2}$  is the oxygen permeation flux through a OTM,  $C_i$  is the oxygen ion concentration,  $D_a$  is the diffusion coefficient of the oxygen ion-electron hole pairs,  $L$  is the thickness of the membrane,  $C_{i1}, C_{i2}$  are the oxygen concentrations of the interfaces of the membrane,  $n$  is the order of the chemical reaction at the gas-MIEC interface. For the oxygen permeation flow through a planar membrane, for this special case  $n = 0.5$ ,  $k_{io}$  is the surface exchange coefficient, and  $P_2$ ,  $P_1$  and  $P_o$  stand for high oxygen partial pressure on the feed side, low oxygen partial pressures on the sweep side and the normalized pressures of 1 bar, respectively.

Many studies indicated that the surface exchange rate can be increased by coating the membrane with porous layer which show a high surface exchange rate such as cobalt-containing perovskites or noble metal Pt. [92-94]

**Dual phase membrane permeator and reactor** Oxygen permeation was studied in a home-made high-temperature oxygen permeation device, as shown in Figure 1.8. The disk membranes were sealed as described onto a quartz tube at 950 °C for 5 h with a gold paste (Heraeus, Germany), the side wall of the membrane disk was also covered with the good paste to avoid a radial contribution to the oxygen permeation flux. The effective areas of the membranes for oxygen permeation were 0.785 cm<sup>2</sup>. The inlet gas flow rates were controlled by gas mass flow controllers (Bronkhorst, Germany), and the flow rates were regularly calibrated by using a bubble

flow meter. The mixture O<sub>2</sub> and N<sub>2</sub> (or synthetic air) was used as feed gas. A mixture of He (or CO<sub>2</sub>, CH<sub>4</sub>) and Ne was used as sweep gas to remove the permeated oxygen. Ne was added to the He or (or CO<sub>2</sub>, CH<sub>4</sub>) as an internal standard gas for gas chromatography to calculate the total flow rate at the outlet of the sweep side. The effluents were analyzed by an online gas chromatograph (GC, Agilent 7890A and 6890A). The GC was frequently calibrated using standard gases in order to ensure the reliability of the experimental data. The leakage is caused by the imperfect sealing at high temperature, which can be determined by the detecting N<sub>2</sub> by GC. In no case, the leakage stream which is larger than 5 % of the oxygen flux through the membrane. Assuming that leakage of nitrogen and oxygen is in accordance with Knudsen diffusion, the fluxes of leaked N<sub>2</sub> and O<sub>2</sub> are related by

$$J_{N_2}^{Leak} : J_{O_2}^{Leak} = \sqrt{\frac{32}{28}} \times \frac{0.79}{0.21} = 4.02 \quad \dots\dots\dots (5)$$

The oxygen permeation flux was then calculated as follows:

$$J_{O_2} (ml / min \cdot cm^2) = \left( C_{O_2} - \frac{C_{N_2}}{4.02} \right) \times \frac{F}{S} \quad \dots\dots\dots (6)$$

where C<sub>O<sub>2</sub></sub>, C<sub>N<sub>2</sub></sub>, are the oxygen and nitrogen concentrations calculated from GC calibration, *F* is the total flow rate of the outlet on the sweep side, which was measured by the change of Ne concentration before and after permeator. The total flow rate of the effluents was calculated from the change in the Ne concentrations before and after the permeator.

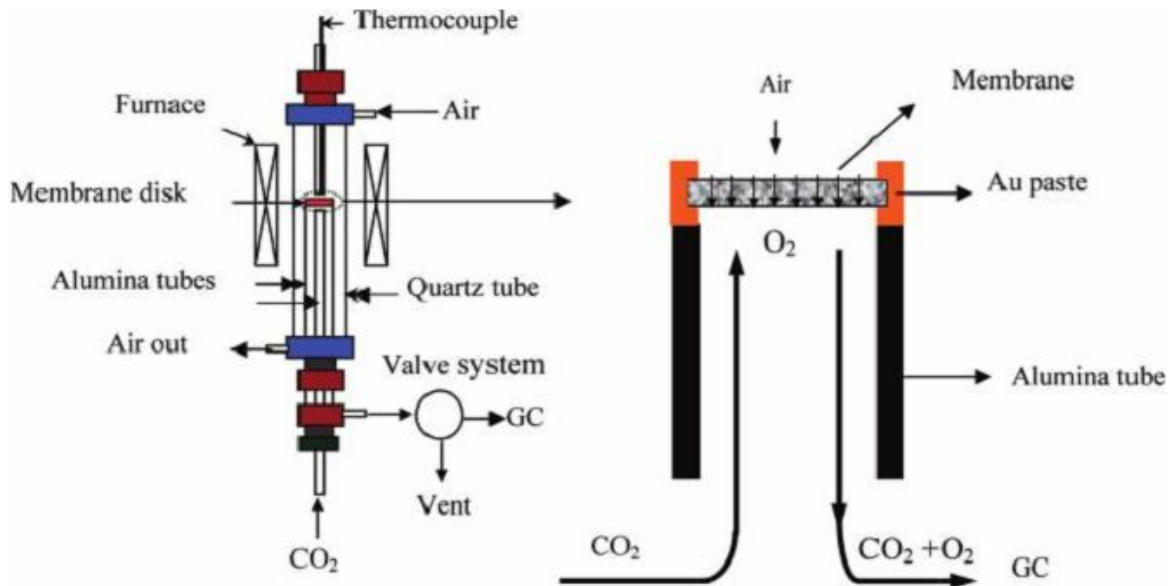


**Figure 1.8** Schematic equipment for oxygen permeation in this work. [95]

Figure 1.9 shows a scheme of the dual phase 40PSFO-60CPO membrane reactor for POM used in this Ph.D. work. The sealing of the membrane was as above mentioned. A Ni-based catalyst (0.3 g, Süd Chemie AG) was loaded on the top of the membrane disc and then the temperature of the reactor was increased to 950 °C with a heating rate of 2 °C/min. The mixture methane of CH<sub>4</sub> and Ne was fed into the permeate side, where CH<sub>4</sub> used as the reactant for the POM to synthesis gas and Ne as an internal standard gas for gas chromatography to calculate the total flow rate at the outlet of the sweep side. All gas lines to the reactor and the gas chromatograph were heated to 180 °C. Gas composition was analyzed by an on-line gas chromatograph (GC, Agilent 6890A) equipped with the Carboxen 1000 column. Concentrations of CH<sub>4</sub>, CO<sub>2</sub>, CO, N<sub>2</sub>, O<sub>2</sub> and H<sub>2</sub> were calculated by calibrating against a standard gas mixture containing all the product species in the known quantities. The quantity of H<sub>2</sub>O was accounted based on hydrogen atom balance. The oxygen permeation flux was calculated based on oxygen atom balance of all the oxygen-containing products. The flow rate at inlet for all the gas was obtained by using the bubble meter. The total flow rate of the effluents at the outlet was determined by using Ne as internal standard. The calculation was based on the facts that the inert Ne didn't take part in the reactions and the flow rate of Ne at the inlet should be equal to that at

exit:

$$F_{total}^{in} C_{Ne}^{in} = F_{total}^{out} C_{Ne}^{out} \dots\dots\dots (8)$$

where  $F_{total}^{in}$  and  $F_{total}^{out}$  are the total flow rate of the stream at inlet and total flow rate of the stream at outlet, respectively.  $C_{Ne}^{in}$  and  $C_{Ne}^{out}$  are the concentration of Ne at inlet and outlet, respectively.

The conversion of  $CH_4$  ( $X_{CH_4}$ ), selectivity of CO ( $S_{CO}$ ) and  $H_2$  ( $S_{H_2}$ ), and the oxygen permeation flux ( $J_{O_2}$ ), were defined as follows:

$$X_{CH_4} = \frac{F_{CH_4}^{out}}{F_{CH_4}^{in} - F_{CH_4}^{out}} \times 100\% \dots\dots\dots (7)$$

$$S_{CO} = \frac{F_{CO}}{F_{CO} + F_{CO_2}} \times 100\% \dots\dots\dots (8)$$

$$S_{H_2} = \frac{F_{H_2}}{F_{H_2} + F_{H_2O}} \times 100\% \dots\dots\dots (9)$$

$$J_{O_2} = \frac{0.5 \times (F_{CO} + F_{H_2O}) + F_{CO_2}}{S} \dots\dots\dots (10)$$

where  $F_i$  is the flow rate of species  $i$  in ml/min,  $S$  the membrane area in  $cm^2$ . [96]

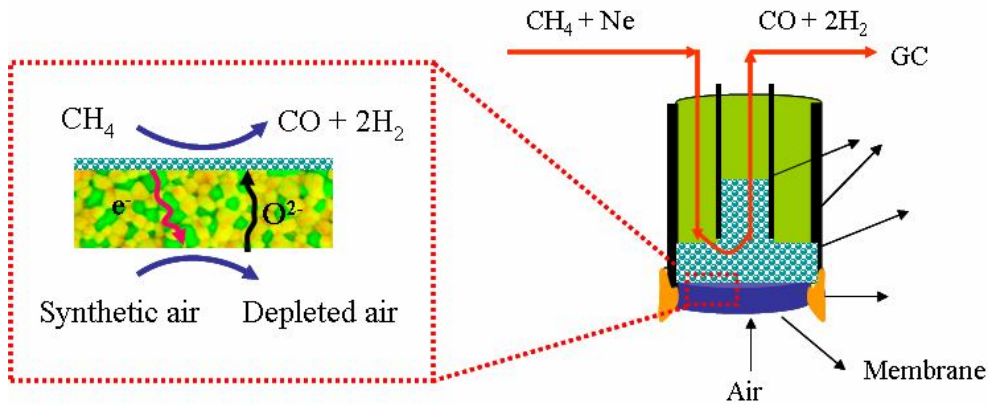


**Figure 1.9** Scheme of the dual phase 40PSFO-60CPO membrane reactor used in this work.

### 1.4.3 Applications of dual phase oxygen permeable membranes

Dual phase oxygen permeable membrane consisting of an oxygen ion conducting phase and electron conducting metal or ceramic phase have many applications, including as membrane separator for oxygen production, membrane reactors for partial oxidation of methane (POM) to synthesis gas and membrane reactors for H<sub>2</sub> generation and separation from H<sub>2</sub>O splitting.

**Membrane separator for oxygen production** Oxygen is ranking among the top five in the production of commodity chemicals in the world. Commercial oxygen is currently produced by cryogenic distillation and pressure swing adsorption but both are energy consuming technologies. Therefore, to get cheap, high-purity oxygen is a very important demand in industry. The oxygen transport through the oxygen permeable membrane is in the form of oxygen ion instead of oxygen molecules, so pure oxygen can be obtained in principle. For a dual phase membrane which consists of a oxygen ionic conductor and a electronic conductor, when both phases form an infinitely continuous or continuous network, the oxygen ions can transport via the oxygen conductive phase while the electron charge compensations diffuse through electronic conductive phase. Dual phase membranes used as the oxygen separators with the inert gas such as He or Ar as sweep gas have reported by most researchers in the published work. Table 1 presents the data of steady-state oxygen permeation flux through various dual phase membranes in disk geometries. The first dual phase membranes were made of noble metal (such as Ag, Pd) powders as electronic conductor and ceramic particles as ionic conductors (such as Bi<sub>1.5</sub>Y<sub>0.3</sub>Sm<sub>0.2</sub>O<sub>3</sub>, (ZrO<sub>2</sub>)<sub>0.94</sub>(Y<sub>2</sub>O<sub>3</sub>)<sub>0.06</sub>).<sup>[24,27,28]</sup> In order to achieve a continuous electron transport network in the bulk, the volume fraction of noble metal phase usually exceeds 30 %, which leads to high costs. It has been reported that 60 vol.% Bi<sub>1.5</sub>Y<sub>0.3</sub>Sm<sub>0.2</sub>O<sub>3-δ</sub> - 40 vol.% Ag dual phase membrane forming the continuous network showed 5 times higher oxygen permeation flux than that of 70 vol.% Bi<sub>1.5</sub>Y<sub>0.3</sub>Sm<sub>0.2</sub>O<sub>3-δ</sub> - 30 vol. % Ag without forming the continuous network.<sup>[97]</sup> The dual phase membrane consisting of two ceramic oxides was first reported by Kharton et al.,<sup>[98]</sup> who developed a dual phase membranes with the composition of 50 wt.% Ce<sub>0.8</sub>Gd<sub>0.2</sub>O<sub>2-δ</sub> - 50 wt.% La<sub>0.8</sub>Sr<sub>0.2</sub>MnO<sub>3-δ</sub>. After then, several groups reported that the dual phase membranes with using ceramic oxides instead of the noble metals as electronic conductors (such as Ce<sub>0.8</sub>Gd<sub>0.2</sub>O<sub>2-δ</sub> - Gd<sub>0.7</sub>Ca<sub>0.3</sub>CoO<sub>3-δ</sub>, Ce<sub>0.8</sub>Sm<sub>0.2</sub>O<sub>2-δ</sub> - La<sub>0.8</sub>Sr<sub>0.2</sub>CrO<sub>3-δ</sub>, Zr<sub>0.6</sub>Y<sub>0.4</sub>O<sub>2-δ</sub> - La<sub>0.8</sub>Sr<sub>0.2</sub>MnO<sub>3-δ</sub>), which cost

lower and but still show low oxygen permeability. Recently, Yang and Zhao group developed a series of new dual phase membranes, comprising ceramic oxide ionic conductors and a mixed ion-electron conductors (such as  $\text{Ce}_{0.8}\text{Gd}_{0.2}\text{O}_{2-\delta}$  -  $\text{Gd}_{0.8}\text{Sr}_{0.2}\text{FeO}_{3-\delta}$ ,  $\text{La}_{0.15}\text{Sr}_{0.85}\text{Ga}_{0.3}\text{Fe}_{0.7}\text{O}_{3-\delta}$  -  $\text{Ba}_{0.5}\text{Sr}_{0.5}\text{Co}_{0.8}\text{Fe}_{0.2}\text{O}_{3-\delta}$ ,  $\text{Ce}_{0.8}\text{Sm}_{0.2}\text{O}_{2-\delta}$  -  $\text{LaBaCo}_2\text{O}_{5+\delta}$ ), which show higher oxygen permeability than the traditional dual phase membranes. [44,101,102]

**Table 1** Steady-state oxygen permeation flux ( $J_{\text{O}_2}$ ) through different dual phase membranes in disk geometries.

Membrane	Temperature (°C)	Thickness (mm)	$\ln(P_2/P_1)$	$J_{\text{O}_2}$ (ml/min·cm <sup>2</sup> )	Refs.
60vol.%(ZrO <sub>2</sub> ) <sub>0.94</sub> (Y <sub>2</sub> O <sub>3</sub> ) <sub>0.06</sub> - 40vol.%(In <sub>0.9</sub> Pr <sub>0.1</sub> ) <sub>0.4</sub>	1100	0.8	-	1.1	24
60vol.%(Bi <sub>2</sub> O <sub>3</sub> ) <sub>0.75</sub> (Er <sub>2</sub> O <sub>3</sub> ) <sub>0.25</sub> -40vol.%Ag	850	1.6	3.75	0.42	27
60vol.%(ZrO <sub>2</sub> ) <sub>0.94</sub> (Y <sub>2</sub> O <sub>3</sub> ) <sub>0.06</sub> -40vol.%Pd	1100	2	7.55	0.06	28
70vol.%Bi <sub>1.5</sub> Y <sub>0.3</sub> Sm <sub>0.2</sub> O <sub>3-δ</sub> -30vol.%Ag	850	1.3	23	0.16	97
60vol.%Bi <sub>1.5</sub> Y <sub>0.3</sub> Sm <sub>0.2</sub> O <sub>3-δ</sub> -40vol.%Ag	850	1.3	23	0.79	97
60vol.%Ce <sub>0.8</sub> Sm <sub>0.2</sub> O <sub>2-δ</sub> - 40vol.%La <sub>0.8</sub> Sr <sub>0.2</sub> CrO <sub>3-δ</sub>	950	0.3	4.69	0.19	94
50wt.%Ce <sub>0.8</sub> Gd <sub>0.2</sub> O <sub>2-δ</sub> - 50wt.%La <sub>0.8</sub> Sr <sub>0.2</sub> MnO <sub>3-δ</sub>	750	1	3.91	0.02	98
Ce <sub>0.8</sub> Gd <sub>0.2</sub> O <sub>3-δ</sub> -15vol.%MnFe <sub>2</sub> O <sub>4-δ</sub>	1000	0.3	-	0.40	99
92.8vol.%La <sub>0.15</sub> Sr <sub>0.85</sub> Ga <sub>0.3</sub> Fe <sub>0.7</sub> O <sub>3-δ</sub> - -7.2vol.%Ba <sub>0.5</sub> Sr <sub>0.5</sub> Co <sub>0.8</sub> Fe <sub>0.2</sub> O <sub>3-δ</sub>	917	2	-	0.47	100
60vol.%Ce <sub>0.8</sub> Gd <sub>0.2</sub> O <sub>2-δ</sub> - 40vol.%Gd <sub>0.8</sub> Sr <sub>0.2</sub> FeO <sub>3-δ</sub>	900	0.6	3.74	0.804	44
60vol.%Ce <sub>0.8</sub> Sm <sub>0.2</sub> O <sub>2-δ</sub> - 40vol.%LaBaCo <sub>2</sub> O <sub>5+δ</sub>	950	0.6	-	0.62	101
60vol.%Ce <sub>0.8</sub> Sm <sub>0.2</sub> O <sub>2-δ</sub> - 40vol.%PrBaCo <sub>2</sub> O <sub>5+δ</sub>	925	0.6	-	0.32	102

**Membrane reactors for partial oxidation of methane (POM) to synthesis gas** One of the most commercially important applications for MIEC membrane is considered to be the POM to syngas (CO + H<sub>2</sub>). Syngas (CO + H<sub>2</sub>) is the most important feedstock for methanol formation and

Fischer-Tropsch (F-T) reaction. Several potential advantages were offered using MIEC membrane reactor to product synthesis gas. The main advantages were as follows: (i) Integration of oxygen separation and POM in the single membrane reactor, the costs can be potentially reduced. (ii) Without premixing of oxygen and natural gas in the ceramic membrane reactor, the formation of hot spots as encountered in a co-feed reactor can be avoided. (iii) Compared to steam reforming, a lower  $H_2/CO$  ratio of 2 is obtained during POM process, which is suitable for methanol synthesis or the F-T process. (iv) The gradual introduction of oxygen reduces contact with the partial oxidized products, which can enhance the yield of the desired products.

Developing MIEC membrane with a high oxygen flux and long-term stability is the main challenge for successful application in the syngas production process. Although many single phase perovskite-type membranes were reported to be successfully used in POM to synthesis gas and showed high oxygen permeation flux, most of their long-term stabilities were not guaranteed due to their poor phase and chemical stability under reducing environments. Dual phase membranes have been suggested as good substitutes with compositions that can be adjusted according to the practical requirements. Many dual phase membranes were developed to the POM reaction. Zhu et al. [44] reported the syngas production by POM in a series of disk-type dual phase membrane reactors. They reported that the dual phase membrane reactor based on 75 wt.%  $Ce_{0.8}Gd_{0.2}O_{1.9}$  - 25 wt.%  $Gd_{0.8}Sr_{0.2}FeO_{3-\delta}$  was operated in the reaction POM for more than 440 h. After 440 h syngas production experiment, morphologies of the surface kept intact, but metal elements transfer up to several microns could not be avoided. On the other hand, 75 wt.%  $Sm_{0.15}Ce_{0.85}O_{1.925}$  - 25 wt.%  $Sm_{0.6}Sr_{0.4}Fe_{1-x}Al_xO_{3-\delta}$  ( $x = 0$  or  $0.3$ ) dual phase membranes were developed. [103,104] They reported that these dual phase reactors were successfully operated for the POM reaction at 950 °C for more than 600 h without failure. Especially, the  $Sm_{0.15}Ce_{0.85}O_{1.925}$  -  $Sm_{0.6}Sr_{0.4}Fe_{0.7}Al_{0.3}O_{3-\delta}$  can be steadily in the POM to syngas generation for more than 1100 h at 950 °C.

**Membrane reactors for  $H_2$  generation and separation from  $H_2O$  splitting**  $H_2$  is regarded as one of the important clean fuel for both the electric power and transportation industries due to the concerns over globe climate change in the world. There is much interest in using water as a hydrogen source since it is clean and abundant. In particular, hydrogen generation from  $H_2O$



splitting with coupling partial oxidation of methane (POM) to synthesis gas employing a MIEC membrane reactor has gaining increasing attention. One of challenges for the process that the chemically and structurally stability of the employed MIEC membrane reactor under the operating conditions that exist on both sides: (i) high water vapor content on one side and (ii) high concentrations of CO and H<sub>2</sub> on the other side. Recently, Jiang et al. [105] in our group successfully used the single phase perovskite-type BaCo<sub>x</sub>Fe<sub>y</sub>Zr<sub>1-x-y</sub>O<sub>3-δ</sub> (BCFZ) hollow fiber membrane in combing water splitting and partial oxidation of methane (POM) to product hydrogen and synthesis gas in the temperature range of 800 to 950 °C. They found that a high H<sub>2</sub> production flux of 3.1 ml/min·cm<sup>2</sup> was obtained at 900 °C. However, the doubt of the long-term stability of this single phase perovskite-type BCFZ membrane still remain since Co-enriched phase was detected on the spent membrane. Gopalan group [106-108] proposed a series of new dual phase membranes (such as Ce<sub>0.8</sub>Gd<sub>0.2</sub>O<sub>1.9</sub> - Y<sub>0.08</sub>Sr<sub>0.88</sub>Ti<sub>0.95</sub>Al<sub>0.05</sub>O<sub>3-δ</sub>, Ce<sub>0.8</sub>Gd<sub>0.2</sub>O<sub>1.9</sub> - Gd<sub>0.08</sub>Sr<sub>0.88</sub>Ti<sub>0.95</sub>Al<sub>0.05</sub>O<sub>3-δ</sub>) comprised of one phase with high oxygen ion conductivity and a second phase with high electron conductivity, both individually stable in the gas atmospheres prevailing on both sides of the membrane during the hydrogen separation process. The concept of using a dual phase membrane to separate hydrogen from water splitting with coupling partial oxidation of methane (POM) to synthesis gas is schematically shown in Figure 1. 10. They investigated the Ce<sub>0.8</sub>Gd<sub>0.2</sub>O<sub>1.9</sub> - Y<sub>0.08</sub>Sr<sub>0.88</sub>Ti<sub>0.95</sub>Al<sub>0.05</sub>O<sub>3-δ</sub> dual phase membrane using conductivity relaxation experiments in the P<sub>O2</sub> range of 10<sup>-18</sup> to 10<sup>-16</sup> atm, which demonstrated excellent chemical stability under the application environment of the hydrogen generation and separation process. Meanwhile, they studied the Ce<sub>0.8</sub>Gd<sub>0.2</sub>O<sub>1.9</sub> - Gd<sub>0.08</sub>Sr<sub>0.88</sub>Ti<sub>0.95</sub>Al<sub>0.05</sub>O<sub>3-δ</sub> dual phase disk-type membrane with 1.2 mm thickness at 900 °C and found that 0.67 ml/min·cm<sup>2</sup> of H<sub>2</sub> can be obtained when 25 % steam fed into this dual phase membrane. Comparing to the single phase perovskite membrane, the H<sub>2</sub> production is lower but the stability was higher.

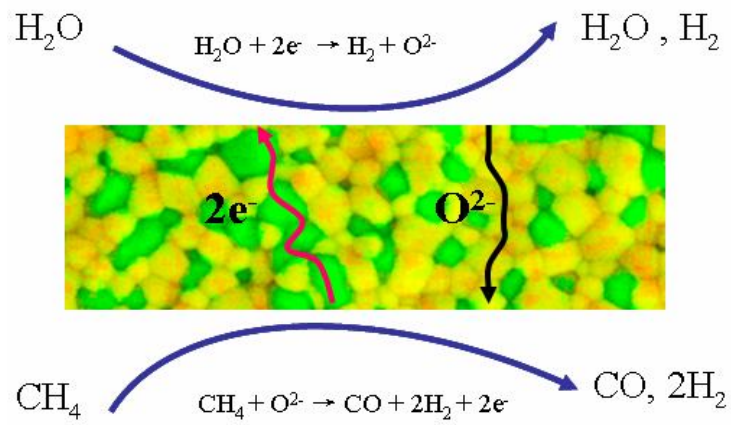


**Figure 1.10** Scheme of hydrogen production process using a dual phase membrane reactor. <sup>[106]</sup>

## 1.5 Bibliography

- [1] A. Schreiber, P. Zapp, W. Kuckshinrichs, Environmental assessment of german electricity generation from coal-fired power plants with amine-based carbon capture, *The international journal of life cycle assessment*, **2009**, *14*, 547-559.
- [2] R. Kneer, D. Toporov, M. Forster, D. Christ, C. Broeckmann, E. Pfaff, M. Zwick, S. Engels and M. Modigell, OXYCOAL-AC: Towards an integrated coal-fired power plant process with ion transport membrane-based oxygen supply, *Energy Environment Science*, **2010**, *3*, 198-207.
- [3] K. Zhang, Z.P. Shao, C.Z. Li, S.M. Liu, Novel CO<sub>2</sub>-tolerant ion-transporting ceramic membranes with an external short circuit for oxygen separation at intermediate temperatures, *Energy Environment Science*, **2012**, *5*, 5257-5264.
- [4] M. Czaperek, P. Zapp, H.J.M. Bouwmeester, M. Modigell, K. Ebert, I. Voigt, W.A. Meulenbergh, L. Singheiser, D. Stöver, Gas separation membranes for zero-emission fossil power plants: MEM-BRAIN, *Journal of Membrane Science*, **2010**, *359*, 149-159.
- [5] S. Engels, F. Beggel, M. Modigell, H. Stadler, Simulation of a membrane unit for oxyfuel power plants under consideration of realistic BSCF membrane properties. *Journal of Membrane Science*, **2010**, *359*, 93-101.
- [6] A. Leo, S. Liu, J.C.D. da Costa, Development of mixed conducting membranes for clean coal energy delivery, *International Journal of Greenhouse Gas Control*, **2009**, *3*, 357-367.
- [7] S.M. Hashim, A.R. Mohamed, S. Bhatia, Current status of ceramic-based membranes for oxygen separation from air, *Advances in Colloid and Interface Science*, **2010**, *160*, 88-100.
- [8] J.F. Vente, W.G. Haije, Z.S. Rak, Performance of functional perovskite membranes for oxygen production, *Journal of Membrane Science*, **2006**, *276*, 178-184.
- [9] S. Baumann, J.M. Serra, M.P. Lobera, S. Escolástico, F. Schulze-Küppers, W.A. Meulenbergh, Ultrahigh oxygen permeation flux through supported Ba<sub>0.5</sub>Sr<sub>0.5</sub>Co<sub>0.8</sub>Fe<sub>0.2</sub>O<sub>3-δ</sub> membranes, *Journal of Membrane Science*, **2011**, *377*, 198-205.
- [10] M. Yoshiya, C.A.J. Fisher, Y. Iwamoto, M. Asanuma, J. Ishii, K. Yabuta, Phase stability of BaCo<sub>1-y</sub>Fe<sub>y</sub>O<sub>3-δ</sub> by first principles calculations, *Solid State Ionics*, **2004**, *172*, 159-163.

- [11] L. Qiu, T.H. Lee, L.M. Liu, Y.L. Yang, A.J. Jacobson, Oxygen permeation studies of  $\text{SrCo}_{0.8}\text{Fe}_{0.2}\text{O}_{3-\delta}$ , *Solid State Ionics*, **1995**, 76, 321-329.
- [12] H. Kruidhof, H.J.M. Bouwmeester, R.H.E.v. Doorn, A.J. Burggraaf, Influence of order-disorder transitions on oxygen permeability through selected nonstoichiometric perovskite-type oxides, *Solid State Ionics*, **1993**, 63-65, 816-822.
- [13] K. Efimov, Q. Xu, A. Feldhoff, Transmission electron microscopy study of  $\text{Ba}_{0.5}\text{Sr}_{0.5}\text{Co}_{0.8}\text{Fe}_{0.2}\text{O}_{3-\delta}$  perovskite decomposition at intermediate temperatures, *Chemistry of Materials*, **2010**, 22, 5866-5875.
- [14] M. Arnold, T.M. Gesing, J. Martynczuk, A. Feldhoff, Correlation of the formation and the decomposition process of the BSCF perovskite at intermediate temperatures, *Chemistry of Materials*, **2008**, 20, 5851-5858.
- [15] U. Balachandran, J.T. Dusek, R.L. Mieville, R.B. Poeppel, M.S. Kleefisch, S. Pei, T.P. Kobylinski, C.A. Udovich, A.C. Bose, Dense ceramic membranes for partial oxidation of methane to syngas, *Applied Catalysis A: General*, **1995**, 133, 19-29.
- [16] J. Kniep, Y.S. Lin, Partial oxidation of methane and oxygen permeation in SrCoFeOx membrane reactor with different catalysts, *Industrial & Engineering Chemistry Research*, **2011**, 50, 7941-7948.
- [17] X.F. Zhu, H.H. Wang, W.S. Yang, Novel cobalt-free oxygen permeable membrane, *Chemical Communications*, **2004**, 1130-1131.
- [18] K. Watanabe, M. Yuasa, T. Kida, Y. Teraoka, N. Yamazoe, K. Shimano, High-performance oxygen-permeable membranes with an asymmetric structure using  $\text{Ba}_{0.95}\text{La}_{0.05}\text{FeO}_{3-\delta}$  perovskite-type oxide, *Advanced Materials*, **2010**, 22, 2367-2370.
- [19] H.H. Wang, C. Tablet, A. Feldhoff, J. Caro, A Cobalt-free oxygen-permeable membrane based on the perovskite-type oxide  $\text{Ba}_{0.5}\text{Sr}_{0.5}\text{Zn}_{0.2}\text{Fe}_{0.8}\text{O}_{3-\delta}$ , *Advanced Materials*, **2005**, 17, 1785-1788.
- [20] K. Efimov, T. Halfer, A. Kuhn, P. Heitjans, J. Caro, A. Feldhoff, Novel cobalt-free oxygen-permeable perovskite-type membrane, *Chemistry of Materials*, **2010**, 22, 1540-1544.
- [21] J. Martynczuk, F.Y. Liang, M. Arnold, V. Šepelák, A. Feldhoff, Aluminum-doped perovskites as high-performance oxygen permeation materials, *Chemistry of Materials*,

- 2009, 21, 1586-1594.
- [22] O. Czuprat, M. Arnold, S. Schirrmeyer, T. Schiestel, J. Caro, Influence of CO<sub>2</sub> on the oxygen permeation performance of perovskite-type BaCo<sub>x</sub>Fe<sub>y</sub>Zr<sub>z</sub>O<sub>3-δ</sub> hollow fiber membranes, *Journal of Membrane Science*, **2010**, 364, 132-137.
- [23] J.X. Yi, M. Schroeder, T. Weirich, J. Mayer, Behavior of Ba(Co, Fe, Nb)O<sub>3-δ</sub> perovskite in CO<sub>2</sub>-containing atmospheres: degradation mechanism and materials design, *Chemistry of Materials*, **2010**, 22, 6246-6253.
- [24] T.J. Mazanec, T.L. Cable, J.G. Frye Jr, Electrocatalytic cells for chemical reaction, *Solid State Ionics*, **1992**, 53–56, Part 1, 111-118.
- [25] K. Wu, S. Xie, G.S. Jiang, W. Liu, C.S. Chen, Oxygen permeation through (Bi<sub>2</sub>O<sub>3</sub>)<sub>0.74</sub>(SrO)<sub>0.26</sub>-Ag (40% v/o) composite, *Journal of Membrane Science*, **2001**, 188, 189-193.
- [26] J. Kim, Y.S. Lin, Synthesis and oxygen permeation properties of ceramic-metal dual-phase membranes, *Journal of Membrane Science*, **2000**, 167, 123-133.
- [27] C.S. Chen, H. Kruidhof, H.J.M. Bouwmeester, H. Verweij, A.J. Burggraaf, Thickness dependence of oxygen permeation through erbiastabilized bismuth oxide-silver composites, *Solid State Ionics*, **1997**, 99, 215-219.
- [28] C.S. Chen, B.A. Boukamp, H.J.M. Bouwmeester, G.Z. Cao, H. Kruidhof, A.J.A. Winnubst, A.J. Burggraaf, Microstructural development, electrical properties and oxygen permeation of zirconia-palladium composites, *Solid State Ionics*, **1995**, 76, 23-28.
- [29] V.V. Kharton, A.V. Kovalevsky, A.P. Viskup, A.L. Shaula, F.M. Figueiredo, E.N. Naumovich, F.M.B. Marques, Oxygen transport in Ce<sub>0.8</sub>Gd<sub>0.2</sub>O<sub>2-δ</sub>-based composite membranes, *Solid State Ionics*, **2003**, 160, 247-258.
- [30] U. Nigge, H.D. Wiemhöfer, E.W.J. Römer, H.J.M. Bouwmeester, T.R. Schulte, Composites of Ce<sub>0.8</sub>Gd<sub>0.2</sub>O<sub>1.9</sub> and Gd<sub>0.7</sub>Ca<sub>0.3</sub>CoO<sub>3-δ</sub> as oxygen permeable membranes for exhaust gas sensors, *Solid State Ionics*, **2002**, 146, 163-174.
- [31] B. Wang, J.X. Yi, L. Winnubst, C.S. Chen, Stability and oxygen permeation behavior of Ce<sub>0.8</sub>Sm<sub>0.2</sub>O<sub>2-δ</sub>-La<sub>0.8</sub>Sr<sub>0.2</sub>CrO<sub>3-δ</sub> composite membrane under large oxygen partial pressure gradients, *Journal of Membrane Science*, **2006**, 286, 22-25.
- [32] I. Kagomiya, T. Iijima, H. Takamura, Oxygen permeability of nanocrystalline

- Ce<sub>0.8</sub>Gd<sub>0.2</sub>O<sub>1.9</sub>-CoFe<sub>2</sub>O<sub>4</sub> mixed-conductive films, *Journal of Membrane Science*, **2006**, 286, 180-184.
- [33] X.F. Zhu, H.H. Wang, W.S. Yang, Relationship between homogeneity and oxygen permeability of composite membrane, *Journal of Membrane Science*, **2008**, 309, 120-127.
- [34] J.S. Yoon, M.Y. Yoon, E.J. Lee, J.W. Moon, H.J. Hwang, Influence of Ce<sub>0.9</sub>Gd<sub>0.1</sub>O<sub>2-δ</sub> particles on microstructure and oxygen permeability of Ba<sub>0.5</sub>Sr<sub>0.5</sub>Co<sub>0.8</sub>Fe<sub>0.2</sub>O<sub>3-δ</sub> composite membrane, *Solid State Ionics*, **2010**, 181, 1387-1393.
- [35] E.M. Logothetis, J.H. Visser, R.E. Soltis, L. Rimai, Chemical and physical sensors based on oxygen pumping with solid-state electrochemical cells, *Sensors and Actuators B: Chemical*, **1992**, 9, 183-189.
- [36] L. Qiu, T.H. Lee, L.M. Liu, Y.L. Yang, A.J. Jacobson, Oxygen permeation studies of SrCo<sub>0.8</sub>Fe<sub>0.2</sub>O<sub>3-δ</sub>, *Solid State Ionics*, **1995**, 76, 321-329.
- [37] Y. Teraoka, H.M. Zhang, N. Yamazoe, Oxygen sorptive properties of defect perovskite-type La<sub>1-x</sub>Sr<sub>x</sub>Co<sub>1-y</sub>Fe<sub>y</sub>O<sub>3-δ</sub>, *Chemistry Letters*, **1995**, 14, 1367-1370.
- [38] J. Kim, Y.S. Lin, Palladium-modified yttria-stabilized zirconia membranes, *Industrial & Engineering Chemistry Research*, **2000**, 39, 2124-2126.
- [39] T.H. Lee, Y.L. Yang, A.J. Jacobson, Electrical conductivity and oxygen permeation of Ag/BaBi<sub>8</sub>O<sub>13</sub> composites, *Solid State Ionics*, **2000**, 134, 331-339.
- [40] C.S. Chen, H. Kruidhof, H.J.M. Bouwmeester, H. Verweij, A.J. Burggraaf, Oxygen permeation through oxygen ion oxide-noble metal dual phase composites, *Solid State Ionics*, **1996**, 86-88, Part 1, 569-572.
- [41] Y. Shen, M. Liu, D. Taylor, S.A. Bolagopal, A. Joshi, K. Krist, in: T.A. Ramanarayanan, W.L. Worrell, H.L. Tuller (Eds.), Proceedings of the 2nd International Symposium on Ionic and Mixed Conducting Ceramics, **1994**, p. 574.
- [42] J. Kim, Inorganic dual-phase membranes for oxygen separation: synthesis and properties, University of Cincinnati, USA, Ph.D defenses, **1999**.
- [43] V.V. Kharton, A.V. Kovalevsky, A.P. Viskup, F.M. Figueiredo, A.A. Yaremchenko, E.N. Naumovich, F.M.B. Marques, Oxygen Permeability of Ce<sub>0.8</sub>Gd<sub>0.2</sub>O<sub>2-δ</sub>-La<sub>0.7</sub>Sr<sub>0.3</sub>MnO<sub>3-δ</sub> composite membranes, *Journal of The Electrochemical Society*, **2000**, 147, 2814-2821.
- [44] X.F. Zhu, W.S. Yang, Composite membrane based on ionic conductor and mixed

- conductor for oxygen permeation, *AIChE Journal*, **2008**, *54*, 665-672.
- [45] Y. Teraoka, T. Fukuda, N. Miura, N. Yamazon, Development of oxygen semipermeable membrane using mixed conductive perovskite-type oxides (Part 2), *Journal of the Ceramic Society of Japan - International Edition*, **1989**, *97*, 523-529.
- [46] H.J.M. Bouwmeester, A.J. Burggraaf, Chapter 10: Dense ceramic membranes for oxygen separation, *Fundamental of Inorganic membrane science and technology*, **1996**, p.436-437.
- [47] D.K. Hohnke., Ionic conduction in doped oxides with the fluorite structure, *Solid State Ionics*, **1981**, *5*, 531-534.
- [48] V. Eyert, K.H. Hock, Electronic structure, itinerant magnetism and orbital ordering of  $K_2NiF_4$ -type compounds, *Journal of Physics: Condensed Matter*, **1993**, *5*, 2987.
- [49] S.Y. Istomin, S.V. Abdyusheva, G. Svensson, E.V. Antipov, Synthesis, crystal and magnetic structure of a novel brownmillerite-type compound  $Ca_2Co_{1.6}Ga_{0.4}O_5$ , *Journal of Solid State Chemistry*, **2004**, *177*, 4251-4257.
- [50] K. Ohgushi, J.I. Yamaura, M. Ichihara, Y. Kiuchi, T. Tayama, T. Sakakibara, H. Gotou, T. Yagi, Y. Ueda, Structural and electronic properties of pyrochlore-type  $A_2Re_2O_7$  (A=Ca, Cd, and Pb), *Physical Review B*, **2011**, *83*, 125103.
- [51] S.E. Jacobo, Novel method of synthesis for double-perovskite  $Sr_2FeMoO_6$ , *Journal of Materials Science*, **2005**, *40*, 417-421.
- [52] S. Uma, A.R. Raju, J. Gopalakrishnan, Bridging the Ruddlesden-Popper and the Dion-Jacobson series of layered perovskites: synthesis of layered oxides,  $A_{2-x}La_2Ti_{3-x}Nb_xO_{10}$  (A = K, Rb), exhibiting ion exchange, *Journal of Materials Chemistry*, **1993**, *3*, 709-713.
- [53] R.D. King-smith, D. Vanderbilt, A first-principles pseudopotential investigation of ferroelectricity in barium titanate, *Ferroelectrics*, **1992**, *136*, 85-94.
- [54] A.S. Bhalla, R.Y. Guo, R. Roy, The perovskite structure - a review of its role in ceramic science and technology, *Materials Research Innovations*, **2000**, *4*, 3-26.
- [55] V.M. Goldschmidt, *Naturwissenschaften*, **1926**, *14*, 477-485.
- [56] R.L. Cook, A.F. Sammells, On the systematic selection of perovskite solid electrolytes for intermediate temperature fuel cells, *Solid State Ionics*, **1991**, *45*, 311-321.

- [57] <http://www.princeton.edu/~cavalab/tutorials/public/structures/perovskites.html>
- [58] X.F. Zhu, Y. Cong, W.S. Yang, Effects of synthesis methods on oxygen permeability of  $\text{BaCe}_{0.15}\text{Fe}_{0.85}\text{O}_{3-\delta}$  ceramic membranes, *Journal of Membrane Science*, **2006**, 283, 158-163.
- [59] L. Tan, X. Gu, L. Yang, W.Q. Jin, L.X. Zhang, N.P. Xu, Influence of powder synthesis methods on microstructure and oxygen permeation performance of  $\text{Ba}_{0.5}\text{Sr}_{0.5}\text{Co}_{0.8}\text{Fe}_{0.2}\text{O}_{3-\delta}$  perovskite-type membranes, *Journal of Membrane Science*, **2003**, 212, 157-165.
- [60] A. Basile, F. Gallucci, Membranes for Membrane Reactors: Preparation, Optimization and Selection, **2011**, p. 130.
- [61] H.X. Luo, B.B. Tian, Y.Y. Wei, H.H. Wang, H.Q. Jiang, J. Caro, Oxygen permeability and structural stability of a novel tantalum-doped perovskite  $\text{BaCo}_{0.7}\text{Fe}_{0.2}\text{Ta}_{0.1}\text{O}_{3-\delta}$ , *AIChE Journal*, **2010**, 56, 604-610.
- [62] H.L. Zhao, N.S. Xu, Y.F. Cheng, W.J. Wei, N. Chen, W.Z. Ding, X.G. Lu, F.S. Li, Investigation of mixed conductor  $\text{BaCo}_{0.7}\text{Fe}_{0.3-x}\text{Y}_x\text{O}_{3-\delta}$  with high oxygen permeability, *The Journal of Physical Chemistry C*, **2010**, 114, 17975-17981.
- [63] X.L. Dong, G.R. Zhang, Z.K. Liu, Z.X. Zhong, W.J. Jin, N.P. Xu,  $\text{CO}_2$ -tolerant mixed conducting oxide for catalytic membrane reactor, *Journal of Membrane Science*, **2009**, 340, 141-147.
- [64] V.V. Kharton, Solid State Electrochemistry I: Fundamentals, Materials and Their applications, **2009**, p. 94.
- [65] Z.P. Shao, W.S. Yang, Y. Cong, H.J. Dong, J.H. Tong, G.X. Xiong, Investigation of the permeation behavior and stability of a  $\text{Ba}_{0.5}\text{Sr}_{0.5}\text{Co}_{0.8}\text{Fe}_{0.2}\text{O}_{3-\delta}$  oxygen membrane, *Journal of Membrane Science*, **2000**, 172, 177-188.
- [66] Y. Teraoka, H.M. Zhang, S.C. Furukawa, N. Yamazoe, Oxygen permeation through perovskite-type oxides, *Chemistry Letters*, **1985**, 14, 1743-1746.
- [67] S. Pei, M.S. Kleefisch, T.P. Kobylinski, J. Faber, C.A. Udovich, V. Zhang-McCoy, B. Dabrowski, U. Balachandran, R.L. Mieville, R.B. Poeppel, Failure mechanisms of ceramic membrane reactors in partial oxidation of methane to synthesis gas, *Catalysis Letters*, **1994**, 30, 201-212.
- [68] K. Zhang, R. Ran, L. Ge, Z.P. Shao, W.Q. Jin, N.P. Xu, Systematic investigation on new



- SrCo<sub>1-y</sub>Nb<sub>y</sub>O<sub>3-δ</sub> ceramic membranes with high oxygen semi-permeability, *Journal of Membrane Science*, **2008**, 323, 436-443.
- [69] X.Z. Chen, L. Huang, Y.Y. Wei, H.H. Wang, Tantalum stabilized SrCoO<sub>3-δ</sub> perovskite membrane for oxygen separation, *Journal of Membrane Science*, **2011**, 368, 159-164.
- [70] T. Nagai, W. Ito, T. Sakon, Relationship between cation substitution and stability of perovskite structure in SrCoO<sub>3-δ</sub>-based mixed conductors, *Solid State Ionics*, **2007**, 177, 3433-3444.
- [71] S. Švarcová, K. Wiik, J. Tolchard, H.J.M. Bouwmeester, T. Grande, Structural instability of cubic perovskite Ba<sub>x</sub>Sr<sub>1-x</sub>Co<sub>1-y</sub>Fe<sub>y</sub>O<sub>3-δ</sub>, *Solid State Ionics* **2008**, 178, 1787-1791.
- [72] M. Arnold, T.M. Gesing, J. Martynczuk, A. Feldhoff, Correlation of the formation and the decomposition process of the BSCF perovskite at intermediate temperatures, *Chemistry of Materials*, **2008**, 20, 5851-5858.
- [73] K. Efimov, Q. Xu, A. Feldhoff, Transmission electron microscopy study of Ba<sub>0.5</sub>Sr<sub>0.5</sub>Co<sub>0.8</sub>Fe<sub>0.2</sub>O<sub>3-δ</sub> perovskite decomposition at intermediate temperatures, *Chemistry of Materials*, **2010**, 22, 5866-5875.
- [74] A.Y. Yan, V. Maragou, A. Arico, M.J. Cheng, P. Tsiakaras, Investigation of a Ba<sub>0.5</sub>Sr<sub>0.5</sub>Co<sub>0.8</sub>Fe<sub>0.2</sub>O<sub>3-δ</sub> based cathode SOFC: II. The effect of CO<sub>2</sub> on the chemical stability, *Applied Catalysis B: Environmental*, **2007**, 76, 320-327.
- [75] M. Arnold, H.H. Wang, A. Feldhoff, Influence of CO<sub>2</sub> on the oxygen permeation performance and the microstructure of perovskite-type (Ba<sub>0.5</sub>Sr<sub>0.5</sub>)(Co<sub>0.8</sub>Fe<sub>0.2</sub>)O<sub>3-δ</sub> membranes, *Journal of Membrane Science*, **2007**, 293, 44-52.
- [76] V.V. Kharton, *Solid State Electrochemistry II: Electrodes, Interfaces and Ceramic membranes*, **2011**, p. 416.
- [77] V.V. Kharton, A.V. Kovalevsky, A.A. Yaremchenko, F.M.M. Snijkers, J.F.C. Cooymans, J.J. Luyten, A.A. Markov, J.R. Frade, F.M.B. Marques, Oxygen transport and thermomechanical properties of SrFe(Al)O<sub>3-δ</sub>-SrAl<sub>2</sub>O<sub>4</sub> composites: microstructural effects, *Journal of Solid State Electrochemistry*, **2006**, 10, 663-673.
- [78] H.H. Luo, H.Q. Jiang, K. Efimov, H.H. Wang, J. Caro, Influence of the preparation methods on the microstructure and oxygen permeability of a CO<sub>2</sub>-stable dual phase membrane, *AIChE Journal*, **2011**, 57, 2738-2745.

- [79] H.X. Luo, K. Efimov, H.Q. Jiang, A. Feldhoff, H.H. Wang, J. Caro, CO<sub>2</sub>-stable and cobalt-free dual-phase membrane for oxygen separation, *Angewandte Chemie International Edition*, **2011**, *50*, 759-763.
- [80] H.X. Luo, H.Q. Jiang, T. Klande, Z.W. Cao, F.Y. Liang, H.H. Wang, J. Caro, A novel cobalt-free noble metal-free oxygen-permeable 40Pr<sub>0.6</sub>Sr<sub>0.4</sub>FeO<sub>3-δ</sub>-60Ce<sub>0.9</sub>Pr<sub>0.1</sub>O<sub>2-δ</sub> composite membrane: Oxygen permeability and stability under CO<sub>2</sub> and methane atmospheres, in preparation.
- [81] M.N. Rahaman, Ceramic processing and sintering, **2003**, p. 721.
- [82] M. Arnold, J. Martynczuk, K. Efimov, H.H. Wang, A. Feldhoff, Grain boundaries as barrier for oxygen transport in perovskite-type membranes, *Journal of Membrane Science*, **2008**, *316*, 137-144.
- [83] P.Y. Zeng, R. Ran, Z.H. Chen, H.X. Gu, Z.P. Shao, J.C.D. da Costa, S.M. Liu, Significant effects of sintering temperature on the performance of La<sub>0.6</sub>Sr<sub>0.4</sub>Co<sub>0.2</sub>Fe<sub>0.8</sub>O<sub>3-δ</sub> oxygen selective membranes, *Journal of Membrane Science*, **2007**, *302*, 171-179.
- [84] Q.M. Li, X.F. Zhu, Y.F. He, Y. Cong, W.S. Yang, Effects of sintering temperature on properties of dual-phase oxygen permeable membranes, *Journal of Membrane Science*, **2011**, *367*, 134-140.
- [85] A.L. Shaula, V.V. Kharton, F.M.B. Marques, A.V. Kovalevsky, A.P. Viskup, E.N. Naumovich, Oxygen permeability of mixed-conducting composite membranes: effects of phase interaction, *Journal of Solid State Electrochemistry*, **2006**, *10*, 28-40.
- [86] H.J.M. Bouwmeester, H. Kruidhof, A.J. Burggraaf, P.J. Gellings, Oxygen semipermeability of erbia-stabilized bismuth oxide, *Solid State Ionics*, **1992**, *53-56, Part I*, 460-468.
- [87] X.L. Dong, W.Q. Jin, N.P. Xu, K. Li, Dense ceramic catalytic membranes and membrane reactors for energy and environmental applications, *Chemical Communications*, **2011**, *47*, 10886-10902.
- [88] R.M. Thorogood, R. Srinivasan, T.F. Yee, M.P. Drake, Composite mixed conductor membranes for producing oxygen, US Patent 5240480, **1993**, p. 3-6.
- [89] C. Wagner, Beitrag zur Theorie des Anlaufvorgangs, *Z. Phys. Chem. B.*, 1933, *21*, 25-41.
- [90] C.S. Chen, Chapter 2 in fine grained zirconia-metal dual phase composites, University of

- Twente, the Netherlands, Ph.D. thesis, **1994**.
- [91] S. Kim, Y.L. Yang, A.J. Jacobson, B. Abeles, Oxygen surface exchange in mixed ionic electronic conductor membranes, *Solid State Ionics*, **1999**, *121*, 31-36.
- [92] X.F. Zhu, H.Y. Liu, Q.M. Li, Y. Cong, W.S. Yang, Unsteady-state permeation and surface exchange of dual-phase membranes, *Solid State Ionics*, **2011**, *185*, 27-31.
- [93] S.M. Fang, C.S. Chen, L. Winnubst, Effect of microstructure and catalyst coating on the oxygen permeability of a novel CO<sub>2</sub>-resistant composite membrane, *Solid State Ionics*, **2011**, *190*, 46-52.
- [94] J.X. Yi, Y.B. Zuo, W. Liu, L. Winnubst, C.S. Chen, Oxygen permeation through a Ce<sub>0.8</sub>Sm<sub>0.2</sub>O<sub>2-δ</sub>-La<sub>0.8</sub>Sr<sub>0.2</sub>CrO<sub>3-δ</sub> dual-phase composite membrane, *Journal of Membrane Science*, **2006**, *280*, 849-855.
- [95] H.X. Luo, H.Q. Jiang, K. Efimov, F.Y. Liang, H.H. Wang, J. Caro, CO<sub>2</sub>-tolerant oxygen-permeable Fe<sub>2</sub>O<sub>3</sub>-Ce<sub>0.9</sub>Gd<sub>0.1</sub>O<sub>2-δ</sub>, dual phase membranes, *Industrial & Engineering Chemistry Research*, **2011**, *50*, 13508-13517.
- [96] H.X. Luo, Y.Y. Wei, H.Q. Jiang, W.H. Yuan, Y.L. Lv, J. Caro, H.H. Wang, Performance of a ceramic membrane reactor with high oxygen flux Ta-containing perovskite for the partial oxidation of methane to syngas, *Journal of Membrane Science*, **2010**, *350*, 154-160.
- [97] J. Kim, Y.S. Lin, Synthesis and oxygen permeation properties of ceramic-metal dual-phase membranes, *Journal of Membrane Science*, **2000**, *167*, 123-133.
- [98] V.V. Kharton, A.V. Kovalevsky, A.P. Viskup, F.M. Figueiredo, A.A. Yaremchenko, E.N. Naumovich, F.M.B. Marques, Oxygen permeability and Faradaic efficiency of Ce<sub>0.8</sub>Gd<sub>0.2</sub>O<sub>2-δ</sub>-La<sub>0.7</sub>Sr<sub>0.3</sub>MnO<sub>3-δ</sub> composites *Journal of the European Ceramic Society*, **2001**, *21*, 1763-1767.
- [99] H. Takamura, H. Sugai, M. Watanabe, T. Kasahara, A. Kamegawa, M. Okada, Oxygen permeation properties and surface modification of acceptor-doped CeO<sub>2</sub>/MnFe<sub>2</sub>O<sub>4</sub> composites, *Journal of Electroceramics*, **2006**, *17*, 741-748.
- [100] H.H. Wang, W.S. Yang, Y. Cong, X.F. Zhu, Y.S. Lin, Structure and oxygen permeability of a dual-phase membrane, *Journal of Membrane Science*, **2003**, *224*, 107-115.

- [101] T. Chen, H.L. Zhao, N.S. Xu, Y. Li, X.G. Lu, W.Z. Ding, F.S. Li, Synthesis and oxygen permeation properties of a  $\text{Ce}_{0.8}\text{Sm}_{0.2}\text{O}_{2-\delta}$ - $\text{LaBaCo}_2\text{O}_{5+\delta}$  dual-phase composite membrane, *Journal of Membrane Science*, **2011**, 370, 158-165.
- [102] T. Chen, H.L. Zhao, Z.X. Xie, L.C. Feng, X.G. Lu, W.Z. Ding, F.S. Li, Electrical conductivity and oxygen permeability of  $\text{Ce}_{0.8}\text{Sm}_{0.2}\text{O}_{2-\delta}$ - $\text{PrBaCo}_2\text{O}_{5+\delta}$  dual-phase composites, *International Journal of Hydrogen Energy*, **2012**, 37, 5277-5285.
- [103] X.F. Zhu, Q.M. Li, Y. Cong, W.S. Yang, Syngas generation in a membrane reactor with a highly stable ceramic composite membrane, *Catalysis Communications*, **2008**, 10, 309-312.
- [104] X.F. Zhu, Q.M. Li, Y.F. He, Y. Cong, W.S. Yang, Oxygen permeation and partial oxidation of methane in dual-phase membrane reactors, *Journal of Membrane Science*, **2010**, 360, 454-460.
- [105] H.Q. Jiang, H.H. Wang, S. Werth, T. Schiestel, J. Caro, Simultaneous production of hydrogen and synthesis gas by combining water splitting with partial oxidation of methane in a hollow fiber membrane reactor, *Angewandte Chemie International Edition*, **2008**, 47, 9341-9344.
- [106] H.D. Cui, A. Karthikeyan, S. Gopalan, U.B. Pal,  $\text{Gd}_{0.2}\text{Ce}_{0.8}\text{O}_{1.9-\delta}$ - $\text{Y}_{0.08}\text{Sr}_{0.88}\text{Ti}_{0.95}\text{Al}_{0.05}\text{O}_{3+\delta}$  composite mixed conductors for hydrogen separation, *Journal of The Electrochemical Society*, **2005**, 152, A1726-A1732.
- [107] H.B. Wang, S. Gopalan, U.B. Pal, Hydrogen generation and separation using  $\text{Gd}_{0.2}\text{Ce}_{0.8}\text{O}_{1.9-\delta}$ - $\text{Gd}_{0.08}\text{Sr}_{0.88}\text{Ti}_{0.95}\text{Al}_{0.05}\text{O}_{3+\delta}$  mixed ionic and electronic conducting membrane, *Electrochim. Acta*, **2011**, 56, 6989-6996.
- [108] H.D. Cui, Mixed ionic and electronic conducting membranes for hydrogen generation and separation, Boston University, USA, Ph.D. thesis, **2007**.

## Chapter 2

### 2. Phase stability and permeation behavior of BSCF perovskite membrane

#### 2.1 Summary

Among many perovskite-type compounds,  $\text{Ba}_{0.5}\text{Sr}_{0.5}\text{Co}_{0.8}\text{Fe}_{0.2}\text{O}_{3-\delta}$  (BSCF), which has a high concentration of the mobile oxygen vacancies, has been regarded as one of the most promising materials for oxygen separation from air and for cathodes in solid-oxide fuel cells. However, the wide applications of BSCF were still hampered by the following reasons: (i) BSCF material was not stable at temperatures below 750 °C. [71-73] (ii) In the presence of  $\text{CO}_2$ , the oxygen permeation flux through BSCF membrane is drastically reduced, the structure was even destroyed because of the formation of carbonates. [74,75]

In this chapter, the phase stability and permeation behavior of a dead-end  $\text{Ba}_{0.5}\text{Co}_{0.5}\text{Fe}_{0.2}\text{Co}_{0.8}\text{O}_{3-\delta}$  tube membrane in the atmosphere of high purity oxygen will be discussed in detail. Powder X-ray diffraction (XRD), energy dispersive X-ray spectroscopy (EDXS), high-angle annular dark-field (HAADF) and scanning transmission electron microscopy (STEM) were used to analyze the spent membrane which was exposed to high purity oxygen. It was found that parts of the cubic perovskite BSCF transformed into a hexagonal perovskite  $\text{Ba}_{0.5\pm x}\text{Sr}_{0.5\pm x}\text{CoO}_{3-\delta}$  ( $x \approx 0.1$ ) and a trigonal mixed oxide  $\text{Ba}_{1-x}\text{Sr}_x\text{Co}_{2-y}\text{Fe}_y\text{O}_{5\pm\delta}$  ( $x \approx 0.15$ ,  $y \approx 0.25$ ) in high-purity oxygen at 750 °C. On the other hand, it was found that the partial degradation of cubic BSCF perovskite at 750 °C was more pronounced under the strongly oxidizing conditions on the oxygen supply (feed) side than on the oxygen release (permeate) side of the membrane. The structural instability of BSCF is attributed to a highly oxidation state of cobalt (+3 and +4), which exhibits an ionic radius that is too small to be tolerated by the cubic perovskite structure, which then becomes unstable.

## **2.2 Phase stability and permeation behavior of a dead-end $\text{Ba}_{0.5}\text{Sr}_{0.5}\text{Co}_{0.8}\text{Fe}_{0.2}\text{O}_{3-\delta}$ tube membrane in high-purity oxygen production**

Fangyi Liang, Heqing Jiang, Huixia Luo, Jürgen Caro and Armin Feldhoff

**Chem. Mater.** 2011, 23, 4765.

**Reprinted (adapted) with permission from (Chemistry of Materials). Copyright (2011) American Chemical Society.**

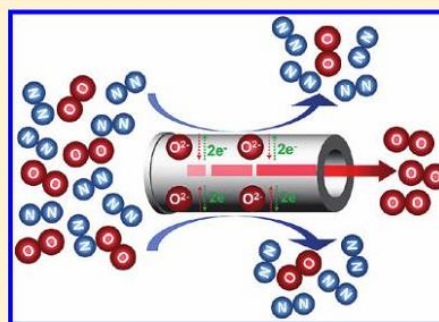
## Phase Stability and Permeation Behavior of a Dead-End $\text{Ba}_{0.5}\text{Sr}_{0.5}\text{Co}_{0.8}\text{Fe}_{0.2}\text{O}_{3-\delta}$ Tube Membrane in High-Purity Oxygen Production

Fangyi Liang,<sup>†</sup> Heqing Jiang,<sup>‡</sup> Huixia Luo,<sup>†</sup> Jürgen Caro,<sup>†</sup> and Armin Feldhoff<sup>\*†</sup>

<sup>†</sup>Institute of Physical Chemistry and Electrochemistry, Leibniz University Hannover, Callinstrasse 3A, D-30167 Hannover, Germany

<sup>‡</sup>Max-Planck-Institut für Kohlenforschung, Kaiser-Wilhelm-Platz 1 D-45470 Mülheim an der Ruhr, Germany

**ABSTRACT:** Phase stability and oxygen permeation behavior of  $\text{Ba}_{0.5}\text{Sr}_{0.5}\text{Co}_{0.8}\text{Fe}_{0.2}\text{O}_{3-\delta}$  (BSCF) dead-end tube membranes were investigated in long-term oxygen production at 950 and 750 °C. At 950 °C, the BSCF tube membranes exhibit good long-term phase stability and a stable oxygen permeation flux. However, at the intermediate temperature of 750 °C, both the oxygen permeation flux and the oxygen purity decrease continuously. This behavior is related to the formation of two secondary phases that are a hexagonal perovskite,  $\text{Ba}_{0.5\pm x}\text{Sr}_{0.5\pm x}\text{CoO}_{3-\delta}$ , and a trigonal mixed oxide,  $\text{Ba}_{1-x}\text{Sr}_x\text{Co}_{2-y}\text{Fe}_y\text{O}_5$ , that evolved in the ceramic membrane made of cubic BSCF perovskite during the dynamic flow of oxygen through it. Tensile stress as a result of phase formation causes the development of cracks in the membrane, which spoil the purity of the permeated oxygen. The partial degradation of cubic BSCF perovskite in the intermediate temperature range (750 °C) was more pronounced under the strongly oxidizing conditions on the oxygen supply (feed) side than on the oxygen release (permeate) side of the membrane. The structural instability of BSCF is attributed to an unsuitable redox state of cobalt, that exhibits an ionic radius that is too small to be tolerated by the cubic perovskite structure, which then becomes unstable. The phase stability of cubic BSCF (i.e., the proper redox states of cobalt) can be maintained by operating the membrane in the high temperature regime (950 °C).



**KEYWORDS:** perovskite, mixed conductor, decomposition, oxygen permeation, oxygen production

### 1. INTRODUCTION

Oxygen is the third-largest-volume chemical produced worldwide,<sup>1</sup> and most of the industrial applications for oxygen require high-purity oxygen. Oxygen-transporting membranes (OTMs) can separate oxygen from air, which is a gas mixture containing approximately 78 vol %  $\text{N}_2$  and 21 vol %  $\text{O}_2$ ,<sup>2</sup> or from other oxygen-containing gases. OTMs can theoretically produce oxygen at purities of up to 100% and are believed to possess the potential to reduce the cost of high-purity oxygen production compared to the conventional cryogenic processes.<sup>3</sup> Moreover, OTM reactors have been developed for such potential applications as the partial oxidation of hydrocarbons,<sup>4–8</sup> the production of hydrogen by thermal water splitting in combination with olefin and synthesis gas production,<sup>9–11</sup> and the decomposition of nitrogen oxides.<sup>12,13</sup>

High-purity oxygen can be obtained with the use of OTMs when the oxygen partial pressure at one surface (feed side) is higher than that at the opposite surface (permeate side). The oxygen partial pressure difference can be achieved through the elevation of the oxygen partial pressure on the feed side by the compression of air to pressures higher than 1 bar, the reduction of the oxygen pressure on the permeate side by a vacuum pump, a combination of both techniques, or the use of steam as a condensable sweep gas on the permeate side.<sup>14</sup> The thermal activation of a membrane's oxygen-transport properties

requires the OTM to operate at temperatures of approximately 700–950 °C. The authors of several studies on the high-purity oxygen production have been reported using tubular membrane geometries, instead of conventional flat disks, which are capillary hollow-fiber<sup>15,16</sup> or tube membranes<sup>17,18</sup> that overcome the problem of high-temperature sealing by allowing the seal to be placed in the cold zone.

In the past few decades, many OTMs with high oxygen permeabilities have been developed that are based on mixed ionic-electronic conductors (MIEC) solid oxides, such as  $\text{SrCo}_{0.8}\text{Fe}_{0.2}\text{O}_{3-\delta}$ ,<sup>19</sup>  $\text{BaCo}_{0.4}\text{Fe}_{0.4}\text{Zr}_{0.2}\text{O}_{3-\delta}$ ,<sup>20</sup>  $\text{BaCo}_{0.7}\text{Fe}_{0.2}\text{Ta}_{0.1}\text{O}_{3-\delta}$ ,<sup>21</sup>  $\text{Ba}_{0.5}\text{Sr}_{0.5}\text{Fe}_{0.9}\text{Al}_{0.1}\text{O}_{3-\delta}$ ,<sup>22</sup>  $\text{Ba}_{0.5}\text{Sr}_{0.5}\text{Fe}_{0.8}\text{Cu}_{0.2}\text{O}_{3-\delta}$ ,<sup>23</sup> and  $\text{Ba}_{0.5}\text{Sr}_{0.5}\text{Co}_{0.8}\text{Fe}_{0.2}\text{O}_{3-\delta}$  (denoted BSCF).<sup>24</sup> Among these compounds, BSCF, which assumes a cubic perovskite structure, has been regarded as one of the most promising materials for oxygen separation from air and for cathodes in solid-oxide fuel cells.<sup>25</sup> Because of the high concentration of the mobile oxygen vacancies in the perovskite lattice,<sup>26</sup> BSCF exhibits a very high oxygen-permeation flux over a wide temperature range.<sup>24</sup> Zhu et al.<sup>18</sup> have observed the stable oxygen permeation behavior of a BSCF perovskite tube membrane under vacuum and elevated pressures

Received: June 24, 2011

Revised: September 20, 2011

Published: October 07, 2011

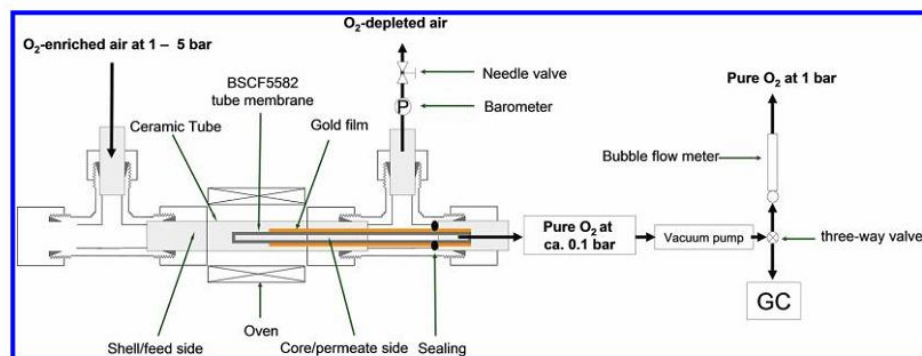


Figure 1. Permeator in dead-end geometry for the production of high-purity oxygen.

for high-purity oxygen production at 925 °C. However, Shao et al.<sup>24</sup> and van Veen et al.<sup>27</sup> have reported that stable oxygen permeation is achieved only when the operating temperatures are higher than 850 °C. During operation in the intermediate temperature (IT, i.e., approximately 500–850 °C) range, however, the oxygen-permeation flux through the BSCF membrane has been observed to decrease, which has been attributed in several reports<sup>24,28–31</sup> to a partial decomposition of the bulk cubic perovskite phase. Shao et al.<sup>24</sup> and Rebeilleau-Dassoneville et al.<sup>28</sup> have observed reflections of noncubic phases in the X-ray diffraction (XRD) patterns of BSCF after the samples were annealed in the IT range. Based on the same experimental technique, Švarcová et al.<sup>30</sup> have described the occurrence of hexagonal perovskite (2H or 4H polymorphs) in addition to the cubic phase. Arnold et al.<sup>29,32</sup> have investigated the formation of cubic BSCF in a sol–gel-based process by analyzing XRD powder patterns that were obtained in situ in the IT range and from quenched intermediate powders. They observed diffraction patterns similar to those observed by Švarcová et al.<sup>30</sup> during partial decomposition of BSCF in the same temperature range. They also noted the reciprocity between the formation and decomposition processes of BSCF. Using transmission electron microscopy (TEM), Arnold et al.<sup>29</sup> clearly showed that some phases, that evolved in the IT range can be described as distorted polytypes with different sequences of cubic and hexagonal close-packed layers, that consist of oxygen and A-site cations (Ba or Sr). These polytypes therefore constitute intergrown structures of cubic and 2H hexagonal perovskite. Using TEM, Mueller et al.<sup>33</sup> observed structural changes not only in the grain boundaries of polycrystalline BSCF ceramic, but also in the BSCF grains themselves by the formation of extended platelets. They mainly addressed the grain boundaries and found barium and cobalt-enriched 2H hexagonal perovskite. Efimov et al.<sup>31</sup> studied, by TEM, BSCF powder and ceramic that had been exposed to IT. They found not only barium- and cobalt-enriched hexagonal perovskite, which was assigned an approximate stoichiometry of  $\text{Ba}_{0.6}\text{Sr}_{0.4}\text{CoO}_{3-\delta}$ , but also barium-enriched and heavily cobalt-enriched trigonal 15R-related  $\text{Ba}_{1-x}\text{Sr}_x\text{Co}_{2-y}\text{Fe}_y\text{O}_{5-\delta}$ . The first XRD diffractograms taken by Shao et al.<sup>24</sup> of a BSCF membrane after it was dynamically operated in an oxygen permeation flux for 400 h at 750 °C showed significantly stronger reflection intensities from additional phases on the feed (air) side as compared to the permeate (helium) side. Microstructure investigations in the aforementioned studies, however, were made solely on BSCF powders or ceramic pellets after they were annealed in a static (air) atmosphere.

In this report, we extend the work of Shao et al.<sup>24</sup> and investigate the microstructure of a BSCF membrane, which developed during operation under a dynamic flow of oxygen in the IT range, by scanning electron microscopy (SEM) analysis, TEM, and XRD. We correlate the observed membrane microstructure, which differs between the feed and permeate side, with the oxygen permeation behavior (i.e., oxygen flux and oxygen purity). Dead-end BSCF tube membranes were used for the high-purity oxygen production using air or oxygen-enriched air as feed gases.

## 2. EXPERIMENTAL SECTION

**Oxygen Production in Dead-End Membrane Reactor.** The  $\text{Ba}_{0.5}\text{Sr}_{0.5}\text{Co}_{0.8}\text{Fe}_{0.2}\text{O}_{3-\delta}$  (BSCF) tubes (400 mm long, 10 mm outer diameter, 1 mm wall thickness) were purchased from Fraunhofer Institute IKTS Dresden/Hermsdorf (Germany). One of the two ends of the tube is closed by an approximately 1 mm thick disk of the same BSCF material.<sup>34</sup>

Oxygen was produced in a dead-end membrane permeator as shown in Figure 1. A stream of air, as a nitrogen/oxygen mixture, is supplied from the left to the dead end of the tube and leaves the setup as oxygen-depleted air. Oxygen permeates the MIEC tube walls via a flux of oxygen anions, which is accompanied by counterflowing electrons. Permeated oxygen leaves the setup to the right via the interior of the tube to the right. In the experiment, parts of the tube membrane were coated by a gold paste (Heraeus), except the 3 cm part near the dead end. The tube segment was painted by the Au paste, which then was sintered at 950 °C for 5 h. This procedure was applied 3-fold to obtain a dense gold film, which the oxygen can not permeate. Inspection by light microscope of the gold sealing after long-term permeation experiment revealed a still hole- and crack-free dense layer. This is consistent with the good compatibility of gold sealant with perovskite membrane as reported by Tong et al.<sup>35</sup> for 2000 h long high-temperature experiments. The uncoated part of our tube with an effective membrane area of 9.1 cm<sup>2</sup> for the outer membrane surface was placed in the middle of the oven, thus ensuring isothermal conditions. Oxygen-enriched air with 50 vol. % O<sub>2</sub> at an elevated pressure of 5 bar was fed at a rate of 500 cm<sup>3</sup>(STP)min<sup>-1</sup> to the feed side. Flow rates were controlled by gas mass-flow controllers (Bronkhorst). High-purity oxygen was produced at approximately 0.1 bar on the core/permeate side. This reduced pressure was achieved with a vacuum pump (Pfeiffer vacuum MVP 015–4). The flow of the outlet on the core/permeate side was mixed with neon (1.0 cm<sup>3</sup>(STP)min<sup>-1</sup>, 99.995%) as an internal standardization gas, which allowed the determination of the absolute flux of the permeate gas by an online coupled gas chromatograph (Agilent 7890A) that was equipped with a Carboxen 1000 column.





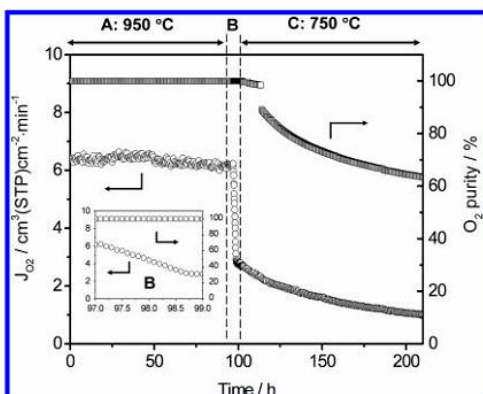


**Figure 2.** Long-term operation of oxygen production using a dead-end BSCF tube membrane at 950 and 750 °C. Shell/feed side: 50 vol % oxygen-enriched air at 5 bar with a flow rate of 500 cm<sup>3</sup>(STP) min<sup>-1</sup>. Core/permeate side: O<sub>2</sub> at approximately 0.1 bar. Inset B shows the continuous decrease of the oxygen flux from the isothermal region A at 950 °C to the isothermal region C at 750 °C. For the associated XRD results, see Figure 7; for SEM micrographs see Figure 8.

The leaking of nitrogen and oxygen through pores or cracks is assumed to be in accordance with the Knudsen diffusion mechanism. Then, for the experiment with 50 vol % oxygen-enriched air at the feed side, the fluxes of leaked nitrogen and oxygen are related by eq 1.

$$J_{N_2}^{\text{Leak}} : J_{O_2}^{\text{Leak}} = \sqrt{\frac{32}{28} \frac{0.5}{0.5}} = 1.07 \quad (1)$$

The oxygen permeation flux  $J_{O_2}$  (cm<sup>3</sup> (STP) min<sup>-1</sup> cm<sup>-2</sup>) can be calculated by eq 2, in which the leakage of oxygen is subtracted by taking into account the leakage of nitrogen.

$$J_{O_2} = \left( C_{O_2} - \frac{C_{N_2}}{1.07} \right) \frac{F}{S} \quad (2)$$

Here,  $C_{O_2}$  and  $C_{N_2}$  are the oxygen and nitrogen concentrations estimated from calibrated gas chromatograph.  $F$  is the total flow rate of the outlet on the core/permeate side, and  $S$  is the effective surface for permeation.

**Tools for Microstructure Analysis.** The XRD data were collected in a  $\theta/2\theta$  geometry on a Bruker D8 Advance instrument equipped with a Cu K $\alpha$  radiation at 40 kV and 40 mA. A receiving slit of 0.05 mm was used and data were collected in step-scan mode in the  $2\theta$  range of  $20^\circ < 2\theta < 80^\circ$  at intervals of  $0.02^\circ$ . Scanning electron microscopy (SEM) was performed with a JEOL JSM-6700F at a low excitation voltage of 2 kV for imaging with secondary electrons and at 5 kV for backscattered-electron channelling contrast imaging. Specimens for the latter purpose were prepared using a Buehler VibroMet 2 vibratory polisher. Transmission electron microscopy (TEM) was performed on a JEOL JEM-2100F that was equipped with a Gatan Imaging Filter (GIF 2001) and an Oxford Instruments INCA TEM 200 light-element energy-dispersive X-ray (EDX) spectrometer. Scanning transmission electron microscopy (STEM) imaging was performed on appropriate bright- and dark-field detectors. TEM imaging, selected area electron diffraction (SAED), and electron energy-loss spectroscopy (EELS) were performed on the charge-coupled device (CCD) camera of the GIF.

### 3. RESULTS AND DISCUSSION

#### Permeation Behavior of Dead-End BSCF Tube Membrane.

The reliability of the dead-end BSCF tube membrane in the

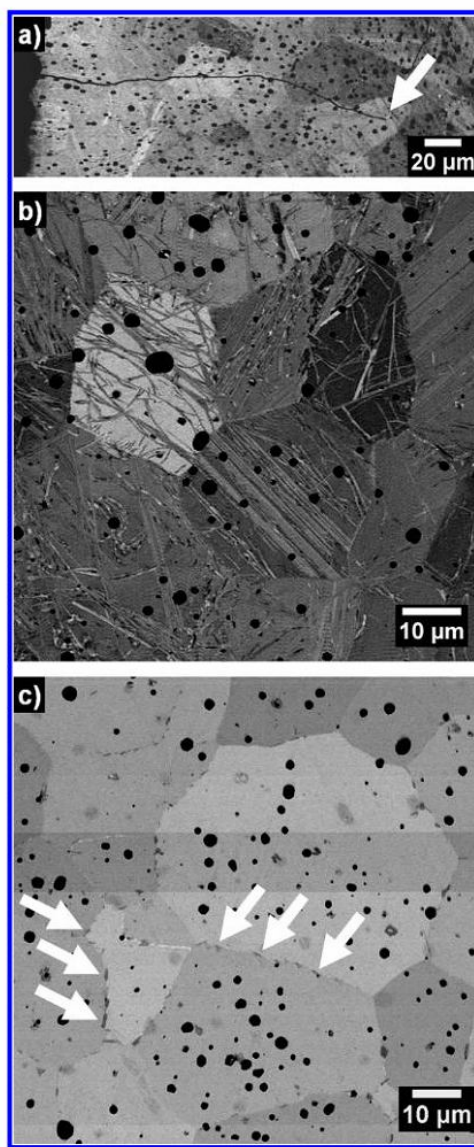


**Figure 3.** Backscattered-electron channelling contrast images of the BSCF perovskite tube membrane cross-section after the long-term permeation experiment shown in Figure 2 (100 h at 950 °C, 120 h at 750 °C): (a) Overview of shell/feed side showing an approximately 200  $\mu\text{m}$  long crack running into the membrane from the left (shell/feed side). The crack tip is marked by an arrow. (b) Area close to the shell/feed side showing secondary phases criss-crossing BSCF grains. (c) Area close to core/permeate side showing secondary phases in the grain boundaries. Some phases are marked by arrows. Note that the closed porosity of the ceramic membrane appears as black dots.

production of oxygen was evaluated with a feed of 50 vol % oxygen-enriched air at 5 bar and a reduced pressure of approximately 0.1 bar on the permeate side at 950 and 750 °C, as shown in Figure 2. The oxygen-enriched air with different oxygen contents can be produced by using either the organic polymeric

hollow-fiber membranes<sup>36</sup> or perovskite hollow-fiber membranes.<sup>15,37</sup> At 950 °C, the oxygen-permeation flux and the oxygen purity were found to be constant over a time period of 100 h. A high oxygen purity of almost 100 vol % (gas chromatograph did not detect any N<sub>2</sub>) and a stable oxygen permeation flux of 6.3 cm<sup>3</sup>cm<sup>-2</sup>min<sup>-1</sup> were observed. The high oxygen purity indicates that the gas leakage is negligible, even at a pressure difference of approximately 6 bar, because of the perfect connection between the BSCF tube and the BSCF disk that forms the dead-end part of the membrane. Moreover, the dead-end tube membrane's geometry can solve the problem of high-temperature sealing by allowing the use of silicon rings outside the high-temperature zone. A stable performance of a dead-end BSCF tube membrane with silver as sealant at 925 °C has also been reported by Zhu et al.<sup>18</sup>

When the temperature was slowly decreased by 2 °Cmin<sup>-1</sup> from 950 to 750 °C, the oxygen purity initially remains constant at 100%, but the oxygen-permeation flux continuously decreases from 6.6 to 2.8 cm<sup>3</sup>(STP) cm<sup>-2</sup> min<sup>-1</sup> (inset in Figure 2). At 750 °C, the oxygen-permeation flux decreases continuously with time from 2.8 cm<sup>3</sup>(STP) cm<sup>-2</sup> min<sup>-1</sup> to 1.0 cm<sup>3</sup>cm<sup>-2</sup>min<sup>-1</sup> after 120 h. This observation is in good agreement with the findings of Shao et al.,<sup>24</sup> van Veen et al.,<sup>27</sup> and Efimov et al.<sup>31</sup> At 750 °C, first the oxygen purity decreases slowly over 10 h. This initial decrease of in the oxygen concentration may be due to a low constant nitrogen flux that results from small sealing imperfections or membrane pin holes, which become increasingly significant if the oxygen flux is decreased by a decrease in the temperature. After approximately 10 h at 750 °C, a sudden decrease in the oxygen purity is observed which is related to the formation of small cracks in the membrane. The further growth of the cracks causes a further decrease of the oxygen purity with time, as shown in Figure 2. Cracks run radially from the perimeter (feed side) into the tube membrane and can be observed in SEM micrographs. After the permeation experiment shown in Figure 2 (100 h at 950 °C and 120 h at 750 °C) was completed, a cross-section of the tube membrane was prepared by vibration polishing to preserve the material's crystallinity to the very surface of the specimen so that backscattered-electron channelling contrast imaging could be applied. Figure 3a shows an overview of the shell/feed side with a crack approximately 200 μm in length. The crack appears black in contrast, because no material is present in the crack opening that could scatter the electrons to the detector. The same holds true for closed porosity, which also is seen as black.

**Microstructure Overview.** At the higher magnification in Figure 3b, orientation-dependent backscattered-electron channelling contrast allows not only individual BSCF grains with sizes of approximately 20–40 μm to be distinguished but also secondary phases in the grain boundaries and, more significantly, those running through the bulk grains. These secondary phases are predominantly observed in a region up to approximately 200 μm below the shell/feed side, which constitutes the side with the highest oxygen chemical potential in the permeation experiment. Remember, cracks are observed in the same region. Obviously, the formation of secondary phases leads to an accumulation of internal stresses. At the core/permeate side, which is shown in Figure 3c, the situation is different. Here, microstructure changes are essentially restricted to the grain boundaries that are decorated by platelike crystals. Almost no secondary phases run through the BSCF grains.

**Microstructure at the Core/Permeate Side.** The situation at the core/permeate side is shown in more detail in Figure 4a by

bright-field TEM. The distribution of secondary phases at the boundary between BSCF grains 1 and 2 (A and B) is sketched in the STEM micrograph of Figure 4b. Based on the elemental distributions of Figures 4c to g, phase B is enriched in oxygen and in cobalt but depleted in strontium, as compared to BSCF. By quantification of the local EDX spectra, a 2:1 ratio of B-site to A-site cations was observed. This ratio is consistent with a complex trigonal oxide of approximate composition Ba<sub>1-x</sub>Sr<sub>x</sub>Co<sub>2-y</sub>Fe<sub>y</sub>O<sub>5-δ</sub>, as reported by Efimov et al.<sup>31</sup> The compositional parameters of approximately  $x = 0.15$  and  $y = 0.25$ , however, vary locally. In the A regions, smaller crystallites with diameters less than 200 nm were formed. These crystallites decorate the interface between the platelet of phase B and grain 1, but are also observed to the lower right. Their occurrence correlates with A regions that are almost free of iron (see Figure 4g). The quantification results of local EDX spectra show less than 1 at % iron. Enrichments of cobalt (Figure 4f) and oxygen (Figure 4c) are observed. It is noteworthy that barium and strontium content varies locally in the opposite manner (compare Figures 4d and e). With reference to Efimov et al.<sup>31</sup> and Mueller et al.,<sup>33</sup> we postulate that hexagonal perovskites Ba<sub>0.5±x</sub>Sr<sub>0.5±x</sub>CoO<sub>3-δ</sub> (with  $x \approx 0.1$ ) were formed in region A. Although a strontium-enriched hexagonal perovskite is not expected according to other investigators, Figures 4d, e, and g clearly indicate that iron depleted regions correlate with different barium and strontium contents.

The different phases in the grain-boundary region appear with characteristic oxygen fine structures in the EEL spectra of Figure 5a. The O–K fine structure from BSCF corresponds to the room-temperature spectrum reported by Arnold et al.<sup>37</sup> and the one for the hexagonal perovskite (A) to the X-ray absorption near-edge structure (XANES) observed by Harvey et al.<sup>39</sup> Hexagonal perovskite is indicated by the absence of the Fe-L<sub>2,3</sub> signal, which can be seen only very weakly in Figure 5a. The oxygen fine structure of Ba<sub>1-x</sub>Sr<sub>x</sub>Co<sub>2-y</sub>Fe<sub>y</sub>O<sub>5-δ</sub> (B) is published here for the first time. Some interesting features are noted at the Co-L<sub>2,3</sub> and Ba-M<sub>4,5</sub> edges. The Ba-M<sub>5</sub> white line appears constant at 788 eV for all phases and can be used as an internal standard (see Arnold et al.<sup>36</sup> and Efimov et al.<sup>31</sup>) to estimate shifts in the Co-L<sub>3</sub> edge. For BSCF, differences between the maxima of Ba-M<sub>5</sub> and Co-L<sub>3</sub> result in an estimate of 4.4 eV, which is smaller than the value that can be read from the spectrum reported by Efimov et al.<sup>31</sup> This result suggests a stronger oxidation of cobalt in BSCF in our experiment as a result of our use of high-pressure oxygen-enriched air on the feed side of the membrane. The increased oxidation of cobalt also explains why the shift of Co-L<sub>3</sub> to the right is only approximately 0.3 eV, compared to 0.7 eV in the experiment by Efimov et al.<sup>31</sup> More interesting is the observation that the Co-L<sub>3</sub> maximum for the hexagonal perovskite is shifted by 1.0 eV to the right as compared to BSCF. This result indicates that the oxidation state of cobalt is the highest in the hexagonal phase, which leads us directly to the reason for the phase decomposition of BSCF under the chosen operating conditions: the decomposition is induced by an unsuitable valence and spin state of cobalt, which is exposed to the strongly oxidizing conditions in the IT range and is associated with a small ionic radius that makes cobalt unstable in the cubic perovskite structure, as reported by Arnold et al.<sup>29</sup> and Efimov et al.<sup>31</sup> The temperature-dependent EELS experiment by Arnold et al.<sup>38</sup> also suggests a 3+ valence and low-spin state of cobalt in BSCF in the IT range. Our EELS observation (Figure 5b) of higher oxidation states of cobalt in the grain-boundary phases, as compared to BSCF, correlates

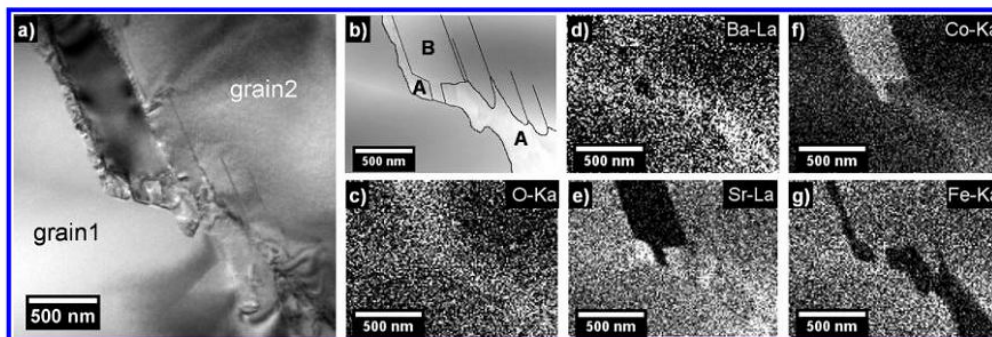


Figure 4. TEM investigation near the core/permeate side showing a grain boundary region. (a) Bright-field TEM, (b) annular dark-field STEM with grain-boundary phases labeled A and B. (c–g) EDXS elemental distributions (bright contrast correlates with high elemental concentration).

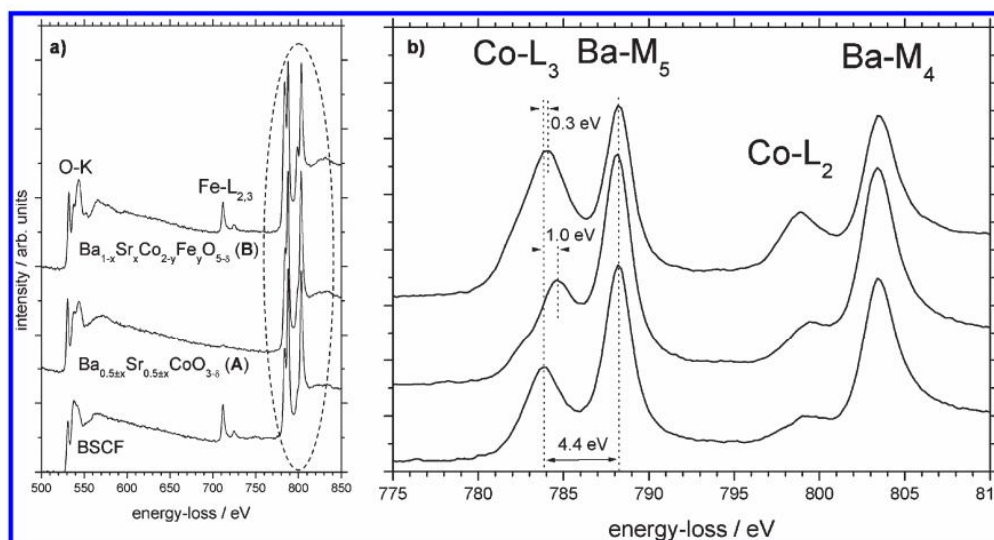
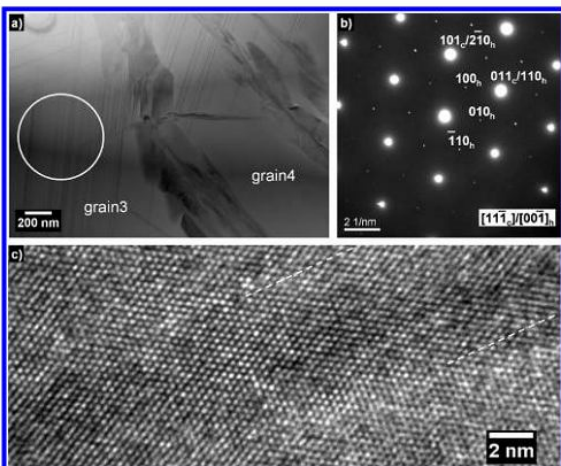


Figure 5. EEL spectra of BSCF and grain-boundary phases near the core/permeate side (see Figure 4b) showing (a) O–K, Fe–L<sub>2,3</sub>, Co–L<sub>2,3</sub>, and Ba–M<sub>4,5</sub> ionization edges; and (b) a close-up of the Co–L<sub>2,3</sub> and Ba–M<sub>4,5</sub> ionization edges.

with the higher amount of oxygen observed in the EDXS elemental distribution in Figure 4c.

**Microstructure at the Shell/Feed Side.** In agreement with the SEM micrographs in Figure 3, the STEM bright-field micrograph of Figure 6a shows that, near the shell/feed side, microstructure changes are not restricted to the grain boundaries. In the grain boundaries, the same phases are observed as those near the core/permeate side. However, the hexagonal phase (A) is the major component relative to the heavily cobalt-enriched trigonal phase (B), which was observed to be wrapped by phase A. Both phase A and phase B form extended platelets and separate grains 3 and 4 in Figure 6a. However, they are also found running straight through grain 4 almost parallel to the grain boundary. More interesting, however, are the dense arrays of hexagonal perovskite phase (A) that are seen in both grains, which differs from our previous observations. The circle in grain 3 marks the area from which the SAED pattern in Figure 6b was observed. The diffraction pattern shows common strong reflections from cubic BSCF and hexagonal perovskite (A) and additional weak reflections that

are attributed only to hexagonal perovskite (A). The pattern was indexed in the same manner reported by Mueller et al.,<sup>33</sup> indicating that the close-packed layers of the cubic and hexagonal perovskite are arranged in parallel. Moreover, a comparison of Figures 6a and b indicates that the hexagonal lamellae are grown along cubic  $\langle 110 \rangle_c$  directions, which are denoted explicitly as  $[101]_c$  and  $[011]_c$  here. The cubic  $\langle 110 \rangle_c$  directions coincide with the average global directions of oxygen migration in cubic perovskite.<sup>40</sup> Therefore, the hexagonal lamellae formed in our experiments correlate with oxygen pathways in cubic BSCF. The hexagonal lamellae intergrew coherently with the cubic BSCF grains as is evident from in the HRTEM micrograph in Figure 6c. The crystals are observed in the projection along  $[111]_c$  such that columns of equal amounts of A-site and B-site cations are observed edge-on and appear as bright spots. Columns of oxygen are located halfway between the bright spots; however, they cannot be seen because of their weak scattering. In any event, the brightness of the spots that represent cationic columns varies locally, which suggests local compositional variations.



**Figure 6.** TEM investigation near the shell/feed side showing a grain-boundary region: (a) Bright-field STEM, (b) SAED pattern of encircled area in a, and (c) HRTEM of hexagonal lamella in cubic BSCF along  $[111]_c$ . Lamella is located between the dashed lines.

**Discussion of BSCF's Partial Decomposition.** With the findings concerning the local oxygen content and the cobalt valence/spin state, as previously discussed in context with Figures 4 and 5 (core/permeate side), and 6 (shell/feed side), we can identify the appearance of the hexagonal perovskite arrays with migration channels of oxygen in cubic BSCF perovskite, which exhibits the most strongly oxidizing local conditions. In addition, the evolved microstructure strongly suggests that the ideal situation of a rigid metal cationic framework has not been achieved, in that only the anionic oxygen is mobile.<sup>41</sup> Now, the cationic cobalt in BSCF appears to migrate to regions of higher oxygen concentration (oxygen migration pathways). There, cobalt changes its valence and spin state, and then the perovskite structure transforms. To expand the findings of Arnold et al.<sup>29</sup> and Efimov et al.,<sup>31</sup> we identify an unsuitable valence and spin state of cobalt as the main reason for the partial decomposition of BSCF while operating at 750 °C, as opposed to 950 °C. This view is supported by the observation (see Figure 3) that the microstructure changes are more severe at the oxygen-supply side (most strongly oxidizing conditions) as compared to the permeate side. Moreover, observation that the partial decomposition is restricted to the grain boundaries at the core/permeate side points out that the grain boundary environment may be significantly different from the grain volume. The preceding arguments lead then to the conclusion that, at the core/permeate side, oxygen content in the grain boundaries is higher than in the grain volume. Probably, here oxygen is transported preferentially in the grain boundary regions.

**More Aspects of Evolved Microstructure.** The phases identified by TEM analysis are also observed in the XRD patterns, which were collected on scans of membrane surfaces. Figure 7 shows the XRD patterns of the BSCF membrane before and after the aforementioned long-term operation. The crystal structures on both the feed and permeate sides of the starting BSCF membrane are a pure cubic-perovskite phase (Figure 3a). After the long-term operation, the cubic BSCF perovskite remains as the major phase. However, a hexagonal perovskite  $\text{Ba}_{0.5\pm x}\text{Sr}_{0.5\pm x}\text{CoO}_{3-\delta}$  (A) has formed on the shell/feed side. Rebeilleau-Dassonneville et al.<sup>28</sup> and Efimov et al.<sup>31</sup> have observed the corresponding signals of

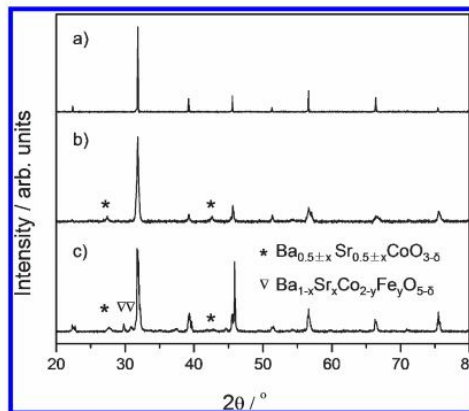


**Figure 7.** XRD patterns of the BSCF tube membrane: (a) shell-side surface (which is identical to the core-side surface) before permeation, (b) shell/feed-side surface, and (c) core/permeation-side surface after the long-term permeation experiment shown in Figure 2 (100 h at 950 °C, 120 h at 750 °C). For SEM micrographs, see Figure 8.

$\text{Ba}_{0.5\pm x}\text{Sr}_{0.5\pm x}\text{CoO}_{3-\delta}$  (A) in XRD patterns and Efimov identified the chemical composition of this phase by STEM-EDXS as  $\text{Ba}_{0.6}\text{Sr}_{0.4}\text{CoO}_{3-\delta}$ . Here, however, the barium and strontium contents vary locally and the phase can be strontium-enriched (see Figure 4d and e). On the shell/feed side, the content of trigonal  $\text{Ba}_{1-x}\text{Sr}_x\text{Co}_{2-y}\text{Fe}_y\text{O}_{5-\delta}$  (B) is too small to be detected by XRD. However, on the core/permeate side, in addition to besides  $\text{Ba}_{0.5\pm x}\text{Sr}_{0.5\pm x}\text{CoO}_{3-\delta}$  (A),  $\text{Ba}_{1-x}\text{Sr}_x\text{Co}_{2-y}\text{Fe}_y\text{O}_{5-\delta}$  (B) is also clearly seen as an additional phase. According to Efimov et al.,<sup>31</sup> trigonal  $\text{Ba}_{1-x}\text{Sr}_x\text{Co}_{2-y}\text{Fe}_y\text{O}_{5-\delta}$  (B) can be indexed in space group  $R\bar{3}m$  and is structurally related to  $\text{BaCo}_{10}\text{O}_{17}$ , which was reported by Sun et al.<sup>42</sup> Because of the structural similarity,  $\text{Ba}_{1-x}\text{Sr}_x\text{Co}_{2-y}\text{Fe}_y\text{O}_{5-\delta}$  (B) is assumed to give an XRD pattern similar to that of  $\text{BaCo}_{10}\text{O}_{17}$ , even though only the structure of the latter phase has been fully resolved thus far (ICSD collection code 240501). We emphasize that the B-site (cobalt and iron) to A-site (barium and strontium) ratio we observed in our analysis is too small to match a stoichiometry of  $\text{BaCo}_{10}\text{O}_{17}$ . The main reflection of cubic BSCF perovskite at approximately 32° seems to be broadened. The additional intensities can be attributed to the aforementioned additional phases of hexagonal and trigonal symmetry, which evolve during the partial decomposition of the bulk cubic BSCF phase.

To sort our findings, let's have a look on Figure 8, which presents secondary-electron micrographs of the shell/feed side surface, the cross-sectional area near the shell/feed side, and the core/permeate-side surface of the BSCF membrane before and after the oxygen-permeation experiment of Figure 2 (100 h at 950 °C and 120 h at 750 °C). After the long-term oxygen-permeation experiment in the IT range, secondary phases protrude from the bulk grains at the surface of the shell/feed side (see Figure 8d). In the corresponding broken cross-section (Figure 8e), an approximately 1 μm thick grain-boundary phase is clearly observed. According to the XRD results (see Figure 7b) and the aforementioned TEM results (Figure 6), the secondary phase is primarily the hexagonal perovskite  $\text{Ba}_{0.5\pm x}\text{Sr}_{0.5\pm x}\text{CoO}_{3-\delta}$  (A). At the core/permeate side (Figure 8f), decoration of grain boundaries is clearly visible, the decorations are composed of trigonal  $\text{Ba}_{1-x}\text{Sr}_x\text{Co}_{2-y}\text{Fe}_y\text{O}_{5-\delta}$  (B) and hexagonal perovskite  $\text{Ba}_{0.5\pm x}\text{Sr}_{0.5\pm x}\text{CoO}_{3-\delta}$  (A), as was analyzed in

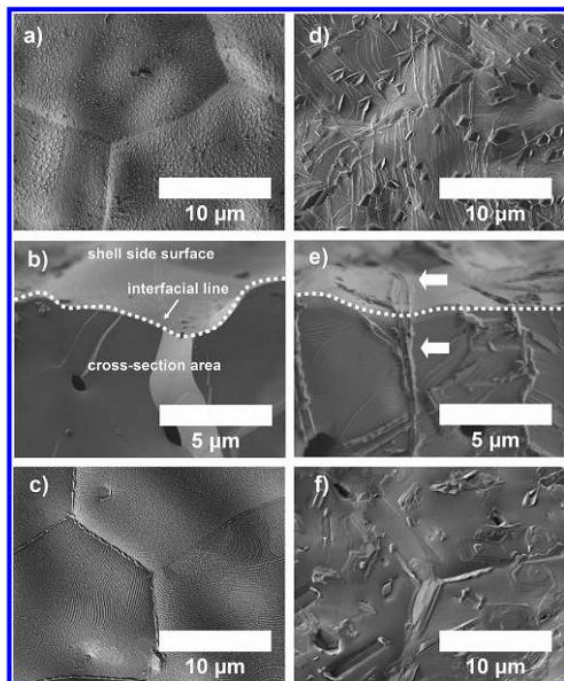


**Figure 8.** Microstructures of the BSCF perovskite tube membrane before and after the oxygen permeation experiment: Surface view of shell/feed side (a) before and (d) after permeation; broken cross-sectional area near the shell/feed side (b) before and (e) after permeation; surface view of the core/permeation side (c) before and (f) after permeation. For the permeation experiment, see Figure 2; for the XRD patterns, see Figure 7c. White arrows in e mark secondary phase at grain boundary.

context with Figure 4. In the vicinity of internal porosity, hexagonal features (A) also appear inside the grains.

## CONCLUSIONS

The long-term phase stability and oxygen permeability of dead-end BSCF tube membranes (400 mm long, 10 mm outer diameter, 1 mm wall thickness) were studied under practice-relevant permeation conditions at 950 and 750 °C. A high oxygen purity of almost 100 vol. % and a stable oxygen-permeation flux were observed during the long-term operation for 100 h at 950 °C. However at 750 °C, the oxygen-permeation flux continuously decreases with time, and the BSCF tube membrane is structurally unstable. The phase instability of BSCF is due to a partial decomposition of the bulk cubic perovskite phase into a hexagonal perovskite,  $\text{Ba}_{0.5\pm x}\text{Sr}_{0.5\pm x}\text{CoO}_{3-\delta}$ , and a trigonal mixed oxide  $\text{Ba}_{1-x}\text{Sr}_x\text{Co}_{2-y}\text{Fe}_y\text{O}_{5-\delta}$ . At the core/permeate side, the formation of secondary phases is predominantly restricted to the grain boundaries. At the shell/feed side, which constitutes the region of highest oxygen chemical potential during dynamic oxygen flux through the BSCF membrane material, the formation of secondary phases is most pronounced. Here, the secondary phase is mainly the cobalt-enriched hexagonal perovskite, which is not only found in grain boundaries, but also runs through the bulk grains, leading to important internal stresses, that give rise to membrane cracking at the oxygen-feed side. The stronger formation of secondary

phases at higher local oxygen chemical potentials during dynamic oxygen flux suggests that the valence and spin state of the most flexible redoxable cation (i.e., cobalt) is the key to an understanding of BSCF's decomposition in the intermediate temperature range. The phase stability of BSCF (i.e., the proper redox states of cobalt) can be maintained by operating BSCF membranes in the high-temperature regime (950 °C).

## AUTHOR INFORMATION

### Corresponding Author

\*E-mail: armin.feldhoff@pci.uni-hannover.de.

## ACKNOWLEDGMENT

The EU is thanked for financing in the 7th Framework Program the IP Innovative Catalytic Technologies & Materials for the Next Gas to Liquid Processes (NEXT-GTL). The State of Lower Saxony is thanked for financing in frame of a bottom-up project to found the Niedersächsisch Technische Hochschule (NTH). G. Centi, Messina, and G. Iaquaniello, Rome, are thanked for their stimulating discussions. The authors appreciate Professor H. H. Wang in Guangzhou for fruitful discussions. The authors thank Dr. R. Kriegel from the Fraunhofer Institute for Ceramic Technologies and Systems (IKTS) for making the BSCF tube and for his helpful remarks.

## REFERENCES

- (1) Bose, A. C., *Inorganic Membranes for Energy and Environmental Applications*; Springer: New York, 2009; p 4.
- (2) Lide, D. R. *CRC Handbook of Chemistry and Physics*; CRC Press: Boca Raton, FL, 1997.
- (3) Armstrong, P. A.; Bennet, D. L.; Fprster, E. P. T.; van Stein, E. E. ITM Oxygen for Gasification. In *2004 Gasification Technology Conference: New Technologies Development*; Washington, D.C., Oct 3–6, 2004; Gasification Technologies Council: Arlington, VA, 2004.
- (4) Bouwmeester, H. J. M. *Catal. Today* **2003**, *82*, 141.
- (5) Tsai, C. Y.; Dixon, A. G.; Moser, W. R.; Ma, Y. H. *AIChE J.* **1997**, *43*, 2741.
- (6) Shao, Z. P.; Dong, H.; Xiong, G. X.; Gong, Y.; Yang, W. S. *J. Membr. Sci.* **2001**, *183*, 181.
- (7) Yang, W. S.; Wang, H. H.; Zhu, X. F.; Lin, L. W. *Top. Catal.* **2005**, *35*, 155.
- (8) Caro, J.; Caspary, K. J.; Hamel, C.; Hoting, B.; Kolsch, P.; Langanke, B.; Nassauer, K.; Schiestel, T.; Schmidt, A.; Schomacker, R.; Seidel-Morgenstern, A.; Tsotsas, E.; Voigt, I.; Wang, H. H.; Warsitz, R.; Werth, S.; Wolf, A. *Ind. Eng. Chem. Res.* **2007**, *46*, 2286.
- (9) Jiang, H. Q.; Cao, Z. W.; Schirrmeister, S.; Schiestel, T.; Caro, J. *Angew. Chem. Int. Ed.* **2010**, *49*, 5656.
- (10) Jiang, H. Q.; Liang, F. Y.; Czuprat, O.; Efimov, K.; Feldhoff, A.; Schirrmeister, S.; Schiestel, T.; Wang, H. H.; Caro, J. *Chem.—Eur. J.* **2010**, *16*, 7898.
- (11) Jiang, H. Q.; Wang, H. H.; Werth, S.; Schiestel, T.; Caro, J. *Angew. Chem. Int. Ed.* **2008**, *47*, 9341.
- (12) Jiang, H. Q.; Wang, H. H.; Liang, F. Y.; Werth, S.; Schiestel, T.; Caro, J. *Angew. Chem. Int. Ed.* **2009**, *48*, 2983.
- (13) Jiang, H. Q.; Xing, L.; Czuprat, O.; Wang, H. H.; Schirrmeister, S.; Schiestel, T.; Caro, J. *Chem. Commun.* **2009**, 6738.
- (14) Wang, H. H.; Kolsch, P.; Schiestel, T.; Tablet, C.; Werth, S.; Caro, J. *J. Membr. Sci.* **2006**, *284*, 5.
- (15) Liang, F. Y.; Jiang, H. Q.; Schiestel, T.; Caro, J. *Ind. Eng. Chem. Res.* **2010**, *49*, 9377.
- (16) Tan, X. Y.; Wang, Z. G.; Meng, B.; Meng, X. X.; Li, K. *J. Membr. Sci.* **2010**, *352*, 189.
- (17) Ito, W.; Nagai, T.; Sakon, T. *Solid State Ionics* **2007**, *178*, 809.

- (18) Zhu, X. F.; Sun, S. M.; Cong, Y.; Yang, W. S. *J. Membr. Sci.* **2009**, *345*, 47.
- (19) Teraoka, Y.; Zhang, H. M.; Furukawa, S.; Yamazoe, N. *Chem. Lett.* **1985**, 1743.
- (20) Yang, L.; Wu, Z. T.; Jin, W. Q.; Xu, N. P. *Ind. Eng. Chem. Res.* **2004**, *43*, 2747.
- (21) Luo, H. X.; Tian, B. B.; Wei, Y. Y.; Wang, H. H.; Jiang, H. Q.; Caro, J. *AIChE J.* **2010**, *56*, 604.
- (22) Martynczuk, J.; Liang, F. Y.; Arnold, M.; Sepelak, V.; Feldhoff, A. *Chem. Mater.* **2009**, *21*, 1586.
- (23) Efimov, K.; Halfer, T.; Kuhn, A.; Heitjans, P.; Caro, J.; Feldhoff, A. *Chem. Mater.* **2010**, *22*, 1540.
- (24) Shao, Z. P.; Yang, W. S.; Cong, Y.; Dong, H.; Tong, J. H.; Xiong, G. X. *J. Membr. Sci.* **2000**, *172*, 177.
- (25) Shao, Z. P.; Haile, S. M. *Nature* **2004**, *431*, 170.
- (26) Kriegel, R.; Kircheisen, R.; Töpfer, J. *Solid State Ionics* **2010**, *181*, 64.
- (27) van Veen, A. C.; Rebeilleau, M.; Farrusseng, D.; Mirodatos, C. *Chem. Commun.* **2003**, 32.
- (28) Rebeilleau-Dassonneville, M.; Rosini, S.; van Veen, A. C.; Farrusseng, D.; Mirodatos, C. *Catal. Today* **2005**, *104*, 131.
- (29) Arnold, M.; Gesing, T. M.; Martynczuk, J.; Feldhoff, A. *Chem. Mater.* **2008**, *20*, 5851.
- (30) Švarcová, S.; Wiik, K.; Tolchard, J.; Bouwmeester, H. J. M.; Grande, T. *Solid State Ionics* **2008**, *178*, 1787.
- (31) Efimov, K.; Xu, Q. A.; Feldhoff, A. *Chem. Mater.* **2010**, *22*, 5866.
- (32) Arnold, M.; Wang, H.; Martynczuk, J.; Feldhoff, A. *J. Am. Ceram. Soc.* **2007**, *90*, 3651.
- (33) Mueller, D. N.; De Souza, R. A.; Weirich, T. E.; Roehrens, D.; Mayer, J.; Martin, M. *Phys. Chem. Chem. Phys.* **2010**, *12*, 10320.
- (34) Kriegel, R.; Kircheisen, R. DE 10 2009 050 019 B3, 2011.03.17, 2009.
- (35) Tong, J.; Yang, W.; Cai, R.; Zhu, B.; Lin, L. *Catal. Lett.* **2002**, *78*, 129.
- (36) Spillman, R. Economics of Gas Separation Membrane Processes. In *Membrane Science and Technology*; Noble, R. D., Stern, S. A., Eds.; Elsevier: New York, 1996; Vol. 2, p 269.
- (37) Wang, H. H.; Werth, S.; Schiestel, T.; Caro, J. *Angew. Chem., Int. Ed.* **2005**, *44*, 6906.
- (38) Arnold, M.; Xu, Q.; Tichelaar, F. D.; Feldhoff, A. *Chem. Mater.* **2009**, *21*, 635.
- (39) Harvey, A. S.; Yang, Z.; Infortuna, A.; Beckel, D.; Purton, J. A.; Gauckler, L. J. *J. Phys.: Condens. Matter* **2009**, *21*, 015801.
- (40) Yashima, M., Structural disorder, diffusion pathway of mobile oxide ions, and crystal structure in perovskite-type oxides and related materials. In *Perovskite Oxide for Fuel Cells*, Ishihara, T., Ed.; Springer: Dordrecht, The Netherlands, 2009; p 117.
- (41) Goodenough, J. B., Crystalline solid electrolytes II: Materials design. In *Solid State Electrochemistry*; Bruce, P. G., Ed.; Cambridge University Press: Cambridge, U.K., 1995; p 43.
- (42) Sun, J. L.; Yang, M.; Li, G. B.; Yang, T.; Liao, F. H.; Wang, Y. X.; Xiong, M.; Lin, J. H. *Inorg. Chem.* **2006**, *45*, 9151.

## **Chapter 3**

### **3. Preparation and characterization of alkaline-earth metals-free CO<sub>2</sub>-stable dual phase membranes**

#### **3.1 Summary**

As mentioned in Section 1.1 and section 1.3.2, in the real process conditions which can include the presence of highly concentrated CO<sub>2</sub>, a dense oxygen separation membrane should possess the following properties: (i) high oxygen permeation flux, (ii) structural stability within appropriate ranges of temperature and oxygen partial pressure, (iii) sufficient mechanical strength and chemical compatibility. Single phase perovskite membranes were hard to meet all the above requirements. One technique to produce CO<sub>2</sub>-stable membranes is to develop alkaline-earth metals-free dual phase membranes. However, many factors affect the properties of the dual phase membranes, like the preparation method, the ratio of two phases or the sintering temperatures. In this chapter, a series of alkaline-earth metals-free CO<sub>2</sub>-stable dual phase membranes (e.g. NFO-CGO, FO-CGO and MCO-CPO) which are composed of a pure oxygen ionic conductor and pure electronic conductor, were developed and studied. Special attention is paid to the CO<sub>2</sub> stability. The effects of the preparation method, ratios of two phase and sintering temperatures on the properties of the dual phase membranes were also demonstrated in detail.

In the first and second article, a novel CO<sub>2</sub>-stable 40NFO-60CGO dual phase membrane was developed using three different preparation ways (i) Powder mixing in a mortar by hand, (ii) Powder mixing by ball-milling and (iii) Direct one-pot EDTA-citric acid sol-gel synthesis. XRD and TEM results showed that both phases were well separated and no interphase was detected. The one-pot method gave the best homogeneous grain size distribution and the smallest mean grain size, thus the 40NFO-60CGO membrane obtained with this method showed the highest oxygen fluxes. At 1000 °C using He and CO<sub>2</sub> as sweep gases, the oxygen permeation fluxes through the membrane prepared with the one-pot material were 0.31 and 0.27 ml/min·cm<sup>2</sup>, respectively. The oxygen permeation fluxes through 40NFO-60CGO stabilized in steady state at



0.31 ml/min·cm<sup>2</sup> for more than 100 h at 1000 °C and no decrease of the oxygen permeation flux was observed, which confirmed that 40NFO-60CGO dual phase membranes are CO<sub>2</sub>-stable.

In the second article, direct one-pot single-step EDTA-citric acid sol-gel synthesis was used to prepare the new CO<sub>2</sub>-stable oxygen-permeable FO-CGO dual phase membranes with the composition  $\chi$  wt. % FO - (100 -  $\chi$ ) wt. % CGO ( $\chi = 25, 40, 50$ ). XRD results confirmed that all the FO-CGO dual phase composed of FO and CGO phase, no other phase was formed. The composition 40FO-60CGO displayed the highest oxygen permeability. The 40FO-60CGO dual phase membrane was CO<sub>2</sub>-stable, which was proven by the *in-situ* XRD and long-term oxygen permeation measurements in the presence of CO<sub>2</sub> in high concentration. The 40FO-60CGO dual phase was sintered at 1300 °C, 1325 °C, and 1350 °C, respectively. It was found that a high sintering temperature had a negative effect on the oxygen permeation flux for 40FO-60CGO dual phase membranes.

In the third article, 40MCO-60CPO dual phase membrane was prepared via a one-pot single-step glycine-nitrate combustion process (GNP). An oxygen permeation flux of 0.2 ml/min·cm<sup>2</sup> was obtained through the uncoated 40MCO-60CPO membrane with a thickness of 0.5 mm using pure CO<sub>2</sub> as sweep gas. No change of the oxygen permeation flux was observed for more than 60 h when pure CO<sub>2</sub> was used as sweep gas, which indicates that 40MCO-60CPO dual phase membranes are CO<sub>2</sub>-stable.

## **3.2 CO<sub>2</sub>-stable and cobalt-free dual phase membrane for oxygen separation**

Huixia Luo, Konstantin Efimov, Heqing Jiang, Armin Feldhoff, Haihui Wang and Jürgen Caro

**Angew. Chem.** 2011, *123*, 785; **Angew. Chem. Int. Ed.** 2011, *50*, 759.

Gas Separation

## CO<sub>2</sub>-Stable and Cobalt-Free Dual-Phase Membrane for Oxygen Separation\*\*

Huixia Luo, Konstantin Efimov, Heqing Jiang, Armin Feldhoff, Haihui Wang,\* and Jürgen Caro\*

The increase in carbon dioxide emissions is considered to be the main contribution to global warming. Therefore, there is an urgent need to reduce the emissions of CO<sub>2</sub> into the atmosphere. Recently, CO<sub>2</sub> capture and storage technologies to reduce the CO<sub>2</sub> emissions from coal-fired power plants have gained the attention of decision makers in governments, industry, and academia. There are three major concepts for CO<sub>2</sub> sequestration: post-combustion capture, pre-combustion separation, and oxyfuel techniques.<sup>[1]</sup> MIECMs, which are ceramic membranes with mixed oxygen ionic and electronic oxygen conductivity, have gained increasing attention owing to their potential applications in oxygen supply<sup>[2]</sup> to power stations for CO<sub>2</sub> capture according to the oxyfuel concept.<sup>[3]</sup> This concept involves burning natural gas with nitrogen-free oxygen, thus allowing CO<sub>2</sub> to be sequestered after steam condensation. Dense MIECMs are promising candidates for this oxygen separation from air. However, when MIECMs are used for this purpose, some of the CO<sub>2</sub> is recycled and used as the sweep gas for the oxygen separation, simultaneously lowering the temperature in the burner. Furthermore, CO<sub>2</sub>-stable MIECMs could be promising for dry reforming and the thermal decomposition of carbon dioxide in combination with the partial oxidation of methane to syngas.<sup>[4]</sup>

Many complex oxides have been investigated as membranes for oxygen separation and in membrane reactors. However, there are two main problems for the proper application of this kind of membrane. First, perovskite membranes with cobalt doping usually show high permeability but poor stability under harsh working conditions;<sup>[5]</sup> by avoiding cobalt, the stability of MIEC membrane materials

can be enhanced.<sup>[6]</sup> Second, for numerous applications such as the oxyfuel process or hydrocarbon partial oxidations, where some CO<sub>2</sub> is formed as a byproduct of an undesired deeper oxidation, the oxygen transporting membranes must sustain their phase stability and oxygen transport properties. Usually, the perovskite-type membranes contain alkaline earth metal ions on the A site, such as barium and strontium, which tend to react with CO<sub>2</sub> and form carbonates.<sup>[7]</sup> However, when using perovskites as oxidation catalysts, the negative effect of CO<sub>2</sub> as product molecule can be reduced if the reaction is carried out in a microwave field.<sup>[8,9]</sup> Also in the case of CO<sub>2</sub> decomposition with a hydrocarbon as oxidant on the other side of the MIECM, the negative influence of CO<sub>2</sub> can be reduced. The aforementioned problems can be overcome by using a cobalt-free and alkaline-earth-metal-free dual-phase membrane, which is composed of two interpenetrating percolated networks of an oxygen conductor (solid oxide electrolyte) and an electron conductor (internally short-circuiting electrode). In an extension of this concept, the dual phases might also consist of MIECMs with deviating transfer rates for oxygen and electrons.<sup>[10]</sup>

The first dual-phase membranes were made of oxygen conductors and noble metals: (Bi<sub>2</sub>O<sub>3</sub>)<sub>0.74</sub>SrO<sub>0.26</sub>-Ag,<sup>[11]</sup> Bi<sub>1.5</sub>Y<sub>0.2</sub>Sm<sub>0.2</sub>O<sub>3</sub>-Ag,<sup>[12]</sup> Bi<sub>1.5</sub>Er<sub>0.5</sub>O<sub>3</sub>-Ag,<sup>[13]</sup> Bi<sub>1.6</sub>Y<sub>0.4</sub>O<sub>3</sub>-Ag,<sup>[14]</sup> and YSZ-Pd.<sup>[15]</sup> However, the application of these materials is limited owing to high materials costs, a mismatch of the coefficient of thermal expansion (CTE) between the ceramic and metallic phases, and poor oxygen permeabilities. In another concept, perovskite- or fluorite-type oxides are used instead of noble metals as electron conductors.<sup>[16–18]</sup> However, these dual-phase membranes have a perovskite phase as electron conductor in which the A site is often occupied by alkaline earth metals, which can be easily eroded by forming carbonates if CO<sub>2</sub> is present. Improved stability against carbonate formation can be expected if both phases are made from oxides, which contain only transition metals and/or lanthanides. Both groups of elements are very tolerant against carbonate formation as shown by thermodynamics as well as by gravimetric considerations.<sup>[19,20]</sup>

Herein, we have prepared a novel alkaline-earth-free CO<sub>2</sub>-stable and cobalt-free composite dual-phase membrane containing 40 wt % NiFe<sub>2</sub>O<sub>4</sub> with a spinel structure and 60 wt % Ce<sub>0.9</sub>Gd<sub>0.1</sub>O<sub>2–δ</sub> with a fluorite structure (abbreviated as 40NFO–60CGO). In the mixture of the two phases, NFO is the electron conductor and CGO is the oxygen-ion conductor. Phase structure and stability and also oxygen permeability were investigated under different atmospheres at high temperatures. Special attention is paid to the CO<sub>2</sub> stability.

The dual phase membrane was synthesized using powder mixing and the one-pot method. X-ray diffraction (Figure 1)

[\*] H. Luo, K. Efimov, Dr. H. Jiang, Dr. A. Feldhoff, Prof. Dr. J. Caro  
Institute for Physical Chemistry and Electrochemistry  
Leibniz University Hannover  
Callinstrasse 3–3A, 30167 Hannover (Germany)  
Fax: (+49) 511-762-19121  
E-mail: juergen.caro@pci.uni-hannover.de  
Prof. Dr. H. Wang  
School of Chemistry & Chemical Engineering  
South China University of Technology  
No. 381 Wushan Road, Guangzhou 510640 (China)  
Fax: (+86) 20-8711-0131  
E-mail: hhwang@scut.edu.cn

[\*\*] H.L. acknowledges the financial support by the China Scholarship Council (CSC) and K.E. and A.F. thank the State of Lower Saxony for the NTH bottom-up grant no. 21-71023-25-7/09. H.W. is grateful for financial support from the NSFC (no. 20706020 and U0834004) and the 973 Plan (no. 2009CB623406). The authors also acknowledge F. Steinbach and F. Liang for technical support.

Supporting information for this article is available on the WWW under <http://dx.doi.org/10.1002/anie.201003723>.

## Communications

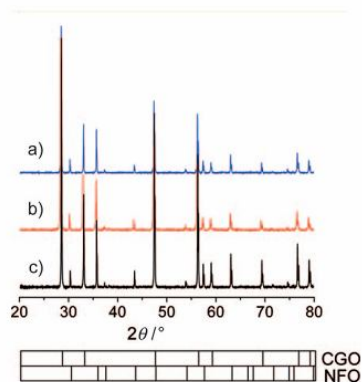


**Figure 1.** XRD pattern of 40NFO–60CGO membranes prepared by different methods and sintered at 1350 °C for 10 h in air. a) Mixing NFO and CGO powders by hand; b) direct one-pot method; c) spent one-pot membrane after the CO<sub>2</sub> stability test shown in Figure 6.

clearly confirmed that both 40NFO–60CGO membranes consist of only the two phases NFO and CGO. The unit-cell parameter of the pure phases NFO (0.83455 nm) and CGO (0.54209 nm) are almost the same as in the 40NFO–60CGO dual-phase material (NFO: 0.83350 nm, CGO: 0.54186 nm). The phase composition was stable with time. As an example, Figure 1c shows the XRD of the spent 40NFO–60CGO membrane after the long-term oxygen separation with CO<sub>2</sub> as sweep gas (Figure 6).

Figure 2 shows the results of scanning electron microscopy (SEM), back-scattered SEM (BSEM), and energy-dispersive X-ray spectroscopy (EDXS) of both membranes. For the membrane prepared by powder mixing (Figure 2a,c,e), the grain size of CGO in these composite membranes is smaller (2–4 μm) than that of NFO (3–7 μm). BSEM in particular (Figure 2c) shows that there is clustering of grains of one and the same type; that is, NFO–NFO and CGO–CGO aggregation. In comparison to powder mixing, the membrane prepared by the direct one-pot method shows much smaller grains and a higher homogenization of the NFO and CGO phases (Figure 2b,d,f). The NFO and CGO grains could be distinguished by BSEM and EDXS. The dark grains in BSEM are NFO and the light grains are CGO, as the contribution of the back-scattered electrons to the SEM signal intensity is proportional to the atomic number. The same information is provided by EDXS. The green color (dark in the black-and-white version) is an overlap of the Fe and Ni signals, whereas the yellow color (light) stems from an average of the Ce and Gd signals.

In situ XRD provides an effective and direct way to characterize the high-temperature structure changes while increasing and decreasing temperatures under certain gas atmospheres. The in situ XRD patterns of the one-pot 40NFO–60CGO in air upon increasing and decreasing the temperature from 30 °C to 1000 °C and back to 30 °C (Supporting Information, Figure S1) indicate that the CGO and NFO phases remain unchanged in the 40NFO–60CGO dual-phase materials. During the oxygen supply for coal-

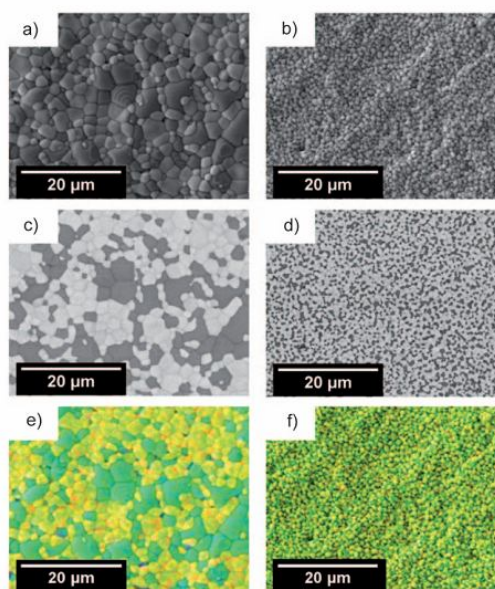


**Figure 2.** Grain structure of the surface (top view) of the 40NFO–60CGO composite membrane after sintering at 1350 °C for 10 h and prepared by different methods. Left line: powder mixing in a mortar by hand (a,c,e); right line: direct one-pot method (b,d,f). a,b) SEM, c,d) BSEM, e,f) EDXS.

based power stations, the membrane would be exposed to CO<sub>2</sub>. Therefore, the high-temperature phase stability in a CO<sub>2</sub>-containing atmosphere was studied by in situ XRD (Supporting Information, Figure S2). The in situ XRD patterns of 40NFO–60CGO dual-phase membranes between room temperature and 1000 °C in an atmosphere of 50 vol% CO<sub>2</sub> and 50 vol% N<sub>2</sub> (Supporting Information, Figure S2) shows that the composite membrane retains its dual phases over the entire temperature range. In an atmosphere of 50 vol% CO<sub>2</sub> and 50 vol% N<sub>2</sub>, no carbonate formation could be detected. These results show that the composite membrane 40NFO–60CGO is stable in a CO<sub>2</sub> atmosphere. The time dependence of the oxygen flux with pure CO<sub>2</sub> as sweep gas also confirmed that the dual-phase membrane was CO<sub>2</sub>-stable (Figure 6).

The scanning transmission electron microscope (STEM) high-angle annular dark-field (HAADF) micrograph in Figure 3a and also the EDXS elemental distributions in Figure 3c reveal a clear phase separation of CGO and NFO in the membrane. The grain size can be determined from these figures to be in the range of 500 nm to 1 μm, which is in accordance with the SEM findings. Similar to BSEM (Figure 2c,d), in the STEM-HAADF micrograph the dark grains are NFO and light grains are CGO (Figure 3a). The electron energy-loss (EEL) spectra (Figure 3b) were taken from circa 150 nm circular areas in the volume of CGO (top) and NFO grains (bottom). The fine-structure of the O<sub>K</sub> ionization edge is characteristic to the respective oxide. No intermixing of cations between the two phases can be observed (that is, CGO

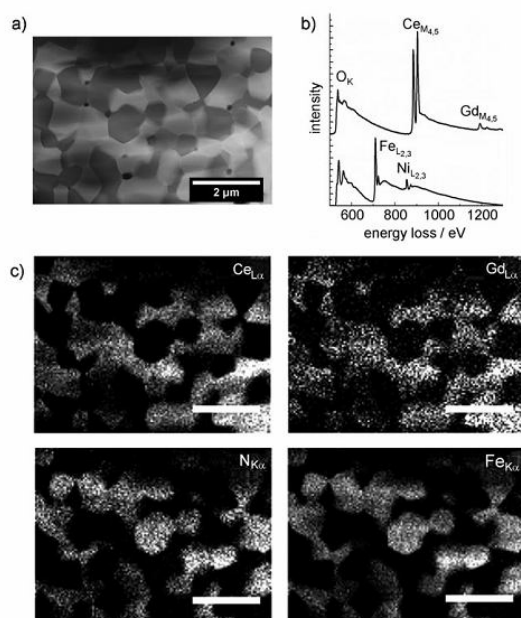


**Figure 3.** a) STEM-HAADF micrograph of a dual-phase membrane obtained by the direct one-pot method, showing CGO by bright contrast and NFO by dark contrast. Very dark contrast corresponds to holes in the as-prepared specimen. b) EEL spectra from the grain volume of CGO and NFO giving clear indication of phase separation. c) EDXS elemental distributions of Ce, Gd, Ni, and Fe. Scale bars: 2  $\mu\text{m}$ .

contains neither Fe nor Ni, and NFO contains neither Ce nor Gd), which shows that a dual-phase membrane with well-separated grains was obtained by the direct one-pot method.

Figure S3a in the Supporting Information shows a CGO–CGO interface with the grain to the left being imaged along  $[111]_{\text{CGO}}$  zone axis and the grain to the right exhibiting  $(111)_{\text{CGO}}$  planes. Figure S3b in the Supporting Information shows an NFO–NFO interface with both grains exhibiting  $(202)_{\text{NFO}}$  lattice planes. In both cases of interfaces between grains of the same kind, the grains are in intimate contact with no interphase between them, which is obvious from the HRTEM micrographs of Figure S3. This result was supported by EDXS and EELS, which could not identify any Fe or Ni at CGO–CGO interfaces and no Ce or Gd at NFO–NFO interfaces.

Figure 4 displays a contact between grains of different type (CGO and NFO). The grain at top is CGO imaged along the  $[110]_{\text{CGO}}$  zone axis, and the grain at bottom is NFO imaged along  $[110]_{\text{NFO}}$  zone axis (see the selected-area electron diffraction (SAED) pattern as insets in Figure 4a). Some Moiré fringes are noted in the right part of Figure 4a, which appear to be due to a slight inclination of the grain boundary with respect to the electron beam and give rise to a circa 1 nm-thick bright contrast feature along the whole grain boundary. Figure 4b shows a close-up of the marked area in Figure 4a and gives no indication of any interphases. Locally varying phase contrast in Figure 4a and b can be attributed to changes

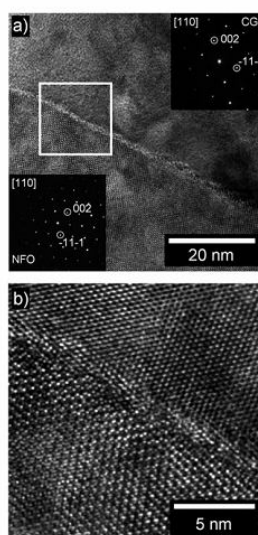


**Figure 4.** HRTEM of a CGO–NFO contact in a dual-phase membrane that was obtained from the direct one-pot method. a) Medium magnification with SAED pattern as insets (CGO at top, NFO at bottom); b) close-up of the marked area in (a).

in the thickness of the as-prepared TEM specimen after ion sputtering. Thus, it is concluded that all interfaces in the dual-phase membrane, which was obtained from direct one-pot method, exhibit well-separated grains in intimate contact.

Figure 5 shows the oxygen permeation fluxes of our dual phase composite membranes prepared by the one-pot method, and by mixing the powders by hand in a mortar, using He and CO<sub>2</sub>, respectively, as sweep gases. For the membrane prepared by one-pot synthesis, oxygen permeation fluxes of 0.31 and 0.27 mL min<sup>-1</sup> cm<sup>-2</sup> are found at 1000 °C when pure He and CO<sub>2</sub> are used as sweep gases.

If the two powders NFO and CGO are mixed by hand in a mortar, only 50 % of the oxygen permeances of the one-pot membrane are obtained (Figure 5). This experimental finding clearly indicates that a homogeneous grain size distribution and a small grain size are a condition for high oxygen fluxes, as mentioned before by Yang<sup>[21]</sup> who reported that the uniformity of dual-phase membrane effects the oxygen permeability. However, when pure CO<sub>2</sub> was taken as the sweep gas, the oxygen permeation flux was only slightly decreased (Figure 5), which demonstrates the high CO<sub>2</sub> stability of the material. On the other hand, there is a slight but remarkable reduction of the oxygen flux when CO<sub>2</sub> instead of He is used as sweep gas. This experimental finding can be explained by the inhibiting effect of carbon dioxide on the oxygen surface exchange reaction; that is, the presence of CO<sub>2</sub> decreases the rate of the oxygen release from the solid. This assumption is in complete agreement with previous findings,<sup>[22]</sup> which state that the oxygen surface-exchange reaction is not the same under different gas atmospheres. From an Arrhenius plot of the oxygen permeation fluxes when He and CO<sub>2</sub> were applied as sweep gases, the apparent

## Communications

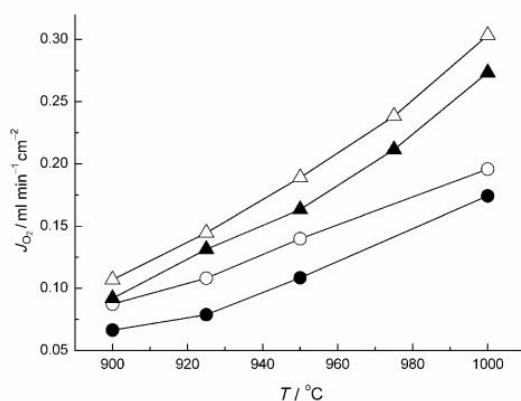


**Figure 5.** Oxygen flux  $J_{O_2}$  of 40NFO–60CGO dual-phase membranes prepared by different methods, and with a thickness of 0.5 mm, at different temperatures and with CO<sub>2</sub> and He as sweep gases. The air flow on the feed side was always  $F_{air} = 150 \text{ mL min}^{-1}$ , the sweep flow was always  $30 \text{ mL min}^{-1}$ . He sweep with  $F_{He} = 29 \text{ mL min}^{-1}$ ,  $F_{Ne} = 1 \text{ mL min}^{-1}$ ;  $\Delta$  = one-pot membrane,  $\circ$  = powder mixing, CO<sub>2</sub> sweep with  $F_{CO_2} = 29 \text{ mL min}^{-1}$ ,  $F_{Ne} = 1 \text{ mL min}^{-1}$ ;  $\blacktriangle$  = one-pot membrane,  $\bullet$  = powder-mixing method.

activation energies  $E_a = (128 \pm 4) \text{ kJ mol}^{-1}$  were found to be the same for the two membrane preparations within experimental error. Tong et al.<sup>[23]</sup> reported that a single activation energy is an important feature for a good stability of oxygen permeation through an oxygen membrane. In our case, a single activation energy was found in the range of 900–1000 °C.

The effect of the sweep rate on the oxygen permeation flux at temperature 1000 °C is shown in Supporting Information, Figure S4. Even when using CO<sub>2</sub> as the sweep gas, we observe the usual behavior, namely that oxygen permeances increase if the gradient of the oxygen partial pressure across the membrane is increased; this increase can be achieved by off-transporting the permeated oxygen as fast as possible, which can be realized with an increased sweep flow.

Figure 6 shows the long-term behavior of oxygen permeation flux through 40NFO–60CGO composite membrane at 1000 °C. During this oxygen permeation test, an oxygen permeation flux of about  $0.30 \text{ mL min}^{-1} \text{ cm}^{-2}$  was obtained at 1000 °C, and no decrease of the oxygen permeation flux was found during the permeation test. After the oxygen permeation test, the sample was characterized by XRD (Figure 1c). The dual-phase structure was retained, which indicates that 40NFO–60CGO exhibits excellent structure stability under a CO<sub>2</sub> atmosphere. The result is in agreement with the finding of in situ high-temperature XRD, indicating that the membrane is CO<sub>2</sub>-stable. It is not like Ba<sub>0.5</sub>Sr<sub>0.5</sub>Fe<sub>0.8</sub>Zn<sub>0.2</sub>O<sub>3-δ</sub> (BSFZ) or Ba<sub>0.5</sub>Sr<sub>0.5</sub>Co<sub>0.8</sub>Fe<sub>0.2</sub>O<sub>3-δ</sub> (BSCF) perovskite materials, where carbonate was formed when CO<sub>2</sub> was the feed gas and the oxygen flux decreased rapidly.<sup>[7]</sup>

In conclusion, a novel CO<sub>2</sub>-stable and cobalt-free dual-phase membrane of the composition 40 wt % NiFe<sub>2</sub>O<sub>4</sub>–60 wt % Ce<sub>0.9</sub>Gd<sub>0.1</sub>O<sub>2-δ</sub> (40NFO–60CGO) was synthesized by a direct one-pot method, and for comparison by powder mixing in a mortar. In situ high-temperature X-ray diffraction

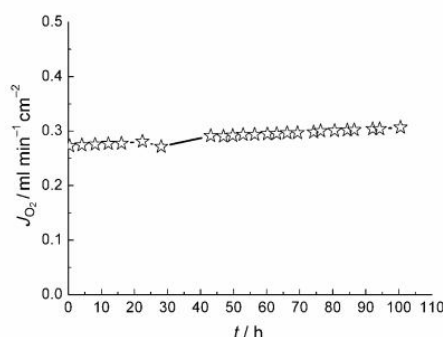


**Figure 6.** Oxygen permeation flux  $J_{O_2}$  through the 40NFO–60CGO composite membrane, prepared by the one-pot method, as a function of time at 1000 °C. Conditions:  $29 \text{ mL min}^{-1}$  CO<sub>2</sub> as sweep gas,  $1 \text{ mL min}^{-1}$  Ne as internal standard gas,  $150 \text{ mL min}^{-1}$  air as feed gas.

demonstrated that the two phases NFO and CGO were stable upon repeated heating and cooling cycles between room temperature and 1000 °C in air and in an atmosphere with 50 vol % CO<sub>2</sub> and 50 vol % N<sub>2</sub>. Energy-dispersive X-ray spectroscopy and back-scattered electron microscopy showed that the one-pot synthesis results in a dual-phase membrane with smaller NFO or CGO grains of uniform size distribution without homoaggregation of grains of the same phase, in comparison with a dual-phase membrane prepared by mixing the two powders. At 1000 °C, oxygen permeation fluxes of 0.31 and  $0.27 \text{ mL min}^{-1} \text{ cm}^{-2}$  were obtained on the membrane prepared with the one-pot material for the sweep gases He and CO<sub>2</sub>, respectively. This value is comparable with that of La<sub>2</sub>NiO<sub>4-δ</sub> and of La<sub>2</sub>Ni<sub>0.9</sub>Fe<sub>0.1</sub>O<sub>4-δ</sub>, which are promising CO<sub>2</sub>-stable membrane materials.<sup>[24]</sup> In a 100 h oxygen permeation using CO<sub>2</sub> as the sweep gas, no decline of the oxygen permeation flux was found, thus indicating that our dual phase membrane is CO<sub>2</sub>-stable.

Received: June 18, 2010

Revised: August 30, 2010

Published online: December 22, 2010

**Keywords:** carbon dioxide · membranes · oxide membranes · oxygen separation

[1] R. Kneer, D. Toporov, M. Förster, D. Christ, C. Broeckmann, E. Pfaff, M. Zwick, S. Engels M. Modigell, *Energy Environ. Sci.* **2010**, *3*, 198–207.

[2] a) H. Q. Jiang, Z. W. Cao, S. Schirmermeister, T. Schiestel, J. Caro, *Angew. Chem.* **2010**, *122*, 5790–5794; *Angew. Chem. Int. Ed.* **2010**, *49*, 5656–5660; b) H. Q. Jiang, H. H. Wang, F. Y. Liang, S. Werth, T. Schiestel, J. Caro, *Angew. Chem.* **2009**, *121*, 3027–3030; *Angew. Chem. Int. Ed.* **2009**, *48*, 2983–2986; c) H. Q. Jiang, H. H. Wang, S. Werth, T. Schiestel, J. Caro, *Angew. Chem.* **2008**, *120*, 9481–9484; *Angew. Chem. Int. Ed.* **2008**, *47*, 9341–9344; d) H. H. Wang, Y. Cong, W. S. Yang, *Chem. Commun.* **2002**, 1468–1469; e) H. Q. Jiang, F. Y. Liang, O. Czuprat, K. Efimov, A. Feldhoff, S. Schirmermeister, T. Schiestel, H. H. Wang, J. Caro, *Chem. Eur. J.* **2010**, *16*, 7898–7903; f) H. Q. Jiang, L. Xing, O. Czuprat, H. H. Wang, S. Schirmermeister, T. Schiestel, J. Caro,

- Chem. Commun.* **2009**, 6738–6740; g) J. Pérez-Ramírez, B. Vigeland, *Angew. Chem.* **2005**, *117*, 1136–1139; *Angew. Chem. Int. Ed.* **2005**, *44*, 1112–1115.
- [3] a) H. H. Wang, S. Werth, T. Schiestel, J. Caro, *Angew. Chem.* **2005**, *117*, 7066–7069; *Angew. Chem. Int. Ed.* **2005**, *44*, 6906–6909; b) G. A. Richards, K. H. Casleton, B. T. Chorpening, *Proc. IMechE Part A* **2005**, *219*, 121–126; c) S. Rezvani, Y. Huang, D. McIlveen-Wright, N. Hewitt, J. D. Mondol, *Fuel* **2009**, *88*, 2463–2472; d) B. J. P. Buhre, L. K. Elliott, C. D. Sheng, R. P. Gupta, T. F. Wall, *Prog. Energy Combust. Sci.* **2005**, *31*, 283–307.
- [4] a) W. J. Jin, C. Zhang, X. F. Chang, Y. Q. Fan, W. H. Xin, N. P. Xu, *Environ. Sci. Technol.* **2008**, *42*, 3064–3068; b) W. Q. Jin, C. Zhang, P. Zhang, Y. Q. Fan, N. P. Xu, *AIChE J.* **2006**, *52*, 2545–2550.
- [5] a) C. S. Chen, S. J. Feng, S. Ran, D. C. Zhu, W. Liu, H. J. M. Bouwmeester, *Angew. Chem.* **2003**, *115*, 5354–5356; *Angew. Chem. Int. Ed.* **2003**, *42*, 5196–5198; b) X. Y. Tan, Y. T. Liu, K. L. *AIChE J.* **2005**, *51*, 1991–2000; c) Z. P. Shao, W. S. Yang, Y. Cong, H. Dong, J. H. Tong, G. X. Xiong, *J. Membr. Sci.* **2000**, *172*, 177–188.
- [6] a) H. H. Wang, C. Tablet, A. Feldhoff, J. Caro, *Adv. Mater.* **2005**, *17*, 1785–1788; b) X. F. Zhu, H. H. Wang, W. S. Yang, *Chem. Commun.* **2004**, 1130–1131; c) K. Watanabe, M. Yuasa, T. Kida, Y. Teraoka, N. Yamazoe, K. Shimano, *Adv. Mater.* **2010**, *22*, 2367–2370; d) K. Efimov, T. Halfer, A. Kuhn, P. Heitjans, J. Caro, A. Feldhoff, *Chem. Mater.* **2010**, *22*, 1540–1544.
- [7] a) J. Martynczuk, K. Efimov, L. Robben, A. Feldhoff, *J. Membr. Sci.* **2009**, *344*, 62–70; b) M. Arnold, H. H. Wang, A. Feldhoff, *J. Membr. Sci.* **2007**, *293*, 44–52.
- [8] J. Beckers, G. Rothenberg, *ChemPhysChem* **2005**, *6*, 223–225.
- [9] C. Zhang, X. Chang, Y. Fan, W. Jin, N. Xu, *Ind. Eng. Chem. Res.* **2007**, *46*, 2000–2005.
- [10] a) I. Kagomiya, T. Iijima, H. Takamura, *J. Membr. Sci.* **2006**, *286*, 180–184; b) S. G. Lia, W. Q. Jin, N. P. Xu, J. Shi, *J. Membr. Sci.* **2001**, *186*, 195–204; c) J. Sunarso, S. Baumann, J. M. Serra, W. A. Meulenber, S. Liu, Y. S. Lin, J. C. Diniz da Costa, *J. Membr. Sci.* **2008**, *320*, 13–41.
- [11] K. Wu, S. Xie, G. S. Jiang, W. Liu, C. S. Chen, *J. Membr. Sci.* **2001**, *188*, 189–193.
- [12] a) F. T. Akin, Y. S. J. Lin, *J. Membr. Sci.* **2004**, *231*, 133–146; b) J. Kim, Y. S. Lin, *J. Membr. Sci.* **2000**, *167*, 123–133.
- [13] J. E. ten Elshof, N. Q. Nguyen, M. W. den Otter, H. J. M. Bouwmeester, *J. Electrochem. Soc.* **1997**, *144*, 4361–4366.
- [14] K. Kobayashi, T. Tsunoda, *Solid State Ionics* **2004**, *175*, 405–408.
- [15] C. S. Chen, Ph.D. Thesis, University of Twente, The Netherlands, **1994**.
- [16] a) V. V. Kharton, A. V. Kovalevsky, A. P. Viskup, F. M. Figueiredo, A. A. Yaremchenko, E. N. Naumovich, F. M. B. Marques, *J. Electrochem. Soc.* **2000**, *147*, 2814–2821; b) A. L. Shaula, V. V. Kharton, F. M. B. Marques, *J. Electrochem. Soc.* **2004**, *24*, 2631–2639; c) V. V. Kharton, A. V. Kovalevsky, A. P. Viskup, A. L. Shaula, F. M. Figueiredo, E. N. Naumovich, F. M. B. Marques, *Solid State Ionics* **2003**, *160*, 247–258.
- [17] a) Q. M. Li, X. F. Zhu, W. S. Yang, *J. Membr. Sci.* **2008**, *325*, 11–15; b) X. F. Zhu, Q. M. Li, Y. Cong, W. S. Yang, *Catal. Commun.* **2008**, *10*, 309–312; c) H. H. Wang, W. S. Yang, Y. Cong, X. F. Zhu, Y. S. Lin, *J. Membr. Sci.* **2003**, *224*, 107–115.
- [18] a) J. X. Yi, Y. B. Zuo, W. Liu, L. Winnubst, C. S. Chen, *J. Membr. Sci.* **2006**, *280*, 849–855; b) W. Li, T. F. Tian, F. Y. Shi, Y. S. Wang, C. S. Chen, *Ind. Eng. Chem. Res.* **2009**, *48*, 5789–5793; c) B. Wang, M. Zhan, D. C. Zhu, W. Liu, C. S. Chen, *J. Solid State Electrochem.* **2006**, *10*, 625–628; d) W. Li, J. J. Liu, C. S. Chen, *J. Membr. Sci.* **2009**, *340*, 266–271.
- [19] a) K. Efimov, M. Arnold, J. Martynczuk, A. Feldhoff, *J. Am. Ceram. Soc.* **2008**, *92*, 876–880; b) A. Feldhoff, M. Arnold, J. Martynczuk, T. M. Gesing, H. Wang, *Solid State Sci.* **2008**, *10*, 689–701.
- [20] S. Liu, R. Ma, R. Jiang, F. Luo, *J. Cryst. Growth* **1999**, *206*, 88–92.
- [21] X. F. Zhu, H. H. Wang, W. S. Yang, *J. Membr. Sci.* **2008**, *309*, 120–127.
- [22] a) J. A. Lane, J. A. Kilner, *Solid State Ionics* **2000**, *136–137*, 927–932; b) K. Yashiro, S. Onuma, A. Kaimai, Y. Nigara, T. Kawada, J. Mizusaki, K. Kawamura, T. Horita, H. Yokokawa, *Solid State Ionics* **2002**, *152–153*, 469–476; c) J. E. ten Elshof, H. J. M. Bouwmeester, H. Verweij, *Solid State Ionics* **1996**, *89*, 81–92.
- [23] J. H. Tong, W. S. Yang, B. C. Zhu, R. Cai, *J. Membr. Sci.* **2002**, *203*, 175–189.
- [24] V. V. Kharton, E. V. Tsipis, E. N. Naumovich, A. Thursfield, M. V. Patrakeev, V. A. Kolotygin, J. C. Waerenborgh, I. S. Metcalfe, *J. Solid State Chem.* **2008**, *181*, 1425–1433.

**Supporting Information for**  
***Angewandte Chemie International Edition***

**CO<sub>2</sub>-stable and cobalt-free dual phase membrane for oxygen separation\*\***

*Huixia Luo<sup>a</sup>, Konstantin Efimov<sup>a</sup>, Heqing Jiang<sup>a</sup>, Armin Feldhoff<sup>a</sup>, Haihui Wang<sup>b\*</sup>, and Jürgen Caro<sup>a\*</sup>*

<sup>a</sup>*Institute of Physical Chemistry and Electrochemistry, Leibniz University of Hannover, Callinstr. 3A, D-30167 Hannover, Germany*

<sup>b</sup>*School of Chemistry and Chemical Engineering, South China University of Technology, Guangzhou, 510640, PR China*



## Experimental Section

**Synthesis of powders and membrane:** The 40NFO-60CGO powder was prepared via a one-pot method.<sup>[1,2]</sup> using appropriate amounts of Ni(NO<sub>3</sub>)<sub>2</sub>, Fe(NO<sub>3</sub>)<sub>3</sub>, Ce(NO<sub>3</sub>)<sub>3</sub> and Gd(NO<sub>3</sub>)<sub>3</sub> dissolved in water and mixed in a beaker. After stirring for certain time, equal molar amounts of citrate and EDTA were added and the pH value was adjusted to ~ 9 by adding ammonia. The molar ratio of EDTA acid : citric acid : total metal ions was 1:1.5:1. Then the solution was stirred while heating at 150 °C, until the water was evaporated and a gel was formed. The gel was calcined in air at 600 °C in a furnace to remove the organic compounds by combustion, and a primary powder was obtained. This powder was calcined at 1000 °C for 10 h. The powders were pressed to disk membranes under a pressure of 10 MPa in a stainless steel module with a diameter of 16 mm. The pure NFO and CGO phases have been prepared in the same way. The NFO and CGO powders were mixed by hand in a mortar for 1.5 h and from the mixed powders a 40NFO-60CGO membrane has been prepared in the identical way as with the powder from the one-pot synthesis. Green disks were pressure-less sintered at 1350 °C for 10 h. The densities of the sintered membranes were determined by the Archimedes method using ethanol. Only those membranes that had relative densities higher than 95 % were chosen for oxygen permeation studies. The disks were polished with 1200 mesh sandpaper from both sides to achieve a 0.5 mm membrane thickness. To improve the oxygen surface exchange rate on the air side, the membranes were coated with an La<sub>0.6</sub>Sr<sub>0.4</sub>CoO<sub>3-δ</sub> (LSC) porous layer<sup>[1,2,3]</sup> on one side with a paste made of 40 wt. % LSC powder and 60 wt. % terpineol. The low CO<sub>2</sub> partial pressure in air does not cause the strontium carbonate formation above 722 °C.<sup>[4]</sup> After coating, the membrane with the LSC layer was calcined at 950 °C for 2 hours.

**Characterization of membrane materials:** The phase composition of the composite membrane was determined by *in-situ* powder X-ray diffraction (XRD) between room temperature and 1000 °C using a PHILIPS-PW1710 (for stability tests in air) and a Bruker D8 (for stability tests in 50 vol.% CO<sub>2</sub>/50 vol.% N<sub>2</sub>). On the PHILIPS-PW1710, the sample was tested in a high temperature cell with a heated Pt sample holder up to 1000 °C in air. The heating and cooling rates amounted to 6 °C/min. At each temperature step, the temperature was held for 70 min to record a data set in a continuous scan mode in the range of 20 ° - 80 ° with intervals of 0.05 °. On the Bruker D8, the

heating and cooling rates amounted to 12 °C/min. At each temperature step, the temperature was held for 30 min to record a data set in a continuous scan mode in the range of 20 ° - 80 ° with intervals of 0.05 °. The disc membranes were studied by scanning electron microscopy (SEM) and back scattered SEM (BSEM) using a JEOL JSM-6700F. The element distribution was studied on the same electron microscope by energy dispersive X-ray spectroscopy (EDXS) at 15 keV. Specimen for transmission electron microscopy (TEM) was thinned mechanically followed by argon ion beam sputtering.<sup>[5,6]</sup> Scanning TEM (STEM) in high-angle annular dark-field (HAADF) mode, EDXS, electron energy-loss spectroscopy (EELS), selected area electron diffraction (SAED), and high-resolution TEM (HRTEM) were conducted at 200 kV primary electron energy in a JEOL JEM-2100F, which was equipped with appropriate spectrometers, detectors, and an ultra-high resolution (UHR) pole-piece.<sup>[5,6]</sup>

**Oxygen permeation:** The oxygen permeation was studied in a self-made high-temperature oxygen permeation cell as shown in.<sup>[7]</sup> A gold paste was used to seal the disk onto a quartz tube at 950 °C for 5 hours. Air was the feed; He and CO<sub>2</sub> have been used as sweep gases (29 ml/min, 99.995 % + 1 ml Ne/min as the internal standard gas). A gas chromatograph (Agilent 6890) was *on line* connected to the permeation apparatus. The leakage of oxygen was subtracted when the oxygen permeation flux was calculated. The total flow rate of the effluents was calculated from the change in the Ne concentrations before and after the permeator. The oxygen permeation flux calculation was shown in detail in.<sup>[7,8]</sup>

## References

- [1] Q.M. Li, X.F. Zhu, W.S. Yang, *J. Membr. Sci.* **2008**, 325, 11-15.
- [2] X.F. Zhu, H.H. Wang, W.S. Yang, *J. Membr. Sci.* **2008**, 309, 120-127.
- [3] X.F. Zhu, W.S. Yang, *AIChE J.* **2008**, 54, 665-672.
- [4] A. Feldhoff, M. Arnold, J. Martynczuk, Th.M. Gesing, H.H. Wang, *Solid State Sci.* **2008**, 10, 689-701.
- [5] J. Martynczuk, K. Efimov, L. Robben, A. Feldhoff, *J. Membr. Sci.* **2009**, 344, 62-70.
- [6] M. Arnold, H.H. Wang, A. Feldhoff, *J. Membr. Sci.* **2007**, 293, 44-52.
- [7] J.H. Tong, W.S. Yang, B.C. Zhu, R. Cai, *J. Membr. Sci.* 2002, 203, 175-189.
- [8] H.X. Luo, B.B. Tian, Y.Y. Wei, H.H. Wang, H.Q. Jiang, J. Caro, *AIChE J.* **2010**, 56, 604-610.

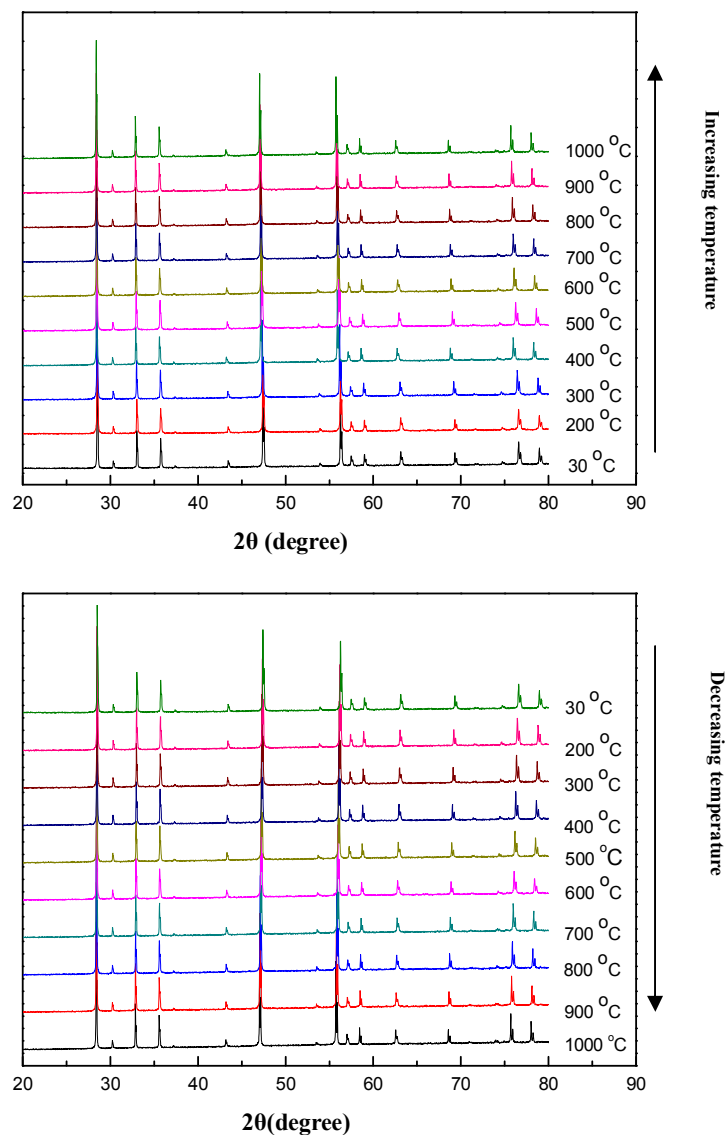


**Figure S1.** *In-situ* XRD patterns of the one-pot 40NFO-60CGO composite membrane under air during increasing and decreasing temperature.

Heating and cooling rates = 6 °C/min, equilibration time at each temperature: 70 minutes for recording the XRD at each temperature.

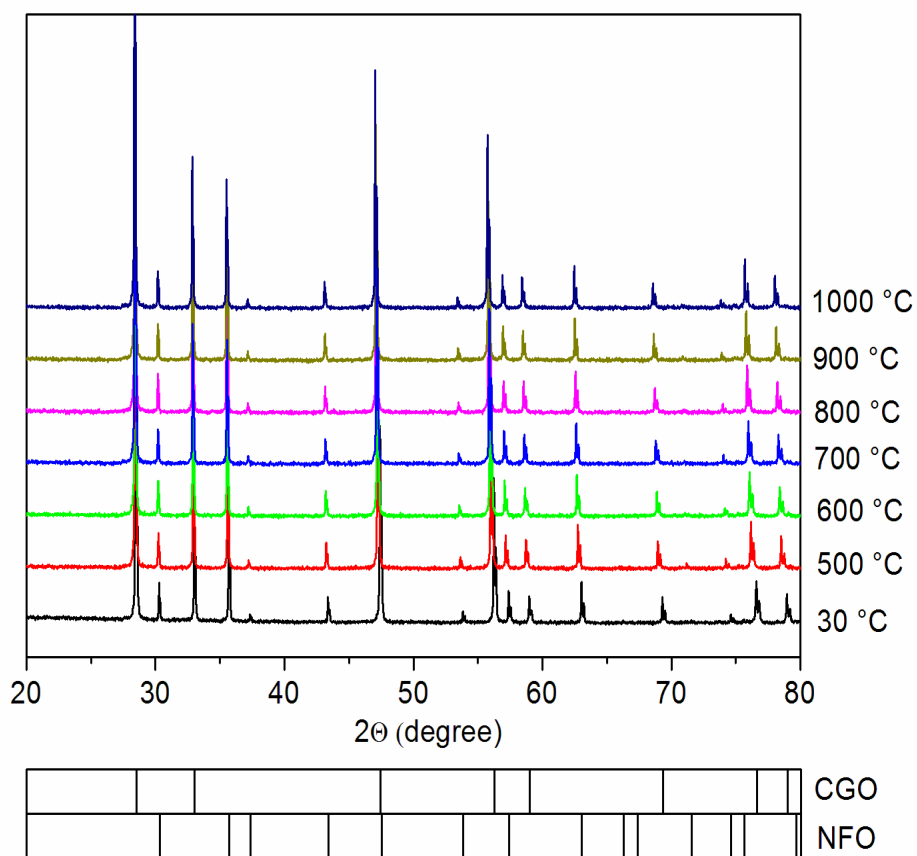


**Figure S2** *In-situ* XRD patterns of the one-pot 40NFO-60CGO composite membrane under 50 vol % CO<sub>2</sub> and 50 vol % N<sub>2</sub> for decreasing temperatures.

Heating and cooling rates = 12 °C/min, equilibration time at each temperature: 30 min for recording the XRD.

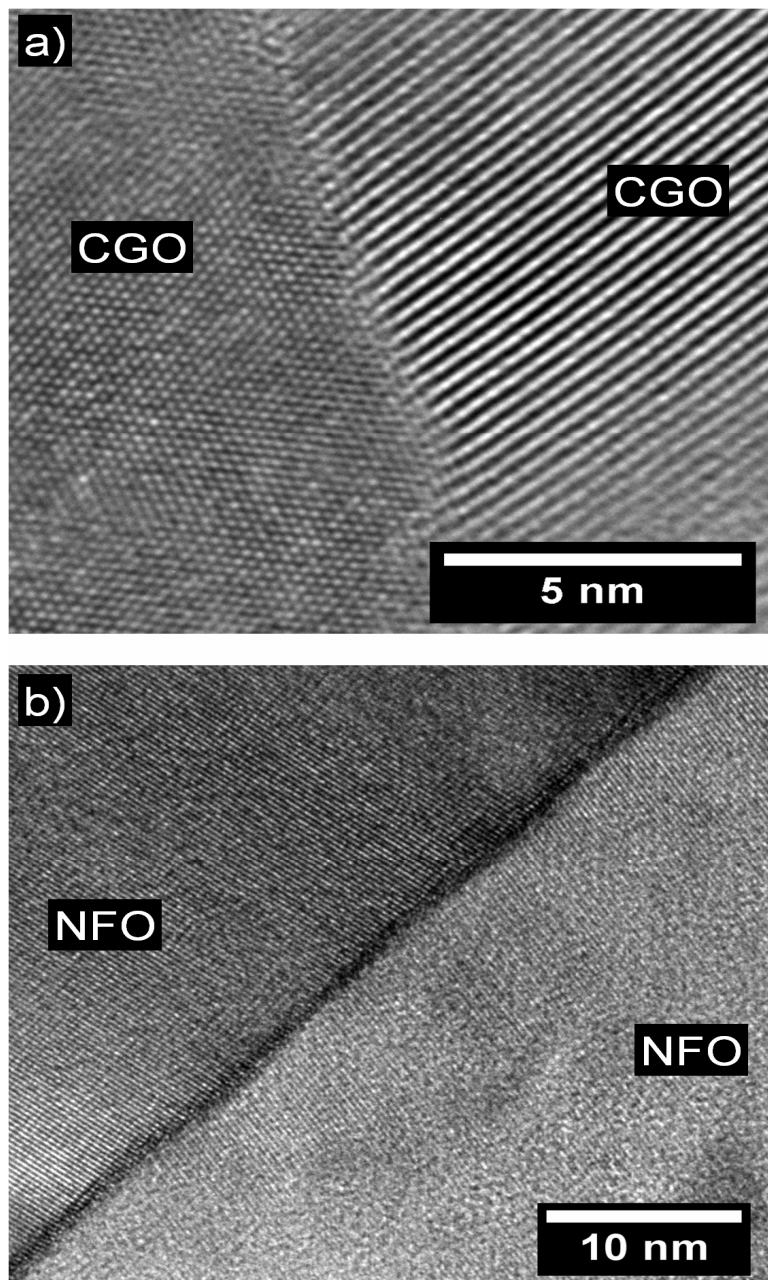


*Figure S3.* HRTEM of a dual phase membrane, which was obtained from direct one-pot method. a) CGO-CGO interface; b) NFO-NFO interface.

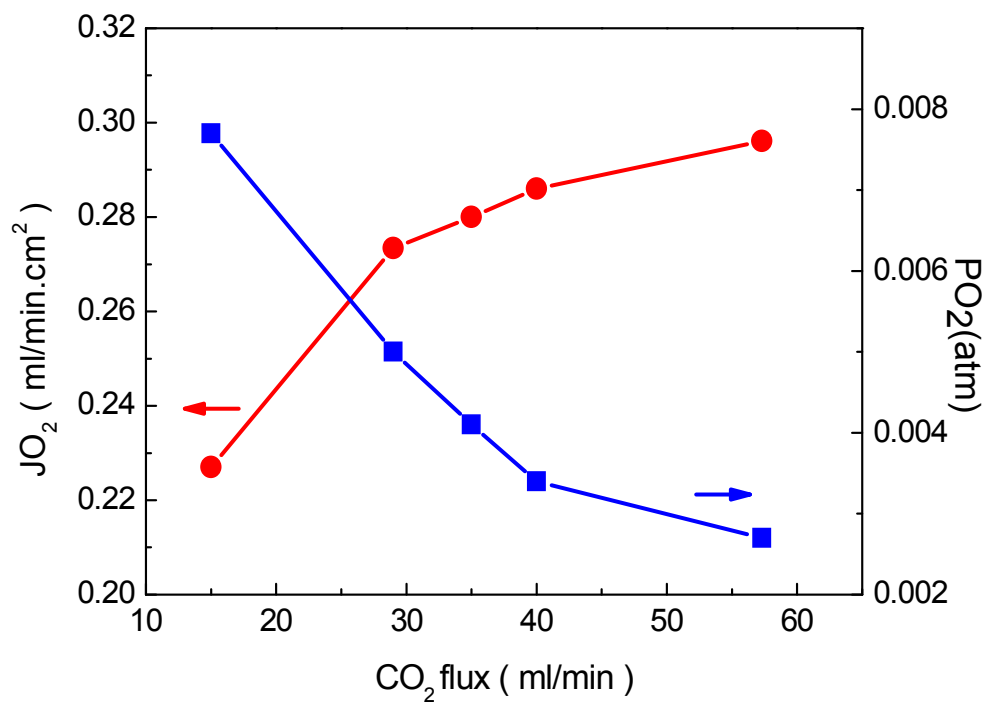


**Figure S4.** Effect of different CO<sub>2</sub> sweep rate on oxygen partial pressure and oxygen permeation flux at 1000 °C.

### **3.3 Influence of the preparation methods on the microstructure and oxygen permeability of a CO<sub>2</sub>-stable dual phase membrane**

Huixia Luo, Heqing Jiang, Konstantin Efimov, Haihui Wang and Jürgen Caro

**AICHE J.** 2011, 57, 2738.

## Influence of the Preparation Methods on the Microstructure and Oxygen Permeability of a CO<sub>2</sub>-Stable Dual Phase Membrane

Huixia Luo, Heqing Jiang, Konstantin Efimov, and Jürgen Caro

Institute of Physical Chemistry and Electrochemistry, Leibniz University of Hannover, D-30167 Hannover, Germany

Haihui Wang

School of Chemistry and Chemical Engineering, South China University of Technology, Guangzhou 510640, China

DOI 10.1002/aic.12488

Published online December 17, 2010 in Wiley Online Library (wileyonlinelibrary.com).

A CO<sub>2</sub>-stable dual phase membrane of the composition 40 wt % NiFe<sub>2</sub>O<sub>4</sub>-60 wt % Ce<sub>0.9</sub>Gd<sub>0.1</sub>O<sub>2-δ</sub> (40NFO-60CGO) was synthesized in three different ways: mixing of the starting powders (1) in a mortar and (2) in a ball-mill as well as by (3) direct in situ one-pot sol-gel powder synthesis. Backscattered scanning electron microscopy revealed that the direct one-pot synthesis of 40NFO-60CGO gives the smallest grains in a homogeneous distribution, compared with powder homogenization in the mortar or the ball-mill. The smaller is the grains, the higher is the oxygen permeability. The permeation of the membrane can be improved by coating a porous La<sub>0.6</sub>Sr<sub>0.4</sub>CoO<sub>3-δ</sub> (LSC) layer on the surface of the air side. The dual phase membrane of 40NFO-60CGO prepared by in situ synthesis shows a steady oxygen flux of 0.30 ml/(min cm<sup>2</sup>) over more than 100 h when pure CO<sub>2</sub> was used as sweep gas, which indicated that the dual phases membrane is CO<sub>2</sub>-resistant at least over this 5 days testing period. © 2010 American Institute of Chemical Engineers *AICHE J*, 57: 2738–2745, 2011

Keywords: homogeneity, dual phase membrane, oxygen separation, CO<sub>2</sub>-stable

### Introduction

The increasing carbon dioxide emission, especially from power generation industry, is considered as the main source of global warming.<sup>1</sup> To minimize the impact of the CO<sub>2</sub> emission on the climate change, great efforts are devoted to recover and sequester CO<sub>2</sub>.<sup>2–4</sup> One potential route is the oxy-fuel concept burning natural gas with nitrogen-free oxygen, which allows to sequester the CO<sub>2</sub> after steam condensation. Dense mixed oxygen ionic-electronic conducting ceramic membranes (MIECM), perovskites are promising candidates for this oxygen separation from air.<sup>5–14</sup> However, when MIECMs are used for the separation of oxygen from

air, some of the CO<sub>2</sub> is recycled and used as the sweep gas for the oxygen separation, simultaneously lowering the temperature in the burner.<sup>15–17</sup>

A handicap of most of the perovskite materials for their application in the oxy-fuel technology is their instability in the presence of CO<sub>2</sub> because of the carbonate formation because the perovskite type membranes usually contain alkaline earth ions like Ba<sup>2+</sup> or Sr<sup>2+</sup> on the A-site, which tend to react with CO<sub>2</sub> and form carbonates.<sup>18,19</sup> An alternative is the development of composite membranes of two separate CO<sub>2</sub>-stable electron and oxygen-ion conducting phases. Up to now, numerous dual phase materials have been developed which can be divided into two major groups: (1) The first generation of dual phase membranes were composites of noble metal powders as electronic and a ceramic particles as ionic conductors.<sup>20–22</sup> However, these composite membranes are expensive, a mismatch of the thermal expansion

Correspondence concerning this article should be addressed to J. Caro at juergen.caro@pci.uni-hannover.de (or) H. Wang at hhwang@scut.edu.cn.



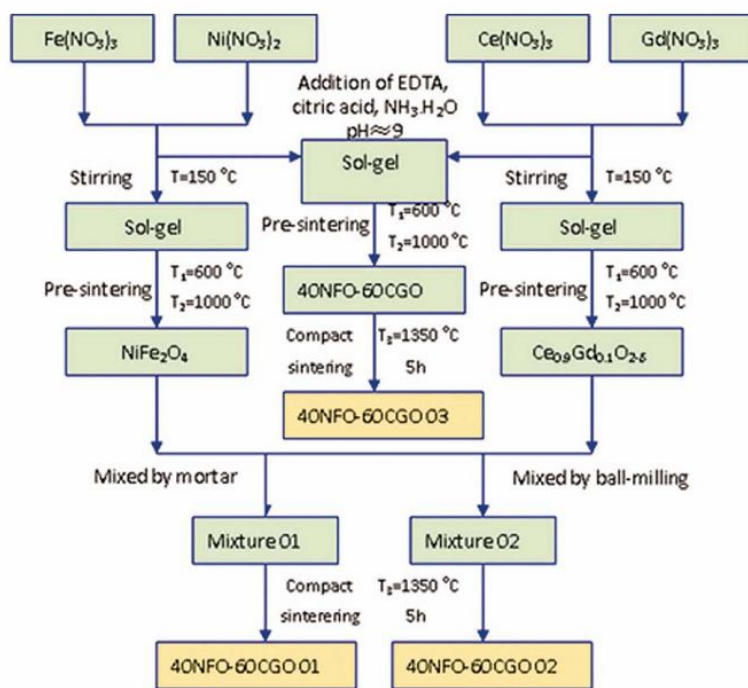


Figure 1. Flowchart for the preparation of dual phase membranes.

[Color figure can be viewed in the online issue, which is available at [wileyonlinelibrary.com](http://wileyonlinelibrary.com).]

coefficients (TEC) of the metallic and the ceramic phase exists, and the oxygen permeabilities were found to be low. (2) The second generation of dual phase membranes were composites of two oxides, where one of the oxides acts as electron conductor instead of the noble metal.<sup>23–25</sup> These dual phase membranes of the second generation show higher oxygen permeabilities, but they usually contain a perovskite phase (ABO<sub>3</sub>, A = alkalin earth metals or lanthanide element; B = transition metal). The alkaline earth metals on the A site easily form carbonates if CO<sub>2</sub> is present. This carbonate formation is found to be reversible but it immediately stops the oxygen flux.<sup>18,19</sup> These dual phase membranes also suffer from a mechanical stress and can mechanically decompose due to swelling by carbonate formation.

In this article, a novel earth alkaline metal-free CO<sub>2</sub>-stable dual phase membrane has been developed. The NiFe<sub>2</sub>O<sub>4</sub> (NFO) and Ce<sub>0.9</sub>Gd<sub>0.1</sub>O<sub>2.δ</sub> (CGO) powders have been mixed in a mortar and a ball-mill, and the NFO-CGO dual phase was also obtained directly in an *in situ* one-pot sol-gel synthesis. The chemical composition of our dual phase membrane is 40 wt % NiFe<sub>2</sub>O<sub>4</sub>-60 wt % Ce<sub>0.9</sub>Gd<sub>0.1</sub>O<sub>2.δ</sub> (40NFO-60CGO). In the mixture of the two phases, NFO is the electron conductor and CGO is the oxygen ion conductor. The microstructure of the membranes will be correlated with the oxygen permeability.

### Experimental Section

The powders of CGO, NFO, and 40 wt % NiFe<sub>2</sub>O<sub>4</sub>-60 wt % Ce<sub>0.9</sub>Gd<sub>0.1</sub>O<sub>2.δ</sub> were synthesized by a combined citrate

and EDTA complexing method. After stirring the metal nitrate solutions for 20 min, calculated amounts of citrate and EDTA were added and the pH value was adjusted to ~9 by ammonia. The molar ratio of EDTA: citric acid: total metal ions was 1:1.5:1. Then, the solutions were stirred when heated to 150 °C, until the water was evaporated and a gel was formed. The gels were calcined in air at 600 °C in a furnace to remove the organic compounds by combustion, and the primary powders were obtained. These powders were calcined at 1000 °C for 10 h.

The 40NFO-60CGO dual phase membranes were prepared in three ways. Figure 1 shows the three methods applied in this article for the dual phase preparation. (1) Powder mixing in a mortar (membrane 40NFO-60CGO 01): The as-obtained CGO and NFO powders were mixed with a weight ratio of 60:40. Then, the mixed powders were ground in an agate mortar for 1.5 h. (2) Powder mixing by ball-milling (membrane 40NFO-60CGO 02): The as-obtained CGO and NFO powders were mixed in a weight ratio 60:40 by ball-milling for 4 h. (3) Direct one-pot sol-gel synthesis (membrane 40NFO-60CGO 03): The powder mixture was obtained *in situ*.

The powders of all three techniques were pressed to disk membranes under a pressure of ~10 MPa in a stainless steel module with a diameter of 16 mm. Then, they were sintered at 1350 °C in air for 10 h with heating and cooling rates of 2 °C/min. The membranes were polished to 0.6 mm thickness by using 1200 grit-sand paper (average particle diameter 15.3 μm), then the membranes were washed with ethanol. To improve the oxygen surface exchange rate on the air

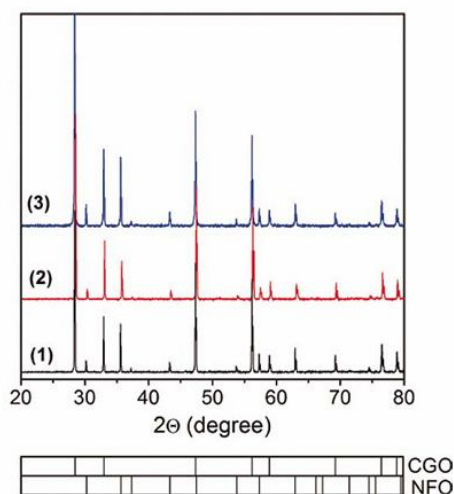


**Figure 2. XRD patterns of 40NFO-60CGO membranes prepared by different methods.**

Mixing of the NFO and CGO powder (1) in an agate mortar and (2) by ball-milling. (3) Direct synthesis of the powder in a one-pot synthesis. The theoretical Bragg position for CGO (PDF 46-507) and NFO (PDF 10-325) are labeled with the ticks at the bottom of the figure. [Color figure can be viewed in the online issue, which is available at [wileyonlinelibrary.com](http://wileyonlinelibrary.com).]

side, a La<sub>0.6</sub>Sr<sub>0.4</sub>CoO<sub>3-δ</sub> (LSC) porous layer<sup>26,27</sup> was deposited with a paste made of 40 wt % LSC powder and 60 wt % terpineol. After coating the membrane with LSC, the composite was calcined at 950°C for 2 h.

The phase structure of the dual phase membranes were studied by X-ray diffraction (XRD, D8 Advance, Bruker-AXS, with Cu K $\alpha$  radiation) after grinding the membranes to a size of 10–100  $\mu$ m. Data sets were recorded in a step-scan mode in the 2 $\theta$  range of 20–80° with intervals of 0.02°. *In situ* XRD tests were conducted in a high-temperature cell HTK-1200N (Anton-Paar) between room temperature and 1000°C. For tests in ambient air, heating and cooling rate were set to 6°C/min. Before each data acquisition, an equilibration time of 70 min was used. Tests in the atmosphere containing 50 vol % CO<sub>2</sub>/50 vol % N<sub>2</sub> were carried out with heating and cooling rate of 12°C/min. At each temperature step, the temperature was held for 30 min before diffraction data collection. The surface and cross section morphology of the membrane disks were studied by scanning electron microscopy (SEM) using the Jeol-JSM-6700F. Some micrographs were taken in the back scattering mode (BSEM).

Oxygen permeation was studied in a self-made high-temperature oxygen permeation cell, described in Ref. 28. A gold paste (Heraeus) was used to seal the disk onto a quartz tube at 950°C for 5 h. As feed a 50 vol % O<sub>2</sub>/50 vol % N<sub>2</sub> mixed gas was used; as sweep gases He and CO<sub>2</sub> have been used (29 ml/min, 99.995% + 1 ml Ne/min as an internal standard gas). A gas chromatograph (GC, Agilent 6890) was connected to the effluents of the sweep side. The GC was frequently calibrated using standard gases to ensure the reliability of the experimental data. The leakage is caused by the imperfect sealing at high temperature, which can be

determined by the detecting N<sub>2</sub> by GC. In no case, the leakage stream is larger than 5% of the oxygen flux through the membrane. Assuming that leakage of nitrogen and oxygen is in accordance with Knudsen diffusion, the fluxes of leaked N<sub>2</sub> and O<sub>2</sub> are related by

$$J_{N_2}^{\text{Leak}} : J_{O_2}^{\text{Leak}} = \sqrt{\frac{32}{28}} \times \frac{0.79}{0.21} = 4.02.$$

The oxygen permeation flux was then calculated as follows:

$$J_{O_2} [\text{ml}/(\text{min cm}^2)] = \left( C_{O_2} - \frac{C_{N_2}}{4.02} \right) \times \frac{F}{S}$$

where  $C_{O_2}$  and  $C_{N_2}$  are the oxygen and nitrogen concentrations, respectively, calculated from GC calibration,  $F$  is the total flow rate of the outlet on the sweep side, which was measured by the change of Ne concentration before and after permeator.

The total flow rate of the effluents was calculated from the change in the Ne concentrations before and after the permeator.

## Results and Discussion

### Characteristics of the dual phase materials

Figure 2 shows the XRD patterns of the 40NFO-60CGO membranes prepared by three different methods, by powder mixing (1) in a mortar and (2) in a ball-milling as well as (3) the direct synthesis of the mixed powders by a one-pot method. All the composite membranes consist of only the two phases, NFO and CGO, and no other crystalline phases have been formed. From the similarity of the lattice parameters of the NFO and CGO phases as shown in Table 1, a good phase compatibility in the mixed material can be expected.

The influence of the different preparation methods on the microstructure of 40NFO-60CGO dual phase membranes is shown in Figure 3. When comparing the SEM and BSEM pictures, we can see clear differences of the size and uniformity of the NFO and CGO grains as well as of their homogeneous distribution of the three membranes under study. Membrane 40NFO-60CGO 03 made by *in situ* direct sol-gel synthesis has the smallest grain size (0.2–1.5  $\mu$ m) but—as shown later—the highest oxygen permeation flux. On the contrary, 40NFO-60CGO 01 made by powder mixing in a mortar has the largest grains and lowest oxygen permeation flux. Furthermore, in this membrane, the NFO grains are bigger (3–7  $\mu$ m) than the CGO grains (2–4  $\mu$ m). Grain size of 40NFO-60CGO 02 made by ball-milling is in the range 0.4–2  $\mu$ m, which is between the grain sizes of 40NFO-60CGO

**Table 1. Lattice Parameters of NFO and CGO as Pure Phases and in the 40NFO-60CGO Dual Phase Membranes Prepared by Different Methods**

Phase	Pure Phase	40NFO-60CGO 01 Mortar	40NFO-60CGO 02 Ball-Milling	40NFO-60CGO 03 One-Pot Method
NFO (Å)	8.3455	8.3641	8.3195	8.3596
CGO (Å)	5.4209	5.4400	5.4106	5.4326

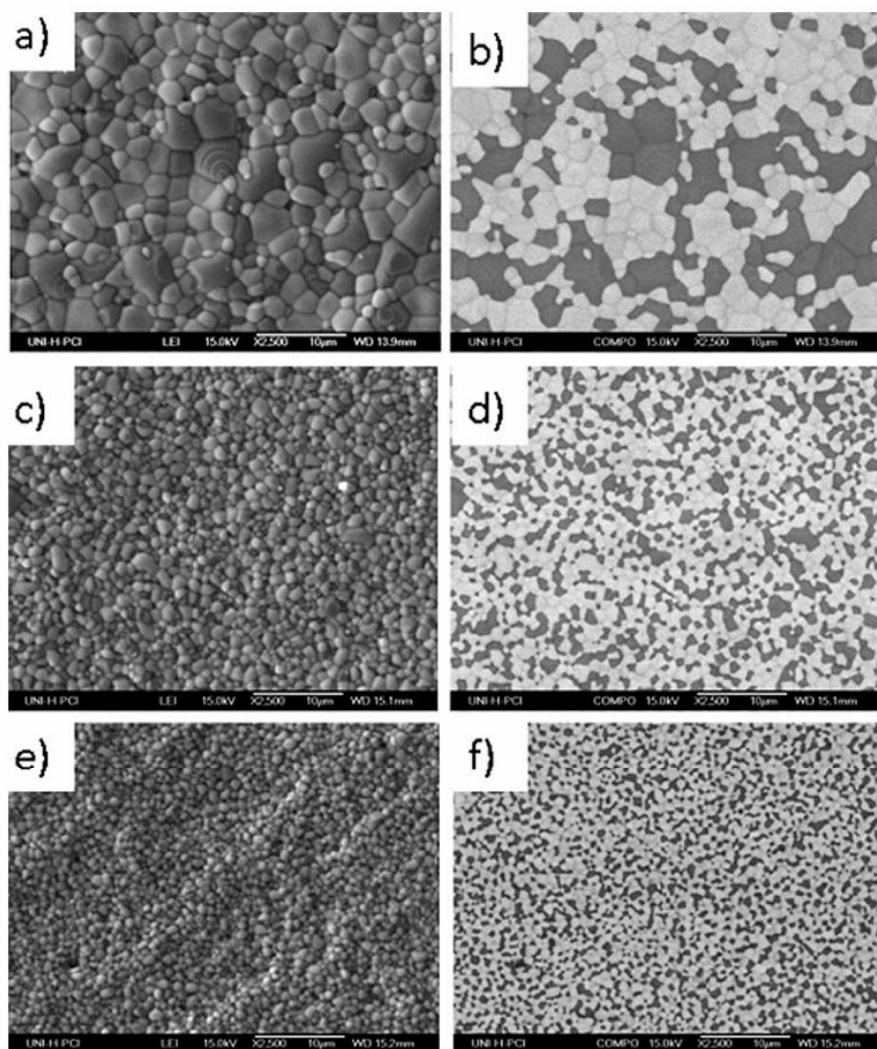


Figure 3. SEM (left column) and BSEM (right column) of the surface grain structure of the membranes 40NFO-60CGO 01, 02, and 03, prepared by powder mixing in a mortar (a and b), ball-milling (c and d), and one-pot method (e and f), respectively.

01 and 40NFO-60CGO 03, and consequently, the oxygen permeation flux is in between.

#### Structure stability and thermal expansion coefficient of the dual phase materials 40NFO-60CGO

*In situ* XRD provides an effective and direct way to characterize the high-temperature structure changes during increasing and decreasing temperatures under certain gas atmospheres. Figures 4 and 5 show the XRD patterns of the NFO and CGO powders in air for increasing and decreasing temperatures between 30°C and 1000°C indicating that the phases CGO and NFO remain unchanged.

Figure 6 shows the lattice constants of NFO and CGO at various temperatures determined from the *in situ* XRD data in air. As expected, the lattice constants depend linearly on temperatures for both NFO and CGO with increasing and decreasing temperatures. The TEC was calculated following the definition  $\frac{d(\Delta a/a_0)}{dT}$  ( $a$  is the lattice constant and  $a_0$  is the lattice constant at room temperature). The values of the TEC of NFO and CGO calculated from the data of Figure 6 for the range of 30–1000°C. The TEC of NFO ( $4.36 \pm 0.3 \times 10^{-5} \text{ K}^{-1}$ ) is higher than that of CGO ( $1.81 \pm 0.1 \times 10^{-5} \text{ K}^{-1}$ ). However, when the membrane was sintered, because of the different TECs of the two phases, the heating and cooling rate should not be faster than 2°C/min to avoid cracking of the membranes.

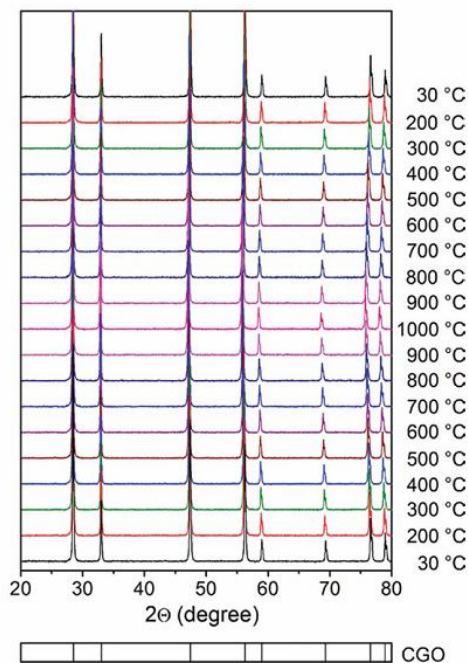


Figure 4. *In situ* XRD patterns of CGO under air during increasing and decreasing temperatures.

Heating and cooling rates = 6°C/min, equilibration time at each temperature: 70 min for recording the XRD. [Color figure can be viewed in the online issue, which is available at [wileyonlinelibrary.com](http://wileyonlinelibrary.com).]

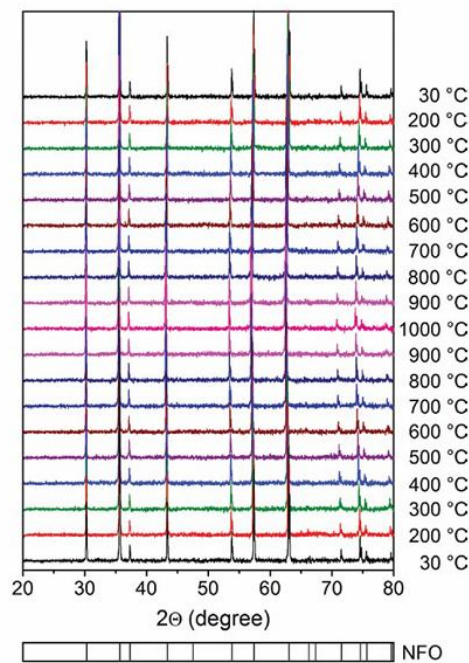


Figure 5. *In situ* XRD patterns of NFO under air during increasing and decreasing temperatures.

Heating and cooling rates = 6°C/min, equilibration time at each temperature: 70 min for recording the XRD. [Color figure can be viewed in the online issue, which is available at [wileyonlinelibrary.com](http://wileyonlinelibrary.com).]

For a potential application of MIECM membranes in the oxy-fuel technology, the membranes must be stable in a carbon dioxide atmosphere. Therefore, the high-temperature phase stability of 40NFO-60CGO 03 in the CO<sub>2</sub> containing atmosphere of 50 vol % CO<sub>2</sub>/50 vol % air has been studied by *in situ* XRD, as shown in Figure 7. The two phases NFO and CGO remained unchanged, no carbonates were found.

#### Influence of grain size on the oxygen permeability of dual phase membrane

Figure 8 shows the oxygen permeation of the three 40NFO-60CGO membranes under study at 950°C. It can be found that the oxygen permeation fluxes of membrane 40NFO-60CGO 01 decreases with increasing permeation time at the initial stage. After around 1200 min, the permeation oxygen fluxes of 40NFO-60CGO 01 reach a steady state. However, the oxygen permeation fluxes through both membrane 40NFO-60CGO 02 and membrane 40NFO-60CGO 03 increase with permeation time at the initial stage and then they reach a steady state. The steady-state oxygen permeances of our 40NFO-60CGO membranes are 01 < 02 < 03, which correlate clearly with the size of the NFO and CGO grains in the mixed matrix. A similar decline of oxygen permeation flux through the dual-phase composite membranes with time has been reported in a previous paper.<sup>27</sup> However, the detailed reason for this time-dependent behavior is not clear.<sup>29</sup> It follows from Figure 8 that the steady

oxygen permeation flux through 40NFO-60CGO 03 is the highest among the three type of membranes. According to the previous studies,<sup>27,30</sup> the oxygen permeation flux is determined not only by the conductivities of both phases but also by the grain sizes as well as grain size distribution, which can be described by the percolation theory. BSEM results (cf. Figure 3) revealed that the direct one-pot synthesis of 40NFO-60CGO 03 gives the smallest grains in a

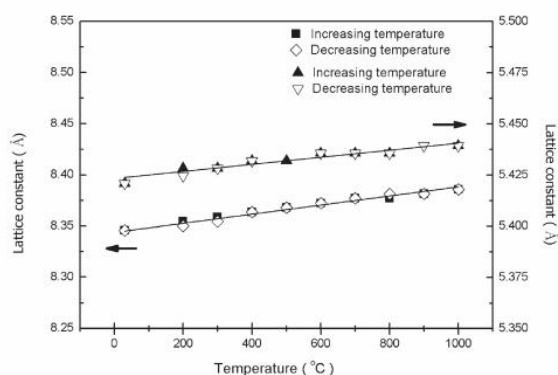
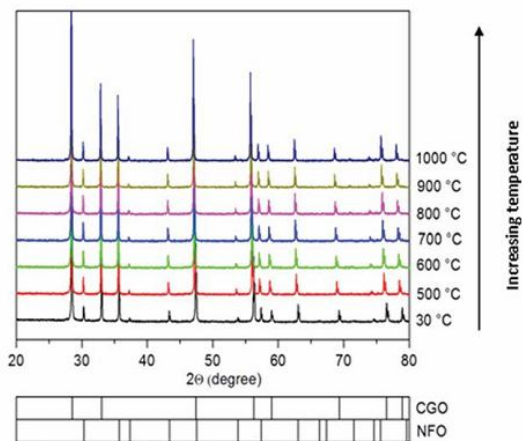


Figure 6. Temperature dependence of the lattice constants for NFO (■ increasing temperature, ◇ decreasing temperature) and CGO (▲ increasing temperature, ▼ decreasing temperature).

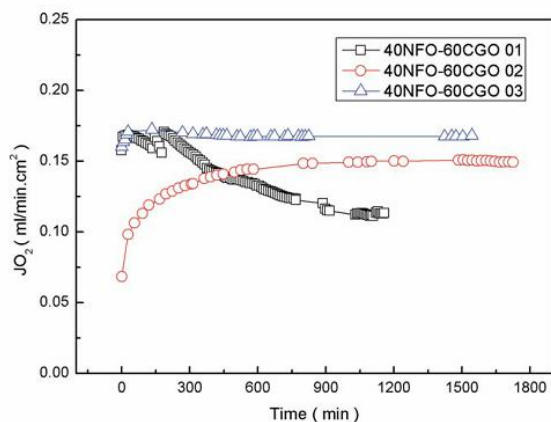


**Figure 7.** *In situ* XRD patterns of the one-pot 40NFO-60CGO 03 powder under 50% CO<sub>2</sub>/50% air at different temperatures.

Heating rates = 12°C/min, equilibration time at each temperature: 30 min for recording the XRD. [Color figure can be viewed in the online issue, which is available at wileyonlinelibrary.com.]

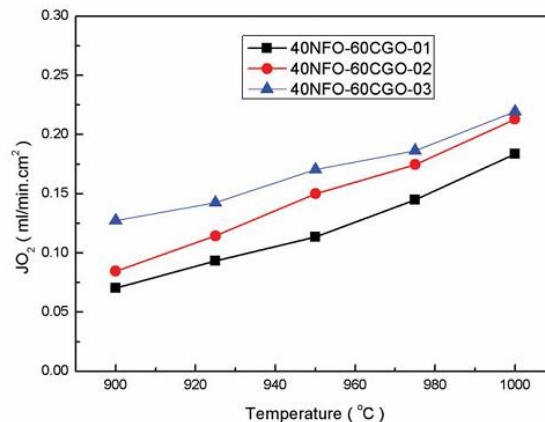
homogeneous distribution, so a highest of oxygen permeation flux was obtained compared with powder homogenization in the mortar or the ball-mill.

Figure 9 shows the oxygen permeability of the three 40NFO-60CGO dual phase membranes as a function of temperature. The data were obtained after the permeation having reached steady state. In agreement with the results shown in Figure 8, in the temperature window between 900°C and 1000°C, the dual phase membrane 03 prepared by the direct *in situ* sol-gel method with the smallest grains shows the



**Figure 8.** Oxygen permeation flux through 40NFO-60CGO composite membranes without coating as a function of time at 950°C.

Feed: 150 ml/min 50 vol % O<sub>2</sub> with 50 vol % N<sub>2</sub>. Sweep: 29 ml/min He + 1 ml/min Ne as internal standard gas, thickness of membranes = 0.6 mm. [Color figure can be viewed in the online issue, which is available at wileyonlinelibrary.com.]



**Figure 9.** Temperature dependence of the oxygen permeation fluxes through 40NFO-60CGO membranes prepared by different methods without coating.

Feed: 150 ml/min 50 vol % O<sub>2</sub> with 50 vol % N<sub>2</sub>. Sweep: 29 ml/min He + 1 ml/min Ne as internal standard gas. Thickness of membranes = 0.6 mm. [Color figure can be viewed in the online issue, which is available at wileyonlinelibrary.com.]

highest oxygen permeation fluxes followed by the membrane 02 made by ball-milling with medium grain size and finally by the membrane 01 with the highest grain size made by powder mixing. The Arrhenius plots of the oxygen permeation fluxes through composite membranes (Figure 10) show that the permeation activation energy of membrane 03  $E_a = 67.48$  kJ/mol is the smallest of the three membranes, whereas the  $E_a$  of membranes 02 and 03 are ~112.0 and ~107.9 kJ/mol, respectively. Similar results were reported in 75 wt % Ce<sub>0.8</sub>Gd<sub>0.2</sub>O<sub>1.9</sub>-25 wt % Gd<sub>0.2</sub>Sr<sub>0.8</sub>FeO<sub>3-δ</sub> (GDC-GSF) dual phase membranes.<sup>27</sup>

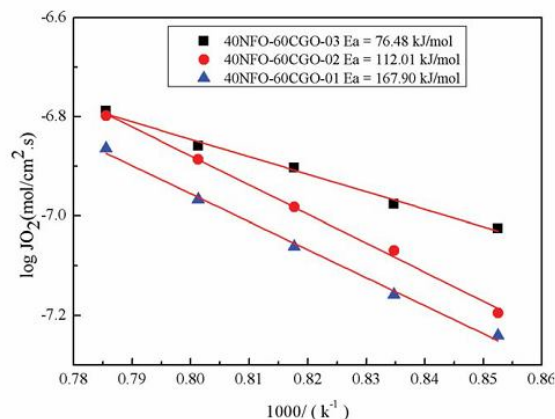


**Figure 10.** Arrhenius plots of the oxygen permeation fluxes through 40NFO-60CGO dual phase membranes (for the experimental conditions see Figure 9).

[Color figure can be viewed in the online issue, which is available at wileyonlinelibrary.com.]

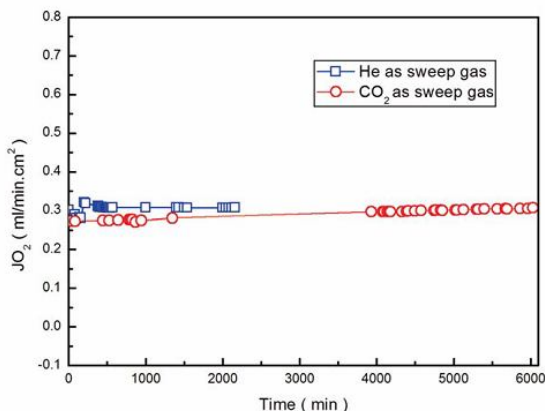


**Figure 11.** Oxygen permeation flux of the 40NFO-60CGO 03 composite membrane with LSC coating as a function of time at 1000°C, membrane thickness = 0.6 mm.

Feed: 150 ml/min synthetic air with 20 vol % O<sub>2</sub>. Sweep: 29 ml/min He + 1 ml/min Ne as an internal standard gas. [Color figure can be viewed in the online issue, which is available at [wileyonlinelibrary.com](http://wileyonlinelibrary.com).]

#### CO<sub>2</sub>-stability of 40NFO-60CGO 03 membrane

Because membrane 40NFO-60CGO 03 made by the direct *in situ* sol-gel synthesis showed the highest oxygen permeation flux, we selected this membrane for CO<sub>2</sub> stability tests and for further surface modification. To improve the oxygen surface exchange rate on the air side, the 40NFO-60CGO 03 membrane was coated with La<sub>0.6</sub>Sr<sub>0.4</sub>CoO<sub>3-δ</sub> (LSC) porous layer on one side using a paste made of 40 wt % LSC powder and 60 wt % terpineol. The low CO<sub>2</sub> partial pressure in natural air will not cause a strontium carbonate formation above 722°C.<sup>31</sup> In our experiments, however, synthetic air was used. After coating with the LSC layer, the membrane 40NFO-60CGO 03 was calcined at 950°C for 2 h in air to burn the organics.

Figure 11 shows the dependence of the oxygen permeation flux of the 40NFO-60CGO 03 composite membrane as a function on time at 1000°C with pure He or CO<sub>2</sub> as sweep gases. From Figure 11, we can find that the LSC coated membrane 03 reaches steady-state oxygen permeation like the uncoated membrane 03 after a relative short time in comparison with the uncoated membranes 01 and 02 (cf. Figure 8). There is almost no difference between using He or CO<sub>2</sub> as sweep gases, which indicates that the membrane 40NFO-60CGO 03 membrane is really CO<sub>2</sub> tolerant. Furthermore, the membrane was operated for 100 h in the oxygen separation with pure CO<sub>2</sub> as the sweep gas which again indicates that the material composition 40NFO-60CGO was found to be CO<sub>2</sub>-stable—at least for our 5 days of testing which is a relative short time scale from an industrial point of view. However, the oxygen permeation flux is found to be slightly lower when CO<sub>2</sub> is used as sweep gas in comparison with He. This difference can be explained by the inhibiting effect of carbon dioxide on the oxygen surface exchange reaction, i.e., the presence of CO<sub>2</sub> reduces the rate of the oxygen release from the solid. This assumption is in complete agreement with previous

papers,<sup>32–34</sup> which report that the oxygen surface exchange reaction is not the same in different gas atmospheres.

#### Conclusions

Different synthesis methods for the preparation of a carbon dioxide resistant dual phase membrane of the composition 40 wt % NiFe<sub>2</sub>O<sub>4</sub>-60 wt % Ce<sub>0.9</sub>Gd<sub>0.1</sub>O<sub>2-δ</sub> (40NFO-60CGO) with NFO as electron conductor and CGO as oxygen ion conductor have been evaluated. The membrane prepared by a direct one-pot synthesis shows the smallest grains and the highest oxygen permeation fluxes in the range 900–1000°C. On the opposite, the membranes prepared by mixing the NFO and CGO powders in a mortar or by ball-milling give larger grains and a lower oxygen permeation flux. High-temperature XRD in CO<sub>2</sub> containing atmospheres showed that the NFO and CGO phases in 40NFO-60CGO 03 remained unchanged, and no carbonate was formed. In long-time permeation studies with CO<sub>2</sub> as sweep gas, we also found that the dual phase membrane 40NFO-60CGO 03 was CO<sub>2</sub> stable and an average oxygen flux of 0.30 ml/(min cm<sup>2</sup>) was obtained at 1000°C for a 0.5-mm-thick membrane. This value is comparable with them of La<sub>2</sub>NiO<sub>4+δ</sub> as well as La<sub>2</sub>Ni<sub>0.9</sub>Fe<sub>0.1</sub>O<sub>4+δ</sub>, which are promising CO<sub>2</sub>-stable membrane materials.<sup>35</sup>

#### Acknowledgments

The author (H.X. Luo) acknowledges the financial support by the China Scholarship Council (CSC). K. Efimov thanks the State of Lower Saxony for the NTH bottom up grant No. 21-71023-25-7/09. H.H. Wang greatly acknowledges the financial support by the National Natural Science Foundation of China (nos. 20706020 and U0834004), the National Basic Research Program of China (no. 2009CB623406), and the International Joint Project of Guangdong Province Science and Technology (2009B050700017). The authors also greatly acknowledge Dr. A. Feldhoff for stimulating discussions as well as F. Steinbach and F.Y. Liang for technical support.

#### Literature Cited

- Herzog H, Golomb D, Zemba, S. Feasibility, modeling and economics of sequestering power plant CO<sub>2</sub> emission in the deep ocean. *Environ Prog.* 2006;10:64–74.
- Lozza G, Chiesa P. Natural gas decarbonization to reduce CO<sub>2</sub> emission from combined cycles. I. Partial oxidation. *ASME J Eng Gas Turbines Power.* 2002;124:82–88.
- Corradetti A, Desideri U. Analysis of gas-steam combined cycles with natural gas reforming and CO<sub>2</sub> capture. *ASME J Eng Gas Turbines Power.* 2005;127:545–552.
- Chiesa P, Consonni S. Natural gas fired combined cycles with low CO<sub>2</sub> emission. *ASME J Eng Gas Turbines Power.* 2000;122:429–436.
- Luo HX, Wei YY, Jiang HQ, Yuan, WH, Lv YX, Caro J, Wang HH. Performance of a ceramic membrane reactor with high oxygen flux Ta-containing perovskite for the partial oxidation of methane to syngas. *J Membr Sci.* 2010;350:154–160.
- Jiang HQ, Wang HH, Werth S, Schiestel T, Caro J. Simultaneous production of hydrogen and synthesis gas by combining water splitting with partial oxidation of methane in a hollow fiber membrane reactor. *Angew Chem Int Ed Engl.* 2008;47:9341–9344.
- Jiang HQ, Cao ZW, Schirmeister S, Schiestel T, Caro J. A coupling strategy to produce hydrogen and ethylene in a membrane reactor. *Angew Chem Int Ed Engl.* 2010;49:5656–5660.
- Jiang HQ, Liang FY, Czuprat O, Efimov K, Feldhoff A, Schirmeister S, Schiestel T, Wang HH, Caro J. Hydrogen production by water dissociation in surface-modified BaCo<sub>2</sub>Fe<sub>1-x</sub>Zr<sub>1-x</sub>O<sub>3-δ</sub> hollow fiber membrane reactor with improved oxygen permeation. *Chem Eur J.* 2010;16:7898–7903.

- Jiang HQ, Wang HH, Liang FY, Werth S, Schiestel T, Caro J. Direct decomposition of nitrous oxide to nitrogen by in situ oxygen removal with a perovskite membrane. *Angew Chem Int Ed Engl.* 2009;48:2983–2986.
- Chen CS, Feng SJ, Ran S, Zhu DC, Liu W, Bouwmeester HJM. Conversion of methane to syngas by a membrane-based oxidation-reforming process. *Angew Chem Int Ed Engl.* 2003;42:5196–5198.
- Jin WQ, Zhang C, Zhang P, Fan YQ, Xu NP. Thermal decomposition of carbon dioxide coupled with POM in a membrane reactor. *AIChE J.* 2006;52:2545–2550.
- Tsai CY, Dixon AG, Moser WR, Ma YH. Dense perovskite membrane reactor for partial oxidation of methane to syngas. *AIChE J.* 1997;43:2741–2750.
- Smart S, Lin CXC, Ding L, Thambimuthu K, Diniz da Costa JC. Ceramic membranes for gas processing in coal gasification. *Energy Environ Sci.* 2010;3:268–278.
- Tan XY, Li K, Thursfield A, Metcalfe IS. Oxyfuel combustion using a catalytic ceramic membrane reactor. *Catal Today.* 2008;131:292–304.
- Zhang N, Lior N. Two novel-fuel power cycles integrated with natural gas reforming and CO<sub>2</sub> capture. *Energy.* 2008;33:340–351.
- Plasynski SI, Litynski JT, McIlvried HG, Srivastava RD. Progress and new developments in carbon capture. *Crit Rev Plant Sci.* 2009;28:123–138.
- Fan YQ, Ren JY, Onstot W, Pasale J, Tsotsis TT, Egolfopoulos FN. Reactor and technical feasibility aspects of a CO<sub>2</sub> decomposition-based power generation cycle, utilizing a high temperature membrane reactor. *Ind Eng Chem Res.* 2003;42:2618–2626.
- Arnold M, Wang HH, Feldhoff A. Influence of CO<sub>2</sub> on the oxygen permeation performance and the microstructure of perovskite-type (Ba<sub>0.5</sub>Sr<sub>0.5</sub>)(Co<sub>0.8</sub>Fe<sub>0.2</sub>)O<sub>3-δ</sub> membranes. *J Membr Sci.* 2007;293:44–52.
- Yi JX, Feng SJ, Zuo YB, Liu YB, Chen CS. Oxygen permeability and stability of Sr<sub>0.95</sub>Co<sub>0.8</sub>Fe<sub>0.2</sub>O<sub>3-δ</sub> in a CO<sub>2</sub> and H<sub>2</sub>O-containing atmosphere. *Chem Mater.* 2005;17:5856–5861.
- Ten Elshof JE, Nguyen NQ, Den Otter MW, Bouwmeester HJM. Oxygen permeation properties of dense Bi<sub>1.5</sub>Er<sub>0.5</sub>O<sub>3</sub>-Ag cermet membranes. *J Electrochem Soc.* 1997;144:4361–4366.
- Kobayashi K, Tsunoda T. Oxygen permeation and electrical transport properties of 60 vol % Bi<sub>1.6</sub>Y<sub>0.4</sub>O<sub>3</sub> and 40 vol % Ag composite prepared by the sol-gel method. *Solid State Ionics.* 2004;175:405–408.
- Kim J, Lin YS. Synthesis and oxygen permeation properties of ceramic-metal dual-phase membranes. *J Membr Sci.* 2000;167:123–133.
- Kharton VV, Kovalevsky AV, Viskup AP, Shaula AL, Figueiredo FM, Naumovich EN, Marques FMB. Oxygen transport in Ce<sub>0.8</sub>Gd<sub>0.2</sub>O<sub>2-δ</sub>-based composite membranes. *Solid State Ionics.* 2003;160:247–258.
- Li W, Tian TF, Shi FY, Wang YS, Chen CS. Ce<sub>0.8</sub>Sm<sub>0.2</sub>O<sub>2-δ</sub>-La<sub>0.8</sub>Sr<sub>0.2</sub>MnO<sub>3-δ</sub> dual-phase composite hollow fiber membrane for oxygen separation. *Ind Eng Chem Res.* 2009;48:5789–5793.
- Wang B, Zhan MC, Liu W, Chen CS. Oxygen permeation and stability of Zr<sub>0.8</sub>Y<sub>0.2</sub>O<sub>3</sub>-La<sub>0.8</sub>Sr<sub>0.2</sub>CrO<sub>3-δ</sub> dual-phase composite. *J Solid State Electrochem.* 2006;10:625–628.
- Li QM, Zhu XF, Yang WS. Single-step fabrication of asymmetric dual-phase composite membranes for oxygen separation. *J Membr Sci.* 2008;325:11–15.
- Zhu XF, Wang HH, Yang WS. Relationship between homogeneity and oxygen permeability of composite membranes. *J Membr Sci.* 2008;309:120–127.
- Luo HX, Tian BB, Wei YY, Wang HH, Jiang HQ, Caro J. Oxygen permeability and structural stability of a novel tantalum-doped perovskite BaCe<sub>0.7</sub>Fe<sub>0.2</sub>Ta<sub>0.1</sub>O<sub>3-δ</sub>. *AIChE J.* 2010;56:604–610.
- Yi JX, Zuo YB, Liu W, Winnubst L, Chen CS. Oxygen permeation through a Ce<sub>0.8</sub>Sm<sub>0.2</sub>O<sub>2-δ</sub>-La<sub>0.8</sub>Sr<sub>0.2</sub>CrO<sub>3-δ</sub> dual-phase composite membrane. *J Membr Sci.* 2006;280:849–855.
- Zhu XF, Cong Y, Yang WS. Effects of synthesis methods on oxygen permeability of BaCe<sub>0.15</sub>Fe<sub>0.85</sub>O<sub>3-δ</sub> ceramic membranes. *J Membr Sci.* 2006;283:158–163.
- Feldhoff A, Arnold M, Martynczuk J, Gesing TM, Wang HH. The sol-gel synthesis of perovskites by an EDTA/citrate complexing method involves nanoscale solid state reactions. *Solid State Sci.* 2008;10:689–701.
- Lane JA, Kilner JA. Oxygen surface exchange on gadolinia doped ceria. *Solid State Ionics.* 2000;136–137:927–932.
- Yashiro K, Onuma S, Kaimai A, Nigara Y, Kawada T, Mizusaki J, Kawamura K, Horita T, Yokokawa H. Mass transport properties of Ce<sub>0.9</sub>Gd<sub>0.1</sub>O<sub>3-δ</sub> at the surface and in the bulk. *Solid State Ionics.* 2002;152–153:469–476.
- ten Elshof JE, Bouwmeester HJM, Verweij H. Oxygen transport through La<sub>1-x</sub>Sr<sub>x</sub>FeO<sub>3-δ</sub> membranes. II. Permeation in air/CO, CO<sub>2</sub> gradients. *Solid State Ionics.* 1996;89:81–92.
- Kharton VV, Tsipis EV, Naumovich EN, Thursfield A, Patrakeeve MV, Kolotygin VA, Waerenborgh JC, Metcalfe IS. Mixed conductivity, oxygen permeability and redox behavior of K<sub>2</sub>NiF<sub>4</sub>-type La<sub>2</sub>Ni<sub>0.9</sub>Fe<sub>0.1</sub>O<sub>4+δ</sub>. *J Solid State Chem.* 2008;181:1425–1433.

Manuscript received July 26, 2010, and revision received Sep. 16, 2010.

### **3.4 CO<sub>2</sub>-tolerant oxygen-permeable Fe<sub>2</sub>O<sub>3</sub> - Ce<sub>0.9</sub>Gd<sub>0.1</sub>O<sub>2-δ</sub> dual phase membranes**

Huixia Luo, Heqing Jiang, Konstantin Efimov, Fangyi Liang, Haihui Wang, Jürgen Caro,

**Ind. Eng. Chem. Res.** 2011, *50*, 13508.

**Reprinted (adapted) with permission from (Industrial Engineering Chemistry Research).  
Copyright (2011) American Chemical Society.**



## CO<sub>2</sub>-Tolerant Oxygen-Permeable Fe<sub>2</sub>O<sub>3</sub>-Ce<sub>0.9</sub>Gd<sub>0.1</sub>O<sub>2-δ</sub> Dual Phase Membranes

Huixia Luo,<sup>†</sup> Heqing Jiang,<sup>†</sup> Konstantin Efimov,<sup>†</sup> Fangyi Liang,<sup>†</sup> Haihui Wang,<sup>†,\*</sup> and Jürgen Caro<sup>†,\*</sup>

<sup>†</sup>Institute of Physical Chemistry and Electrochemistry, Leibniz University of Hannover, Callinstrasse 3-3A, D-30167 Hannover, Germany

<sup>\*</sup>School of Chemistry & Chemical Engineering, South China University of Technology, No. 381 Wushan Road, 510640 Guangzhou, China

**ABSTRACT:** CO<sub>2</sub>-stable oxygen-permeable Fe<sub>2</sub>O<sub>3</sub> (FO) - Ce<sub>0.9</sub>Gd<sub>0.1</sub>O<sub>2-δ</sub> (CGO) dual phase composite membranes of the composition  $\chi$  wt % FO - (100 -  $\chi$ ) wt % CGO with  $\chi = 25, 40, 50$  were successfully prepared via a one-pot single-step method. X-ray diffraction (XRD) demonstrated that all FO - CGO composite membranes after sintering at 1300 °C for 5 h represent a microscale mixture of only the two pure phases FO and CGO. Scanning electron microscopy (SEM), energy dispersive X-ray spectroscopy (EDXS), and oxygen permeation revealed that the microstructure of the composition of the  $\chi$  FO - (100 -  $\chi$ ) CGO dual phase membranes has a great influence on the oxygen permeability including its time-dependence. It was found that the composition of 40FO - 60CGO displays the highest oxygen permeability. An oxygen permeation flux of 0.18 mL/min · cm<sup>2</sup> was obtained through the uncoated 40FO - 60CGO membrane with a thickness of 0.5 mm under an air/He oxygen gradient at 1000 °C. *In situ* XRD demonstrates that the 40FO - 60CGO material possesses a good phase stability not only in an atmosphere of 50 vol % CO<sub>2</sub>/50 vol % Ar but also in other atmospheres with a low oxygen partial pressure like reduced pressure (vacuum) and 5 vol % H<sub>2</sub>/95 vol % He. After coating the 40FO - 60CGO dual phase membrane with a porous La<sub>0.6</sub>Sr<sub>0.4</sub>CoO<sub>3-δ</sub> (LSC) layer of a few  $\mu$ m thicknesses on the air side, the oxygen permeation flux reaches the steady state immediately. This steady oxygen permeation flux of the LSC coated membrane was found to be 0.20 mL/min · cm<sup>2</sup> unchanged for more than 150 h even when pure CO<sub>2</sub> was used as the sweep gas, which indicates that the coated 40FO - 60CGO dual phase membrane is CO<sub>2</sub> stable.

### 1. INTRODUCTION

In recent years, owing to their potential applications in separation of oxygen from air,<sup>1,2</sup> partial oxidation of methane to synthesis gas,<sup>3-5</sup> hydrogen production by water splitting,<sup>6-8</sup> and as cathode in solid oxide fuel cells (SOFCs),<sup>8,9</sup> oxygen-permeable dense ceramic membranes with mixed ionic-electronic conductivity (MIEC) have been intensively investigated. At high temperatures, MIEC membranes with high oxygen permeability and infinite selectivity provide a promising way to supply pure oxygen to power plants with CO<sub>2</sub> capture following the oxy-fuel concept.<sup>11-13</sup> It is accepted that oxygen-permeable membranes can be operated in a vacuum driven (3-end operation) and in a sweep gas driven oxy-fuel process (4-end operation).<sup>14</sup>

So far, the most studied oxygen-permeable materials are single-phase perovskite-type materials since these materials possess a high oxygen permeability. However, most of these perovskite-type materials have stability problems in a low oxygen partial pressure atmosphere and especially in a CO<sub>2</sub> containing atmosphere.<sup>15,16</sup> Dual phase membranes which consist of an oxygen ionic conducting (OIC) phase and an electronic conducting (EC) phase in a microscale phase mixture are considered to be promising substitutes for the single phase MIEC materials. In addition to good phase stability in CO<sub>2</sub> and reducing atmospheres, their chemical compositions can be tailored according to practical requirements.<sup>17</sup> However, due to the use of noble metals as electronic conductor<sup>18-20</sup> and reactions between OIC and EC phases forming mixed oxides at high operation temperature,<sup>21-23</sup> most of these composite membranes are too expensive or unstable. Therefore, the development of new oxygen-permeable membranes with high chemical/phase

stability under low oxygen partial pressures or CO<sub>2</sub> atmospheres is highly desired.

Recently, a novel alkaline earth metal-free, noble metal-free dual phase membrane 40 wt % NiFe<sub>2</sub>O<sub>4</sub> (NFO) - 60 wt % Ce<sub>0.9</sub>Gd<sub>0.1</sub>O<sub>2-δ</sub> (CGO) with CO<sub>2</sub>-stability has been developed in our group for oxygen separation.<sup>24,25</sup> This membrane was steadily operated for more than 150 h under an air/CO<sub>2</sub> oxygen partial pressure gradient. However, it is found that 40NFO - 60CGO composite membranes were not stable under low oxygen partial pressure. Kharton et al.<sup>26,27</sup> and Ishihara et al.<sup>28,29</sup> recently reported that Fe-doped LaSrGaO<sub>3</sub> was more stable than Ni-doped LaSrGaO<sub>3</sub> in a reducing atmosphere. On the other hand, it is well-known that iron is one of most abundant elements on earth, which is cheaper than Ni and benefits from a wide industrial application. Moreover, the solubility of Fe in CGO has been reported to be as low as 0.5 atom %.<sup>30</sup> It can be expected, therefore, that the low solubility of Fe in CGO would promote Fe oxide segregation as a separate phase in the composite system. Therefore, based on our previous studies,<sup>24,25</sup> it should be possible to design a new dual phase oxygen-permeable material replacing Ni by Fe. It is expected that this oxygen transporting material will exhibit both adequate CO<sub>2</sub> stability and sufficient chemical/phase stability at low oxygen partial pressure for a practical application in the oxy-fuel process.

Received: March 15, 2011

Accepted: October 27, 2011

Revised: October 11, 2011

Published: October 27, 2011

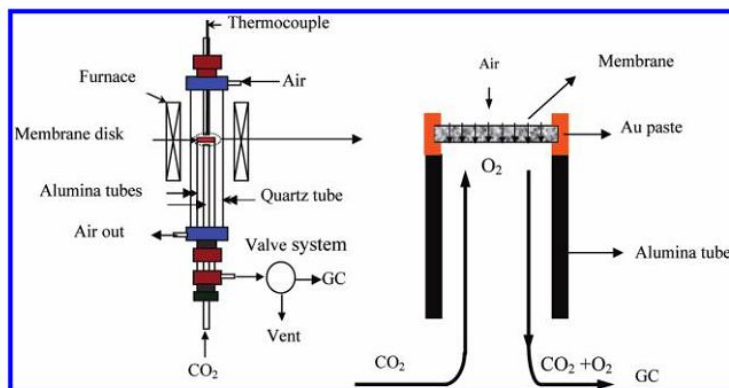


Figure 1. Equipment schematic for oxygen permeation.

Herein, we report the preparation and evaluation of a series of dual phase composite membranes of the compositions  $\chi$  wt % FO - (100 -  $\chi$ ) wt % CGO, with FO as the electron conductor and CGO as the oxygen ion conducting phase. The influences of the FO:CGO ratio and of the sintering temperature on the oxygen permeability are investigated. Phase structure and stability as well as oxygen permeability are studied for different sweep gas atmospheres on the permeate side. Special attention is paid to the CO<sub>2</sub> stability and the chemical/phase stability of FO and CGO, especially in low oxygen partial pressure atmospheres. Phase stability means that no changes of the two coexisting crystallographic phases FO and CGO in their microscale mixture could be observed by X-ray diffraction. Chemical stability means that no changes of the chemical composition of the dual phase material have been detected by energy-dispersive X-ray spectroscopy.

## 2. EXPERIMENT

**2.1. Preparation of Powders and Membranes.** The  $\chi$  wt % FO - (100 -  $\chi$  wt %) CGO ( $\chi = 25, 40$ , and  $50$ , and denoted 25FO - 75CGO, 40FO - 60CGO, and 50FO - 50CGO, respectively) composite powders were synthesized via a one-pot single-step method. This preparation technique is described elsewhere.<sup>24,25</sup> The composite powders obtained after heat treatment for 10 h at 950 °C were pressed to disk-shaped membranes under a pressure of 10 MPa in a stainless steel module with a diameter of 18 mm. The green disks were sintered at 1300 °C, 1325 °C, and 1350 °C for 5 h in air, respectively. All the membranes used for oxygen permeation tests had relative densities of more than 95% of the theoretical density. All types of disks were carefully polished with 1200 mesh sandpaper from both sides to achieve a 0.5 mm membrane thickness. Before oxygen permeation, both surfaces of the polished disks were cleaned with ethanol. To improve the oxygen surface exchange rate on the air side, the 40FO - 60CGO membrane was coated with a La<sub>0.6</sub>Sr<sub>0.4</sub>CoO<sub>3- $\delta$</sub>  (LSC) porous layer, which is known to show a good oxygen reducing activity when it acts as cathode materials for SOFC.<sup>31</sup> After coating with the LSC layer, the membrane was calcined again at 950 °C for 2 h. The disk membranes were sealed onto a quartz tube with a gold paste (Heraeus, Germany) as described previously.<sup>32</sup> From the presence of small amounts of nitrogen in the permeated gas, it follows that this sealing was imperfect. If the oxygen flux which goes through imperfections was higher than 5% of the total oxygen

flux, the process of gold sealing had to be repeated several times (see 2.3 Oxygen Permeation Performance).

**2.2. Membrane Characterization.** X-ray diffraction (XRD, D8 Advance, Bruker-AXS, with Cu K $\alpha$  radiation) was used to determine the phase structure. Data sets were recorded in a step-scan mode in the  $2\theta$  range of 20°–80° with intervals of 0.02°. Structural data for FO and CGO phases were taken from ICDD PDF 2009 database:  $\alpha$ -Fe<sub>2</sub>O<sub>3</sub>: [00-003-0800], and Ce<sub>0.9</sub>Gd<sub>0.1</sub>O<sub>1.95</sub> [01-075-0161]. *In situ* XRD was conducted in a high-temperature cell HTK-1200N (Anton - Paar) from room temperature to 1000 °C. The *in situ* XRD tests in a 50 vol % CO<sub>2</sub>/50 vol % Ar atmosphere and at reduced pressure (vacuum, 10<sup>-6</sup> bar) were performed with a heating rate of 12 °C/min. At each temperature step, samples of the crushed membranes were held for 30 min for thermal and chemical equilibration before the diffraction data collection. For phase stability studies, the membranes sintered at 1300 °C for 5 h in air were crushed into small particles in the 40–60 mesh range and then exposed to a 5 vol % H<sub>2</sub>/95 vol % He mixed gas at 900 °C for 2 and 4 h, respectively. The morphology of the membranes was investigated by scanning electron microscopy (SEM) using the Jeol-JSM-6700F operating at 15 keV. The element distribution of the membranes was studied on the same electron microscope by energy dispersive X-ray spectroscopy (EDXS) with Oxford Instruments INCA-300 EDX spectrometer at 15 keV.

**2.3. Oxygen Permeation Performances of Membranes.** Oxygen permeation was studied in a home-made high-temperature oxygen permeation cell, described elsewhere.<sup>32</sup> The disk membranes were sealed as described onto a quartz tube at 950 °C for 5 h with a gold paste (Heraeus, Germany), the side wall of the membrane disk was also covered with the gold paste to avoid a radial contribution to the oxygen permeation flux, as shown in Figure 1. The effective areas of the membranes for oxygen permeation were 0.785 cm<sup>2</sup>. The inlet gas flow rates were controlled by gas mass flow controllers (Bronkhorst), and the flow rates were regularly calibrated by using a bubble flow meter. Synthetic air (20% O<sub>2</sub> and 80% N<sub>2</sub>) with a flow rate of 150 mL/min was used as feed gas. He or CO<sub>2</sub> was used (29 mL/min) as sweep gas to remove the permeated oxygen. One milliliter of Ne/min was added to the He or CO<sub>2</sub> as an internal standard gas for gas chromatography to calculate the total flow rate at the outlet of the sweep side. The effluents were analyzed by an online gas chromatograph (GC, Agilent 7890A). The GC was frequently calibrated using standard gases in order to ensure the reliability of

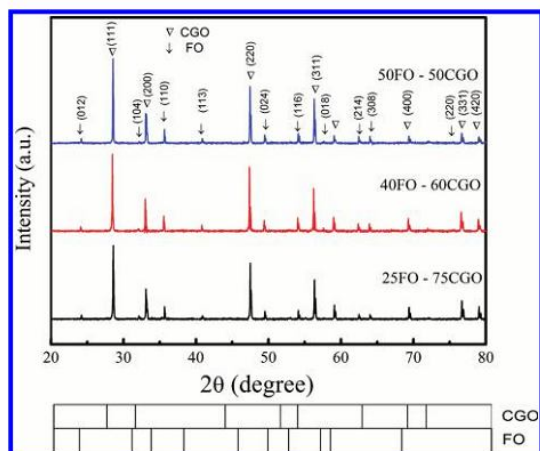


**Figure 2.** XRD patterns of FO - CGO dual phase membranes of different compositions after sintering at 1300 °C for 5 h in air.

the experimental data. As stated in 2.1, the leakage caused by an imperfect sealing can be determined by detecting N<sub>2</sub> in the permeated O<sub>2</sub> by GC. Here, we assume that leakage of nitrogen and oxygen is in accordance with Knudsen diffusion. The leakage of oxygen was subtracted from the oxygen permeation flux (the oxygen leakage through imperfections of the gold sealing and/or through pinholes or microcracks of the membrane never exceeded 5% of the oxygen that regularly permeated through the membrane). The total flow rate of the effluents was calculated based on the change in the Ne concentrations before and after the permeator. The oxygen permeation flux calculation was shown in detail elsewhere.<sup>25</sup> However, in the case of dual phase membranes the oxygen flux could be influenced by an additional electronic conductivity originating from the metal sealing as discussed in ref 33 for EMF measurements. We could experimentally exclude this possible error by using a glass sealing without any electron or oxygen ion conductivity instead of gold, as described in ref 34 for the gastight attachment of the disk membrane to the quartz tube. No difference in the oxygen permeation flux between metal (gold) and glass sealings could be found.

### 3. RESULTS AND DISCUSSIONS

**3.1. Characterizations of the FO - CGO Dual Phase Materials.** Figure 2 presents the XRD patterns of the  $\chi$  FO - (100 -  $\chi$ ) CGO dual phase composite membranes after sintering at 1300 °C for 5 h before its use in oxygen separation. All three membranes under study (25FO - 75CGO, 40FO - 60CGO, and 50FO - 50CGO) consist of only the two phases FO and CGO, indicating that the coexistence of the phases FO and CGO is stable. The exact compositions of the FO and CGO phases present are most probably near to the stoichiometric ones, since there is only a tiny solubility of CeO<sub>2</sub> and GdO<sub>2</sub> in FO and of Fe<sub>2</sub>O<sub>3</sub> in CGO.<sup>30</sup> It has been reported by Jivaganont et al.<sup>35</sup> that the solubility limit of Fe<sub>2</sub>O<sub>3</sub> into Ce<sub>0.9</sub>Gd<sub>0.1</sub>O<sub>1.95</sub> is less than 0.5 atom %. If the Fe content is >0.5 atom %, a new Gd-Fe-O phase will be formed.<sup>35</sup> However, in our case, this GdFeO<sub>3</sub> phase has not been observed from the XRD (limit of detection in this case about 5%). From the absence of foreign phase signals different from FO and CGO, it is concluded that the dual phase

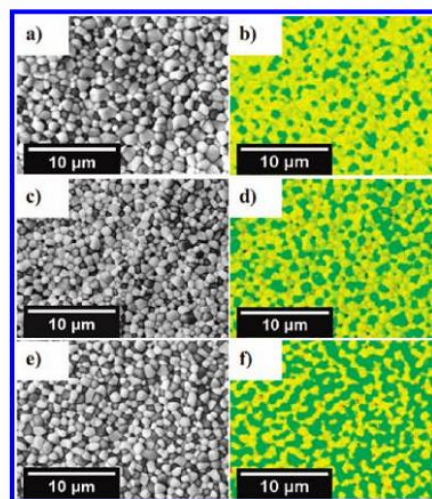


**Figure 3.** SEM (left line, a, c, e) and EDXS (right line, b, d, f) micrographs of the surface of 25FO - 75CGO (a, b), 40FO - 60CGO (c, d), and 50FO - 50CGO (e, f) dual phase membranes after sintering at 1300 °C for 5 h. In SEM, the dark grains represent the FO grains, the light ones represent the CGO grains, since the contribution of the secondary electrons to the SEM signal intensity is proportional to the ionization potential (first ionization potential Ce  $\ll$  Fe). In EDXS, the green grains represent FO grains (Fe 3p  $\rightarrow$  2s line), and the yellow grains represent CGO grains (averaged and calibrated signals of Ce 4s  $\rightarrow$  3p and Gd 5p  $\rightarrow$  3s).

membranes  $\chi$  FO - (100 -  $\chi$ ) CGO could be successfully synthesized via the one-pot single-step method.

Figure 3 shows the SEM and EDXS of the  $\chi$  FO - (100 -  $\chi$ ) CGO dual phase membranes after sintering at 1300 °C for 5 h in air. No cracks or pin holes are visible, and it is seen that all three membranes consist of only well separated FO and CGO grains. Kharton et al.<sup>21</sup> reported that a sintering temperature of up to 1600 °C was necessary to obtain a dense CGO membrane. Since the addition of transition metal oxides can decrease the sintering temperature of Gd-doped ceria, we could obtain dense  $\chi$  FO - (100 -  $\chi$ ) CGO dual phase membranes after sintering at only 1300 °C because of FO acting as a sintering agent. Comparing the SEM and EDXS pictures in Figure 3, we can see that the chemical composition, i.e. the FO:CGO ratio, has only little effect on the grain sizes, but it remarkably influences the distribution of the two phases. It is known that the grain size influences the oxygen permeation flux through MIEC membranes.<sup>36,37</sup> In two previous papers,<sup>24,25</sup> we have shown the influence of the grain size on the oxygen permeation flux by applying different preparation techniques for dual phase membranes: (i) sintering of a powder mixed in a mortar by hand, (ii) sintering of a ball-milled mixed powder, and (iii) sintering of a single-step one-pot directly synthesized powder mixture. The direct single-step one-pot sol-gel synthesis gave the smallest grain size with the highest oxygen flux. Therefore, we applied the latter technique for the powder synthesis also in this paper. Further, there are slight differences in the grain size of the FO - CGO dual phase membranes of this paper as function of the FO - CGO ratio (see Figure 3). In all cases, the CGO grains are larger than the FO grains. From the analysis of 50 grains, we obtain the following mean grain size areas: 25FO (0.047  $\mu\text{m}^2$ ) - 75CGO (0.085  $\mu\text{m}^2$ ), 40FO (0.064  $\mu\text{m}^2$ ) - 60CGO (0.093  $\mu\text{m}^2$ ), and

50FO (0.079 μm<sup>2</sup>) - 50CGO (0.087 μm<sup>2</sup>). The remarkable effects of the sintering temperatures on the grain sizes and the oxygen permeabilities, will be discussed in detail in section 3.3 Influence of the Sintering Temperatures on Oxygen Permeability.

For the 25FO - 75CGO (Figure 3a and b), the FO phase is finely distributed as isolated islands in the CGO phase, whereas the CGO phase forms a well interpenetrating continuous network. For 40FO - 60CGO (Figure 3c, d) and 50FO - 50CGO (Figure 3e, f), both phases form a continuous interpenetrating network. This optical impression can be correlated with the results of oxygen permeation which show that the FO content in the dual phase membrane FO - CGO should be 25 < FO < 50 (see Figures 4 and 9). If the FO content is lower 25 wt %, the electronic conductor FO forms isolated islands, which lead to a low oxygen permeation flux due to the lack of electronic conductivity. An FO content >50 wt % FO also reduces the oxygen permeability since in this case oxygen permeation is limited by the oxygen ion conductivity rather than by the electron conductivity (see Figures 4 and 9). On the other hand, M. Mogensen et al.<sup>38</sup> and B. M. Warnes et al.<sup>39</sup> have examined the conductivity of CGO and FO. The oxygen ionic conductivity of CGO was found to be 0.259 S · cm<sup>-1</sup> and the electronic conductivity of Fe<sub>2</sub>O<sub>3</sub> was 0.398 S · cm<sup>-1</sup> at 975 °C. Therefore, 40FO - 60CGO has an oxygen ionic conductivity of 0.155 S · cm<sup>-1</sup> and electronic conductivity of 0.159 S · cm<sup>-1</sup>. Only if the electronic conductivity is equal to the oxygen ionic conductivity, a dual phase membrane shows its maximum oxygen permeation flux. Therefore, in our case, the optimum oxygen permeation flux can be expected near to the chemical composition 40FO - 60CGO (see Figure 9).

3.2. Influence of the FO:CGO Ratio on Oxygen Permeability. The χFO - (100 - χ) CGO dual phase membranes show

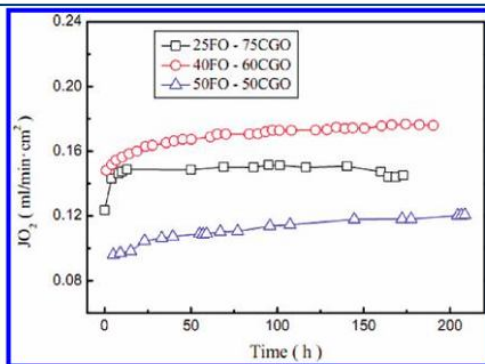


Figure 4. Time dependence of oxygen permeation fluxes at 1000 °C for FO - CGO composite membranes after sintering at 1300 °C for 5 h with He as sweep gas. Conditions: 150 mL/min air as feed gas, 29 mL/min He as sweep gas; 1 mL/min Ne as internal standard gas. Membrane thickness: 0.5 mm.

different oxygen permeation fluxes. Surprisingly, it takes different times for the oxygen permeation flux to reach a steady state (Figure 4). With increasing iron content, the initialization time of the oxygen permeation flux before steady state increases: For 25, 40, and 50 wt % FO in CGO, the initialization times are 10, 150, and 200 h, respectively. Obviously, the FO:CGO ratio controls the oxygen permeability in steady state as well as influences the initiation period. In previous investigations of NFO - CGO dual phase membranes,<sup>24,25</sup> we also found that the oxygen permeation fluxes increased with time in the initial stage, before they reached a steady state. A similar time-dependent behavior could be found for dual phase membranes made of fluorite/perovskite oxides or perovskite/perovskite oxides as reported by Yang et al.<sup>40,41</sup> The initiation period of the 25 wt % Gd<sub>0.2</sub>Sr<sub>0.8</sub>FeO<sub>3-δ</sub> (GSF) - 75 wt % Ce<sub>0.8</sub>Gd<sub>0.2</sub>O<sub>1.9</sub> (CGO) membrane was about 50 h for 40 wt % GSF - 60 wt % CGO membrane the initiation period has risen to even 600 h. Wang et al.<sup>42</sup> observed that the oxygen permeation flux of 92.8 vol % La<sub>0.15</sub>Sr<sub>0.85</sub>Ga<sub>0.3</sub>Fe<sub>0.7</sub>O<sub>3-δ</sub> - 7.2 vol % Ba<sub>0.5</sub>Sr<sub>0.5</sub>Fe<sub>0.2</sub>Co<sub>0.8</sub>O<sub>3-δ</sub> (LSGF - BSCF) dual phase membrane

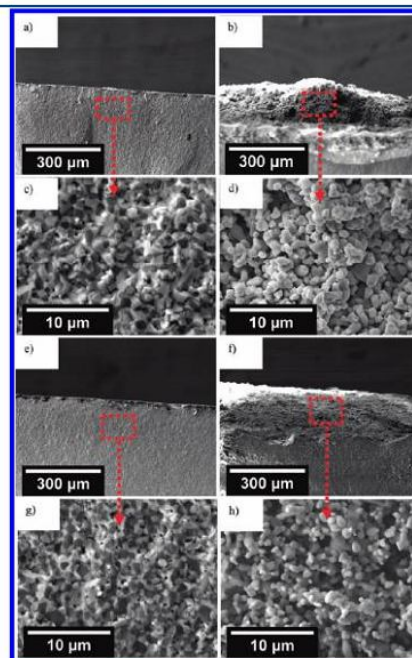


Figure 6. Cross sections of the fresh and spent FO - CGO dual phase membranes after sintering at 1300 °C for 5 h. 40FO - 60CGO: (a,c) fresh membrane, (b,d) sweep side of the spent membrane. 50FO - 50CGO: (e,g) fresh membrane, (f,h) sweep side of the spent membrane.

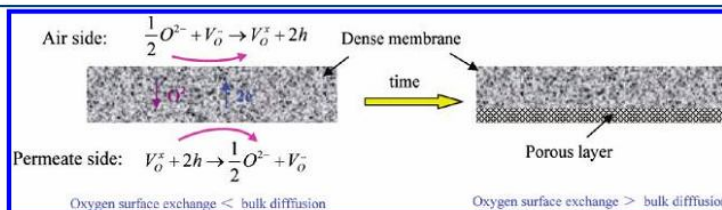


Figure 5. Model for the membrane activation during initialization time.

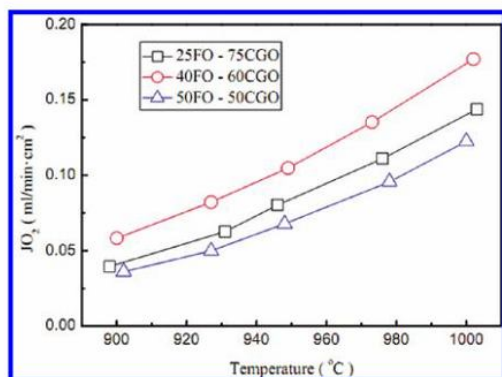


Figure 7. Temperature dependence of oxygen permeation fluxes for FO - CGO composite membranes after sintering at 1300 °C for 5 h with He as sweep gas. Conditions: 150 mL/min air as feed gas, 29 mL/min He as sweep gas, 1 mL/min Ne as internal standard gas. Membrane thickness: 0.5 mm.

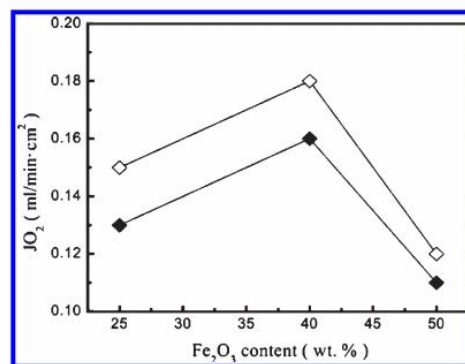


Figure 9. Oxygen permeation flux of  $\chi$  FO - (100 -  $\chi$ ) CGO dual phase membranes after sintering at 1300 °C for 5 h as a function of FO content at 1000 °C with He ( $\diamond$ ) or CO<sub>2</sub> ( $\blacklozenge$ ) as sweep gas. Conditions: 150 mL/min air as feed gas, 29 mL/min He or CO<sub>2</sub> as sweep gas, 1 mL/min Ne as internal standard gas. Membrane thickness: 0.5 mm.

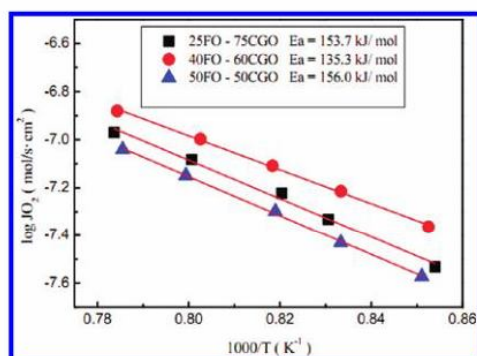


Figure 8. Arrhenius plots of the oxygen permeation fluxes through FO - CGO dual phase membranes after sintering at 1300 °C for 5 h (for the experimental conditions see Figure 7).

increases with time during the first 20 h, before it reaches a steady state. In these papers, the unsteady oxygen permeation in the initialization stage was attributed to surface exchange effects. As shown schematically in Figure 5, we postulate that the unsteady initialization period of oxygen permeation is related to the formation of a porous layer on the low oxygen partial pressure side (sweep side) of the membrane. If there is a remarkable influence of the surface reaction on the overall oxygen transport (thin membrane and high oxygen ions/electrons mobility), an enlargement of the membrane surface can enhance the surface exchange reaction and thus the oxygen transport. Figure 6 shows that on the low oxygen partial pressure side (sweep gas side) a porous layer with a thickness of about 100–150  $\mu\text{m}$  forms which enlarges the effective surface area of the membrane thus leading to an enhancement of the oxygen permeation flux during the initialization period. EDXS indicates that the chemical compositions of the bulk and the porous layer were identical within the error of this method ( $\pm 3$  atom %) and also the XRD analysis of the fresh and spent membranes gave no differences (not shown here). Therefore, in our case, the initialization period process may be related to the surface exchange process of the FO - CGO membrane as discussed by Zhu et al.<sup>43</sup>

Figure 7 shows the oxygen flux through the  $\chi$  FO - (100 -  $\chi$ ) CGO dual phase membranes as a function of temperature with He as sweep gas. All data were collected after the oxygen permeation had reached steady state. As shown in Figure 7, the oxygen permeation fluxes increase with increasing temperature in the following order: 50FO - 50CGO < 25FO - 75CGO < 40FO - 60CGO. Contrarily, the apparent activation energies  $E_a$  for oxygen permeation were found to decrease in the order of 50FO - 50CGO ( $E_a = 156.0$  kJ/mol) > 25FO - 75CGO ( $E_a = 153.7$  kJ/mol) > 40FO - 60CGO ( $E_a = 135.3$  kJ/mol), as shown in Figure 8. Membranes with a lower oxygen permeation flux exhibit a higher activation energy of oxygen permeation. Furthermore, a single activation energy in the temperature range of 900–1000 °C was found for all three membranes. Following Tong et al.,<sup>44</sup> a single activation energy is an important feature for a good phase stability for oxygen permeation through the MIEC membranes. The *in situ* XRD of 40FO - 60CGO (Figures 12 and 13) has proven that this dual phase material possesses a good phase stability in the temperature range between 30 and 1000 °C.

Figure 9 shows the oxygen permeation flux of  $\chi$  FO - (100 -  $\chi$ ) CGO dual phase membranes as a function of the FO content at 1000 °C with He and CO<sub>2</sub> as sweep gases. The 40FO - 60CGO oxygen-permeable dual phase membrane shows an oxygen permeation flux of 0.18 mL/min · cm<sup>2</sup> at 1000 °C under an Air/He oxygen gradient, which is the highest oxygen flux among the three membranes under study. The oxygen permeation fluxes through the 50FO - 50CGO and 25FO - 75CGO membranes were found to be 0.12 mL/min · cm<sup>2</sup> and 0.15 mL/min · cm<sup>2</sup>, respectively. Following the percolation theory, it is reported that the interconnectivity of the two phases is important for the preparation of a mixed conducting composite oxygen transporting membrane.<sup>45,46</sup> The SEM and EDXS microscopy results (cf. Figure 3) showed that the FO particles did not form a continuous interconnecting phase in the 25FO - 75CGO dual phase membrane. Combining the results of SEM, EDXS, and oxygen permeability studies, we can suggest that the isolated FO islands prevent a continuous electronic conductivity and block the transport of oxygen ions through the 25FO - 75CGO dual phase membrane. When combining equal amounts of FO and CGO in a 50FO - 50CGO dual phase material, a continuous interpenetrating network is formed, but only low oxygen permeation fluxes are measured due to the low oxygen ion conductivity in CGO as a

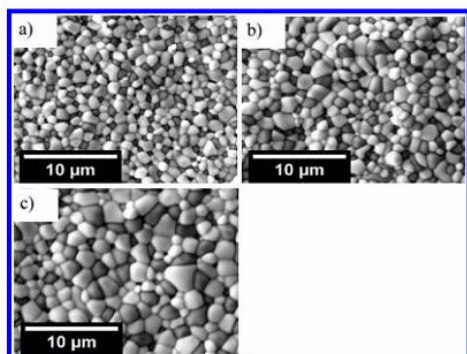


Figure 10. SEM micrographs of the surfaces of 40FO - 60CGO dual phase membranes after sintering at 1300 °C (a), 1325 °C (b), and 1350 °C (c) for 5 h, respectively. Dark grains represent FO, light ones CGO (for an explanation see Figure 3).

bottleneck for the whole oxygen transport process. From published data,<sup>38,39</sup> we know that the oxygen ionic conductivity of CGO and the electronic conductivity of Fe<sub>2</sub>O<sub>3</sub> are around 0.259 S·cm<sup>-1</sup> and 0.398 S·cm<sup>-1</sup> at 975 °C, respectively. Thus, assuming a simple linear ideal relationship, 40FO - 60CGO should possess an oxygen ionic conductivity of 0.155 S·cm<sup>-1</sup> and an electronic conductivity of 0.159 S·cm<sup>-1</sup>. If the electronic conductivity is equal to the oxygen ionic conductivity, then the membrane shows its maximum permeation flux. Therefore, for both pure CO<sub>2</sub> and He as sweep gases, the oxygen permeation flux through the 40FO - 60CGO dual phase membrane is the highest among the three dual phase membranes under study. However, for all membranes the oxygen permeation flux is slightly reduced if pure CO<sub>2</sub> instead of pure He is applied as the sweep gas. A similar observation was made recently for the La<sub>0.8</sub>Sr<sub>0.2</sub>MnO<sub>3-δ</sub> - Ce<sub>0.8</sub>Sm<sub>0.2</sub>O<sub>2-δ</sub> dual phase composite material by Chen et al.,<sup>47</sup> they attributed this finding to the interaction of CO<sub>2</sub> with the surface of the dual phase membrane which influences the surface process of oxygen exchange. The slight reduction of oxygen permeability when using CO<sub>2</sub> as sweep gas is also in complete accordance with our previous study on 40NFO - 60CGO dual phase material.<sup>24,25</sup>

**3.3. Influence of the Sintering Temperatures on Oxygen Permeability.** The aforementioned experiments revealed that the ratio of FO and CGO can affect the oxygen permeability and the composition 40FO - 60CGO shows the highest oxygen permeability. Therefore, we studied the influence of the sintering temperatures on the grain sizes for this composition. Figure 10 shows the SEM pictures of the 40FO - 60CGO membrane after sintered at different temperatures. As shown in Figure 10, the sintering temperatures obviously affect the grain sizes of FO and CGO phases in the 40FO - 60CGO dual phase membranes. The higher the sintering temperature, the larger is the size of both the FO and CGO grains. Moreover, in all cases, the CGO grains are larger than the FO grains. From the analysis of 50 grains, we obtain the following mean grain size areas: 40FO (0.064 μm<sup>2</sup>) - 60CGO (0.093 μm<sup>2</sup>) sintered at 1300 °C for 5 h, 40FO (0.1368 μm<sup>2</sup>) - 60CGO (0.1497 μm<sup>2</sup>) sintered at 1325 °C for 5 h, and 40FO (0.1947 μm<sup>2</sup>) - 60CGO (0.2243 μm<sup>2</sup>) sintered at 1350 °C for 5 h.

In previous studies,<sup>48,49</sup> a grain growth with increasing sintering temperatures also has been observed for the single-phase perovskite membranes Ba<sub>0.5</sub>Sr<sub>0.5</sub>Co<sub>0.8</sub>Fe<sub>0.2</sub>O<sub>3-δ</sub> and La<sub>0.6</sub>Sr<sub>0.4</sub>Co<sub>0.2</sub>Fe<sub>0.8</sub>O<sub>3-δ</sub>. Oxygen permeation demonstrated, however,

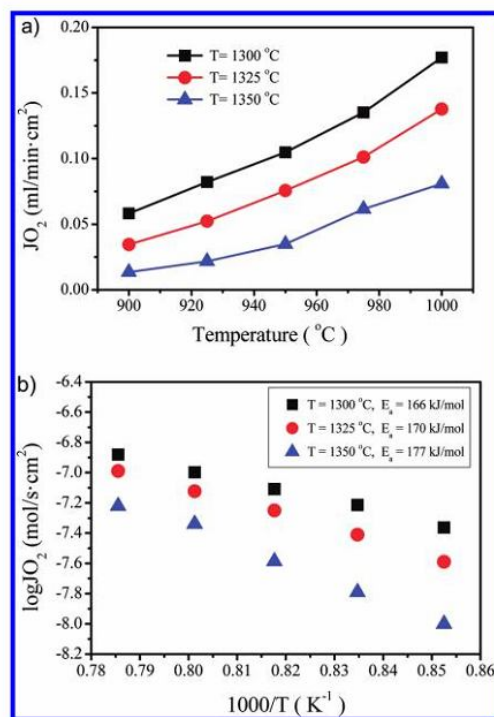


Figure 11. Temperature dependence of oxygen permeation fluxes for 40FO - 60CGO composite membranes sintered at 1300 °C (■), 1325 °C (●), and 1350 °C (▲) for 5 h with He as sweep gas.

that in the case of single-phase membranes the grain growth has a positive effect on the oxygen permeability, since the grain boundaries in single-phase perovskite membranes act as barriers for the oxygen transport. However, in the case of dual phase membranes, the grain growth has a negative effect on the oxygen permeability of 40FO - 60CGO dual phase membrane (Figure 11). As shown in Figure 11a, the oxygen permeation fluxes decrease with increasing sintering temperature, i.e. increasing grain size. For example, the oxygen permeation flux of 0.18, 0.14, and 0.08 mL/min·cm<sup>2</sup> were obtained for the membranes sintered at 1300 °C, 1325 °C, and 1350 °C, respectively, at the same operating temperatures 1000 °C. As usual, with increasing operating temperatures, the oxygen permeation flux increases as well. It was found that membranes sintered at a higher temperature show a smaller oxygen flux with a higher activation energy (Figure 11b). It is well-known that a low activation energy means an easier oxygen transfer in the bulk and oxygen exchange at the surface.<sup>50</sup> With increasing sintering temperatures of dual phase membranes, the grain growth can interrupt the continuity of the FO percolation network, which will block the electronic transport through the dual phase 40FO - 60CGO membrane. Therefore, it can be concluded that a high sintering temperature has a negative influence on the oxygen permeation flux for our dual phase membranes. The similar phenomenon was also observed for 75 wt % Se<sub>0.85</sub>Sm<sub>0.15</sub>O<sub>2-δ</sub> - 25 wt % Sm<sub>0.6</sub>Sr<sub>0.4</sub>FeO<sub>3-δ</sub> dual phase membrane.<sup>51</sup>

**3.4. Characterization and Oxygen Permeation Performance of 40FO - 60CGO Membranes.** Since the highest oxygen permeability was obtained from the dual phase membranes of the

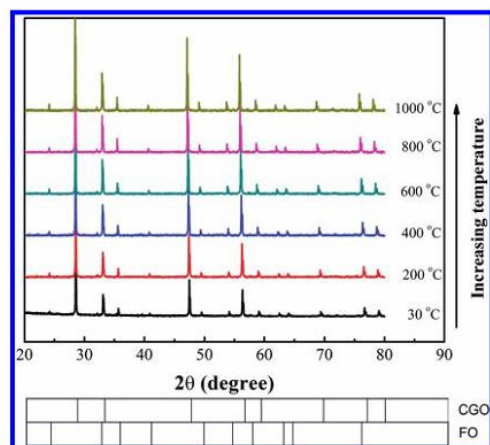


Figure 12. *In situ* XRD patterns of the 40FO - 60CGO composite membrane in 50 vol % CO<sub>2</sub>/50 vol % Ar atmosphere for increasing temperature. Heating rate = 12 °C/min, equilibration time at each temperature: 30 min for recording the XRD data at each temperature.

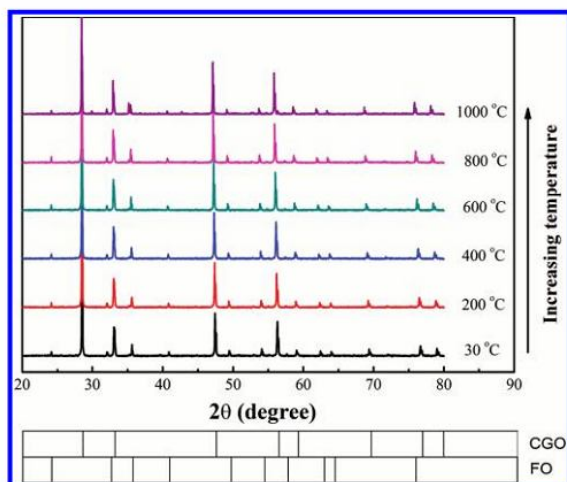


Figure 13. *In situ* XRD patterns of the 40FO - 60CGO composite membrane under vacuum for increasing temperature. Heating rate = 12 °C/min, equilibration time at each temperature: 30 min for recording the XRD data at each temperature.

chemical composition 40FO - 60CGO, we focused the further tests of the thermal stability and of the CO<sub>2</sub> stability on this material. The *in situ* XRD patterns of 40FO - 60CGO particles (mean grain size 100 μm), obtained by crushing dense membranes, and treating them in different atmospheres in the temperature range of 30–1000 °C, are shown in Figures 12 and 13. Confirmed by *in situ* XRD (Figure 12), the dual phase structure of 40FO - 60CGO is completely unchanged in a 50 vol % CO<sub>2</sub>/50 vol % Ar atmosphere. No carbonate reflexes were detected indicating that the dual phase membrane displays a high CO<sub>2</sub> stability. On the other hand, it follows from Figure 13, that the two coexisting phases FO and CGO remained unchanged even under the low oxygen partial pressure <1 ppm (vacuum) and no reflexes of other phases appeared. These results confirm that the

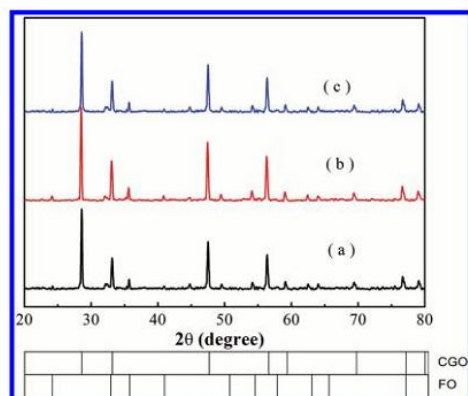


Figure 14. XRD patterns for the fresh 40FO - 60CGO dual phase (a) and the membrane after treatment in 5 vol % H<sub>2</sub>/95 vol % He at 900 °C for 2 h (b) and 4 h (c), respectively.

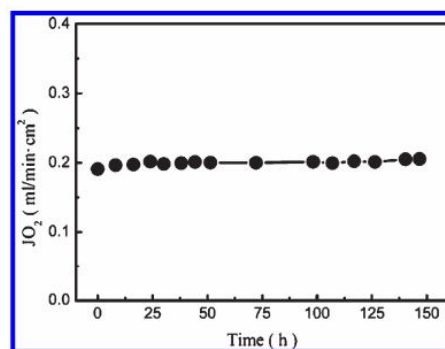


Figure 15. Oxygen permeation flux through LCS-coated 40FO - 60CGO dual phase composite membrane after sintering at 1300 °C for 5 h as a function of time using pure CO<sub>2</sub> as sweep gas. Conditions: 150 mL/min air as feed gas, 29 mL/min CO<sub>2</sub> as sweep gas, 1 mL/min Ne as internal standard gas. Membrane thickness: 0.5 mm. Temperature: 1000 °C.

40FO - 60CGO material is not only stable in CO<sub>2</sub> but also in atmospheres with an oxygen concentration <1 ppm. For the further investigation of the phase stability of 40FO - 60CGO under low oxygen partial pressures, the 40FO - 60CGO was exposed to a 5 vol % H<sub>2</sub>/95 vol % He atmosphere at 900 °C for 2 and 4 h hours, respectively, and then characterized by XRD. Figure 14 shows that the XRD patterns of the fresh and the 40FO - 60CGO material treated in 5 vol % H<sub>2</sub>/95 vol % He atmosphere are identical, indicating that the stability of Fe<sub>2</sub>O<sub>3</sub> - as the most easy to reduce oxide present - can be improved in the dual phase system.

We also found that the oxygen permeation flux through a 40FO - 60CGO dual phase membrane can be slightly increased by about 10% if the membrane is coated with a porous LSC layer on the feed side. Furthermore, whereas the membrane without LSC coating needs a long initialization time before it reaches as steady oxygen flux (see Figure 4), the LSC-coated membrane shows no initialization time (Figure 15). The porous LSC coating enlarges the gas–solid interface of the membranes on the air side and facilitates the oxygen exchange. Correspondingly, the oxygen permeation flux through the membrane with LSC

coating is 10% higher than that through the membrane without LSC coating. The enhancement of the oxygen permeation flux is because LaSr(Fe)CoO<sub>3</sub> (LSC) exhibits a high mixed conductivity and catalytic activity for the oxygen insertion.<sup>31,52</sup> Many researchers have reported that the oxygen permeation through MIEC membranes could be improved by coating them with an LSC porous layer to accelerate oxygen dissociation.<sup>52,53</sup> This LSC-coated 40FO - 60CGO membrane was operated successfully in the oxygen separation from air with pure CO<sub>2</sub> as sweep gas, as shown in Figure 15. The oxygen flux through the LSC-coated 40FO - 60CGO dual phase membrane remains constant at 0.2 mL/min·cm<sup>2</sup> over 150 h. This CO<sub>2</sub>-stability is an important property of our FO - CGO dual phase membrane since the presence of CO<sub>2</sub> deteriorated the oxygen permeation flux through different MIEC materials which normally contain alkaline earth metal elements. For examples, Yi et al.<sup>15,16</sup> studied the degradation behavior of Sr<sub>0.95</sub>Co<sub>0.8</sub>Fe<sub>0.2</sub>O<sub>3-δ</sub> and BaCo<sub>0.4</sub>Fe<sub>0.4</sub>Nb<sub>0.2</sub>O<sub>3-δ</sub> materials in CO<sub>2</sub>-containing atmospheres and attributed these degradations to the carbonate formation. Similarly, it has been reported by Kharton et al.<sup>54</sup> that supplying CO<sub>2</sub> led to a significant decrease of the oxygen permeation flux through SrCo<sub>0.8</sub>Fe<sub>0.2</sub>O<sub>3-δ</sub>-SrAl<sub>2</sub>O<sub>4</sub> composite membranes due to strontium carbonate formation. Yan et al.<sup>55</sup> observed the degradation of Ba<sub>0.5</sub>Sr<sub>0.5</sub>Co<sub>0.8</sub>Fe<sub>0.2</sub>O<sub>3-δ</sub> even in a 1 vol % CO<sub>2</sub>/99 vol % O<sub>2</sub> mixture atmosphere. In this paper, no degradation was observed during 150 h oxygen permeation although pure CO<sub>2</sub> was used as the sweep gas which demonstrates that the 40FO - 60CGO material possesses a good chemical stability in a CO<sub>2</sub> atmosphere due to the absence of alkaline earth metal elements (see Figure 15).

It is noteworthy that the initialization stage of the oxygen flux disappears after LSC coating on the air side of the 40FO - 60CGO membrane. A similar elimination of this initialization period after LSC coating was observed by Zhu et al.<sup>43</sup> who found that the oxygen permeation through the 75 wt % Ce<sub>0.85</sub>Sm<sub>0.15</sub>O<sub>1.925</sub> - 25 wt % Sm<sub>0.6</sub>Sr<sub>0.4</sub>FeO<sub>3-δ</sub> (75CSO - 25SSF) dual phase membrane with LSC porous layers coated on both sides reached steady state immediately. However, if only the air side of the 75CSO - 25SSF membrane was coated with LSC, the unsteady oxygen initialization period was shortened from 40 to 18 h; if coating only the sweep side of the 75CSO - 25SSF membrane, the unsteady period was shortened from 40 to 8 h. From the above results, Zhu et al. attributed the unsteady oxygen permeation to the surface exchange process. The surface oxygen exchange in dual phase membranes is believed to occur at the three phase boundaries (TPB) of gas/oxygen ion conductor/electron conductor.<sup>56</sup> For our uncoated 40FO - 60CGO dual phase membrane, the surface oxygen exchange is proposed to occur at the TPB of gas/CGO/FO. However, the surface oxygen exchange for the LSC-coated 40FO - 60CGO dual phase membrane occurs at the gas/porous perovskite particle LSC.

#### 4. CONCLUSIONS

A series of dual phase composite membranes based on Fe<sub>2</sub>O<sub>3</sub> (FO) and Ce<sub>0.9</sub>Gd<sub>0.1</sub>O<sub>2-δ</sub> (CGO) was prepared in the compositions 25, 40, and 50 wt % FO and correspondingly 75, 60, and 50 wt % CGO with FO as an electronic conductor and CGO as oxygen ionic conductor in a one-pot single-step synthesis. XRD and EDXS results indicate that all FO - CGO membranes under study consist of well separated μm-sized grains of only the two phases FO and CGO. Oxygen permeation showed that the FO:CGO ratio remarkably affects the oxygen permeability. The highest oxygen permeability of 0.18 mL/min·cm<sup>2</sup> was found

for a mixed matrix membrane of the composition 40FO - 60CGO at 1000 °C. The 40FO - 60CGO material possesses a good phase stability not only in an atmosphere of 50 vol % CO<sub>2</sub>/50 vol % Ar but also in other atmospheres with low oxygen partial pressure like reduced pressure (vacuum) and 5 vol % H<sub>2</sub>/95 vol % He. An increased oxygen permeation flux of 0.20 mL/min·cm<sup>2</sup> was obtained at 1000 °C under an air/CO<sub>2</sub> gradient if the 40FO - 60CGO membrane was coated on the air side with a porous layer of La<sub>0.6</sub>Sr<sub>0.4</sub>CoO<sub>3-δ</sub> (LSC). After LSC coating, the initialization period of the oxygen flux disappears. No change of the oxygen permeation flux was observed for more than 150 h when pure CO<sub>2</sub> was used as sweep gas, which indicates that both the parent and the LSC-coated 40FO - 60CGO dual phase membranes are CO<sub>2</sub> stable. These properties recommend FO - CGO dual phase membranes as a good candidate for the oxygen separation from air in the oxy-fuel process.

#### ■ AUTHOR INFORMATION

##### Corresponding Author

\*Phone: +86-20-87110131. Fax: +86-20-87110131. E-mail: hhwang@scut.edu.cn (H.H.W.). Phone: +49-511-762-3175. Fax: +49-511-762-19121. E-mail: juergen.caro@pci.uni-hannover.de (J.C.).

#### ■ ACKNOWLEDGMENT

The authors thank the financial support from the Chinese-German Centre for Science (GZ676). The EU is also thanked for financing in the 7th Framework Program the IP Innovative Catalytic Technologies & Materials for the Next Gas to Liquid Processes (NEXT-GTL). H. X. Luo acknowledges the financial support by the China Scholarship Council (CSC). The authors also greatly acknowledge Dr. A. S. Huang for stimulating discussions and F. Steinbach and Z. W. Cao for technical support.

#### ■ REFERENCES

- (1) Zhu, X. F.; Wang, H. H.; Yang, W. S. Novel cobalt-free oxygen permeable membrane. *Chem. Commun.* **2004**, *9*, 1130.
- (2) Watanabe, K.; Yuasa, M.; Kida, T.; Teraoka, Y.; Yamazoe, N.; Shimano, K. High-performance oxygen-permeable membranes with an asymmetric structure using Ba<sub>0.95</sub>La<sub>0.05</sub>FeO<sub>3-δ</sub> perovskite-type oxide. *Adv. Mater.* **2010**, *22*, 2367.
- (3) Chen, C. S.; Feng, S. J.; Ran, S.; Zhu, D. C.; Liu, W.; Bouwmeester, H. J. M. Conversion of methane to syngas by a membrane-based oxidation-reforming process. *Angew. Chem., Int. Ed.* **2003**, *42*, 5196.
- (4) Balachandran, U.; Dusek, J. T.; Mieville, R. L.; Poeppel, R. B.; Kleefisch, M. S.; Pei, S.; Kobylinski, T. P.; Udovich, C. A.; Bose, A. C. Dense ceramic membranes for partial oxidation of methane to syngas. *Appl. Catal., A* **1995**, *133*, 19.
- (5) Tsai, C. Y.; Dixon, A. G.; Moser, W. R.; Ma, Y. H. Dense perovskite membrane reactors for partial oxidation of methane to syngas. *AIChE J.* **1997**, *43*, 2741.
- (6) Jiang, H. Q.; Wang, H. H.; Werth, S.; Schiestel, T.; Caro, J. Simultaneous production of hydrogen and synthesis gas by combining water splitting with partial oxidation of methane in a hollow fiber membrane reactor. *Angew. Chem., Int. Ed.* **2008**, *47*, 9341.
- (7) Jiang, H. Q.; Cao, Z. W.; Schirmeister, S.; Schiestel, T.; Caro, J. A coupling strategy to produce hydrogen and ethylene in a membrane reactor. *Angew. Chem., Int. Ed.* **2010**, *49*, 5656.
- (8) Jiang, H. Q.; Liang, F. Y.; Czuprat, O.; Efimov, K.; Feldhoff, A.; Schirmeister, S.; Schiestel, T.; Wang, H. H.; Caro, J. Hydrogen production by water dissociation in surface-modified BaCo<sub>2</sub>Fe<sub>7</sub>Zr<sub>1-x-y</sub>O<sub>3-δ</sub> hollow fiber membrane reactor with improved oxygen permeation. *Chem.—Eur. J.* **2010**, *16*, 7898.



- (9) Shao, Z. P.; Haile, S. M. A high-performance cathode for the next generation of solid-oxide fuel cells. *Nature* 2004, 431, 170.
- (10) Shao, Z. P.; Haile, S. M.; Ahn, J. M.; Rooney, P. D.; Zhan, Z. L.; Barnett, S. A. A thermally self-sustained micro solid-oxide fuel-cell stack with high power density. *Nature* 2005, 435, 795.
- (11) Wang, H. H.; Werth, S.; Schiestel, T.; Caro, J. Perovskite hollow-fiber membranes for the production of oxygen-enriched air. *Angew. Chem., Int. Ed.* 2005, 42, 7066.
- (12) Zhang, N.; Lion, N. Two novel oxy-fuel cycles integrated with natural gas reforming and CO<sub>2</sub> capture. *Energy* 2008, 33, 340.
- (13) Plasynski, S. L.; Litynski, J. T.; McIlvried, H. G.; Srivastava, R. D. Progress and new development in carbon capture and storage. *Crit. Rev. Plant Sci.* 2009, 28, 123.
- (14) Engels, S.; Beggel, F.; Modigell, M.; Stadler, H. Simulation of a membrane unit for oxyfuel power plants under consideration of realistic BSCF membrane properties. *J. Membr. Sci.* 2010, 359, 93.
- (15) Yi, J. X.; Feng, S. J.; Zuo, Y. B.; Liu, W.; Chen, C. S. Oxygen permeability and stability of Sr<sub>0.95</sub>Co<sub>0.8</sub>Fe<sub>0.2</sub>O<sub>3-δ</sub> in a CO<sub>2</sub>- and H<sub>2</sub>O-containing atmosphere. *Chem. Mater.* 2005, 17, 5856.
- (16) Yi, J. X.; Schroeder, M.; Weirich, T.; Mayer, J. Behavior of Ba(Co,Fe,Nb)O<sub>3-δ</sub> perovskite in CO<sub>2</sub>-containing atmosphere degradation mechanism materials design. *Chem. Mater.* 2010, 22, 6246.
- (17) Ten, E. J. E.; Nguyen, N. Q.; Den, O. M. W.; Bouwmeester, H. J. M. Oxygen permeation properties of dense Bi<sub>1.5</sub>Er<sub>0.5</sub>O<sub>3</sub>-Ag cermet membranes. *J. Electrochem. Soc.* 1997, 144, 4361.
- (18) Kobayashi, K.; Tsunoda, T. Oxygen permeation and electrical transport properties of 60 vol % Bi<sub>1.6</sub>Y<sub>0.4</sub>O<sub>3</sub> and 40 vol % Ag composite prepared by the Sol-Gel method. *Solid State Ionics* 2004, 175, 405.
- (19) Wu, K.; Xie, S.; Jiang, G. S.; Liu, W.; Chen, C. S. Oxygen permeation through (Bi<sub>2</sub>O<sub>3</sub>)<sub>0.74</sub>(SrO)<sub>0.26</sub>-Ag (40% v/o) composite. *J. Membr. Sci.* 2001, 188, 189.
- (20) Kim, J.; Lin, Y. S. Synthesis and oxygen permeation properties of ceramic-metal dual-phase membranes. *J. Membr. Sci.* 2000, 167, 123.
- (21) Kharton, V. V.; Kovalevsky, A. V.; Viskup, A. P.; Shaula, A. L.; Figueiredo, F. M.; Naumovich, E. N.; Marques, F. M. B. Oxygen transport in Ce<sub>0.8</sub>Gd<sub>0.2</sub>O<sub>2-δ</sub>-based composite membranes. *Solid State Ionics* 2003, 160, 247.
- (22) Kharton, V. V.; Kovalevsky, A. V.; Viskup, A. P.; Yaremchenko, A. A.; Figueiredo, F. M.; Naumovich, E. N.; Marques, F. M. B. Oxygen permeability of Ce<sub>0.8</sub>Gd<sub>0.2</sub>O<sub>2-δ</sub>-La<sub>0.8</sub>Sr<sub>0.2</sub>MnO<sub>3-δ</sub> composite membranes. *J. Electrochem. Soc.* 2000, 147, 2814.
- (23) Kharton, V. V.; Kovalevsky, A. V.; Viskup, A. P.; Yaremchenko, A. A.; Figueiredo, F. M.; Naumovich, E. N.; Marques, F. M. B. Oxygen permeability and faradaic efficiency of Ce<sub>0.8</sub>Gd<sub>0.2</sub>O<sub>2-δ</sub>-La<sub>0.8</sub>Sr<sub>0.2</sub>MnO<sub>3-δ</sub> composites. *J. Eur. Ceram. Soc.* 2001, 21, 1763.
- (24) Luo, H. X.; Efimov, K.; Jiang, H. Q.; Feldhoff, A.; Wang, H. H.; Caro, J. CO<sub>2</sub>-stable and cobalt-free dual phase membrane for oxygen separation. *Angew. Chem., Int. Ed.* 2011, 50, 759.
- (25) Luo, H. X.; Jiang, H. Q.; Efimov, K.; Wang, H. H.; Caro, J. Influence of the preparation methods on the microstructure and oxygen permeability of a CO<sub>2</sub>-stable dual phase membrane. *AIChE J.* 2011, 57, 2738.
- (26) Shaula, A. L.; Yaremchenko, A. A.; Kharton, V. V.; Logvinovich, D. I.; Naumovich, E. N.; Kovalevsky, A. V.; Frade, J. R.; Marques, F. M. B. Oxygen permeability of LaGaO<sub>3</sub> based ceramic membranes. *J. Membr. Sci.* 2003, 221, 69.
- (27) Yaremchenko, A. A.; Kharton, V. V.; Viskup, A. P.; Naumovich, E. N.; Tikhonovich, V. N.; Lapchuk, N. M. Mixed electronic and ionic conductivity of LaCo(M)O<sub>3</sub> (M=Ga, Cr, Fe or Ni). V. Oxygen permeability of Mg-doped La(Ga,Co)O<sub>3-δ</sub> perovskites. *Solid State Ionics* 1999, 120, 65.
- (28) Ishihara, T.; Yamada, T.; Arikawa, H.; Nishiguchi, H.; Takita, Y. Mixed electronic-oxide ionic conductivity and oxygen permeating property of Fe-, Co- or Ni-doped LaGaO<sub>3</sub> perovskite oxide. *Solid State Ionics* 2000, 135, 631.
- (29) Ishihara, T.; Tsuruta, Y.; Todaka, T.; Nishiguchi, H.; Takita, Y. Fe doped LaGaO<sub>3</sub> perovskite oxide as an oxygen separating membrane for CH<sub>4</sub> partial oxidation. *Solid State Ionics* 2002, 152–153, 709.
- (30) Zhang, T. S.; Ma, J.; Kong, L. B.; Chan, H. S.; Hing, P.; Kilner, J. A. Iron oxide as an effective sintering aid and grain boundary scavenger for ceria-based electrolytes. *Solid State Ionics* 2004, 167, 203.
- (31) Tao, Y. K.; Shao, J.; Wang, W. G.; Wang, J. X. Optimization and evaluation of La<sub>0.6</sub>Sr<sub>0.4</sub>CoO<sub>3-δ</sub> cathode for intermediate temperature solid oxide fuel cells. *Fuel Cells* 2009, 9, 679.
- (32) Luo, H. X.; Tian, B. B.; Wei, Y. Y.; Wang, H. H.; Jiang, H. Q.; Caro, J. Oxygen permeability and structural stability of a novel tantalum-doped perovskite BaCo<sub>0.7</sub>Fe<sub>0.2</sub>Ta<sub>0.1</sub>O<sub>3-δ</sub>. *AIChE J.* 2010, 56, 604.
- (33) Hoelscher, U.; Elektrochemische Untersuchungen zur Punktfehlordnung und von Transporteigenschaften des Co<sub>1-x</sub>O bei hohen Temperaturen, Ph.D. Thesis, Technical University Clausthal, Germany, 1983.
- (34) Qi, X.; Akin, F. T.; Lin, Y. S. Ceramic-glass composite high temperature seals for dense ionic-conducting ceramic membranes. *J. Membr. Sci.* 2001, 193, 185.
- (35) Jivaganont, P.; Loyma, W.; Charojrochkul, S.; Limthongkul, P. Second phase investigation and sintering of Fe-doped nano- and ceramic grade Ce<sub>0.9</sub>Gd<sub>0.1</sub>O<sub>1.95</sub>. *J. Microsc. Soc. Thailand* 2010, 24, 121.
- (36) Martynczuk, J.; Arnold, M.; Feldhoff, A. Influence of grain size on the oxygen permeation performance of perovskite-type (Ba<sub>0.5</sub>Sr<sub>0.5</sub>)(Fe<sub>0.8</sub>Zn<sub>0.2</sub>)O<sub>3-δ</sub> membranes. *J. Membr. Sci.* 2008, 322, 375.
- (37) Arnold, M.; Martynczuk, J.; Efimov, K.; Wang, H. H.; Feldhoff, A. Grain boundaries as barrier for oxygen transport in perovskite-type membranes. *J. Membr. Sci.* 2008, 316, 137.
- (38) Mogensen, M.; Sammes, N. M.; Tomsett, G. A. Physical, chemical and electrochemical properties of pure and doped ceria. *Solid State Ionics* 2000, 129, 63.
- (39) Warnes, B. M.; Aplan, F. F.; Simkovich, G. Electrical conductivity and seebeck voltage of Fe<sub>2</sub>O<sub>3</sub>, pure and doped, as a function of temperature and oxygen pressure. *Solid State Ionics* 1984, 12, 271.
- (40) Zhu, X. F.; Yang, W. S. Composite membrane based on ionic conductor and mixed conductor for oxygen permeation. *AIChE J.* 2008, 54, 665.
- (41) Zhu, X. F.; Wang, H. H.; Yang, W. S. Relationship between homogeneity and oxygen permeability of composite membranes. *J. Membr. Sci.* 2008, 309, 120.
- (42) Wang, H. H.; Yang, W. S.; Cong, Y.; Zhu, X. F.; Lin, Y. S. Structure and oxygen permeability of a dual-phase membrane. *J. Membr. Sci.* 2003, 224, 107.
- (43) Zhu, X. F.; Liu, H. Y.; Li, Q. M.; Cong, Y.; Yang, W. S. Unsteady-state permeation and surface exchange of dual-phase membranes. *Solid State Ionics* 2011, 185, 27.
- (44) Tong, J. H.; Yang, W. S.; Zhu, B. C.; Cai, R. Investigation of ideal zirconium-doped perovskite-type ceramic membrane materials for oxygen separation. *J. Membr. Sci.* 2002, 203, 175.
- (45) Shaula, A. L.; Kharton, V. V.; Marques, F. M. B.; Kovalevsky, A. V.; Viskup, A. P.; Naumovich, E. N. Oxygen permeability of mixed-conducting composite membranes: effect of phase interaction. *J. Solid State Electrochem.* 2006, 10, 28.
- (46) Chen, C. C.; Prasad, R.; Amberst, E.; Mazanec, T. J.; Besecker, C. J. Multi-phase solid ion and electron conducting membrane with low volume percentage electron conducting phase and methods for fabrication. 2001; United States Patent. Patent No.: US6332964 B1.
- (47) Li, W.; Tian, T. F.; Shi, F. Y.; Wang, Y. S.; Chen, C. S. Ce<sub>0.8</sub>Sm<sub>0.2</sub>O<sub>2-δ</sub>-La<sub>0.8</sub>Sr<sub>0.2</sub>MnO<sub>3-δ</sub> dual-phase composite hollow fiber membrane for Oxygen Separation. *Ind. Eng. Chem. Res.* 2009, 48, 5789.
- (48) Arnold, M.; Martynczuk, J.; Efimov, K.; Wang, H. H.; Feldhoff, A. Grain boundaries as barrier for oxygen transport in perovskite-type membranes. *J. Membr. Sci.* 2008, 316, 137.
- (49) Zeng, P. Y.; Ran, R.; Chen, Z. H.; Gu, H. X.; Shao, Z. P.; J.C. Costa, D. D.; Liu, S. M. Significant effects of sintering temperature on the performance of La<sub>0.6</sub>Sr<sub>0.4</sub>Co<sub>0.2</sub>Fe<sub>0.8</sub>O<sub>3-δ</sub> oxygen selective membranes. *J. Membr. Sci.* 2007, 302, 171.
- (50) Shao, Z. P.; Xiong, G. X.; Tong, J. H.; Dong, H.; Yang, W. S. Ba effect in doped Sr(Co<sub>0.8</sub>Fe<sub>0.2</sub>)O<sub>3-δ</sub> on the phase structure and oxygen permeation properties of the dense ceramic membranes. *Sep. Purif. Technol.* 2001, 25, 419.

(51) Li, Q. M.; Zhu, X. F.; He, Y. F.; Cong, Y.; Yang, W. S. Effects of sintering temperature on properties of dual-phase oxygen permeable membranes. *J. Membr. Sci.* **2011**, *367*, 134.

(52) Lee, S. W.; Lee, K. S.; Woo, S. K.; Kim, J. W.; Ishihara, T.; Kim, D. K. Oxygen-permeating properties of LaSrBFeO<sub>3</sub> (B = Co, Ga) perovskite membrane surface-modified by LaSrCoO<sub>3</sub>. *Solid State Ionics* **2003**, *158*, 287.

(53) Hong, W. K.; Choi, G. M. Oxygen permeation of BSCF membrane with varying thickness and surface coating. *J. Membr. Sci.* **2010**, *346*, 353.

(54) Yaremchenko, A. A.; Kharton, V. V.; Avdeev, M.; Shaula, A. L.; Marques, F. M. B. Oxygen permeability, thermal expansion and stability of SrCo<sub>0.8</sub>Fe<sub>0.2</sub>O<sub>3-δ</sub>-SrAl<sub>2</sub>O<sub>4</sub> composites. *Solid State Ionics* **2007**, *178*, 1205.

(55) Yan, A. Y.; Maragou, V.; Arico, A.; Cheng, M.; Tsiakaras, P. Investigation of a Ba<sub>0.5</sub>Sr<sub>0.5</sub>Co<sub>0.8</sub>Fe<sub>0.2</sub>O<sub>3-δ</sub> based cathode SOFC II. The effect of CO<sub>2</sub> on the chemical stability. *Appl. Catal. B* **2007**, *76*, 320.

(56) Wang, B.; Zhan, M. C.; Liu, W.; Chen, C. S. Oxygen permeation and stability of Zr<sub>0.8</sub>Y<sub>0.2</sub>O<sub>0.9</sub> - La<sub>0.8</sub>Sr<sub>0.2</sub>CrO<sub>3-δ</sub> dual-phase composite. *J. Solid State Electrochem.* **2006**, *10*, 625.

### **3.5 Rapid glycine-nitrate combustion synthesis of the CO<sub>2</sub>-stable dual phase membrane 40Mn<sub>1.5</sub>Co<sub>1.5</sub>O<sub>4-δ</sub> - 60Ce<sub>0.9</sub>Pr<sub>0.1</sub>O<sub>2-δ</sub> for CO<sub>2</sub> capture via an oxy-fuel process**

Huixia Luo, Heqing Jiang, Tobias Klande, Fangyi Liang, Zhengwen Cao, Haihui Wang,

Jürgen Caro

**J. Membr. Sci. submitted, May, 2012.**

Journal Name

Dynamic Article Links ►

Cite this: DOI: 10.1039/c0xx00000x

www.rsc.org/xxxxxx

ARTICLE TYPE

## Rapid glycine-nitrate combustion synthesis of the CO<sub>2</sub>-stable dual phase membrane 40Mn<sub>1.5</sub>Co<sub>1.5</sub>O<sub>4-δ</sub> - 60Ce<sub>0.9</sub>Pr<sub>0.1</sub>O<sub>2-δ</sub> for CO<sub>2</sub> capture via an oxy-fuel process

Huixia Luo<sup>a</sup>, Heqing Jiang<sup>b</sup>, Tobias Klande<sup>a</sup>, Fangyi Liang<sup>a</sup>, Zhengwen Cao<sup>a</sup>, Haihui Wang<sup>\*c</sup> and Jürgen Caro<sup>\*c</sup>

Received (in XXX, XXX) Xth XXXXXXXXX 20XX, Accepted Xth XXXXXXXXX 20XX

DOI: 10.1039/b000000x

A rapid one-pot combustion synthesis method based on glycine-nitrate, has been applied to prepare a novel oxygen transporting dual phase CO<sub>2</sub>-stable membrane of the composition 40 wt.% Mn<sub>1.5</sub>Co<sub>1.5</sub>O<sub>4-δ</sub> - 60 wt.% Ce<sub>0.9</sub>Pr<sub>0.1</sub>O<sub>2-δ</sub> (40MCO-60CPO). After sintering at 1300 °C in air for 10 h, the 40MCO-60CPO membranes were characterized by X-ray diffraction (XRD), scanning electron microscopy (SEM), back scattered SEM (BSEM), and energy dispersive X-ray spectroscopy (EDXS), showing that the 40MCO-60CPO composite represents a micro-scale mixture of mainly the two phases MCO and CPO, but small amounts of MnO<sub>2</sub> and (MnCo)(MnCo)<sub>2</sub>O<sub>4.5</sub> were detected in the sintered membranes as well. The oxygen permeation fluxes through the 40MCO-60CPO dual phase membrane were measured at elevated temperatures (900-1000 °C) with one side of the membrane exposed to synthetic air and the other side to a CO<sub>2</sub>/He sweep gas stream. A stable oxygen permeation rate of 0.48 mL cm<sup>-2</sup> min<sup>-1</sup> was obtained for a 0.3 mm thick membrane under an air/CO<sub>2</sub> oxygen partial pressure gradient at 1000 °C. It was also found that 40MCO-60CPO dual phase membranes are stable for more than 60 h even when pure CO<sub>2</sub> was used as the sweep gas, which recommends 40MCO-60CPO membranes as promising candidates for 4-end membrane operation in an oxy-fuel power plant.

### Introduction

Recently, oxygen-permeable dense ceramic membranes with mixed ionic-electronic conductivity (MIEC) have attracted much attention as economical, efficient, and environment-friendly means to produce oxygen from air or other oxygen-containing gas mixtures.<sup>1</sup> In fact, an integration of oxygen transport membranes (OTMs) into oxy-fuel power plants can integrate CO<sub>2</sub> capture and sequestration strategies in order to reduce CO<sub>2</sub> emission. Further, OTMs allow process intensification<sup>2,3</sup> and enable thermal integration and energy saving.<sup>4-7</sup> A promising process route in the oxy-fuel power plant concept is the so-called 4-end membrane operation mode,<sup>8</sup> in which a part of the flue gas is recycled as sweep gas on the permeate side of OTMs. The heat from natural gas or coal combustion offers the possibility of efficient membrane integration into the oxy-fuel process. However, the development of the 4-end membrane operation mode technology is hampered since the state-of-the-art OTMs suffer from low chemical stability towards corrosive components of the flue gas such as CO<sub>2</sub> and SO<sub>2</sub>, which lead to a poor oxygen permeation performance and even membrane destruction.<sup>9-14</sup> It is known that single phase perovskite-type OTM materials (ABO<sub>3</sub>) with a high content of alkaline-earth metals on the A site, easily react with CO<sub>2</sub> and SO<sub>2</sub> forming carbonates and sulphates.<sup>15-18</sup>

Another type of MIEC membranes is called "dual phase

membranes", which consist of a micro-scale mixture of well-separated grains of an oxygen ion conductor (OIC) and an electron conductor (EC). Dual phase membranes offer a promising approach for the 4-end membrane operation mode technology since their constituents can be tailored according to practical requirements. Since their constituents can be tailored according to practical requirements. However, if noble metals are used as EC, their high price turns out as drawback. Further, often reactions between the OIC and EC at the high operational temperatures take place; new phases of lower ionic and electronic conductivity are formed and stability problems are reported. Recently, we have proposed that novel dual-phase membranes without noble metals and alkaline-earth metals show a much higher CO<sub>2</sub> stability than the common alkaline-earth-containing membranes.<sup>19,21</sup> However, the traditional synthesis of dual phase oxides consists in a simple mixing of the two oxide powders,<sup>22,23</sup> which often requires several sintering-milling steps to get uniform mixtures. This conventional preparation can be replaced by recent developments such as the one-pot one-step EDTA-citric acid process or the glycine-nitrate combustion process (GNP). Especially the GNP is reported to rapidly produce complex oxide ceramic powders of uniform composition on an atomic scale and fine enough in grain size for sintering to a ceramic with a high density.<sup>24-26</sup> Herein, we combine the rapid one-pot one-step and GNP techniques to develop a new CO<sub>2</sub>-stable oxygen-permeable

GNP techniques to develop a new CO<sub>2</sub>-stable oxygen transporting membrane of the composition 40wt.% Mn<sub>1.5</sub>Co<sub>1.5</sub>O<sub>4.8</sub> (MCO) - 60wt.% Ce<sub>0.9</sub>Pr<sub>0.1</sub>O<sub>2.8</sub> (CPO), with MCO as the EC and CPO as the OIC.

It is generally accepted that oxygen permeation properties of dual phase membrane are dependent on their electronic and ionic conductivity, structural and phase stability, as well as thermal expansion compatibility between OIC and EC.<sup>22</sup> Thus, with these conclusions in mind, we designed our dual phase membrane as follows: (i) MCO spinel is reported to show excellent electronic conductivity and satisfactory thermal and structural stability as well as a thermal expansion which matches ferritic stainless steel. Therefore, MCO has been widely studied in solid oxide fuel cells (SOFCs) as a protective coating on stainless steel interconnections and as cathodes for intermediate temperature SOFCs.<sup>23-25</sup> (ii) Pr-doped ceria is well-known to exhibit high oxygen ionic conductivity and a good structural stability in a wide oxygen partial pressure range. These properties recommend CPO as solid electrolyte<sup>26</sup> and oxygen storage material<sup>27</sup> in SOFCs. (iii) Because of the lack of alkaline- earth metals in MCO and CPO, high CO<sub>2</sub> stability can be expected. (vi) To guarantee a sufficient electron transport in the percolation network, the concentration of the highly electron conducting component MCO in the dual phase materials should not be < 40 wt.%.

Therefore, the aim of this study is the fabrication of 40MCO - 40CPO dual phase membrane via a one-pot one-step GNP. Phase structure and stability as well as oxygen permeability for different CO<sub>2</sub> atmosphere on the permeate side of the membrane are investigated in detail.

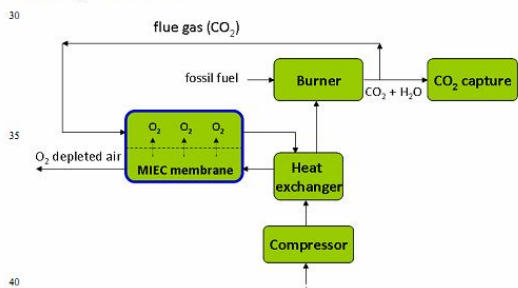


Fig.1 The 4-end concept of CO<sub>2</sub> capture with oxygen permeable membrane in an oxy-fuel process. (after [5])

## Experimental

### Preparation of powders and membranes

The glycine-nitrate combustion process (GNP), as a proven means to obtain fine and homogeneous powders<sup>21</sup>, was used to prepare the 40wt.%Mn<sub>1.5</sub>Co<sub>1.5</sub>O<sub>4.8</sub>-60wt.%Ce<sub>0.9</sub>Pr<sub>0.1</sub>O<sub>2.8</sub> (40MCO-60CPO) dual phase composite powders directly. As shown in the process flow chart (Figure 2), a precursor was prepared by combining glycine and the metal nitrates Mn(NO<sub>3</sub>)<sub>2</sub>, Co(NO<sub>3</sub>)<sub>2</sub>, Ce(NO<sub>3</sub>)<sub>3</sub> and Pr(NO<sub>3</sub>)<sub>3</sub> in their appropriate stoichiometric ratios in an aqueous solution. The molar ratio of glycine : total metal ions was 2 : 1. The precursor was stirred and heated at 150 °C in air to evaporate excess water until a viscous liquid was obtained. Further heating of the viscous liquid up to

300 °C caused the precursor liquid to auto-ignite. Combustion was rapid and self-sustaining, and a precursor ash was obtained. This precursor ash was calcined at 950 °C for 10 h. The resulting powders were pressed to disk membranes under a pressure of 5 MPa in a stainless steel module with a diameter of 18 mm to get green membranes. These green disks were pressure-less sintered at 1300 °C in air for 10 h. The surfaces of the disks were carefully polished to 0.3 mm and 0.5 mm thickness, respectively, by using 1200 grit-sand paper (average particle diameter 15.3 μm), then the membranes were washed with ethanol.

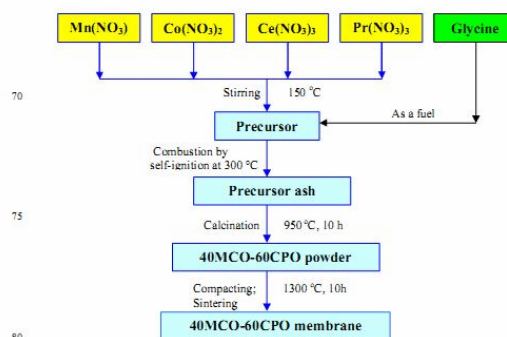


Fig. 2 Flow chart for the one-pot one-step preparation of dual phase 40Mn<sub>1.5</sub>Co<sub>1.5</sub>O<sub>4.8</sub>-60Ce<sub>0.9</sub>Pr<sub>0.1</sub>O<sub>2.8</sub>(40MCO-60CPO) membranes by the glycine-nitrate combustion process.

### Characterization of powders and membranes

X-ray diffraction (XRD, D8 Advance, Bruker-AXS, with Cu Kα radiation) was used to determine the phase structure. Data sets were recorded in a step-scan mode in the 2θ range of 20° - 80° with intervals of 0.02° and using a counting time of 1 s per point. The morphology of precursor ash and dual phase oxide powder were characterized by scanning electron microscopy (SEM) and by energy dispersive X-ray spectroscopy (EDXS) at 15 keV. SEM and back scattered SEM (BSEM) were made using a Jeol-JSM-6700F operating at 15 keV. The element distribution in the grains of the dual phase membrane was studied on the same electron microscope by EDXS with Oxford Instruments INCA-300 EDX spectrometer at 15 keV.

### Oxygen permeation performances of membranes

Oxygen permeation measurement was conducted in a home-made high-temperature oxygen permeation cell.<sup>28</sup> The disc-shaped membranes were sealed onto an alumina tube (Ø = 16mm) at 950 °C in air for 5 hours with a gold paste (Heraeus, Germany). Another quartz tube (Ø = 24 mm) served as the air side of the permeator. The temperature was maintained with a microprocessor temperature controller (HTM Reetz GmbH, Germany) coupled to a tubular furnace with a type K thermocouple setting inside the furnace. The effective areas of the membranes for oxygen permeation were 0.785 cm<sup>2</sup>. The inlet gas flow rates were controlled by mass flow controllers (Bronkhorst, Germany) and the flow rates were regularly calibrated by using a bubble flow meter. During oxygen permeation measurement, synthetic air (20 % O<sub>2</sub> and 80 % N<sub>2</sub>) at the rate of 200 ml/min

membrane of the composition 40 wt.% Mn<sub>1.2</sub>Co<sub>1.2</sub>O<sub>4.8</sub> - 60 wt.% Ce<sub>0.9</sub>Pr<sub>0.1</sub>O<sub>2.8</sub> (40MCO-60CPO), with MCO as the EC and CPO as the OIC.

It is generally accepted that oxygen permeation properties of dual phase membrane are dependent on their electronic and ionic conductivity, structural and phase stability, as well as thermal expansion compatibility between OIC and EC.<sup>27</sup> Thus, with these conclusions in mind, we designed our dual phase membrane as follows: (i) MCO spinel is reported to show excellent electronic conductivity and satisfactory thermal and structural stability as well as a thermal expansion which matches ferritic stainless steel. Therefore, MCO has been widely studied in solid oxide fuel cells (SOFCs) as a protective coating on stainless steel interconnections and as cathodes for intermediate temperature SOFCs.<sup>28-30</sup> (ii) Pr-doped ceria is well-known to exhibit high oxygen ionic conductivity and a good structural stability in a wide oxygen partial pressure range. These properties recommend CPO as solid electrolyte<sup>31</sup> and oxygen storage material<sup>32</sup> in SOFCs. (iii) Because of the lack of alkaline-earth metals in MCO and CPO, high CO<sub>2</sub> stability can be expected. (vi) To guarantee a sufficient electron transport in the percolation network, the concentration of the highly electron conducting component MCO in the dual phase materials should not be < 40 wt.%.

Therefore, the aim of this study is the fabrication of 40MCO-60CPO dual phase membrane via a one-pot one-step GNP. Phase structure and stability as well as oxygen permeability for different CO<sub>2</sub> atmosphere on the permeate side of the membrane are investigated in detail.

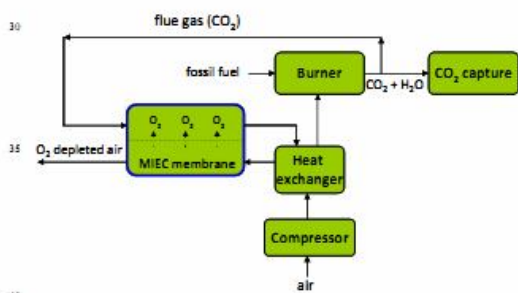


Fig. 1 The 4-end concept of CO<sub>2</sub> capture with oxygen permeable membrane in an oxy-fuel process. (after<sup>8</sup>)

## Experimental

### Preparation of powders and membranes

The glycine-nitrate combustion process (GNP), as a proven means to obtain fine and homogeneous powders,<sup>24</sup> was used to prepare the 40 wt.% Mn<sub>1.2</sub>Co<sub>1.2</sub>O<sub>4.8</sub> - 60 wt.% Ce<sub>0.9</sub>Pr<sub>0.1</sub>O<sub>2.8</sub> (40MCO-60CPO) dual phase composite powders directly. As shown in the process flow chart (Fig. 2), a precursor was prepared by combining glycine and the metal nitrates Mn(NO<sub>3</sub>)<sub>2</sub>, Co(NO<sub>3</sub>)<sub>2</sub>, Ce(NO<sub>3</sub>)<sub>3</sub> and Pr(NO<sub>3</sub>)<sub>3</sub> in their appropriate stoichiometric ratios in an aqueous solution. The molar ratio of glycine : total metal ions was 2 : 1. The precursor was stirred and

heated at 150 °C in air to evaporate excess water until a viscous liquid was obtained. Further heating of the viscous liquid up to 300 °C caused the precursor liquid to auto-ignite. Combustion was rapid and self-sustaining, and a precursor ash was obtained. This precursor ash was calcined at 950 °C for 10 h. The resulting powders were pressed to disk membranes under a pressure of 5 MPa in a stainless steel module with a diameter of 18 mm to get green membranes. These green disks were pressure-less sintered at 1300 °C in air for 10 h. The surfaces of the disks were carefully polished to 0.3 mm and 0.5 mm thickness, respectively, by using 1200 grit-sand paper (average particle diameter 15.3 μm), then the membranes were washed with ethanol for oxygen permeation.

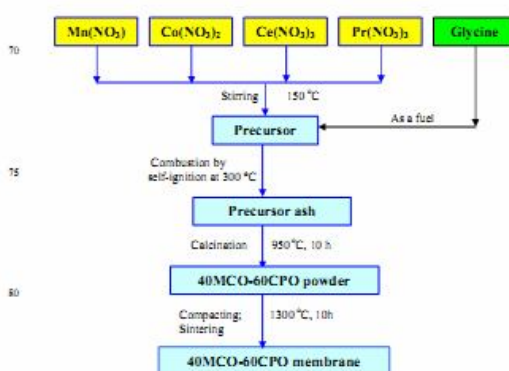


Fig. 2 Flow chart for the one-pot one-step preparation of dual phase 40MCO-60CPO membranes by the glycine-nitrate combustion process.

### Characterization of powders and membranes

X-ray diffraction (XRD, D8 Advance, Bruker-AXS, with Cu Kα radiation) was used to determine the phase structure. Data sets were recorded in a step-scan mode in the 2θ range of 20°-80° with intervals of 0.02° and using a counting time of 1 s per point. The morphology of precursor ash and dual phase oxide powder were characterized by scanning electron microscopy (SEM) and by energy dispersive X-ray spectroscopy (EDXS) at 15 keV. SEM and back scattered SEM (BSEM) were made using a Jeol JSM-6700F operating at 15 keV. The element distribution in the grains of the dual phase membrane was studied on the same electron microscope by EDXS with Oxford Instruments INCA-300 EDX spectrometer at 15 keV.

### Oxygen permeation performances of membranes

Oxygen permeation measurement was conducted in a home-made high-temperature oxygen permeation cell.<sup>33</sup> The disc-shaped membranes were sealed onto an alumina tube (Ø = 16 mm) at 950 °C in air for 5 hours with a gold paste (Heraeus, Germany). Another quartz tube (Ø = 24 mm) served as the air side of the permeator. The temperature was maintained with a microprocessor temperature controller (HTM Reetz GmbH, Germany) coupled to a tubular furnace with a type K thermocouple setting inside the furnace. The effective areas of the membranes for oxygen permeation were 0.785 cm<sup>2</sup>. The inlet gas flow rates were controlled by mass flow controllers (Bronkhorst,

Germany) and the flow rates were regularly calibrated by using a bubble flow meter. During oxygen permeation measurement, synthetic air (20% O<sub>2</sub> and 80% N<sub>2</sub>) at the rate of 200 ml/min was used as feed gas. He/CO<sub>2</sub> was used as sweep gas to remove the permeated oxygen. 1 ml Ne/min was used as an internal standard gas for calculating the total flow rate at the outlet on the sweep side. The effluents were analyzed by an on-line gas chromatograph (GC, Agilent 7890A) equipped with a Carboxen 1000 column. The GC was frequently calibrated using standard gases in order to ensure the reliability of the experimental data. The calculation of oxygen permeation flux was demonstrated in detail in our previous papers.<sup>19,20</sup>

### Results and discussion

#### Characterization of the 40MCO-60CPO dual phase materials

Fig. 3a and b show the XRD patterns of the membrane after sintering at 1300 °C in air for 10 h and of the powder after calcining the precursor ash at 950 °C in air for 10 h (Fig. 3a and b). For comparison, the XRD patterns of the pure phase CPO and MCO powders – also synthesized by the GNP and calcined at 950 °C in air for 10 h - are given (Fig. 3c and d). The XRD patterns of CPO (Fig. 3c) confirm its cubic structure (space group 225, Fm-3m) in agreement with literature.<sup>34</sup> From the Scherrer formalism, the mean crystallite size of pure CPO is determined to be about 85.4 nm. From the analysis of the XRD patterns of MCO (Fig. 3d) it follows that the MCO spinel phase consists of 57.9 wt.% cubic MnCo<sub>2</sub>O<sub>4.8</sub> (space group 227, Fd-3mZ) and 42.1 wt.% tetragonal Mn<sub>2</sub>CoO<sub>4.8</sub> (space group 141, 141/amdS), as known from literature.<sup>28-30</sup> According to the Scherrer equation, the mean crystallite size of MnCo<sub>2</sub>O<sub>4.8</sub> and Mn<sub>2</sub>CoO<sub>4.8</sub> are calculated to be 22 nm and 25.2 nm, respectively. Similar crystallite sizes can be derived from the XRD pattern of the mixture 40MCO-60CPO powder after calcination at 950 °C (Fig. 3b). Mean MCO and CPO crystallite sizes of 16.4 nm and 66.4 nm have been obtained, respectively. The mean particle size of the 40MCO-60CPO membrane after pressing and sintering at 1300 °C is estimated by SEM analysis (see Fig. 5c, d and 6a) to be 580 nm (MCO) and 647 nm (CPO). This means, after high temperature treatment at 1300 °C, the 40MCO-60CPO powder no longer exhibits nanocrystallinity since grain ripening took place. Comparing in Fig. 3 the XRD of the 40MCO-60CPO powder with those of the pure MCO and CPO phases, no other crystalline phases except those of MCO and CPO were detected in the powder after calcination at 950 °C. Since MCO gives much weaker XRD signals than CPO, the 2θ range between 30 and 40 degrees was measured over 10 h, and the MCO line at 36 degrees can be taken as a fingerprint for the existence of crystalline MCO. However, from the XRD patterns of the 40MCO-60CPO dual phase membrane sintered at 1300 °C in air for 10 h, small amounts of MnO<sub>2</sub> and the tetragonal (MnCoMnCo)<sub>2</sub>O<sub>4.8</sub> can be found. This behavior may be related to the tetragonal-cubic structure transformations of Mn<sub>2-x</sub>Co<sub>x</sub>O<sub>4.8</sub> (1.54 ≥ x ≥ 0.98) with temperature.<sup>35</sup> According to the phase diagram of the Mn-Co-O system reported by Aukrust et al., at 1300 °C exists in air for X = 1.5 a stable mixture of cubic MnCo<sub>2</sub>O<sub>4.8</sub>, tetragonal Mn<sub>2</sub>CoO<sub>4.8</sub> and the mixed oxide

(Mn<sub>2</sub>Co)O.<sup>36</sup>

The precursor ash obtained by the combustion of the precursor in the GNP shows a foam-like structure open-pore structure because of the vigorous gas evolution (H<sub>2</sub>O, N<sub>2</sub> and CO<sub>2</sub>) during the GNP combustion synthesis (Fig. 4a). After sintering the precursor ash at 950 °C for 10 h, some densification can be stated (Fig. 4b). From the comparison of the EDXS of the precursor ash (Fig. 4c) and the powder after 950 °C calcination (Fig. 4d) it follows that the chemical composition of the ash and the powder is unchanged. Quantitative analysis based on the Cliff-Lorimer ratio technique, gave the element ratios Mn/Co = 1 : 1 and Ce/Pr = 9 : 1, which are in accurate agreement with the stoichiometry of the Mn<sub>1.5</sub>Co<sub>1.5</sub>O<sub>4.8</sub> spinel and of the Ce<sub>0.9</sub>Pr<sub>0.1</sub>O<sub>2</sub> cubic fluorite structure.

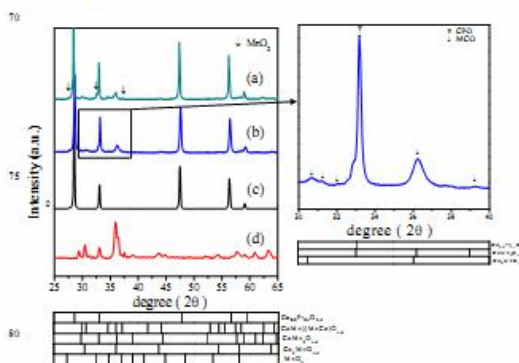


Fig. 3. XRD patterns of the 40MCO-60CPO membrane after sintered at 1300 °C in air for 10 h (a) and the mixed powder 40MCO-60CPO (b), pure phase powders CPO (c) and MCO (d), produced by the GNP method and calcined at 950 °C for 10 h in air (flow chart see Fig. 2, for the SEM see Fig. 4). Since MCO gives poor XRD patterns, the 30 - 40 2θ range of all samples has been measured for long time (10 h).

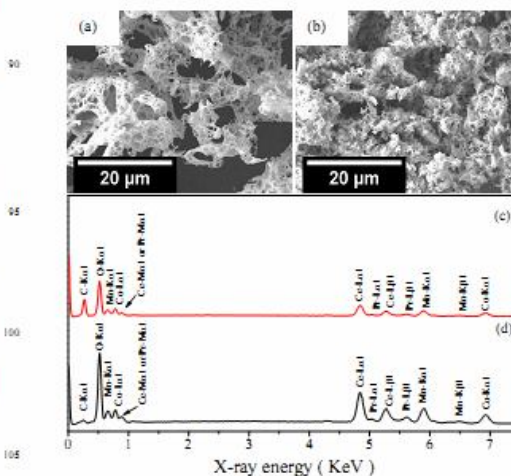


Fig. 4 SEM (a,b) pictures and EDXS (c,d) analysis of the precursor ash after burning the precursor (a,c) and the 40MCO-60CPO powder (b,d) after calcination of the precursor ash at 950 °C for 10 h in air (see Fig. 2).

Fig. 5 shows the SEM and BSEM images of the 40MCO-60CPO dual phase membranes after sintering at 1300 °C for 10 h at two different magnifications. The grains of the two phases are well distributed with clear grain boundaries. The MCO and CPO grains can be easily distinguished by BSEM, the dark grains are MCO and the light ones represent CPO since the contribution of the backscattered electrons to the SEM signal intensity is proportional to the atomic number. Furthermore, in the BSEM images of Fig. 5c and d, the mean grain size areas of MCO and CPO are found to be 0.265 μm<sup>2</sup> and 0.329 μm<sup>2</sup> through the analysis of 50 grains, respectively. The EDXS of the membrane (Fig. 6) shows the presence of Mn, Co, Ce, and Pr (Fig. 6b). Fig. 6a shows the elemental mapping of the top view of the 40MCO-60CPO membrane obtained by EDXS. The green color (dark in BSEM) is an overlap of the Mn and Co signals, whereas the yellow color (light in BSEM) stems from an average of the Ce and Pr signals.

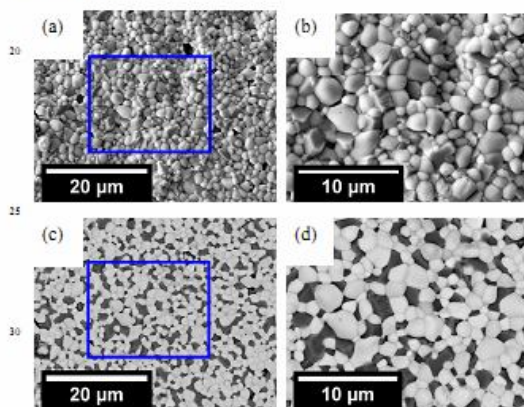


Fig. 5 SEM (a,b) and BSEM (c,d) of the surface of the 40MCO-60CPO dual phase membrane after sintered at 1300 °C in air for 10 h for different magnifications. In BSEM, the dark grains represent the MCO grains, the light ones represent the CPO grains, since the contribution of the backscattered electrons to the SEM signal intensity is proportional to the atomic number.

#### Oxygen permeation properties and stability of the 40MCO-60CPO dual phase materials

The oxygen permeability through the 40MCO-60CPO dual phase membranes as a function of temperature with CO<sub>2</sub> as sweep gas is presented in Fig. 7. All the data were collected after oxygen permeation had reached steady state (after about 24 h). As shown in Fig. 7a, the oxygen permeation fluxes increase with increasing temperature. For example, when the temperature increases from 900 °C to 1000 °C, the oxygen permeation flux increases from 0.26 ml/min·cm<sup>2</sup> to 0.48 ml/min·cm<sup>2</sup>. At 950 °C, a stable oxygen permeation flux of 0.37 ml/min·cm<sup>2</sup> is obtained through a membrane with a thickness of 0.3 mm. These are relative high oxygen fluxes in comparison with literature data. The Ce<sub>0.8</sub>Sm<sub>0.2</sub>O<sub>2.8</sub> - La<sub>0.8</sub>Sr<sub>0.2</sub>CrO<sub>3.8</sub> dual phase membrane with a thickness of 0.3 mm exhibits an oxygen permeation flux of 1.4 ×

10<sup>-7</sup> mol/s·cm<sup>2</sup> (0.19 ml/min·cm<sup>2</sup>) under an air/He oxygen partial pressure gradient at 950 °C,<sup>37</sup> which is nearly two times lower than that on our 40MCO-60CPO membrane. Furthermore, the Arrhenius plot (Fig. 7b) indicates that oxygen permeation can be described by a single apparent activation energy of 77 kJ/mol in the temperature range of 900-1000 °C with pure CO<sub>2</sub> as the sweep gas. It is accepted that a single activation energy is an important indication that there is no phase transformation in the membrane under study.<sup>38</sup> This conclusion is in agreement with the finding that the oxygen flux with pure CO<sub>2</sub> as sweep gas is found to be long-time stable (see Fig. 12).

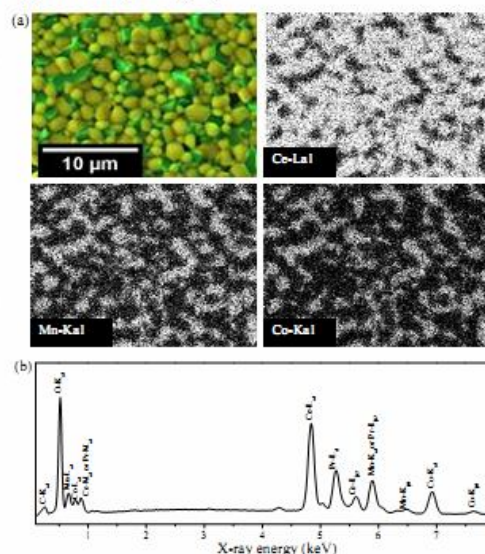


Fig. 6 EDXS analysis of 40MCO-60CPO composite membranes after sintered at 1300 °C for 10 h. In the EDXS map, the green grains represent MCO grains (averaged and calibrated signals of Mn Kα1, 2p → 1s and Co Kα1, 2p → 1s), and the yellow grains represent CPO grains (averaged and calibrated signals of Ce Lα1, 3d → 2p and Pr Lα1, 3d → 2p).

It is known that the rate-limiting step of oxygen permeation through an MIEC membrane can be controlled either by oxygen surface exchange or by oxygen ions bulk diffusion. In order to identify the rate limiting step of oxygen transport through our 40MCO-60CPO membrane with CO<sub>2</sub> sweep gas, we studied the oxygen permeation under different oxygen partial pressures on the sweep side at different temperatures while keeping the oxygen pressure on the air side constant at 0.20 bar. The different oxygen partial pressures on the sweep side were adjusted by changing the CO<sub>2</sub> flow rate and measured by gas chromatography in this study. Fig. 8 displays the influence of different CO<sub>2</sub> flow rates on oxygen permeation on the 40MCO-60CPO membrane with 0.5 mm thickness at different temperatures. It was found for all temperatures that the oxygen permeation fluxes were increased with increasing the CO<sub>2</sub> flow rate. For example, when the CO<sub>2</sub> flow rate increased from 19 to 116 mL min<sup>-1</sup>, the oxygen partial pressures on the permeate side decrease from 0.007 bar to 0.002 bar; whereas the oxygen permeation fluxes increased from 0.19 mL cm<sup>-2</sup> min<sup>-1</sup> to 0.23 mL cm<sup>-2</sup> min<sup>-1</sup> at 1000 °C. When



using CO<sub>2</sub> as the sweep gas, we can observe the usual behavior, namely that the oxygen permeances increase if the gradient of the oxygen partial pressure across the membrane is increased, which can be achieved by off-transporting the permeated oxygen as fast as possible, by an increased sweep flow.

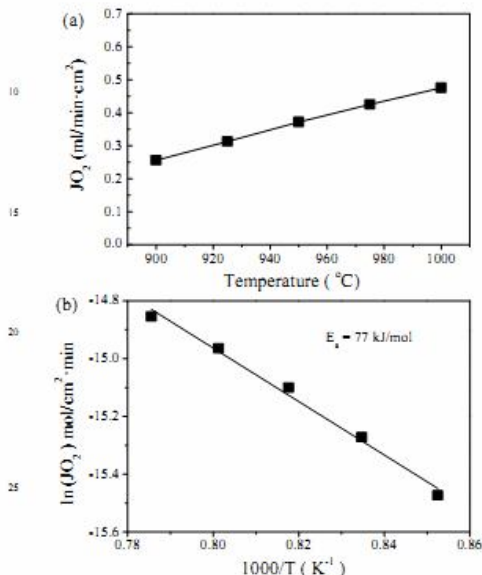


Fig. 7 Oxygen permeation fluxes (a) and its Arrhenius plot (b) through the 40MCO-60CPO dual phase membranes as a function of temperature with pure CO<sub>2</sub> as sweep gas. Conditions: 200 ml/min air as feed gas, 29 ml/min CO<sub>2</sub> as sweep gas; 1 ml/min Ne as internal standard gas; Membrane thickness: 0.3 mm.

Following Kim et al.<sup>39</sup>,  $J_{O_2}$  shows a linear relationship with  $(P_h/P_a)^{0.5} - (P_l/P_a)^{0.5}$  according to

$$J_{O_2} = \frac{1}{2} \frac{C_1 C_2}{C_{i1} + C_{i2}} k_w [(P_h/P_a)^n - (P_l/P_a)^n] \quad (1)$$

if the oxygen permeation process is limited by the surface exchange reaction. If the oxygen permeation process is controlled by oxygen ion bulk diffusion,  $J_{O_2}$  would be linearly proportional to  $\ln(P_h/P_l)$  according to<sup>39</sup>

$$J_{O_2} = \frac{1}{4} \frac{(C_i D_o)}{L} \ln \frac{P_h}{P_l} \quad (2)$$

where  $J_{O_2}$  is the oxygen permeation flux,  $C_i$  is the oxygen ion concentration,  $D_o$  is the diffusion coefficient of the oxygen ion-electron hole pairs,  $L$  is the thickness of the membrane,  $C_{i1}, C_{i2}$  are the oxygen concentrations at the interfaces of the membrane.  $n$  is the order of the chemical reaction at the gas-MIEC interface which is for the special case of a planar membrane  $n = 0.5$ .  $k_w$  is the surface-exchange coefficient, and  $P_h, P_l$  and  $P_a$  stand for high oxygen partial pressures on the feed side, low oxygen partial pressures on the sweep side and the normalized pressures of 1 bar, respectively.

Correlating and evaluating our oxygen permeation data according to the above theory of Kim et al.,<sup>39</sup> we can state that the oxygen permeation fluxes  $J_{O_2}$  are a linear function of  $(P_h/P_a)^{0.5} - (P_l/P_a)^{0.5}$  and not of  $\ln(P_h/P_l)$  as shown in Fig. 9. From this result, it suggests that the oxygen permeation through the 40MCO-60CPO dual phase membrane of 0.5 mm thickness is controlled in the temperature region studied by the surface reaction rather than by bulk diffusion.

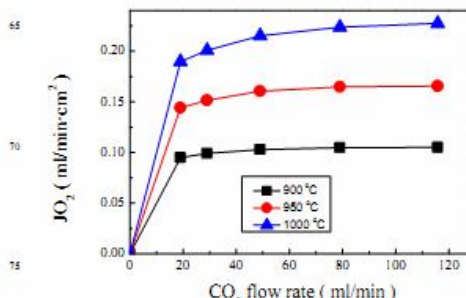


Fig. 8 Effect of different CO<sub>2</sub> sweep rates on oxygen permeation flux at different temperatures. Conditions: 200 ml/min air as feed gas; 1 ml/min Ne as internal standard gas; Membrane thickness: 0.5 mm.

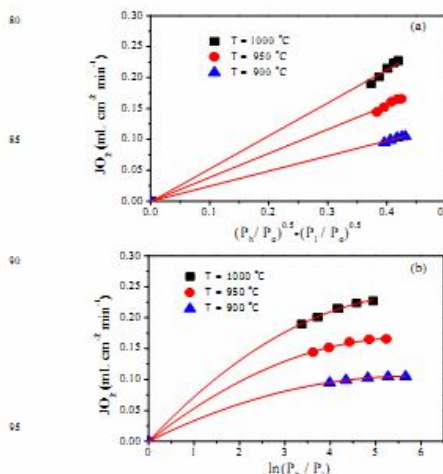


Fig. 9 Relationship between oxygen permeation fluxes through the 40MCO-60CPO membrane with 0.5 mm thickness at different temperatures and  $\ln(P_h/P_l)$ .  $P_h, P_l$  and  $P_a$  denote for high oxygen partial pressure on the feed side, low oxygen partial pressures on the sweep side and the normalized pressures of 1 bar, respectively. Conditions: (see Fig. 8). Conditions: 200 ml/min air as feed gas,  $F_{CO_2+He+Ne} = 30$  ml/min as sweep gas; 1 ml/min Ne as internal standard gas. Membrane thickness: 0.5 mm.

Fig. 10 shows the oxygen permeation flux through 40MCO-60CPO dual phase composite membrane with a thickness 0.5 mm as a function of the CO<sub>2</sub> concentration in the sweep gas at 1000 °C. The different CO<sub>2</sub> concentrations have been obtained by mixing with He, the total flow rate of the sweep gas was kept

constant at 30 ml/min with 1 ml Ne/min as calibration gas. With increasing CO<sub>2</sub> concentration of the sweep gas, only a slight decrease of the oxygen permeation flux can be seen. This behavior is different to those of alkaline-earth metals containing perovskites. Schulz et al. reported a strong decrease of the oxygen permeation flux through the perovskites Ba<sub>0.5</sub>Sr<sub>0.5</sub>Co<sub>0.8</sub>Fe<sub>0.2</sub>O<sub>3-δ</sub> (BSCF) and SrCo<sub>1-x</sub>Nb<sub>x</sub>O<sub>3-δ</sub> (SCN; x = 0.1, 0.2) due to carbonate formation with increasing CO<sub>2</sub> concentrations in the sweep gas.<sup>40</sup> The slight decrease of the oxygen permeation flux can be explained by a stronger influence of CO<sub>2</sub> on the surface process compared with pure He which is in complete agreement with previous reports.<sup>19,21</sup> This finding is also in correspondence with our previous studies on NiFe<sub>2</sub>O<sub>4-δ</sub>-Ce<sub>0.9</sub>Gd<sub>0.1</sub>O<sub>2-δ</sub> composite materials and similar to the La<sub>0.8</sub>Sr<sub>0.2</sub>MnO<sub>3-δ</sub>-Ce<sub>0.8</sub>Sm<sub>0.2</sub>O<sub>2-δ</sub> dual phase composite membrane of Chen et al., where also a slight reduction of the oxygen permeation flux was observed when pure CO<sub>2</sub> instead of a more inert sweep gas was used.<sup>41</sup>

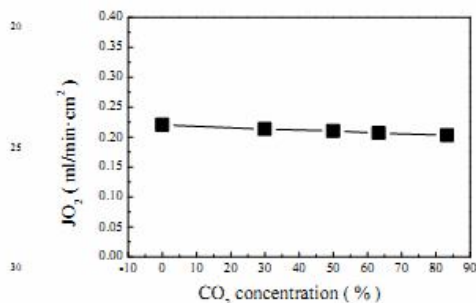


Fig. 10 Oxygen permeation flux through 40MCO-60CPO dual phase composite membrane as function of CO<sub>2</sub> concentration in the sweep gas at 1000 °C. Conditions: 200 ml/min air as feed gas, F<sub>CO<sub>2</sub>-He-Ne</sub> = 30 ml/min as sweep gas; 1 ml/min Ne as internal standard gas. Membrane thickness: 0.5 mm.

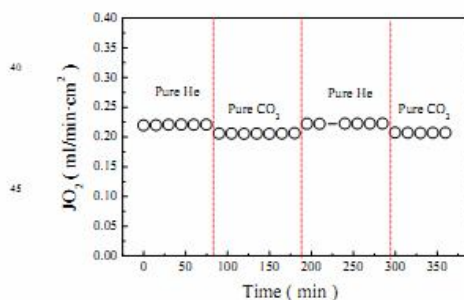


Fig. 11 Oxygen permeation fluxes as function of time while periodically changing the sweep gas. Conditions: 200 ml/min air as feed gas, 29 ml/min He and 1 ml/min Ne or 29 ml/min CO<sub>2</sub> and 1 ml/min Ne as sweep gas; Membrane thickness: 0.5 mm. Temperature: 1000 °C.

Fig. 11 presents the reversibility of the oxygen permeation flux through the 40MCO-60CPO membrane while periodically changing the sweep gas between He and CO<sub>2</sub> at 1000 °C. When

using He as sweep gas, a stable oxygen permeation flux of 0.22 ml/min·cm<sup>2</sup> can be obtained, whereas the oxygen permeation flux decreases immediately to the slightly lower value of 0.20 ml/min·cm<sup>2</sup> if CO<sub>2</sub> instead of He is used as sweep gas. This behavior is different to previous findings on the perovskite-type membranes. Arnold et al. reported an immediate stop of the oxygen permeation for BSCF membrane when pure CO<sub>2</sub> was used as sweep gas at 875 °C but the oxygen permeation flux recovered if the sweep gas is switched back to pure helium.<sup>16</sup> It also has been reported that a rapid breakdown of the oxygen permeability through (Ba,Sr)(Zn,Fe)O<sub>3-δ</sub> membrane at 750 °C in a CO<sub>2</sub> atmosphere due to the formation of a small amount of carbonate on the surface of the membrane.<sup>42</sup> Yi et al. demonstrated that the oxygen permeability of Ba(Co<sub>0.4</sub>Fe<sub>0.2</sub>Nb<sub>0.2</sub>)O<sub>3-δ</sub> perovskite membrane deteriorates significantly upon exposure of the membrane to a CO<sub>2</sub>-containing sweep gas. Further, it was found that the reaction of the membrane with CO<sub>2</sub> leads to a decomposition of the membrane material and to the formation of a compact BaCO<sub>3</sub> surface layer as well as a porous decomposed zone; the latter consists of mainly CoO and the Co-depleted perovskite phase.<sup>13</sup> However, in our study, only a slight decrease of the oxygen permeation flux was observed. This behavior is ascribed to the slight inhibiting effect of CO<sub>2</sub> on the oxygen surface-exchange reaction but not to the formation of carbonates. Numerous papers have shown that the oxygen surface-exchange reaction is influenced by the kind of sweep gas. Ten Elshof et al. have reported that the activation energy obtained from La<sub>1-x</sub>Sr<sub>x</sub>FeO<sub>3-δ</sub> (x = 0.1 - 0.3) under air/CO<sub>2</sub> oxygen partial pressure gradients is much lower than that under air/He gradient due to the difference of oxygen exchange reaction in the presence of CO, CO<sub>2</sub> or He gas.<sup>43</sup>

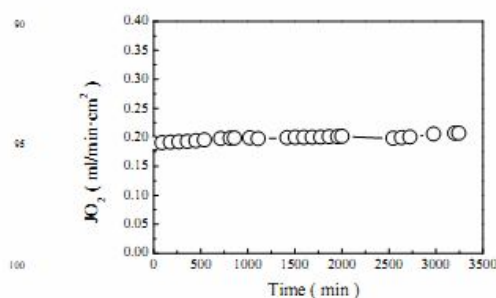


Fig. 12 Oxygen permeation flux through 40MCO-60CPO dual phase composite membrane as a function of time using pure CO<sub>2</sub> as sweep gas. Conditions: 200 ml/min air as feed gas, 29 ml/min CO<sub>2</sub> as sweep gas; 1 ml/min Ne as internal standard gas. Membrane thickness: 0.5 mm. Temperature: 1000 °C.

The oxygen permeation flux through the 40MCO-60CPO dual phase composite membrane with CO<sub>2</sub> as sweep gas is shown in Fig. 12 as a function of time. During the whole oxygen permeation test, an oxygen permeation flux of about 0.20 ml/min·cm<sup>2</sup> was obtained at 1000 °C and no decrease was found. In the previous studies of the perovskite-type materials containing alkaline-earth metals e.g. Ba<sub>0.5</sub>Co<sub>0.7</sub>Fe<sub>0.2</sub>Nb<sub>0.1</sub>O<sub>3-δ</sub> (BCFN),<sup>13</sup> Ba<sub>0.5</sub>Sr<sub>0.5</sub>Co<sub>0.8</sub>Fe<sub>0.2</sub>O<sub>3-δ</sub> (BSCF),<sup>16</sup> and Ba<sub>0.5</sub>Sr<sub>0.5</sub>Fe<sub>0.8</sub>Zn<sub>0.2</sub>O<sub>3-δ</sub>

(BSFZ),<sup>42</sup> it has been found that oxygen permeation flux through these single perovskite-type membranes decreased sharply due to the formation of carbonates once if CO<sub>2</sub> gas was present. Moreover, Kharton et al. have reported that obvious degradation of the oxygen permeation flux through Ce<sub>0.8</sub>Gd<sub>0.2</sub>O<sub>2-δ</sub>-La<sub>0.7</sub>Sr<sub>0.3</sub>MnO<sub>3-δ</sub> dual phase composite membrane with time was observed due to the formation of Sr(Ce, Ln)O<sub>3-δ</sub> (Ln is Gd, La) in the grain boundaries, which can block the ionic transport.<sup>44</sup> From the stable oxygen permeation fluxes on our 40MCO-60CPO, we can exclude chemical reactions between the two MCO and CPO phases involved like reported in previous studies of dual phase membranes.

### Conclusions

A novel oxygen transporting dual phase membrane of the composition 40 wt.% Mn<sub>1.5</sub>Co<sub>1.5</sub>O<sub>4.5</sub> - 60 wt.% Ce<sub>0.9</sub>Pr<sub>0.1</sub>O<sub>2-δ</sub> (40MCO-60CPO) was prepared with MCO as an electron conductor and CPO as oxygen ion conductor via a rapid one-pot one-step glycine-nitrate combustion process. XRD confirmed that the 40MCO-60CPO membrane sintered at 1300 °C in air, represents a micro-scale mixture of mainly the two phases MCO and CPO, but also traces of MnO<sub>2</sub> and (MnCoMnCo)<sub>2</sub>O<sub>4.8</sub> have been detected. An oxygen permeation flux of 0.48 ml/min·cm<sup>2</sup> was obtained at 1000 °C under an air/CO<sub>2</sub> oxygen partial pressure gradient through a membrane with a thickness 0.3 mm. The 40MCO-60CPO dual phase membrane can be operated for at least 60 h when pure CO<sub>2</sub> was used as sweep gas, suggesting that the 40MCO-60CPO dual phase membrane is CO<sub>2</sub> stable. The good stability under pure CO<sub>2</sub> recommends the 40MCO-60CPO material as a good candidate for the oxygen separation from air in the 4-end membrane operation mode in the oxy-fuel process.

### Acknowledgements

H. X. Luo acknowledges the financial support by the China Scholarship Council (CSC). The authors acknowledge financial support from EU through FP7 NASA-OTM project (grant agreement n° 228701) and from the Sino-German centre for Science Promotion (GZ 676). T. Klande thanks the State of Lower Saxony for the NTH bottom up grant No. 21-71023-25-7/09. The authors thank Dr. Feldhoff for stimulating discussions and F. Steinbach for technical support.

### Notes and References

- <sup>a</sup> Institute of Physical Chemistry and Electrochemistry Leibniz University of Hannover, Callinstraße 3-3A, D-30167 Hannover, Germany. Fax: +49-511-762 1912; Tel.: +49-511-762 3175; E-mail address: juergen.caro@pci.uni-hannover.de
- <sup>b</sup> Max-Planck-Institut für Kohlenforschung, Kaiser-Wilhelm-Platz 1, D-45470 Mülheim an der Ruhr, Germany.
- <sup>c</sup> School of Chemistry & Chemical Engineering, South China University of Technology, No. 381 Wushan Road, 510640 Guangzhou, China. Fax: +86-20-87110131; Tel.: +86-20-87110131;

E-mail address: hhwang@scut.edu.cn

- S. Baumann, J. M. Serra, M. P. Lobera, S. Escolástico, F. Schulze-Küppers and W. A. Meulenber, *J. Membr. Sci.*, 2011, **377**, 198-205.
- J. Pérez-Ramírez and B. Vigeland, *Angew. Chem. Int. Ed.*, 2005, **44**, 1112-1115.
- E. Drioli, A. Brunetti, G. Di Profio and G. Barbieri, *Green Chem.*, 2012, DOI: 10.1039/C2GC16668B.
- M. A. Habib, H. M. Badr, S. F. Ahmed, R. Ben-Mansour, K. Mezghani, S. Imashuku, G. J. la O', Y. Shao-Horn, N. D. Mancini, A. Mitsos, P. Kirchen and A. F. Ghoneim, *Int. J. Energy Res.*, 2011, **35**, 741-764.
- S. Smart, C. X. C. Lin, L. Ding, K. Thambimuthu and J. C. D. da Costa, *Energy Environ. Sci.*, 2010, **3**, 268-278.
- S. S. Hashim, A. R. Mohamed and S. Bhatia, *Renew. Sust. Energy Rev.*, 2011, **15**, 1284-1293.
- S. Engels, T. Markus, M. Modigell and L. Singheiser, *J. Membr. Sci.*, 2011, **370**, 58-69.
- S. Engels, F. Beggel, M. Modigell and H. Stadler, *J. Membr. Sci.*, 2010, **359**, 93-101.
- A. Waindich, A. Möbius and M. Müller, *J. Membr. Sci.*, 2009, **337**, 182-187.
- M. Schulz, R. Kriegel and A. Kämpfer, *J. Membr. Sci.*, 2011, **378**, 10-17.
- E. Tzimpilisi, N. Moschoudis, M. Stoukides and P. Bekiaroglou, *Appl. Catal. B: Environ.*, 2009, **87**, 9-17.
- N. P. Xu, S. G. Li, W. Q. Jin, J. Shi and Y. S. Lin, *AIChE J.*, 1999, **45**, 2519-2526.
- J. X. Yi, M. Schroeder, T. Weirich and J. Mayer, *Chem. Mater.*, 2010, **22**, 6246-6253.
- Q. Jiang, S. Faraji, K. J. Nordheden and S. M. Stagg-Williams, *J. Membr. Sci.*, 2011, **368**, 69-77.
- J. X. Yi, S. J. Feng, Y. B. Zuo, W. Liu and C. S. Chen, *Chem. Mater.*, 2005, **17**, 5856-5861.
- M. Arnold, H. H. Wang and A. Feldhoff, *J. Membr. Sci.*, 2007, **293**, 44-52.
- X. Tan, N. Liu, B. Meng, J. Sunarso, K. Zhang and S. Liu, *J. Membr. Sci.*, 2012, **389**, 216-222.
- S. Li, W. Jin, P. Huang, N. Xu, J. Shi and Y. S. Lin, *J. Membr. Sci.*, 2000, **166**, 51-61.
- H. X. Luo, H. Q. Jiang, K. Efimov, H. H. Wang and J. Caro, *AIChE J.*, 2011, **57**, 2738-2745.
- H. X. Luo, K. Efimov, H. Q. Jiang, A. Feldhoff, H. H. Wang and J. Caro, *J. Angew. Chem. Int. Ed.*, 2011, **50**, 759-763.
- H. X. Luo, H. Q. Jiang, K. Efimov, F. Y. Liang, H. H. Wang and J. Caro, *Ind. Eng. Chem. Res.*, 2011, **50**, 13508-13517.
- V. V. Kharton, A. V. Kovalevsky, A. P. Viskup, A. L. Shaula, F. M. Figueiredo, E. N. Naumovich and F. M. B. Marques, *Solid State Ionics*, 2003, **160**, 247-258.
- E. J. E. Ten, N. Q. Nguyen, O. M. W. Den and H. J. M. Bouwmeester, *J. Electrochem. Soc.*, 1997, **144**, 4361-4366.
- L. A. Chick, L. R. Pederson, G. D. Maupin, J. L. Bates, L. E. Thomas and G. J. Exarhos, *Mater. Letter.*, 1990, **10**, 6-12.
- R. D. Purohit, S. Saha and A. K. Tyagi, *J. Nucl. Mater.*, 2001, **288**, 7-10.
- Y. L. Zhang, H. C. Shin, J. Dong and M. L. Liu, *Solid State Ionics*, 2004, **171**, 25-31.
- H. H. Wang, W. S. Yang, Y. Cong, X. F. Zhu and Y. S. Lin, *J. Membr. Sci.*, 2003, **224**, 107-115.
- Z. G. Yang, G. G. Xia, X. H. Li and J. W. Stevenson, *Int. J. Hydrogen Energy*, 2007, **32**, 3648-3654.
- M. C. Tucker, L. Cheng and L. C. DeJonghe, *J. Power Sources*, 2011, **196**, 8435-8443.
- H. Y. Liu, X. F. Zhu, M. J. Cheng, Y. Cong and W. S. Yang, *Chem. Commun.*, 2011, **47**, 2378-2380.
- D. L. Maricle, T. E. Swarr and S. Karavolis, *Solid State Ionics*, 1992, **52**, 173-182.
- P. Knauth and H. L. Tuller, *J. Eur. Ceram. Soc.*, 1999, **19**, 831-836.
- H. X. Luo, B. B. Tian, Y. Y. Wei, H. H. Wang, H. Q. Jiang and J. Caro, *AIChE J.*, 2010, **56**, 604-610.

- 34 Z. Y. Pu, J. Q. Lu, M. F. Luo and Y. L. Xie, *J. Phys. Chem. C*, 2007, **111**, 18695-18702.
- 35 H. Bordeneuve, S. Guillemet-Fritsch, A. Rousset, S. Schuurman and V. Poulain, *J. Solid State Chem.*, 2009, **182**, 396-610.
- 36 E. Aukrust and A. Muan, *J. Am. Ceram. Soc.-Discussions and notes*, 1963, **46**, 511.
- 37 J. X. Yi, Y. B. Zuo, W. Liu, L. Winnubst and C. S. Chen, *J. Membr. Sci.*, 2006, **280**, 849-855.
- 38 J. H. Tong, W. S. Yang, B. C. Zhu and R. Cai, *J. Membr. Sci.*, 2002, **203**, 175-189.
- 39 S. Kim, Y. L. Yang, A. J. Jacobson and B. Abeles, *Solid State Ionics*, 1999, **121**, 31-36.
- 40 M. Schulz, R. Kriegel and A. Kämpfer, *J. Membr. Sci.*, 2011, **378**, 10-17.
- 41 W. Li, T. F. Tian, F. Y. Shi, Y. S. Wang and C. S. Chen, *Ind. Eng. Chem. Res.*, 2009, **48**, 5789-5793.
- 42 J. Martynczuk, K. Efimov, L. Robben and A. Feldhoff, *J. Membr. Sci.*, 2009, **344**, 62-70.
- 43 J. E. Ten Elshof, H. J. M. Bouwmeester and H. Verweij, *Solid State Ionics*, 1996, **89**, 81-92.
- 44 V. V. Kharton, A. V. Kovalevsky, A. P. Viskup, F. M. Figueiredo, E. N. Naumovich and F. M. B. Marques, *J. Electrochem. Soc.*, 2000, **147**, 2814-2821.

## Chapter 4

### 4. Dual phase membrane as reactor for partial oxidation of methane

#### 4.1 Summary

The above mentioned noble metal-free and alkaline metal-free dual phase membrane materials described in chapter 3 showed very good CO<sub>2</sub> stability. However, it was found that most of these dual phase materials contain easily reducible metals oxides of Co or Ni in their compositions, which is unfavorable for the membrane stability in reducing atmospheres.

In this chapter, a novel dual phase membrane cobalt-free noble metal-free 40PSFO-60CPO dual phase material was developed via a one-pot single-step GNP, as a proven means to obtain fine and homogeneous powders. The concept of this dual phase membrane was to prepare a mixture of a pure oxygen ionic conductor and a mixed (oxygen ionic and electronic) conductor. XRD and BSEM confirmed that the 40PSFO-60CPO dual phase membrane was successfully prepared. *In-situ* XRD demonstrated that the 40PSFO-60CPO dual phase membrane shows a good phase stability not only in air but also in 50 vol.% CO<sub>2</sub>/50 vol.% N<sub>2</sub> atmosphere. At 950 °C using pure He as sweep gas, a stable oxygen permeation flux of 0.26 ml/min·cm<sup>2</sup> is obtained through the 40PSFO-60CPO dual phase membrane. Whereas, an oxygen permeation flux of 0.18 ml/min·cm<sup>2</sup> through the 40PSFO-60CPO dual phase membrane was obtained when using pure CO<sub>2</sub> as sweep gas. The partial oxidation of methane (POM) to syngas was also successfully investigated in the 40PSFO-60CPO dual phase membrane reactor. At 950 °C under a steady state, methane conversion was found to be higher than 99 % with 97 % CO selectivity, and 7.81 ml/min·cm<sup>2</sup> oxygen permeation flux is obtained. The dual phase membrane, without any noble metals like Ag, Pd or easily reducible metals oxides of Co or Ni, exhibits high oxygen permeation fluxes as well as good phase stability at high temperatures. Furthermore, the dual phase membrane shows a good chemical stability under the harsh conditions of the POM reaction and in a CO<sub>2</sub> atmosphere at high temperatures.

## **4.2 A novel cobalt-free noble-free oxygen-permeable $40\text{Pr}_{0.6}\text{Sr}_{0.4}\text{FeO}_{3-\delta}$ - $60\text{Ce}_{0.9}\text{Pr}_{0.1}\text{O}_{2-\delta}$ dual phase membrane**

Huixia Luo, Heqing Jiang, Tobias Klande, Zhengwen Cao, Fangyi Liang, Haihui Wang, Jürgen  
Caro,

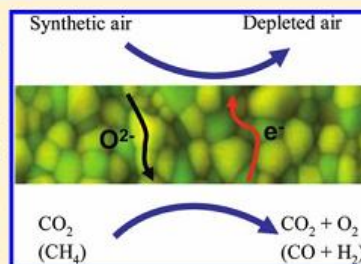
**Chem. Mater.** 24 (2012), 2148-2154

**Reprinted (adapted) with permission from (Chemistry of Materials). Copyright (2012)  
American Chemical Society.**

Novel Cobalt-Free, Noble Metal-Free Oxygen-Permeable  
40Pr<sub>0.6</sub>Sr<sub>0.4</sub>FeO<sub>3-δ</sub>-60Ce<sub>0.9</sub>Pr<sub>0.1</sub>O<sub>2-δ</sub> Dual-Phase MembraneHuixia Luo,<sup>†</sup> Heqing Jiang,<sup>‡</sup> Tobias Klande,<sup>†</sup> Zhengwen Cao,<sup>†</sup> Fangyi Liang,<sup>†</sup> Haihui Wang,<sup>\*,§</sup>  
and Jürgen Caro<sup>\*,†</sup><sup>†</sup>Institute of Physical Chemistry and Electrochemistry, Leibniz University Hannover, Callinstrasse 3A, D-30167 Hannover, Germany<sup>‡</sup>Max-Planck-Institut für Kohlenforschung, Kaiser-Wilhelm-Platz 1, D-45470 Mülheim an der Ruhr, Germany<sup>§</sup>School of Chemistry & Chemical Engineering, South China University of Technology, No. 381 Wushan Road, 510640 Guangzhou, China

**ABSTRACT:** A novel cobalt-free and noble metal-free dual-phase oxygen-transporting membrane with a composition of 40 wt % Pr<sub>0.6</sub>Sr<sub>0.4</sub>FeO<sub>3-δ</sub>-60 wt % Ce<sub>0.9</sub>Pr<sub>0.1</sub>O<sub>2-δ</sub> (40PSFO-60CPO) has been successfully developed via an in situ one-pot one-step glycine-nitrate combustion process. In situ XRD demonstrated that the 40PSFO-60CPO dual-phase membrane shows a good phase stability not only in air but also in 50 vol % CO<sub>2</sub>/50 vol % N<sub>2</sub> atmosphere. When using pure He or pure CO<sub>2</sub> as sweep gases, at 950 °C steady oxygen permeation fluxes of 0.26 cm<sup>3</sup> min<sup>-1</sup> cm<sup>-2</sup> and 0.18 cm<sup>3</sup> min<sup>-1</sup> cm<sup>-2</sup> are obtained through the 40PSFO-60CPO dual-phase membrane. The partial oxidation of methane (POM) to syngas was also successfully investigated in the 40PSFO-60CPO dual-phase membrane reactor. Methane conversion was found to be higher than 99.0% with 97.0% CO selectivity and 4.4 cm<sup>3</sup> min<sup>-1</sup> cm<sup>-2</sup> oxygen permeation flux in steady state at 950 °C. Our dual-phase membrane - without any noble metals such as Ag, Pd or easily reducible metals oxides of Co or Ni - exhibits high oxygen permeation fluxes as well as good phase stability at high temperatures. Furthermore, the dual-phase membrane shows a good chemical stability under the harsh conditions of the POM reaction and in a CO<sub>2</sub> atmosphere at high temperatures.

**KEYWORDS:** dual-phase membrane, CO<sub>2</sub>-stable membrane, glycine-nitrate combustion process (GNP), oxygen permeation, partial oxidation of methane (POM)



## 1. INTRODUCTION

Clean energy delivery is a global goal to avert the climate change impacts arising from greenhouse gas emissions. Oxygen transport membranes (OTMs) with mixed ionic-electronic conductivity are attractive as environmentally friendly, economical, and efficient means of producing oxygen from air,<sup>1,2</sup> for example, for catalytic hydrocarbon partial oxidations such as the conversion of natural gas into synthesis gas.<sup>3,4</sup> In addition, oxygen permeable membranes have been rapidly becoming attractive because of their potential oxygen supply to power stations with CO<sub>2</sub> capture according to the oxy-fuel concept<sup>5,6</sup> by using flue gas as sweep gas. Further promising applications are high-temperature catalytic membrane reactors for hydrocarbon conversion into syngas and added-value products<sup>7,8</sup> and the thermal decomposition of carbon dioxide in combination with the partial oxidation of methane to syngas.<sup>9,10</sup>

Over the last two decades, much efforts have been directed on the development of perovskite-type oxide membranes with the general formula ABO<sub>3</sub> (A = alkaline earth metals or lanthanide element; B = transition metal). Typically, alkaline earth cobaltites such as Ba<sub>1-x</sub>Sr<sub>x</sub>Co<sub>1-y</sub>Fe<sub>y</sub>O<sub>3-δ</sub>,<sup>11,12</sup> BaCo<sub>1-y</sub>Fe<sub>y</sub>O<sub>3-δ</sub>,<sup>13</sup> and SrCo<sub>1-y</sub>Fe<sub>y</sub>O<sub>3-δ</sub><sup>14</sup> were fabricated as

high oxygen permeation membranes. However, their widespread applications of the above oxygen permeation membranes are hampered owing to the poor phase stability and chemical stability under a large oxygen concentration gradient, with one side of the membrane exposed to air as oxidizing atmosphere and the other side to a reducing or CO<sub>2</sub> containing atmosphere.<sup>15,16</sup> At present, new CO<sub>2</sub>-stable materials are attracting much interest. So far, some CO<sub>2</sub>-tolerant OTMs, such as K<sub>2</sub>NiF<sub>4</sub>-type (Pr<sub>0.9</sub>La<sub>0.1</sub>)<sub>2</sub>(Ni<sub>0.74</sub>Cu<sub>0.21</sub>Gd<sub>0.05</sub>)O<sub>4-δ</sub>,<sup>17,18</sup> La<sub>2</sub>NiO<sub>4-δ</sub>,<sup>19</sup> perovskite-type La<sub>0.6</sub>Ca<sub>0.4</sub>Co<sub>0.8</sub>Fe<sub>0.2</sub>O<sub>3-δ</sub>,<sup>20</sup> fluorite-type Ce<sub>1-x</sub>Tb<sub>x</sub>O<sub>2-δ</sub> + Co,<sup>21</sup> have been reported. Recently, we have developed novel cobalt-free CO<sub>2</sub>-tolerant dual-phase OTMs which consist of a mixture of pure ionic and pure electronic conducting oxides, such as NiFe<sub>2</sub>O<sub>4</sub>-Ce<sub>0.9</sub>Gd<sub>0.1</sub>O<sub>2-δ</sub>(NFO-CGO)<sup>22,23</sup> and Fe<sub>2</sub>O<sub>3</sub>-Ce<sub>0.9</sub>Gd<sub>0.1</sub>O<sub>2-δ</sub>(FO-CGO).<sup>24</sup> Very recently, Zhu et al.<sup>25</sup> have reported a novel CO<sub>2</sub>-stable dual-phase membrane which is made of ionic conducting oxides and mixed conducting oxides, showing 1 order of magnitude higher oxygen permeation fluxes than the

Received: March 5, 2012

Revised: May 16, 2012

Published: May 16, 2012

traditional dual-phase membranes. However, most of the above-mentioned materials contain easily reducible metals oxides of Co or Ni in their composition, which is unfavorable for the membrane stability in reducing atmospheres. Therefore, it is highly desired to develop novel OTMs with high stability under real application conditions, especially in the presence of gases like  $\text{CO}_2$ ,  $\text{CH}_4$ , etc.

In the present work, we report the development a novel cobalt-free noble-metal free dual-phase membrane material, 40 wt %  $\text{Pr}_{0.6}\text{Sr}_{0.4}\text{FeO}_{3-\delta}$ -60 wt %  $\text{Ce}_{0.9}\text{Pr}_{0.1}\text{O}_{2-\delta}$  (abbreviated as 40PSFO-60CPO). The 40PSFO-60CPO dual-phase material was prepared via an in situ one-pot one-step glycine-nitrate combustion process. In this dual-phase system, CPO is the main phase for ionic transport, and PSFO is the main phase for electronic transport, however, the latter phase PSFO also assists the ionic transport. Phase structure and stability as well as oxygen permeability are investigated under different atmospheres at high temperatures. Special attention is paid to the stability under  $\text{CO}_2$  and the reducing atmosphere of  $\text{CH}_4$ .

## 2. EXPERIMENTAL SECTION

**2.1. Preparation of Powders and Membranes.** The 40 wt %  $\text{Pr}_{0.6}\text{Sr}_{0.4}\text{FeO}_{3-\delta}$ -60 wt %  $\text{Ce}_{0.9}\text{Pr}_{0.1}\text{O}_{2-\delta}$  (40PSFO-60CPO) dual-phase powder mixture was directly synthesized via an in situ one-pot one-step glycine-nitrate combustion process (GNP), a proven means of obtaining fine and homogeneous powders.<sup>26</sup> The process flowchart

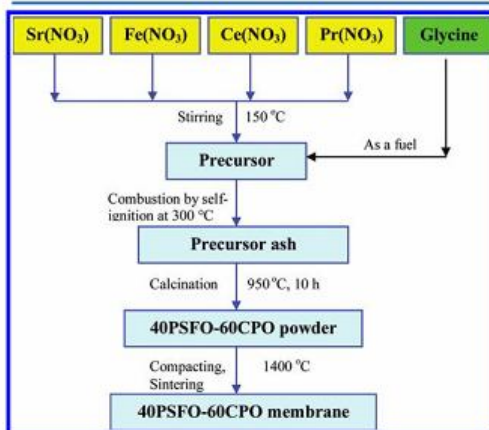


**Figure 1.** Flowchart for the one-pot one-step preparation of dual-phase 40 wt %  $\text{Pr}_{0.6}\text{Sr}_{0.4}\text{FeO}_{3-\delta}$ -60 wt %  $\text{Ce}_{0.9}\text{Pr}_{0.1}\text{O}_{2-\delta}$  (40PSFO-60CPO) membranes by the glycine-nitrate combustion process.

is shown in Figure 1. A precursor was prepared by combining glycine and the metal nitrates  $\text{Sr}(\text{NO}_3)_2$ ,  $\text{Fe}(\text{NO}_3)_3$ ,  $\text{Ce}(\text{NO}_3)_3$  and  $\text{Pr}(\text{NO}_3)_3$  in their appropriate stoichiometric ratios in an aqueous solution. The molar ratio of glycine: total metal ions was 2: 1. The precursor was stirred and heated at 150 °C in air to evaporate excess water until a viscous liquid was obtained. Further heating of the viscous liquid up to 300 °C caused the precursor liquid to autoignite. Combustion was rapid and self-sustaining, and a precursor ash was obtained. For comparison, the single phase  $\text{Pr}_{0.6}\text{Sr}_{0.4}\text{FeO}_{3-\delta}$  (PSFO) and  $\text{Ce}_{0.9}\text{Pr}_{0.1}\text{O}_{2-\delta}$  (CPO) materials were also prepared via the GNP method. All the powders were calcined at 950 °C in air for 10 h. The 40PSFO-60CPO powders were pressed to disk membranes under a pressure of 5 MPa in a stainless steel module with a diameter of 18

mm to get green disk membranes. These green disks were sintered at 1400 °C in air for 5 h. The surfaces of the disks were carefully polished to 0.6 mm thickness by using 1200 grit-sandpaper (average particle diameter 15.3  $\mu\text{m}$ ), then the membranes were washed with ethanol.

**2.2. Characterizations of Powders and Membranes.** X-ray diffraction (XRD, D8 Advance, Bruker-AXS, with  $\text{Cu K}\alpha$  radiation) was used to determine the phase structure of the dual-phase membranes after sintering at 1400 °C for 5 h. Data sets were recorded in a step-scan mode in the  $2\theta$  range of 20° - 80° with intervals of 0.02°. In situ XRD was conducted in a high-temperature cell HTK-1200N (Anton-Paar) from 30 to 1000 °C. The in situ XRD studies in air and a 50 vol %  $\text{CO}_2$ /50 vol %  $\text{N}_2$  atmosphere were performed with a heating rate of 12 °C  $\text{min}^{-1}$ . At each temperature step, the sample was held for 50 min for the thermal equilibrium before diffraction data collection. The disk membranes were studied by scanning electron microscopy (SEM) and back scattered SEM (BSEM) using a JEOL JSM-6700F at an excitation voltage of 20 keV. The element distribution in the grains of the fresh dual-phase membranes under study was investigated on the same electron microscope by energy dispersive X-ray spectroscopy (EDXS), Oxford Instruments INCA-300 EDX spectrometer with an ultrathin window at an excitation voltage of 20 keV.

**2.3. Oxygen Permeation and POM Performances of Membranes.** Oxygen permeation was studied using air as feed gas and He or  $\text{CO}_2$  as sweep gas using a homemade high-temperature oxygen permeation device, which is described in a previous paper.<sup>24</sup> The disk membranes were sealed onto a alumina tube at 950 °C for 5 h with a gold paste (Heraeus, Germany), the side wall of the membrane disk was also covered with the gold paste to avoid any radial contribution to the oxygen permeation flux. The effective areas of the membranes for oxygen permeation were 0.785  $\text{cm}^2$ . All the inlet gas flow rates were controlled by gas mass flow controllers (Bronkhorst, Germany) and all flow rates were regularly calibrated by using a bubble flow meter. Synthetic air (20%  $\text{O}_2$  and 80%  $\text{N}_2$ ) with a flow rate of 150  $\text{cm}^3 \text{min}^{-1}$  was the feed; a mixture of He or  $\text{CO}_2$  (29  $\text{cm}^3 \text{min}^{-1}$ ) and Ne (1  $\text{cm}^3 \text{min}^{-1}$ ) as the internal standard gas was fed to the sweep side.

In addition, the 40PSFO-60CPO dual-phase membrane has been used as a membrane reactor for POM. The membrane reactor configuration for POM was described elsewhere.<sup>25</sup> A Ni-based catalyst (0.3 g, Süd Chemie AG) was loaded on the top of the membrane disk and then the temperature of the reactor was increased to 950 °C with a heating rate of 2 °C  $\text{min}^{-1}$ . All gas lines to the reactor and the gas chromatograph were heated to 180 °C. High-purity methane of 7.32  $\text{cm}^3 \text{min}^{-1}$  without dilution was used as the reactant for the POM to synthesis gas. Gas composition was analyzed by an online gas chromatograph (GC, Agilent 6890A).

## 3. RESULTS AND DISCUSSION

**3.1. Characterizations of the 40PSFO-60CPO Dual-Phase Materials.** Figure 2 shows the XRD patterns of the PSFO, CPO, 40PSFO-60CPO powders after calcination at 950 °C for 10 h and the 40PSFO-60CPO dual-phase membrane after sintered at 1400 °C for 5 h. The XRD characterization indicates that both the calcined dual-phase powder and the sintered membrane consist of only the orthorhombic distorted perovskite PSFO and the cubic fluorite CPO phases, suggesting that the coexistence of PSFO and CPO is stable. The unit cell parameters of the pure CPO ( $a = b = c = 5.4110$  Å, space group No. 225:  $Fm\bar{3}m$ ) and PSFO ( $a = 5.4828$  Å,  $b = 7.7855$  Å,  $c = 5.4855$  Å, space group No. 74:  $Imma$ ) are similar in the 40PSFO-60CPO dual-phase powder (CPO:  $a = b = c = 5.4132$  Å, PSFO:  $a = 5.4906$  Å,  $b = 7.7667$  Å,  $c = 5.5244$  Å) and the sintered membrane (CPO:  $a = b = c = 5.4117$  Å, PSFO:  $a = 5.4930$  Å,  $b = 7.7974$  Å,  $c = 5.4945$  Å). It is worth to note that even though the dual-phase mixture preparation by the one-pot one-step GNP method, no additional phases, such



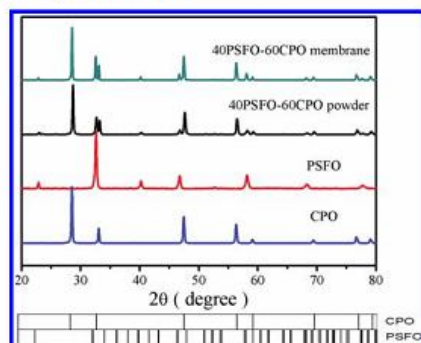


Figure 2. XRD patterns of CPO, PSFO and the dual-phase 40PSFO–60CPO powder calcined at 950 °C for 10 h and the 40PSFO–60CPO dual-phase membrane sintered at 1400 °C for 5 h (see Figure 1).

as  $\text{PrFeO}_3$  and  $\text{SrPrFeO}_4$ , were observed. Therefore, from the absence of foreign phase signals different from PSFO and CPO, it is concluded that the dual-phase membranes 40PSFO–60CPO can be successfully synthesized via a one-pot one-step GNP combustion process.

Figure 3 depicts the SEM, BSEM, and EDXS pictures of the 40PSFO–60CPO dual-phase membrane after sintering at 1400 °C for 5 h and before polishing at two different magnifications. Obviously, the micro-sized grains are packed closely; no major cracks are visible. The PSFO and CPO grains could be

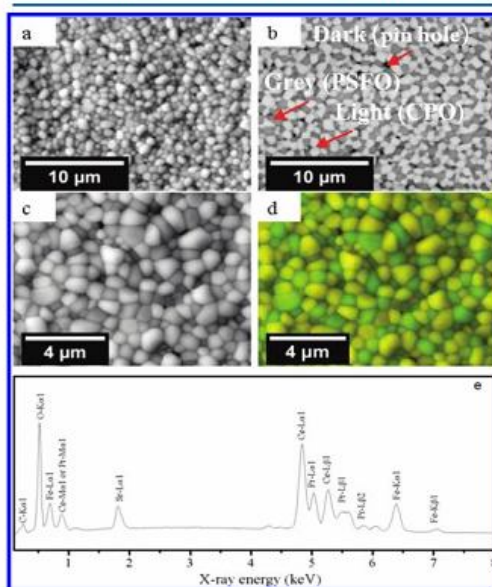


Figure 3. (a, c) SEM, (b) BSEM, and (d, e) EDXS images of the 40PSFO–60CPO membrane after sintered at 1400 °C for 5 h in air before polishing (see Figure 1). For the EDXS mapping in d, superimpositions of the Pr-L $\alpha$ , Pr-L $\beta$ , Sr-L $\alpha$ , and Fe-K $\alpha$  and Fe-K $\beta$  (green) and Pr-L $\alpha$ , Pr-L $\beta$  and Ce-L $\alpha$ , Ce-L $\beta$  (yellow) signals have been used.

distinguished by BSEM and EDXS (Figure 3b, d). The two phases are well-distributed with clear grain boundaries, demonstrating the good chemical compatibility between the PSFO and CPO phases, which is in good agreement with the XRD results (Figure 2). However, there are three different contrast levels observable (dark, gray and light) in the BSEM. The dark spots in BSEM are pin holes, the gray grains are PSFO and the light ones are CPO since the contribution of the back scattered electrons to the SEM signal intensity is proportional to the atomic number (Figure 3b). The same information is provided by EDXS (Figure 3d, e), which suggests that the green color (gray in the black-and-white version) is an overlap of the Pr, Fe, and Sr signals, whereas the yellow color (light) stems from an average of the Ce and Pr signals. The mean grain size areas of PSFO and CPO have been estimated to 0.146 and 0.230  $\mu\text{m}^2$  from the analysis of 100 grains, respectively. Furthermore, the two phases are well-distributed and form a percolation network of both phases that can be clearly observed in the BSEM and EDXS micrographs, which is beneficial to the oxygen ion and electron transport.

**3.2. Phase Stability of the 40PSFO–60CPO Dual-Phase Material.** In situ XRD provides an effective and direct way to characterize high-temperature structure changes during increasing and decreasing temperatures under different atmospheres. The in situ XRD patterns of the calcined 40PSFO–60CPO powder in air with increasing temperature from 30 to 1000 °C, as shown in Figure 4, indicate that the

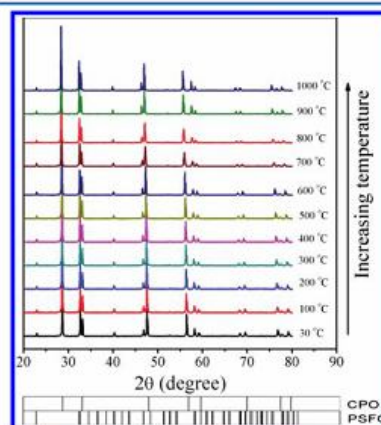
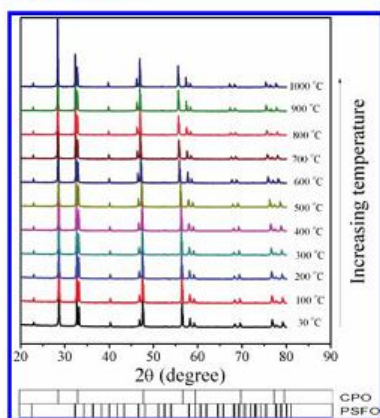


Figure 4. In situ XRD patterns of the 40PSFO–60CPO dual-phase powder after calcination at 950 °C (see Figure 1) in air for increasing temperature. Conditions: heating rate = 12 °C  $\text{min}^{-1}$ ; equilibration time at each temperature, 50 min for recording the XRD data at each temperature.

phases CPO and PSFO remain unchanged in the 40PSFO–60CPO dual-phase material. The high-temperature phase stability has been studied by in situ XRD (Figure 5) between 30 and 1000 °C in an atmosphere of 50 vol %  $\text{CO}_2$  and 50 vol %  $\text{N}_2$ . Figure 5 shows that the dual-phase membrane completely keeps its dual phases PSFO and CPO. No carbonate formation was observed in an atmosphere of 50 vol %  $\text{CO}_2$  and 50 vol %  $\text{N}_2$  in the temperature range of 30 and 1000 °C. These results suggest that the dual-phase membrane



**Figure 5.** In situ XRD patterns of the 40PSFO–60CPO dual-phase powder after calcination at 950 °C (see Figure 1) in 50 vol % CO<sub>2</sub> and 50 vol % N<sub>2</sub> atmosphere for increasing temperatures. Conditions: heating rate = 12 °C min<sup>-1</sup>; equilibration time at each temperature, 50 min for recording the XRD data at each temperature.

40PSFO–60CPO is thermally and chemically stable both in air and in CO<sub>2</sub> between 30 and 1000 °C.

**3.3. Oxygen Permeability and Chemical Stability under CO<sub>2</sub> and CH<sub>4</sub> Atmospheres.** To further assess the CO<sub>2</sub> stability of our dual-phase material during oxygen permeation, the oxygen permeation performance through the 40PSFO–60CPO dual-phase membrane was studied over 150 h using pure CO<sub>2</sub> as sweep gas. Figure 6 shows the oxygen

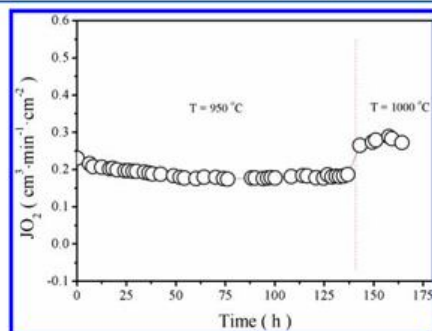


**Figure 6.** Oxygen permeation flux through 40PSFO–60CPO dual-phase membrane as a function of time with pure CO<sub>2</sub> as sweep gas. Conditions: 150 cm<sup>3</sup> min<sup>-1</sup> air as feed gas, 29 cm<sup>3</sup> min<sup>-1</sup> CO<sub>2</sub> as sweep gas; 1 cm<sup>3</sup> min<sup>-1</sup> Ne as internal standard gas. Membrane thickness: 0.5 mm. Temperature: 950–1000 °C.

permeation flux as a function of time. It is found that the oxygen permeation flux decreased slightly from 0.22 cm<sup>3</sup> min<sup>-1</sup> cm<sup>-2</sup> and stabilized at the level of 0.18 cm<sup>3</sup> min<sup>-1</sup> cm<sup>-2</sup> with pure CO<sub>2</sub> as sweep gas at 950 °C. At 1000 °C, the oxygen permeation flux was kept constant at 0.28 cm<sup>3</sup> min<sup>-1</sup> cm<sup>-2</sup> for 20 h. This stable performance in CO<sub>2</sub> suggests that the 40PSFO–60CPO dual-phase membrane possess a high CO<sub>2</sub> stability. To benchmark the 40PSFO–60CPO material, the

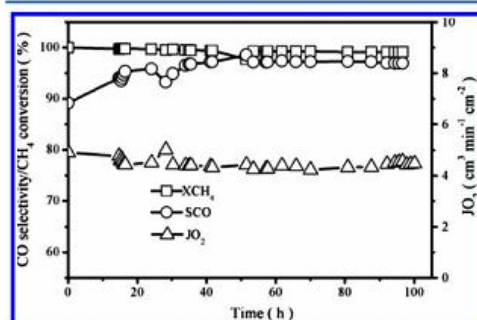
oxygen permeation flux and stability under CO<sub>2</sub> have been compared with results of previously reported materials. From the comparison shown in Table 1, it follows that the oxygen permeation flux through the alkaline earth metal-containing single-phase perovskite membranes is higher than that of the dual-phase membranes, when He as sweep gas has been used. However, if CO<sub>2</sub> becomes the sweep gas, the oxygen permeation flux sharply decreased. The decrease of the oxygen permeation flux through most of these perovskite membranes was more than 90%. In some cases, the materials were even decomposed due to the carbonate formation.

It has been reported by Yi et al.<sup>15</sup> that the reaction of the BaCO<sub>3</sub>·Fe<sub>0.2</sub>Nb<sub>0.1</sub>O<sub>3-δ</sub> membrane with CO<sub>2</sub> leads to a decomposition of the membrane and to the formation of a compact BaCO<sub>3</sub> surface layer and a porous decomposed zone; the latter consists of mainly CoO and a Co-depleted perovskite phase. However, 40PSFO–60CPO dual-phase membrane shows lower oxygen permeation fluxes than most of the alkaline earth metal-containing single-phase perovskite membranes, but it shows a much higher stability in CO<sub>2</sub>. Moreover, compared with the dual-phase membranes NiFe<sub>2</sub>O<sub>4</sub>–Ce<sub>0.9</sub>Gd<sub>0.1</sub>O<sub>2-δ</sub> and Fe<sub>2</sub>O<sub>3</sub>–Ce<sub>0.9</sub>Gd<sub>0.1</sub>O<sub>2-δ</sub>, we can see that our 40PSFO–60CPO membrane shows a higher oxygen permeation flux. However, the oxygen flux can be increased as well by technical measures such as an asymmetric membrane structures<sup>28–30</sup> or by surface enlargement as demonstrated for a hollow fiber.<sup>31</sup> Combining an asymmetric structure and surface enlargement, it was shown by Baumann et al.<sup>28</sup> that a sophisticated material processing using tape casting and cofiring results in high oxygen fluxes of up to 12.2 cm<sup>3</sup> (STP) min<sup>-1</sup> cm<sup>-2</sup> at 1000 °C for an oxygen partial pressure gradient with air on the feed side and Ar on the sweep side. The disk-shaped membrane consists of only the material BSCF: a gastight layer (70 μm) is deposited by tape casting on a porous substrate (830 μm) with 34% open porosity. An open-porous surface activation layer on the air side was prepared via screen printing and increases substantially the surface exchange rate and notably the oxygen permeation rate. A CGO membrane with an asymmetric structure, which was tested under oxy-fuel and syngas conditions by Kaiser et al.,<sup>29,30</sup> consists of an about 30 μm thick gastight CGO layer on top of an about 300 μm thick porous CGO support. The basic membrane structure was produced by tape casting, lamination and cosintering. For this type of asymmetric CGO membranes, three measures have been taken to increase the oxygen fluxes: (i) A thin dense CGO layer of only 30 μm thickness was used. (ii) Co<sub>3</sub>O<sub>4</sub> (or Fe<sub>2</sub>O<sub>3</sub>) was used as sintering aids for membrane layer (and support) and as electronically conductive grain boundary phase. These metal oxides with high electron conductivities were found to be enriched in the grain boundaries, and (iii) the porous support layer was infiltrated with the perovskite La<sub>0.8</sub>Sr<sub>0.4</sub>CoO<sub>3-δ</sub> (LSC) as air catalyst for incorporation of oxygen into the membrane.

Furthermore, we also found that the 40PSFO–60CPO dual-phase membrane reactor was successfully operated in the partial catalytic oxidation of methane (POM) to synthesis gas (see Figure 7). There is an activation period at the beginning, which is attributed to the reduction of Ni oxide to Ni<sup>0</sup> in the catalyst. A similar behavior was found in previous studies.<sup>31</sup> As shown in Figure 7, a CO selectivity of more than 90.0% was obtained in our POM, with about 99.0% methane conversion. After an activation period of 14 h, the CO selectivity can reach 97.0%, the CH<sub>4</sub> conversion remained 99.0% and the oxygen permeation flux through the 40PSFO–60CPO dual-phase

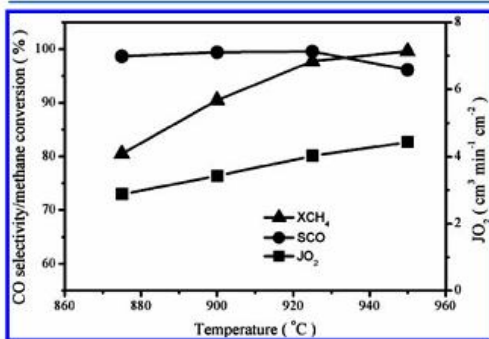
Table 1. Effect of CO<sub>2</sub> as sweep Gas on the Oxygen Permeation Flux through Several MIEC Membranes in Disk Geometry in Comparison with the Sweep Gas He

membrane materials	thickness (mm)	T (°C)	oxygen flux (cm <sup>3</sup> min <sup>-1</sup> cm <sup>-2</sup> ) air/He	oxygen flux (cm <sup>3</sup> min <sup>-1</sup> cm <sup>-2</sup> ) air/CO <sub>2</sub>	ref
BaCo <sub>0.8</sub> Fe <sub>0.2</sub> Nb <sub>0.1</sub> O <sub>3-δ</sub>	1	900	0.70	0	15
Ba <sub>0.5</sub> Sr <sub>0.5</sub> Fe <sub>0.8</sub> Zr <sub>0.2</sub> O <sub>3-δ</sub>	1.15	750	0.36	0	16
Ba <sub>0.5</sub> Sr <sub>0.5</sub> Co <sub>0.8</sub> Fe <sub>0.2</sub> O <sub>3-δ</sub>	1	875	1.9	0	27
40wt.%NiFe <sub>2</sub> O <sub>4</sub> -60wt.%Ce <sub>0.9</sub> Gd <sub>0.1</sub> O <sub>2-δ</sub>	0.5	950	0.18	0.16	22, 23
40wt.%Fe <sub>2</sub> O <sub>3</sub> -60wt.%Ce <sub>0.9</sub> Gd <sub>0.1</sub> O <sub>2-δ</sub>	0.5	950	0.10	0.08	24
40wt.%Pr <sub>0.6</sub> Sr <sub>0.4</sub> FeO <sub>3-δ</sub> -60wt.%Ce <sub>0.9</sub> Pr <sub>0.1</sub> O <sub>2-δ</sub>	0.6	950	0.27	0.18	this work

Figure 7. Time dependence of oxygen permeation flux ( $\Delta$ ), CH<sub>4</sub> conversion ( $\square$ ), and CO selectivity ( $\circ$ ) for 40PSFO-60CPO dual-phase membrane at 950 °C in the POM to synthesis gas. Conditions: 150 cm<sup>3</sup> min<sup>-1</sup> air as feed gas, 7.32 cm<sup>3</sup> min<sup>-1</sup> CH<sub>4</sub> as sweep gas; 1 cm<sup>3</sup> min<sup>-1</sup> Ne as internal standard gas. Membrane thickness: 0.6 mm.

membrane reached 4.4 cm<sup>3</sup> min<sup>-1</sup> cm<sup>-2</sup> at 950 °C. These results indicate that 40PSFO-60CPO membranes possess good chemical stability under a reducing atmosphere such as in the POM, in combination with a high oxygen permeation flux.

After the steady state was reached, the influence of temperature on the CH<sub>4</sub> conversion, the CO selectivity and the oxygen permeation flux was investigated (Figure 8). It was found that the methane conversions increased from 80.5% to

Figure 8. Influence of temperature on the CH<sub>4</sub> conversion ( $\blacktriangle$ ), CO selectivity ( $\bullet$ ), and oxygen permeation flux ( $\blacksquare$ ) through the 40PSFO-60CPO dual-phase membrane in the POM to synthesis gas. Conditions: 150 cm<sup>3</sup> min<sup>-1</sup> air as feed gas, 7.32 cm<sup>3</sup> min<sup>-1</sup> CH<sub>4</sub> as sweep gas; 1 cm<sup>3</sup> min<sup>-1</sup> Ne as internal standard gas. Membrane thickness: 0.6 mm.

99.6%, and the oxygen permeation fluxes increased from 2.9 cm<sup>3</sup> min<sup>-1</sup> cm<sup>-2</sup> to 4.4 cm<sup>3</sup> min<sup>-1</sup> cm<sup>-2</sup> with increasing temperatures from 875 to 950 °C. However, the CO selectivity decreased from 99.0% to 96.0%. This behavior has been observed also for single phase perovskite-type membrane reactors, e.g. using BaCo<sub>0.7</sub>Fe<sub>0.2</sub>Ta<sub>0.1</sub>O<sub>3-δ</sub>.<sup>33</sup> The explanation for this phenomenon is as follows: (i) The increased oxygen permeation flux was ascribed to the increase of oxygen diffusion rate through the 40PSFO-60CPO membrane and the faster surface kinetics with increasing temperature. (ii) The methane conversion was mainly controlled by the amount of the permeated oxygen through the dense membrane. Therefore, the increase in the oxygen permeation flux results in an increase of methane conversion. (iii) With the increased oxygen permeation flux, there is more oxygen available than needed for the stoichiometric POM. Consequently, CO was deeper oxidized to CO<sub>2</sub>, resulting in the decrease in the CO selectivity with increasing temperature.

In the POM to synthesis gas under industrial conditions, oxygen permeable membranes are operated under a highly reducing environment. Unfortunately, only a few perovskite-type membranes can keep their structures in such a harsh environment. In the open literature, it has been reported that carbonates and metals were found on the surface of the spent membrane in the POM because of the corrosive gases H<sub>2</sub>, CO, CO<sub>2</sub>, and H<sub>2</sub>O destroying the membrane. For example, it has been found that cobalt-enriched particles were formed on the surface of a BaCo<sub>0.7</sub>Fe<sub>0.2</sub>Ta<sub>0.1</sub>O<sub>3-δ</sub> membrane after operating in the POM to synthesis gas for 400 h.<sup>32</sup> The perovskite-type Ba<sub>0.5</sub>Sr<sub>0.5</sub>Co<sub>0.8</sub>Fe<sub>0.2</sub>O<sub>3-δ</sub> membrane has been found to be completely destroyed in a hydrogen-containing environment.<sup>34</sup> On the other hand, doped ceria is known as very prone to chemical expansion because of partial reduction of the cations, particularly at high temperatures in highly reducing atmospheres such as H<sub>2</sub> and CH<sub>4</sub>.<sup>12,35</sup> It has been reported that ceria-based electrolytes (e.g., Ce<sub>0.8</sub>Gd<sub>0.2</sub>O<sub>2-δ</sub>) is hindered by poor mechanical strength, a problem notably undesirable for electrolyte-supported cells<sup>36,37</sup> or is limited to intermediate temperatures because of cracks induced by a chemical expansion gradient across the electrolyte (membrane) at temperatures above ca. 700 °C.<sup>30,38</sup> The CPO is reported to be even worse.<sup>38</sup> Therefore, it is necessary to test the structural stability of the dual-phase membrane under POM reaction conditions. After 100 h operation in POM to synthesis gas, both sides of the 40PSFO-60CPO dual-phase membrane were studied by XRD (see Figure 9). Comparing the fresh and spent 40PSFO-60CPO dual-phase membrane, no obvious difference in the XRD patterns except the gold diffraction peaks from the gold paste sealant was observed. Therefore, it can be concluded that the 40PSFO-60CPO dual-phase membrane keeps its dual-

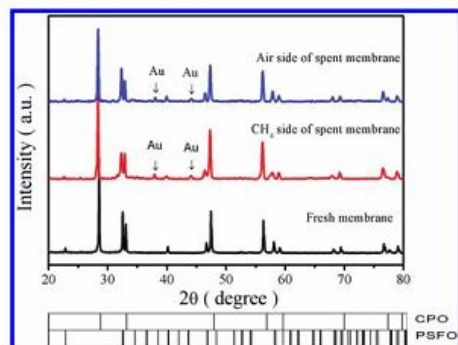


Figure 9. XRD patterns of fresh and spent 40PSFO-60CPO dual-phase membranes in the POM to synthesis gas after 100 h time on stream at 950 °C (see Figure 7).

phase structure, which suggests that 40PSFO-60CPO has a good chemical stability in the reducing POM atmosphere.

Figure 10 shows the temperature dependence of the oxygen permeation fluxes for the 40PSFO-60CPO dual-phase

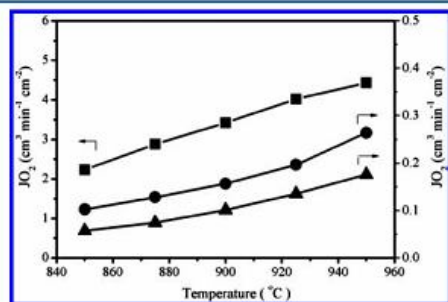


Figure 10. Temperature dependence of oxygen permeation fluxes through 40PSFO-60CPO dual-phase membranes using different gases as the sweep gas: CH<sub>4</sub> (■), He (●), or CO<sub>2</sub> (▲). Conditions: 150 cm<sup>3</sup> min<sup>-1</sup> air as feed gas, 29 cm<sup>3</sup> min<sup>-1</sup> He or CO<sub>2</sub> as sweep gas, or in POM reaction condition (7.32 cm<sup>3</sup> min<sup>-1</sup> CH<sub>4</sub> as sweep gas, Ni-based catalyst as catalyst); 1 cm<sup>3</sup> min<sup>-1</sup> Ne as internal standard gas. Membrane thickness: 0.6 mm.

membrane under different gas atmospheres. At 950 °C, a stable oxygen permeation flux of 0.26 cm<sup>3</sup> min<sup>-1</sup> cm<sup>-2</sup> is obtained through a membrane with a thickness of 0.6 mm, when He as sweep gas has been used. In the POM to synthesis gas, the oxygen permeation flux can be enhanced to 4.4 cm<sup>3</sup> min<sup>-1</sup> cm<sup>-2</sup>. According to the well-known Wagner theory, the

driving force is the oxygen partial pressure gradient between the two sides of the membrane. The presence of the reactive CH<sub>4</sub> lowers the oxygen partial pressure on the reaction side much more than He. Thus, the oxygen permeation flux through 40PSFO-60CPO with CH<sub>4</sub> as reactant was remarkably increased compared with the inert He. The oxygen permeation flux of our dual-phase membrane is higher or comparable with some single-phase perovskite-type and dual-phase-type OTMs in the POM to synthesis gas. As shown in Table 2, the oxygen permeation flux through our 40PSFO-60CPO membrane is higher than that of the single-phase perovskite-type membrane Ba<sub>0.5</sub>Sr<sub>0.5</sub>Fe<sub>0.8</sub>Zn<sub>0.2</sub>O<sub>3-δ</sub> and comparable with them of dual-phase-type membranes (e.g., 40 wt % Gd<sub>0.6</sub>Sr<sub>0.4</sub>FeO<sub>3-δ</sub>-60 wt % Ce<sub>0.8</sub>Gd<sub>0.2</sub>O<sub>2-δ</sub>, 25 wt % Sm<sub>0.6</sub>Sr<sub>0.4</sub>FeO<sub>3-δ</sub>-75 wt % Ce<sub>0.85</sub>Sm<sub>0.15</sub>O<sub>2-δ</sub>, and 25 wt % Sm<sub>0.6</sub>Sr<sub>0.4</sub>Fe<sub>0.7</sub>Al<sub>0.3</sub>O<sub>3-δ</sub>-75 wt % Ce<sub>0.85</sub>Sm<sub>0.15</sub>O<sub>2-δ</sub><sup>31,39-42</sup> under similar POM reaction conditions. Thus, we propose that the 40PSFO-60CPO dual-phase membrane is a promising membrane material for applications in the oxy-fuel process using CO<sub>2</sub> flue gas as sweep gas and high-temperature catalytic membrane reactors for hydrocarbon conversion into syngas and added-value products or thermal decomposition of carbon dioxide in combination with the partial oxidation of methane to syngas.

#### 4. CONCLUSIONS

By using the one-pot one-step glycine-nitrate combustion technique, a novel cobalt-free noble metal-free dual-phase oxygen transporting membrane with the composition 40 wt % Pr<sub>0.6</sub>Sr<sub>0.4</sub>FeO<sub>3-δ</sub>-60 wt % Ce<sub>0.9</sub>Pr<sub>0.1</sub>O<sub>2-δ</sub> (40PSFO-60CPO) has been developed. The membrane consists of a microscale mixture of well-separated PSFO (mixed ion-electron conductor) and CPO (oxygen ions conductor) grains forming a percolation network. According to its chemical composition, the new 40PSFO-60CPO dual-phase membrane is CO<sub>2</sub>-stable. For a 0.6 mm thick membrane, a stable oxygen flux of 0.18 cm<sup>3</sup> min<sup>-1</sup> cm<sup>-2</sup> has been found at 950 °C when using CO<sub>2</sub> as sweep gas. The POM to syngas in the 40PSFO-60CPO dual-phase reactor was successfully performed. Methane conversion was found to be higher than 99.0% with 97.0% CO selectivity, a 4.4 cm<sup>3</sup> min<sup>-1</sup> cm<sup>-2</sup> oxygen permeation flux was obtained under a steady state condition at 950 °C. XRD indicated that the spent membrane operated for 100 h in the POM to synthesis gas retained its dual-phase structure, which suggests that the 40PSFO-60CPO dual-phase membrane is chemically stable under a reducing atmosphere.

#### AUTHOR INFORMATION

##### Corresponding Author

\*E-mail: hhwang@scut.edu.cn (H.W.); juergen.caro@pci.uni-hannover.de (J.C.). Tel.: +86-20-8711-0131 (H.W.); +49-511-762-3175 (J.C.). Fax: +86-20-8711-0131 (H.W.); +49-511-762-19121 (J.C.).

Table 2. Comparison of MIEC OTMs in Disk Geometries for Oxygen Separation under Similar POM Conditions

Membrane materials	thickness (mm)	T (°C)	oxygen flux (cm <sup>3</sup> min <sup>-1</sup> cm <sup>-2</sup> )	catalyst	ref
Ba <sub>0.5</sub> Sr <sub>0.5</sub> Fe <sub>0.8</sub> Zn <sub>0.2</sub> O <sub>3-δ</sub>	1.25	900	2.6	Ni-based catalyst	31
BaCe <sub>0.15</sub> Fe <sub>0.85</sub> O <sub>3-δ</sub>	1.5	950	4.2	LiLaNiO/γ-Al <sub>2</sub> O <sub>3</sub>	39
40 wt % Gd <sub>0.6</sub> Sr <sub>0.4</sub> FeO <sub>3-δ</sub> -60 wt % Ce <sub>0.8</sub> Gd <sub>0.2</sub> O <sub>2-δ</sub>	0.5	950	2-5	LiLaNiO/γ-Al <sub>2</sub> O <sub>3</sub>	40
25 wt % Sm <sub>0.6</sub> Sr <sub>0.4</sub> FeO <sub>3-δ</sub> -75 wt % Ce <sub>0.85</sub> Sm <sub>0.15</sub> O <sub>2-δ</sub>	0.6	950	~4	LiLaNiO/γ-Al <sub>2</sub> O <sub>3</sub>	41
25 wt % Sm <sub>0.6</sub> Sr <sub>0.4</sub> Fe <sub>0.7</sub> Al <sub>0.3</sub> O <sub>3-δ</sub> -75 wt % Ce <sub>0.85</sub> Sm <sub>0.15</sub> O <sub>2-δ</sub>	0.5	950	~4.3	LiLaNiO/γ-Al <sub>2</sub> O <sub>3</sub>	42
40 wt % Pr <sub>0.6</sub> Sr <sub>0.4</sub> FeO <sub>3-δ</sub> -60 wt % Ce <sub>0.9</sub> Pr <sub>0.1</sub> O <sub>2-δ</sub>	0.6	950	~4.4	Ni-based catalyst	This work

## Notes

The authors declare no competing financial interest.

## ACKNOWLEDGMENTS

H.X.L. acknowledges the financial support by the China Scholarship Council (CSC). T.K. thanks the State of Lower Saxony for the NTH bottom up Grant 21-71023-25-7/09. The authors acknowledge the financial support by EU through FP7 NASA-OTM project (Grant 228701) and from the Sino-German centre for Science Promotion (GZ 676). The authors also greatly acknowledge Dr. A. Huang for stimulating discussions and F. Steinbach for technical support.

## REFERENCES

- (1) Watanabe, K.; Yuasa, M.; Kida, T.; Teraoka, Y.; Yamazoe, N.; Shimano, K. *Adv. Mater.* 2010, 22, 2367.
- (2) Watanabe, K.; Yuasa, M.; Kida, T.; Shimano, K.; Teraoka, Y.; Yamazoe, N. *Chem. Mater.* 2008, 20, 6965.
- (3) Kniep, J.; Lin, Y. S. *Ind. Eng. Chem. Res.* 2011, 50, 7941.
- (4) Chen, C. S.; Feng, S. J.; Ran, S.; Zhu, D. C.; Liu, W.; Bouwmeester, H. J. M. *Angew. Chem., Int. Ed.* 2003, 42, 5196.
- (5) Smart, S.; Lin, C. X. C.; Ding, L.; Thambimuthu, K.; Diniz da Costa, J. C. *Energy Environ. Sci.* 2010, 3, 268.
- (6) Engels, S.; Beggel, F.; Modigell, M.; Stadler, H. J. *Membr. Sci.* 2010, 359, 93.
- (7) Yaremchenko, A. A.; Kharton, V. V.; Valente, A. A.; Snijkers, F. M. M.; Cooymans, J. F. C.; Luyten, J. J.; Marques, F. M. B. *J. Membr. Sci.* 2008, 319, 141.
- (8) Slade, D. A.; Duncan, A. M.; Nordheden, K. J.; Stagg-Williams, S. M. *Green Chem.* 2007, 9, 577.
- (9) Zhang, C.; Chang, X. F.; Fan, Y. Q.; Jin, W. J.; Xu, N. P. *Ind. Eng. Chem. Res.* 2007, 46, 2000.
- (10) Jin, W. J.; Zhang, C.; Chang, X. F.; Fan, Y. Q.; Xin, W. H.; Xu, N. P. *Environ. Sci. Technol.* 2008, 42, 3064.
- (11) Fang, S. M.; Yoo, C. Y.; Bouwmeester, H. J. M. *Solid State Ionics* 2011, 195, 1.
- (12) Sunarso, J.; Baumann, S.; Serra, J. M.; Meulenberg, W. A.; Liu, S.; Lin, Y. S.; Diniz da Costa, J. C. *J. Membr. Sci.* 2008, 320, 13.
- (13) Tong, J. H.; Yang, W. S.; Zhu, B. C.; Cai, R. J. *Membr. Sci.* 2002, 203, 175.
- (14) Qiu, L.; Lee, T. H.; Liu, L. M.; Yang, Y. L.; Jacobson, A. J. *Solid State Ionics* 1995, 76, 321.
- (15) Yi, J. X.; Schroeder, M.; Weirich, T.; Mayer, J. *Chem. Mater.* 2010, 22, 6246.
- (16) Martynczuk, J.; Efimov, K.; Robben, L.; Feldhoff, A. *J. Membr. Sci.* 2009, 344, 62.
- (17) Wei, Y. Y.; Tang, J.; Zhou, L. Y.; Xue, J.; Li, Z.; Wang, H. H. *AIChE J.* 2011, DOI: 10.1002/aic.12802.
- (18) Tang, J.; Wei, Y. Y.; Zhou, L. Y.; Li, Z.; Wang, H. H. *AIChE J.* 2011, DOI: 10.1002/aic.12742.
- (19) Klande, T.; Efimov, K.; Cusenza, S.; Becker, K. D.; Feldhoff, A. *J. Solid State Chem.* 2011, 184, 3310.
- (20) Efimov, K.; Klande, T.; Juditzki, N.; Feldhoff, A. *J. Membr. Sci.* 2011, 389, 205.
- (21) Balaguer, M.; Solis, C.; Serra, J. M. *Chem. Mater.* 2011, 23, 2333.
- (22) Luo, H. X.; Efimov, K.; Jiang, H. Q.; Feldhoff, A.; Wang, H. H.; Caro, J. *Angew. Chem., Int. Ed.* 2011, 50, 759.
- (23) Luo, H. X.; Jiang, H. Q.; Efimov, K.; Wang, H. H.; Caro, J. *AIChE J.* 2011, 57, 2738.
- (24) Luo, H. X.; Jiang, H. Q.; Efimov, K.; Liang, F. Y.; Wang, H. H.; Caro, J. *Ind. Eng. Chem. Res.* 2011, 50, 13508.
- (25) Zhu, X. F.; Liu, H. Y.; Cong, Y.; Yang, W. S. *Chem. Commun.* 2012, 48, 251.
- (26) Mokkelbost, T.; Kaus, I.; Grande, T.; Einarsrud, M. A. *Chem. Mater.* 2004, 16, 5489.
- (27) Arnold, M.; Wang, H. H.; Feldhoff, A. *J. Membr. Sci.* 2007, 293, 44.
- (28) Baumann, S.; Serra, J. M.; Lobera, M. P.; Escolástico, S.; Schulze-Küppers, F.; Meulenberg, W. A. *J. Membr. Sci.* 2011, 377, 198.
- (29) Lobera, M. P.; Serra, J. M.; Foghmoes, S. P.; Sogaard, M.; Kaiser, A. *J. Membr. Sci.* 2011, 385–386, 154.
- (30) Kaiser, A.; Foghmoes, S.; Chatzichristodoulou, C.; Sogaard, M.; Glasscock, J. A.; Frandsen, H. L.; Hendriksen, P. V. *J. Membr. Sci.* 2011, 378, 51.
- (31) Tan, X. Y.; Wang, Z. G.; Meng, B.; Meng, X. X.; Li, K. J. *Membr. Sci.* 2010, 352, 189.
- (32) Wang, H. H.; Tablet, C.; Feldhoff, A.; Caro, J. *Adv. Mater.* 2005, 17, 1785.
- (33) Luo, H. X.; Wei, Y. Y.; Jiang, H. Q.; Yuan, W. H.; Lv, Y. X.; Caro, J.; Wang, H. H. *J. Membr. Sci.* 2010, 350, 154.
- (34) Tong, J. H.; Yang, W. S.; Suda, H.; Haraya, K. *Catal. Today* 2006, 118, 144.
- (35) Pu, Z. Y.; Lu, J. Q.; Luo, M. F.; Xie, Y. L. *J. Phys. Chem. C* 2007, 111, 18695.
- (36) Fagg, D. P.; Mather, G. C.; Frade, J. R. *Ionics* 2003, 9, 214.
- (37) Fagg, D. P.; Kharton, V. V.; Frade, J. R. *J. Electroceram.* 2002, 9, 199.
- (38) Fagg, D. P.; Marozau, I. P.; Shaula, A. L.; Kharton, V. V.; Frade, J. R. *J. Solid State Chem.* 2006, 179, 3347.
- (39) Zhu, X. F.; Wang, H. H.; Cong, Y.; Yang, W. S. *Catal. Lett.* 2006, 111, 179.
- (40) Zhu, X. F.; Yang, W. S. *AIChE J.* 2008, 54, 665.
- (41) Zhu, X. F.; Li, Q. M.; He, Y. F.; Yang, W. S. *J. Membr. Sci.* 2010, 360, 454.
- (42) Zhu, X. F.; Li, Q. M.; Cong, Y.; Yang, W. S. *Catal. Commun.* 2008, 10, 309.



## 5. Conclusions

In this thesis, first the issues of phase stability and oxygen permeation behavior of single phase-type perovskite membrane were demonstrated by the example of BSCF tube membrane in high purity oxygen. It was found at 950 °C, that the BSCF tube membranes exhibit good long-term phase stability and a stable oxygen permeation flux. However, at the intermediate temperature of 750 °C, both the oxygen permeation flux and the oxygen purity decrease continuously due to a partial decomposition of the bulk cubic perovskite phase into a hexagonal perovskite ( $\text{Ba}_{0.5\pm x}\text{Sr}_{0.5\pm x}\text{CoO}_{3-\delta}$ ,  $x \approx 0.1$ ) and a trigonal mixed oxide ( $\text{Ba}_{1-x}\text{Sr}_x\text{Co}_{2-y}\text{Fe}_y\text{O}_{5-\delta}$ ,  $x \approx 0.15$ ,  $y \approx 0.25$ ). The structural instability of BSCF is attributed to an oxidation of cobalt from  $\text{Co}^{2+}$  to  $\text{Co}^{3+}$  and  $\text{Co}^{4+}$ , which exhibits an ionic radius that is too small to be tolerated by the cubic perovskite structure, which then becomes unstable.

As described in Section 1.3.2 and the first part, the wide applications of single phase perovskite membrane were still hampered not only by its phase instability at intermediate temperatures of 750 °C but also by its decomposition due to the formation of carbonates in the presence of  $\text{CO}_2$ . Dual phase oxygen permeable membranes were proposed to avoid this dilemma since their compositions can be tailored in the practical applications. In the second part of this thesis, the preparation and characterization of  $\text{CO}_2$ -stable dual phase membranes are demonstrated. Three types of noble metal-free and alkaline metal-free dual phase membranes of the compositions: (i)  $\text{NiFe}_2\text{O}_4\text{-Ce}_{0.9}\text{Gd}_{0.1}\text{O}_2$  (NFO-CGO), (ii)  $\text{Fe}_2\text{O}_3\text{-Ce}_{0.9}\text{Gd}_{0.1}\text{O}_2$  (FO-CGO) and (iii)  $\text{Mn}_{1.5}\text{Co}_{1.5}\text{O}_4\text{-Ce}_{0.9}\text{Pr}_{0.1}\text{O}_2$  (MCO-CPO) have been developed via different methods including mixing powder by hand, mixing powder by ball-milling, one-pot single-step EDTA-citric acid sol-gel method and one-pot single-step combustion method. The one-pot methods gave the best homogeneous grain size distribution and the smallest grain size, leading to the highest oxygen permeability. The oxygen permeation fluxes through these dual phase membranes were performed as a function of time using pure  $\text{CO}_2$  as sweep gas. It was found that the oxygen permeation fluxes through 40NFO-60CGO, 40FO-60CGO and 40MCO-60CPO stabilized at the level of 0.3 ml/min·cm<sup>2</sup>, 0.2 ml/min·cm<sup>2</sup> and 0.2 ml/min·cm<sup>2</sup>, respectively at 1000 °C, and no decrease of the oxygen permeation flux was observed, which indeed confirms that these dual phase membranes are  $\text{CO}_2$ -stable. However, most of these dual phase membranes, which contain easily reducible oxides like Co, Ni, were not stable in harsh reducing atmosphere.

In the third part of this thesis, a novel cobalt-free noble metal-free 40PSFO-60CPO dual phase material was developed via a one-pot single-step GNP, which is a proven means to obtain fine and homogeneous powders. *In-situ* XRD demonstrated that the 40PSFO-60CPO dual phase membrane shows a good phase stability not only in air but also in 50 vol.% CO<sub>2</sub>/50 vol.% N<sub>2</sub> atmosphere. At 950 °C, stable oxygen permeation fluxes of 0.26 ml/min·cm<sup>2</sup> and 0.18 ml/min·cm<sup>2</sup> were obtained through the 40PSFO-60CPO dual phase membrane when using pure He and CO<sub>2</sub> as sweep gases, respectively. The partial oxidation of methane (POM) to syngas was also successfully investigated in the 40PSFO-60CPO dual phase membrane reactor. At 950 °C in steady state, methane conversion was found to be higher than 99 % with 97 % CO selectivity, and a 7.81 ml/min·cm<sup>2</sup> oxygen permeation flux has been obtained. XRD confirmed the unchanged dual phase structure of the spent 40PSFO-60CPO in POM to synthesis gas for more than 100 h, indicating that this dual phase was very stable in hash reducing atmosphere.

In conclusion, this Ph.D. work presents the issues of phase stability of BSCF perovskite membrane in high purity oxygen. Four novel CO<sub>2</sub>-stable dual phase membranes of the compositions of 40NFO-60CGO, 40FO-60CGO, 40MCO-60CPO and 40PSFO-60CPO were synthesized successfully via the direct one-step one-pot synthesis method. They possess high CO<sub>2</sub> stabilities and provide a promising way to supply pure oxygen to power plants with CO<sub>2</sub> capture according to the oxy-fuel concept.



## Publications and conferences

### Publications included in this thesis

1. **Huixia Luo**, Heqing Jiang, Tobias Klande, Zhengwen Cao, Fangyi Liang, Haihui Wang, Jürgen Caro, *A novel cobalt-free noble metal-free oxygen-permeable  $40\text{Pr}_{0.6}\text{Sr}_{0.4}\text{FeO}_{3-\delta}-60\text{Ce}_{0.9}\text{Pr}_{0.1}\text{O}_{2-\delta}$  composite membrane*, **Chem. Mater.** **2012**, **24**, 2148.
2. **Huixia Luo**, Heqing Jiang, Tobias Klande, Fangyi Liang, Zhengwen Cao, Haihui Wang, Jürgen Caro, *Rapid glycine-nitrate combustion synthesis of  $\text{CO}_2$ -stable dual phase membrane  $40\text{Mn}_{1.5}\text{Co}_{1.5}\text{O}_{4-\delta}-60\text{Ce}_{0.9}\text{Pr}_{0.1}\text{O}_{2-\delta}$  for  $\text{CO}_2$  capture via a oxyfuel process*, **J. Membr. Sci.** Submitted, 2012.
3. **Huixia Luo**, Heqing Jiang, Konstantin Efimov, Fangyi Liang, Haihui Wang, Jürgen Caro,  *$\text{CO}_2$ -tolerant oxygen-permeable  $\text{Fe}_2\text{O}_3\text{-Ce}_{0.9}\text{Gd}_{0.1}\text{O}_{2-\delta}$  dual phase membranes*, **Ind. Eng. Chem. Res.** **2011**, **50**, 13508.
4. **Huixia Luo**, Heqing Jiang, Konstantin Efimov, Jürgen Caro, Haihui Wang, *Influence of the preparation method on the microstructure and oxygen permeability of a  $\text{CO}_2$ -stable dual phase membrane*, **AIChE J.** **2011**, **57**, 2738.
5. **Huixia Luo**, Konstantin Efimov, Heqing Jiang, Armin Feldhoff, Haihui Wang, and Jürgen Caro,  *$\text{CO}_2$ -stable and cobalt-free dual phase membrane for oxygen separation*, **Angew. Chem. Int. Ed.** **2011**, **50**, 759.  *$\text{CO}_2$ -stabile und kobaltfreie Zweiphasenmembranen zur Sauerstoffabtrennung*, **Angew. Chem.** **2011**, **123**, 785.
6. Fangyi Liang, Heqing Jiang, **Huixia Luo**, Juergen Caro and Armin Feldhoff, *Phase Stability and Permeation Behavior of a Dead-End  $\text{Ba}_{0.5}\text{Sr}_{0.5}\text{Co}_{0.8}\text{Fe}_{0.2}\text{O}_{3-\delta}$  Tube Membrane in High-Purity Oxygen Production*, **Chem. Mater.** **2011**, **23**, 4765.

## Publications not included in this thesis

7. Fangyi Liang, Heqing Jiang, **Huixia Luo**, Ralf Kriegel, Jürgen Caro, High-purity oxygen production by a dead-end  $Ba_{0.5}Sr_{0.5}Co_{0.8}Fe_{0.2}O_{3-\delta}$  tube membrane, **Catal. Today (2012)**, doi:10.1016/j.cattod.2011.12.016
8. Zhengwen Cao, Heqing Jiang, **Huixia Luo**, Stefan Baumann, Wilhelm A. Meulenber, Hartwig Voss and Jürgen Caro, Simultaneous overcome of the equilibrium-limitations in BSCF oxygen-permeable membrane reactors: water splitting and methane coupling, **Catal. Today (2012)**, doi:10.1016/j.cattod.2011.12.018
9. **Huixia Luo**, Yanying Wei, Heqing Jiang, Wenhui Yuan, Yangxiao Lv, Jürgen Caro, Haihui Wang, *Performance of a ceramic membrane reactor with high oxygen flux Ta-containing perovskite for the partial oxidation of methane to syngas*, **J. Membr. Sci. 2010, 350, 154**. (Selected as one of “Top 100 most cited Chinese papers published in internationals in 2010”)
10. **Huixia Luo**, Bingbing Tian, Yanying Wei, Haihui Wang, Heqing Jiang, Jürgen Caro, *Oxygen permeability and structural stability of a novel tantalum-doped perovskite  $BaCo_{0.7}Fe_{0.2}Ta_{0.1}O_{3-\delta}$* , **AIChE J., 2010, 56, 604**.
11. **Huixia Luo**, LingHui Yu, XinZhi Chen, HaiHui Wang, Jürgen Caro, *Novel  $Ba_{0.5}Sr_{0.5}Fe_{0.8}Zn_{0.2}O_{3-\delta}$  membranes for POM*, **Chin. Chem. Lett. 2009, 20, 250**.
12. Mingya Cai, **Huixia Luo**, Zhong Li, Armin Feldhoff, Jürgen Caro, Haihui Wang, *Preparation and hydrogen permeation properties of  $Ba_{0.5}Ce_{0.95}Nd_{0.05}O_{3-\delta}$  membranes*, **Chin. Chem. Lett. 2008, 19, 1256**.
13. Haihui Wang, **Huixia Luo**, Qiaosheng Liu, XinZhi Chen, *Zinc-containing series perovskite mixing conductor oxygen-penetrating film and its preparation method and application*, **Patent Nr. CN 101265080 B**.

## Contribution to the conference

1. **Huixia Luo**, Konstantin Efimov, Heqing Jiang, Armin Feldhoff, Haihui Wang, and Jürgen Caro, *CO<sub>2</sub>-stable and cobalt-free dual phase membrane for oxygen separation*, **2<sup>nd</sup> ICEPE International conference on energy process engineering-Efficient carbon capture for coal power plants**, 2011, p.193, Frankfurt, Germany. (Poster)
2. **Huixia Luo**, zhengwen Cao and Jürgen Caro, *Oxidative Coupling of Methane (OCM)*, **Semi-annual Meeting on nanostructured Surface Activated ultra-thin Oxygen Transport Membranes**, Seville, Spain, 2011. (Talk)
3. **Huixia Luo** and Jürgen Caro, *Oxidative Coupling of Methane (OCM)*, **Semi-annual Meeting on nanostructured Surface Activated ultra-thin Oxygen Transport Membranes**, Jülich, Germany, 2012. (Talk)
4. **Huixia Luo** and Jürgen Caro, *Oxidative Coupling of Methane (OCM)*, **Semi-annual Meeting on nanostructured Surface Activated ultra-thin Oxygen Transport Membranes**, BASF, Germany, 2012. (Talk)
5. **Huixia Luo**, Haihui Wang and Jürgen Caro, *Development of novel CO<sub>2</sub>-tolerant oxygen-permeable dual phase membranes for CO<sub>2</sub> capture via an oxy-fuel process by a new one-step one-pot synthesis*, **12<sup>th</sup> International Conference on Inorganic Membranes**, University of Twente, Enschede, The Netherlands, 9-13<sup>th</sup> July 2012. (Poster)



# Curriculum Vitae

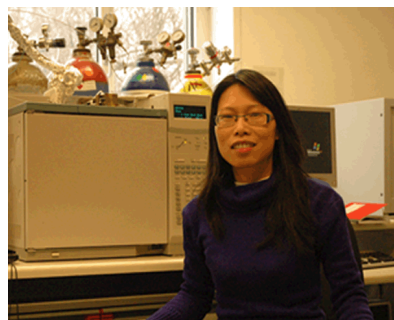
## **Personal data:**

Date of birth: July 29<sup>th</sup>, 1984,

Place of birth: Guangdong, China

Nationality: Chinese

Marital status: Single



## **Awards:**

**08/2009 - 08/2012:** China Scholarship Council (CSC) awards and financed for Ph.D. study in Germany

**2010:** First class of Award of Excellent Paper of Nature Science in Guangdong Province

## **Education and work experiments:**

**09/2009 – 08/2012:** Ph.D. student financed by China Scholarship Council (CSC) and Scientific co-worker at the group of Prof. Dr. Jürgen Caro, Institute of Physical Chemistry and Electrochemistry, Leibniz University of Hannover, Germany

**09/2007 – 06/2009:** Graduate student at the group of Prof. Dr. Haihui Wang, School of Chemistry and Chemical Engineering, South China University of Technology, China

**Degree: Master of engineering**

**09/2003 – 06/2007:** Undergraduate student at School of Chemical Engineering and Energy & School of management engineering, Zhengzhou University, China.

**Degree: Bachelor of engineering & double degree program in business administration**



# **Erklärung zur Dissertation**

Hiermit erkläre ich, dass ich die vorliegende Arbeit selbstständig verfasst und nur unter Verwendung der angegebenen Quellen und Hilfsmittel angefertigt habe. Die Dissertation ist nicht schon als Diplomarbeit oder ähnliche Prüfungsarbeit verwendet worden.

Hannover, im Mai 2012

---

(Unterschrift)

Name: Huixia Luo